THE UNIVERSITY
of EDINBURGH

Dynamic Optimisation and Parameter Estimation for Biochemical Process Systems

Alistair Rodman

Doctor of Philosophy
University of Edinburgh
2019

Declaration

I declare that this thesis was composed by myself and that the work contained therein is my own, except where explicitly stated otherwise in the text.

(*Alistair Rodman*)

Acknowledgements

I would like to thank and acknowledge the following persons and entities:

Dr Dimitrios Gerogiorgis, my principal supervisor, for his guidance, support and mentorship throughout the duration of this project.

Professor Krist Gernaey and Dr Francesco Falco for providing essential assistance with the experimental portion of this thesis.

Professor Eric Fraga for an exciting and thought provoking collaboration.

Professor Constantinos Theodoropoulos and Dr Nicholas Polydorides, my viva examiners, for invaluable feedback towards improving the final version of this thesis.

The Eric Birse Charitable Trust for the generous funding which made this project possible.

Abstract

A vast number of contemporary production processes rely on living cells or biomolecules preforming chemical transformations as a vital step in the manufacture of valuable products. Providing sustainable supplies of food and drink relies on such biochemical processes which are essentially unchanged for millennia, and will remain quintessential for future communities and societies. Likewise many pharmaceutical products and produced from similar systems, and have formed an essential component of modern civilisation. To ensure high productivity without wasting resources (agricultural feedstock, equipment, time), it is critical to determine optimal dynamic operating profiles toward prescribing implementable control methodologies. Mathematical models have been developed for many important food and drink manufacturing processes operated using suboptimal recipes: these journal publications are quite rigorous and extensive (often describing not only composition, but also how flavour can be tuned as desired), but they frequently require consistent kinetic parameter estimation on the basis of industrial data, which is itself a dynamic optimisation problem (multi-parametric error minimisation). Dynamic optimisation of biochemical processes is of extreme technoeconomic interest and importance in industrial control practice, particularly for biochemical process systems which display steady-state and/or operating regime multiplicity, and require sizeable vectors of time-dependent concentrations and temperature-dependent kinetic parameters. Alcohol fermentation is undergoing continuous development for several millennia via concurrent advances in chemistry and chemical engineering (which greatly affected the art of bringing yeast, barley and hops together); at the same time, the biological evolution of yeast strands by natural selection as well as empirical recipes and procedures

have impacted brewing even more. Ensuring high product quality is not a trivial task, particularly when strong market demand dictates process intensification. Producing food and drink in shorter times (more efficiently) with optimised processes (more cost-effectively) requires in-depth knowledge of reactive systems. The problems of consistent kinetic parameter estimation and systematic determination of optimal operating profiles to improve industrial practice are explored in this thesis for several different biochemical systems. For the first time attainable performance in beer fermentation has been exhaustively mapped under a comprehensive family of realistic time dependent temperature manipulations, providing invaluable insight to industrial brewing collaborators. This is expanded upon with the computation of optimal dynamic fermentor temperature profiles subject to a range of realistic threshold constraints on flavour degrading compounds in the product. Herein the influence of each individual by-product level on the achievable process performance can be explicitly quantified and visualised. Furthermore, the inherent trade-off in brewing process targets (batch time vs product quality) has been explored for the first time in this work, mapping the Pareto front via multi-objective dynamic optimisation. These results can be used by decision makers to better inform process decisions with significant economic implications. Following an extensive experimental campaign the first lumped parameter model and associated parameter values for the enzymatic hydrolysis of keratin waste is also proposed in this work. The model is used to formulate a dynamic optimisation problem, demonstrating that treatment of this waste can be accelerated with novel feed strategies. This work highlights the immense value in systematic and rigorous model based simulation and optimisation campaigns for biochemical process systems.

Lay Summary

This PhD thesis involves the modelling and optimisation of biochemical networks: that is any system where at least one stage involves a living organism or an active biomolecule undergoing or performing a chemical transformation. These systems can be manipulated on an industrial level to produce products for sale and consumption including bread, yoghurt, beer and wine; other applications include pharmaceutical production, waste treatment and energy recovery from waste. To ensure high productivity without wasting resources, it is of great value to determine to detirmine how the process should be operated for optimal performance. Mathematical models have been developed for many important food and drink manufacturing processes operated using suboptimal recipes. Such models frequently require parameter estimation on the basis of industrial data: determination of properties and constants which may not be directly measured, which is itself an optimisation problem. This thesis presents a framework for bioprocess model parameter estimation, rapid dynamic simulation of viable operational cases with visualisation of the attainable performance, followed by multi-objective dynamic optimisation strategies. The problems of consistent kinetic parameter estimation and systematic determination of optimal operating profiles to improve industrial practice are explored, with best practices presented in this thesis. Specific studies are centred on two pertinent process systems: beer fermentation and keratin hydrolysis, with significant and viable improvement demonstrated in each case via dynamic optimisation. Valuable insight into these systems has been gained via visualisation of attainable performance, exploration of inherent target trade-offs and by computation of optimal protocols under varying product specifications.

Contents

List of Figures

List of Tables

Part I

Introduction & Background

Chapter 1

Introduction

A vast number of contemporary production processes rely on living cells or biomolecules preforming chemical transformations, as a vital step in the manufacture of valuable products. Many food and drink products which we consume daily are produced via a range of such processes which have been essentially unchanged for thousands of years (e.g. bread, yoghurt, beer, wine). Biochemical processes are not specific to consumer good manufacturing: they also play an essential step in a wide range of areas including pharmaceutical production, waste water treatment, energy recovery from biomass, the production of added value chemicals and even a vast range of biological phenomena taking place with the human body. Biochemical process operation tends to rely on historically established and proven recipes due to system complexity and the limited understanding of the underlying mechanisms; as a result the current protocol or recipe in place is often suboptimal, creating wide scope for viable improvements.

1.1 General Problem Definition

Determining how a modern industrial production process shall be best operated typically involves mathematical optimisation in some form. Computational prediction and performance assessment of a biochemical process toward process optimisation requires a mathematical model representing species consumption and production in addition to cell growth (and death). This strategy is applied fre-

quently in the context of continuous pharmaceutical manufacturing (Engell and Toumi, 2005; Schaber et al., 2011), among a wide array of further bioprocesses (e.g. Chachuat et al. 2001; Tse et al. 2007; Lam 2009; Guebila and Thiele 2016; Spann et al. 2018). Often this will include an optimal control problem, where a system of state variables (x) are influenced by an externally manipulatable control variable, u, so the optimal control vector $u(t)$ is sought to minimise an objective, J, which can consider a terminal pay-off (φ) and a running pay-off ($\int_{t_0}^{t_f}\gamma$) across the process duration from t_0 to t_f (Biegler, 2010; Biegler et al., 2012):

$$J(u) = \varphi(x(t_f), u(t_f), t_f) + \int_{t_0}^{t_f} \gamma(x(t), u(t), t)\ \mathrm{dt} \tag{1.1}$$

Subject to:

$$\frac{dx(u,t)}{dt} = f(x(t), u(t)) \text{ for all } t\in [t_0,t_f] \tag{1.2}$$

$$x(t_0) = x_0 \tag{1.3}$$

The ordinary differential equations (ODEs) which dictate the state trajectories (Eq. 1.2) of known initial value (x_0, Eq. 1.3) are influenced at any time by the current control (u) value. Eqs. 1.4–1.5 represent equality (h) and inequality constraints (g) across the entire time horizon, $t \in [t_0, t_f]$, with terminal equality (h_f) and inequality (g_f) constraints given by Eqs. 1.6 and 1.7 respectively. Lastly the state and control profiles are constrained within permissible bounds by Eqs. 1.8–1.9, where $u(t)_L$ and $x(t)_L$ define the lower bounds across the process horizon and $u(t)_U$ and $x(t)_U$the corresponding upper bounds.

$$h(x(t), u(t)) = 0 \tag{1.4}$$

$$g(x(t), u(t)) \leq 0 \tag{1.5}$$

$$h_f(x(t_f)) = 0 \tag{1.6}$$

$$g_f(x(t_f)) \leq 0 \tag{1.7}$$

$$u(t)_L \leq u(t) \leq u(t)_U \tag{1.8}$$

$$x(t)_L \leq x(t) \leq x(t)_U \tag{1.9}$$

To ensure high productivity in an efficient manner, it is necessary to determine optimal dynamic operating profiles and implementable control methodologies for these processes by solving this problem form. Prior authors have developed mathematical kinetic models for many important biochemical processes via taking repeated concentration measurements as a process progresses under an array of operational conditions (e.g DiStefano III (1969); Bajpai and Reuss (1980); de Andrés-Toro et al. (1998); Henze et al. (2000); Niu et al. (2013); Spann et al. (2018)). These non-linear dynamic ODE/DAE systems can be explored computationally using a range of mathematical techniques with the goal of postulating optimal operational procedures, the criteria of which is process specific. Dynamic optimisation of biochemical processes is of extreme technoeconomic interest and importance in industrial control practice. Ensuring high product quality and the longest shelf life possible is not a trivial task, particularly when strong consumer demand and market competitiveness dictates process intensification. Producing food and drink more efficiently (in terms of time and cost) while maintaining an adequate product quality requires in-depth knowledge of reactive systems, as well as rigorous consideration of the operability restrictions imposed by existing process equipment. Furthermore, in modern times demands for 'green' engineering practices are at the forefront of public discussion and ever-tightening legislation. Approaches to process optimisation fall under three areas (Bonvin, 1998):

- off-line optimisation (open loop optimal control)
- run-to-run optimisation
- on-line optimisation

This thesis is concerned with the former: determining solutions to the off-line optimisation problem to provide optimal open loop trajectories for the manipulated and state variables. These profiles are computed once, off-line, thus feedback elements are not included, and rather an ideal recipe for optimal production is produced. This approach can be limited in usefulness as in the presence of disturbances these trajectories lose their optimal character (Balsa-Canto et al., 2010), however on-line optimisation is not practical: online concentration readings are extremely cumbersome to monitor in many cases.

1.2 Review of Strategies for Dynamic Optimisation

A wide range of optimisation methodologies exist for solving optimal control trajectory problems defined by Eqs. 1.1 - 1.9, summarised in Fig. 1.1 (Biegler, 2007). These may be described as either variational methods or finite approximation methods. Variational methods, also known as indirect methods, attempt to produce a solution satisfying the classical conditions of optimality. In contrast finite methods first apply discretisation to the original continuous time problem. These methods are further divided depending on the extent the problem is discretised; methods that discretise only the control profile(s) (partial discretisation, PD) and those that discretise both the state and control profiles (complete discretisation, CD). The resulting problem from partial discretisation is solved either via non-linear programming (NLP) methods or dynamic programming, while NLP strategies are also used to solve the finite system in complete discretisation approaches. The primary difference is that CD methods solve the DAE system only once, at the optimum, in contrast to PD methods whereby a feasible solution of the DAE system is obtained by model integration at every iteration. As such these PD methods produce smaller discrete problems when compared to CD, however CD problems have better stability properties than PD methods at the expense of increased problem size which may require special solution techniques. An overview of each of the solution strategy follows, based on Cervantes and Biegler (2001).

1.2.1 Variational Methods

Variational methods require optimality conditions from Pontryagin's maximum principle (Pontryagin, 2018), formulated as a set of DAEs where the Hamiltonian is a scalar function of the adjoint variables. The challenging aspect in obtaining a solution to the adjoint equations is satisfying the boundary conditions. State variables are typically assigned initial values while adjoint variables are assigned terminal (final) values. The result is a two point boundary value problem, TP-

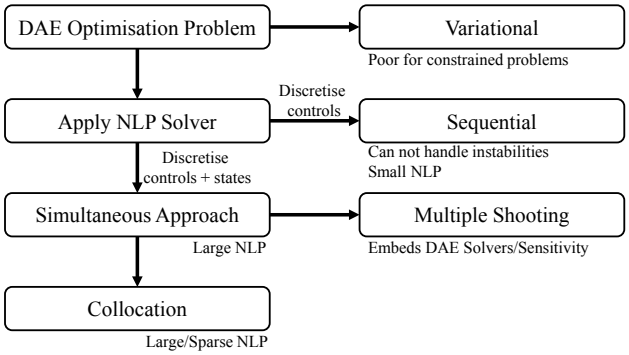

Figure 1.1: Solution strategies for dynamic optimisation (from Biegler, 2007).

BVP. The TPBVP may be solved with several methods: single shooting, invariant embedding, multiple shooting, collocation on finite elements or finite differences.

For the single shooting approach the missing initial conditions of the adjoint equations are guessed, integrating the DAE forward. A Newton iteration adjusts the guessed values so that the final conditions are those specified. The approach can fail if problem cannot be solved for a specific initial condition guess, as a result of non-linearities and instabilities of the system of equations.

Invariant embedding (Støren and Hertzberg, 1995) converts the TPBVP to an initial value problem (IVP), by assuming the structure of the solution. This leads to a solution methodology analogous to the Riccati matrix differential equation (Bittanti et al., 2012), with the primary limitation the resulting high dimensionality of the transformed problem.

Multiple shooting methods apply the same concept as single shooting, however the integration span is sub-divided into discreet intervals such that costate values are guessed at several points in addition to the initial point. The system of equations is decomposed by either solving a collocation system for each interval or by using an integrator along the nominal trajectory on each subinterval. As the entire solution to the TPBVP is produced simultaneously it is no longer necessary to guess the initial conditions. Various factorisation methods (Lentini and Pereyra, 1977; Wright, 1992) are used to reduce the computational burden within each iteration of the solution procedure. These methods work well for unbounded problems, but often struggle handling inequality constraints if information about the active constraints at any point is now known (Cervantes and Biegler, 2001).

1.2.2 Partial Discretisation

Control Vector Parametrisation

In control vector parametrisation (CVP) the time horizon is divided into N elements, within each of which the control variable(s) are represented with a piecewise constant/linear, higher order polynomial or Lagrange polynomials (Almeida and Secchi, 2011). Given the initial state values and an initial discretised control trajectory the ODE/DAE system is solved in each iteration. In doing so the objective function may be evaluated, used by a non-linear programming (NLP) solver to find the optimal value of the parameters which define the piecewise control vectors. Since in every iteration the DAE system is solved, the procedure is very robust providing the system contains only stable modes; otherwise finding a feasible solution can be difficult. Gradients of the objective function with respect to the control parameters can be calculated with the sensitivity equations of the DAE system (Reverberi et al., 1993; Støren and Hertzberg, 1995) or by integration of the adjoint equations (Sargent and Sullivan, 1979; Hasdorff, 1976; Bryson, 2018). CVP is effective for problems with few decision variables and constraints (Osorio et al., 2005) which has been widely applied to engineering problems (i.e. Farhat et al. 1990; Mujtaba and Macchietto 1993; Sørensen et al. 1996).

Dynamic Programming

Iterative dynamic programming (IDP) has been applied to optimal control problems, however the associated high dimensionality has restricted the approaches applicability. To prevent problem size explosion a very course grid can be used, a valuable approach for certain problems where this remains practically accurate. IDP is a slow algorithm when compared to gradient-based methods, but has particular value in cross-validating results of smaller problems when the global optimum is unknown. The likelihood of obtaining the global optimum is good providing the grid is well chosen (Dadebo and McAuley, 1995). The algorithm for IDP for dynamic optimisation problems is detailed by Luus (1993).

1.2.3 Complete Discretisation

Unlike the partial discretisation methods (PD) the complete discretisation methods (CD) discretise all the variables of the DAE system, now also including any continuous control vectors, producing a large scale non-linear programming problem (NLP). Here the DAE system is only solved at the optimal point, rather than at each and every iteration. As such this class of methods may be described as an infeasible path approach, in which the NLP is larger than corresponding partial discretisation methods, but function evaluations are much more rapid. Theses simultaneous approaches are favourable when path constraints are imposed and where instabilities are present. They also circumvent troublesome intermediate solutions, i.e. which are be difficult to obtain or require excessive CPU time, by not solving the DAE system at every step. Two primary approaches for CD methods exist: multiple shooting (Bock and Plitt, 1984) and collocation on finite elements (Cuthrell and Biegler, 1987).

Multiple Shooting

Here control trajectories are approximated with a finite set of control parameters, generally piecewise constant or piecewise linear. A time transformation is made onto a dimensionless grid such that the control approximation is a basic function of dimensionless time and the local control parameters. The DAE system is discretised on the same grid using multiple shooting (Bock et al., 1987), such that it is integrated in each element separately. Values of state profiles at each grid point are treated as further unknowns, producing a set of initial value problems (IVP). Implementing continuity conditions on the state variables at element boundaries into the NLP means that the solution obtained must satisfy the ODE/DAE model. The NLP can be solved using a SQP-type algorithm, calculating the objective gradient and the constraint Jacobians in every iteration. For standard function forms the corresponding derivatives can easily be calculated (Bock and Plitt, 1984). With this approach it is possible for path constraints to be violated within each time element, since constraints are only imposed at the boundaries.

Collocation

Families of polynomials on finite elements are used to approximate the control and state trajectories allowing the continuous problem to be converted to NLP form. Polynomials may be power series, summations of orthogonal polynomials or Lagrange polynomials. Thus the DAE system is converted to a system of algebraic equations, where decision variables of the derived NLP problem include coefficients of the linear combinations of these AEs. The NLP formulation now consists of the DAE process model discretised on finite elements. Continuity equations for state variables and the inequality constraints on the system are added to the NLP, which is large scale and compatible with a number of NLP solvers. Specialised methods can be used to efficiently solve the large scale NLP: full space methods exploit the sparsity of the DAE problem, while reduced space methods exploit the structure of the problem (Biegler, 2007). Precision is known to vary with collocation point locations and element lengths used (Tanartkit and Biegler, 1995; Logsdon and Biegler, 1989). The strategy offers numerous benefits, being faster to solve and able to handle problems with a greater number of decision variables and constraints compared to PD methods (Cervantes and Biegler, 1998; Cervantes et al., 2000).

1.3 Application in Process Engineering

Since the early work of Denbigh (1958) optimal control of batch reactors has received a vast amount of research interest (i.e Logsdon 1991; Logsdon and Biegler 1993; Luus 1994; Garcia et al. 1995; Aziz and Mujtaba 2002). Logsdon (1991) considered a maximum conversion and fixed time-frame optimisation problem for a consecutive reaction scheme. This work sought the optimal temperature profile, $T(t)$, to maximise conversion of the desired product in a predefined reaction time, solved with a two-point collocation method. Later Logsdon and Biegler (1993) solved the same problem with a relaxed simultaneous approach requiring less CPU time to solve. Luus (1994) also considered a maximum conversion for consecutive reactions. Here the piecewise constant $T(t)$ profile with fixed switching is opti-

mised with IDP to maximise conversion. Garcia et al. (1995) considered another conversion maximisation problem for a consecutive parallel reaction scheme. The dynamic optimal control is discretised into an NLP problem and solved by a generalised reduced gradient method coupled with a golden search technique. The authors compared considering 5 and 10 time intervals to discretise the temperature profile, concluding that there is no significant improvement upon increasing the discretisation density and resultant NLP problem size. Aziz and Mujtaba (2002) consider a CVP method for both maximum conversion (operation time is fixed a priori) and minimum time problems (conversion is fixed a priori) for a typical consecutive reaction scheme in batch reactors. They explore the effect of waste and/or temperature constraints (both path constraints and terminal value constraints) on the optimal operation policies and on the attainable performance (solution objective function values). Aside from batch reactor optimisation, unconventional chemical process applications of systematic process simulation and optimisation include high-temperature multiple reactor design (Gerogiorgis and Ydstie, 2005), fossil fuel production (Arashi et al., 2003; Gerogiorgis et al., 2006), polygeneration (Liu et al., 2007; Gassner and Maréchal, 2012), cyclic dynamics (Akinlabi et al., 2007; Logist and Van Impe, 2012) and structured products (Angelopoulos et al., 2013; 2014; Tsikouras et al., 2016).

1.4 Chapter Conclusions

It can be concluded that first-principles mathematical modelling for systematic process simulation and optimisation on the basis of validated ODE/DAE system models is well established in several (but not all) chemical and material process industries. Due to the system complexity many existing biochemical systems are currently operated in a suboptimal manor, and can potentially benefit significantly from rigorous computational optimisation. Similarly the development of novel biotechnologies can be accelerated by seeking optimal operation as the technology advances from infancy to improve competitiveness versus mature alternatives. A range of approaches have been successfully applied to control trajectory optimisation for improved chemical process operation, with sequential and simultaneous strategies both favourable depending on the specific problem being solved. This thesis explores several lucrative methodologies for dynamic optimisation in the context improving the performance of specific bioprocesses identified as having significant scope for attainable process improvement.

Chapter 2

Thesis Aims & Objectives

This project aims to produce novel dynamic operational manipulations (control trajectories) capable of improving upon current performance for select bioprocesses under consideration. One primary objective of this thesis is to apply optimisation strategies described in Chapter 1 for an established and widespread industrial bioprocess to gain insight into the viable scope for process improvident to be made. Additionally, a further objective is also consider a less developed or novel bioprocess, to attempt to accelerate development and adoption via the construction, experimental validation and use of a high-fidelity model for dynamic optimisation. Achieving more efficient bioprocess operation with shorter throughput times without any compromise on quality is a challenging task so the following deliverables are outlined to form a systematic workflow to fulfil the primary remits of this thesis.

Selection of candidate processes: To be compatible with the general problem form outlined in Chapter 1 the process progression must be effected by an externally manipulatable dynamic control profile, the formulation of which ultimately becomes the optimisation target. An incentive to improve upon current practice must exist, which can include economical or environmental factors. Additionally, kinetic models of the process must exist to permit computational simulation and optimisation where data acquisition and model development for a specific process is out of the scope of this work.

Assessment of published kinetic models: It is necessary to ensure published models are adequate in scope, describing all observables of interest. In addition to any feed, cells or product, it is of particular importance that any problematic pollutants or by-products are described, since constraints on these species which ensure quality are often the performance bottleneck. All assumptions made in any model formulation must be cross-checked in order to ensure computational results are not non-useful in practice on the real process. Model applicability under realistic operation (scale and valid ranges of input conditions) must also be ensured, by comparing scales and conditions of the industrial process to those used for model validation. Consideration of any specific scale effects should be made where validation has only been performed on small scale systems relative to industry. If published parameter vectors are used it is essential that a suitable data-set was used and that the fitting performed is not ill-conditioned. Where several models exist for a specific process the relative benefits of each (number of species, scale, data quality, validation scope, model accuracy etc.) shall be evaluated to choose the most useful for simulation and optimisation.

Evaluation of existing protocols/recipes: Simulating process progression following control profiles obtained from literature sources or consultation with plant operators shall allow their performance to be assessed, acting as a benchmark which any improvement can be measured against.

Experimental data acquisition: Subject to a lack of published or available industrial data, targeted experiments are to be performed to generate necessary concentration data over time for model parametrisation. Collaboration with the Process and Systems Engineering Centre (PROSYS) at the Technical University of Denmark (DTU) to take place to this end.

Model development: Where data availability permits; mathematical formulation and experimental validation of process models correlating adjustable inputs (feed quality, process conditions, recipe specifications) with measurable outputs (product component concentrations, pH, shelf life) is to be performed.

Kinetic parameter estimation: Kinetic parameter estimation using process-specific concentration vectors, to obtain high-fidelity ordinary-differential-equation (ODE) system models describing processes of interest, in conjunction with literature and/or industrial data.

Formulation of appropriate objective(s) and process constraints: The relative importance of various factors, such as batch time, product/effluent concentrations or energy consumption will be process specific and something essential to ensure optimisation results are valuable.

Systematic determination of optimal operating profiles: A range of optimisation techniques are to be used towards systematic determination of optimal implementable operating profiles (e.g. fermentation cooling profile or wastewater aerator schedule) to significantly enhance current practice. Control vector parametrisation can be used to solve the mathematical problem: parametrisation of the control domain converts the problem to one which may be solved with a wide range of non-linear programming (NLP) algorithms (i.e. Biegler et al. 2002; Schlegel et al. 2005).

Sensitivity analysis: Applying efficient algorithms for sensitivity analysis of resultant output ranges as a function of input parameter variation is another important aspect which will be considered, to elucidate the design and operational variables with potential for improvement.

Comparative analysis of optimisation protocols: Both stochastic and deterministic dynamic optimisation algorithms are considered in this work, so the relative benefits of each on a process specific level can be considered including CPU time, objective value and solution profile implementability.

The systematic methodology defined by the above objectives represents the necessary steps to reliably fulfil the primary objectives of this thesis. In doing so novel control trajectories for optimal operation of key bioprocesses shall be produced, and any scope for industrial improvements shall be elucidated. Additionally, procedure(s) are to be formulated to use validated process models and favourable optimisation methodologies to gain process insight, in addition to computing the unique solution to optimal control problems.

Chapter 3

Bioprocess Systems Considered

This thesis considers several specific bioprocess systems. These processes are introduced in this chapter, along with the driving motivation which renders them promising candidates to benefit from dynamic process optimisation.

3.1 Enzymatic Keratin Hydrolysis

Keratin-rich waste material is an abundant by-product from agro-industrial activities, particularly the meat and poultry industries (Daroit and Brandelli, 2014): skin remains, bristle, animal hair, horns and hooves, feathers, etc. It is estimated that five million tonnes per year of keratin waste is produced in these industries (Brebu and Spiridon, 2011), which is classified as a low-risk animal by-product. This constitutes the third most abundant renewable polymeric material present in nature after cellulose and chitin. This solid residue is not suitable for human consumption and must to be treated for safe disposal into the environment. Keratins are insoluble and resistant to enzymatic proteases due to a high number of disulphide bonds in their structure (Fraser et al., 1988). Their favourable structural properties for defensive skin appendages become troublesome when attempting to decompose the waste material, for which a range of strategies are investigated and employed.

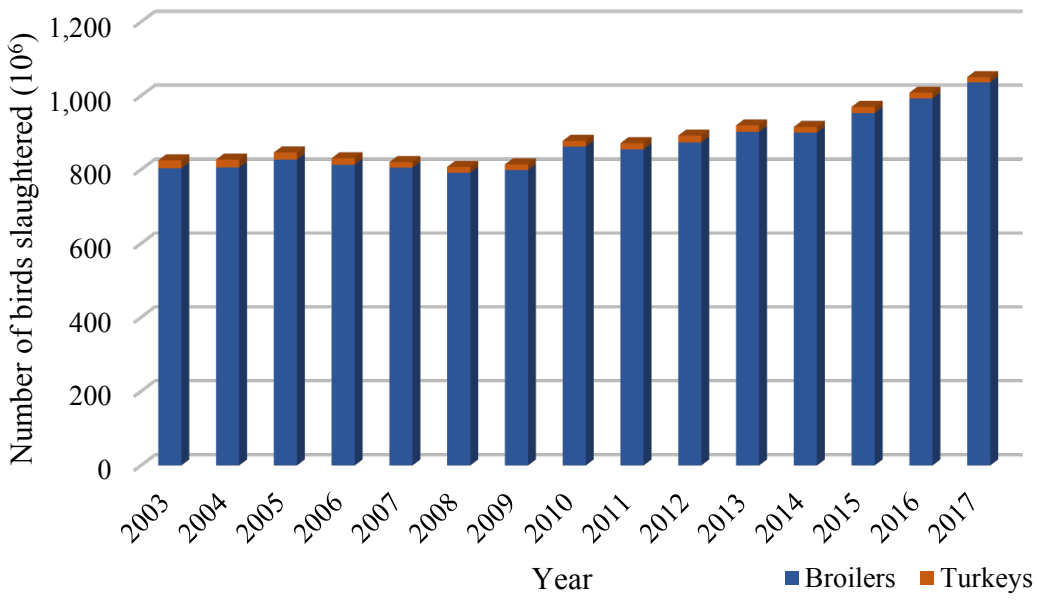

Figure 3.1: Poultry slaughtered in the UK, 2003–2017, by type (DEFRA, 2018).

3.1.1 Motivation

Consumption of popular meat products has been continuously growing in recent years in certain markets. Figure 3.1 shows the annual UK poultry consumption by number of birds over the past 14 years (DEFRA, 2018). While turkey consumption (red) has been relatively static over this time frame, broiler (chickens bred specifically for their meat, blue) consumption has been growing at a rate faster than the population. Similarly Fig. 3.2 shows the number of clean pigs slaughtered for their meat in the UK over the same time frame. Again a growth rate exceeding that of the population is observed, highlighting the increasing supply and demand for these meat products in this market. In recent years there has been considerable interest in developing strategies for improving the sustainability of global food consumption (Lichtfouse et al., 2009). While reducing meat consumption and maintaining vegetarian or vegan diets appear as the most direct steps an individual can take towards sustainability, the consumption statistics suggest that this is unlikely to be widely adopted in the near future. As such there is growing pressure due to the increasing volume hazardous animal by-products produced from these and other agro-industrial activities each year.

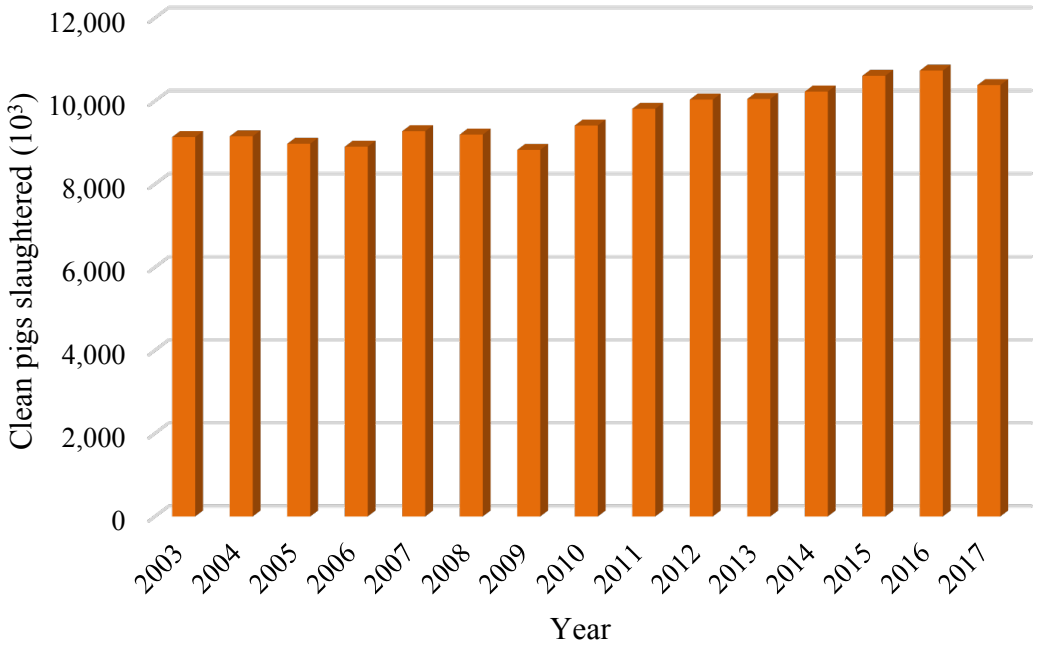

Figure 3.2: Number of pigs slaughtered in the UK, 2003–2017 (DEFRA, 2018).

Where possible, operators seek to extract as much value as possible from the animal by-products, once the meat has been stripped from the animal carcasses. Figure 3.3 presents the export value of animal by-products from the UK in 2017, showing that aside from guts, bladders, stomachs and skin there is very little value in additional by-products from slaughterhouses. In particular the extremely abundant keratin-rich bristles and hair highlighted in Figure 3.3 have a particularly low export value, as a result of the soluble protein content not being useful in its polymer keratin form. For this reason producers seek waste valorization by upcycling this non-biodegradable by-product by de-polymerization to extract soluble proteins from the residual biomass to produce a saleable by-product, for example as an animal feed supplement.

An additional strategy towards developing and maintaining a sustainable global food source is that of fish-farming (aquaculture). Figure 3.4 compares the mass of fish produced over the past 10 years via conventional open fishing versus that from aquaculture. It is demonstrated that the capture volume is not increasing, as a result of tariffs in place to prevent unsustainable overfishing, while in contrast the aquaculture portion is increasing dramatically year on year. This makes the aquaculture industry one of the fastest growing sectors in food

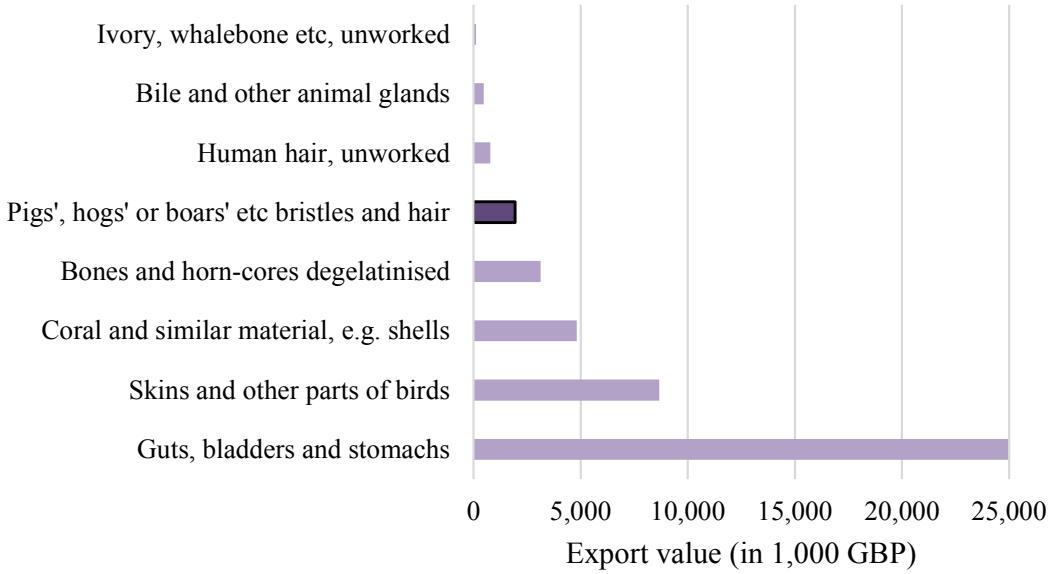

Figure 3.3: UK animal by-product exports by value (ITC, 2017).

production accounting for close to 50% of global production in 2017.

Deemed more sustainable than open fishing, due to the ability to control fish populations, fish farming still requires a vast amount of feed to be supplied in order for the fish to grow. The specific requirements for a fish feed vary depending on the species and region (FAO, 2018), where regardless of the specific product or the stage of fish development a minimum crude protein content (%) must be ensured in all feeds. This essential nutrient is required for the organism to synthesize muscle tissue which is the desired product for consumption.

The availability of risk-free, easily accessible and economical feed ingredients capable of meeting this protein requirement for sustainable aquaculture production plays a key role in global food security. The protein and amino acid composition of a range of ingredients which may be used as components of fish feed id documented (NRC, 1993), where poultry by-product meal (PBM) containing a reported 59.7% protein by weight with a favourable blend of amino acids, suggesting that proteins obtained from the biodegradation of keratin could replace a significant fraction of the fish meal used in aquaculture feed formulation. Conventional fish meal constitutes one of the main ingredients of fish feed and represents about 40% of its total weight (Fang et al., 2013), suggesting vast potential demand for such a product.

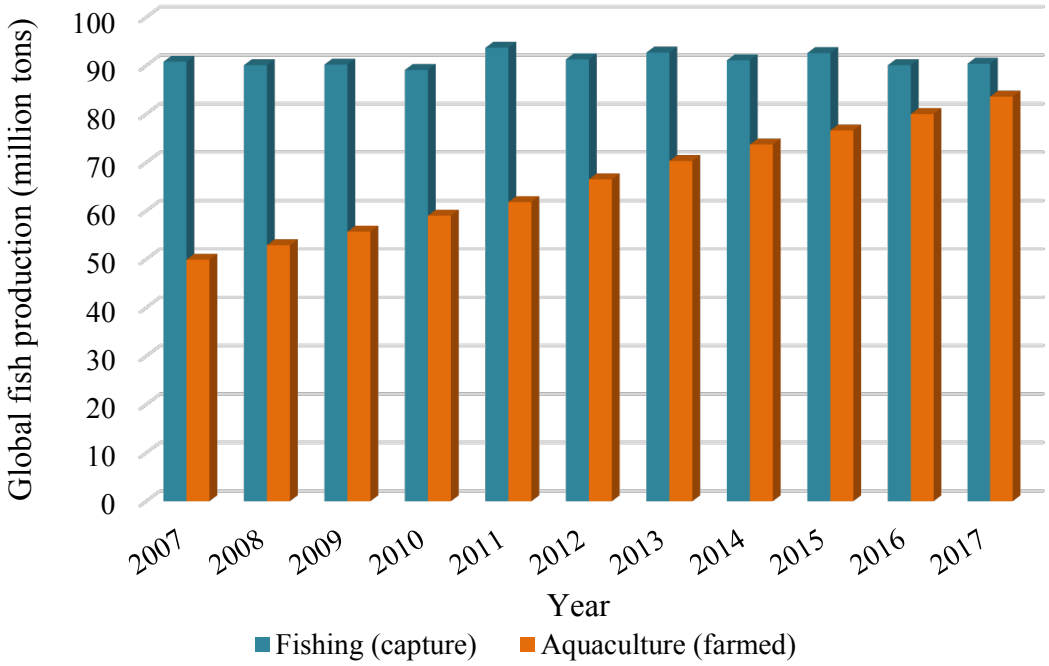

Figure 3.4: World fish production, 2007-2017 (FAO, 2017).

3.1.1.1 Keratin Waste Management

Keratins are insoluble and resistant to enzymatic proteases due to a high number of disulphide bonds in their structure. Their favourable structural properties for defensive skin appendages become troublesome when attempting to decompose the waste material, for which a range of strategies are investigated and employed (Ayyaldaz, 2018).

Thermal Processing Traditionally keratin hydrolysis has been performed via incineration (Jeske et al., 1976; Orzeszko and Sutarzewicz, 1979). Hydrothermal treatment has been a favoured mechanism to treat feather and bristle wastes to produce animal feeds via pressure cooking and subsequent milling. Here high pressure steam is introduced along with select acids, and by maintaining the waste mixture at a boil for several hours the keratin polypeptide chains are opened to release water-soluble peptides, oligo-peptides and amino acids. The product from this hydrothermal treatment contains a high protein content, in addition to nitrogen, fat and mineral substances. However, in addition to substantial fumes being produced with a foul odour (Suzuki et al., 2006), high temperature processing destroys amino acids necessary for the product to be used as animal feed,

which are costly to supplement afterwards. Because of temperature, pressure, and chemicals, hydrolysis ultimately causes the partial or complete destruction of essential amino acids like lysine, methionine and tryptophan and formation of non-nutritive amino acids like lysine, alanine, and lanthionine. As such these methods decrease the nutritional quality and digestibility of the products, which are classified as low-quality animal feed due to their low content of essential amino acids (Karthikeyan et al., 2007; Korniłłowicz-Kowalska and Bohacz, 2011). An alternative approach reported considers thermally decomposing keratin-rich wastes in two main steps. The degradation step is performed between $170 - 300$ °C and is dominated by the evolution of inorganic gases. During the second step, nitriles and aromatics are formed at temperatures above 300 °C. Pyrolysis can be considered as an alternative method to treat keratin-rich wastes, cleaving the disulphide bonds and releasing constituent amino acids from the polypeptide chains. However, this mechanism has economic and environmental drawbacks induced by the need for high temperature and the production of undesirable by-products (Brebu and Spiridon, 2011).

Acidic or alkaline hydrolysis Acidic or alkaline hydrolysis can be used to solubilize keratin material in a heated organic solvent. Proteins may be precipitated with acetone, before distillation and drying to remove residual solvents. It is demonstrated that the hydrolysate is rich in amino acids and polypeptides with a protein composition similar to that of soybean rendering it suitable for use as a diet supplement for ruminant mammals. However its arginine, histidine, lysine, methionine and threonine content were all too low to be viable as an animal feed (Korniłłowicz-Kowalska and Bohacz, 2011).

Microbial fermentation The high operational costs and environmental impact of thermal and chemical methods has resulted in growing interest towards microbial treatment. Microbial degradation methods are considered an environmentally favourable and potentially economical alternative to manage the vast amount of keratin-rich waste material, without excessive energy consumption nor undesired degradation of the product amino acid profile. Studies performed

demonstrating microbiological degradation of wool with fungus, Bacillus and thermophilic and mesophilic actinomycetes show that they can efficiently degrade keratin by synthesis of keratinases. They attack keratin residues and extract the valuable proteins at much lower temperature than the aforementioned treatment strategies. Products obtained from feather waste with keratinolytic strains show a high content of soluble proteins and amino acids. Unlike thermal and chemical treatment, the microbial hydrolysis products show a high content of lysine, threonine, leucine, isoleucine and valine and high digestibility. These favourable properties suggest this route as a viable means of producing an animal feed supplement to add value to the abundant keratin rich waste material. Keratinolytic microorganisms have started to be used in select countries such as India, Brazil, and Venezuela to obtain protein hydrolysates. However, microbial hydrolysis is not commercially used for keratin reuse as animal feed at present (Brandelli, 2008; Fang et al., 2013).

Aerobic and anaerobic digestion of keratin waste Previously certain keratin wastes were simply disposed of in landfills, however this does not fulfil environmental legislation due to degradation issues, the foul smell and the danger of spreading pathogens that grow on keratinous waste. In the 1980s waste feathers were first trailed in the production of fertilizing agents like keratin-bark-urea granulates. Experiments showed the fertilizer agents affected soil properties and some plants positively, however in some cases they reduced respiratory activities of light soils, causing a disturbance to nitrification and nitrogen losses (Korniłłowicz-Kowalska and Bohacz, 2011). A more recent study demonstrated that waste feathers can be treated by aerobic or anaerobic digestion. This involves composting chicken feather together with plant waste rich in lignocellulosic material to perform biological conversion of keratin waste to a hygienic, stable, and mature product that can be used to enrich soil properties. This method may be considered the safest and most cost-effective technologies to utilize keratinous waste as fertilizer (Korniłłowicz-Kowalska and Bohacz, 2011). Poultry waste can also be used in bioenergy production: it is possible to produce natural gas, methane gas fuel pellets and bio-hydrogen via sufficient utilization of keratinolytic microor-

ganisms. Keratinases hydrolyse keratin waste after which anaerobic digestion is used to produce biogas from via methane fermentation with methane-producing bacteria. The remaining protein-rich feather by product from biogas production could then potentially be used as an animal feed. Alternatively, the feather meal might be used to produce more keratinase, and the spent keratinous material can act as a fertilizer (Anbu et al., 2007).

3.1.1.2 Novel Enzymatic Keratin Hydrolysis Process

Many of the established keratin treatment routes feature significant drawbacks. High utility costs are incurred, their pose a detrimental effect on the environment from by-products produced, as well as the losses of essential amino acids due to harsh chemical and thermal conditions. New regulations considering management of category three waste material emphasize the need for environmentally-friendly technologies. Therein there is an increasing need for the adoption of a more sustainable method to treat keratin-rich residues which can lower the environmental, financial and public health risks (Daroit and Brandelli, 2014). Recent studies have considered keratin waste as a possible renewable source for production of sustainable materials. The enzymatic hydrolysis of keratin waste employs microbial keratinases to decompose keratin-rich substrates. The soluble proteins, peptides and free amino acids are released during the process, and not degraded by the reaction conditions. Therefore, biodegradation using keratinolytic bacteria is an attractive way of converting keratinic waste into products of practical industrial value (Al-Musallam et al., 2003). This can include acting as a fish meal replacement in feeds for the aquaculture industry, where the product has an improved amino acid profile compared to thermal keratin processing (Korniłłowicz-Kowalska and Bohacz, 2011). Therein a novel two stage process can be performed for the conversion of keratin-rich waste material into a useful protein-rich product. Firstly, a keratin sample is used as a bacteria feed to promote the synthesis of microbial keratinases. Here, keratin consumption is not of interest and the process stage should be optimised solely for enzyme production and growth. Subsequently keratin hydrolysis may be performed using the

enzyme produced in the previous stage. The two processes (enzyme synthesis and hydrolysis) are favoured in drastically different conditions. The two stages can be physically separated by means of a cross-flow ultrafiltration membrane step, with each stage cyclically repeated to achieve semi-continuous operation. It is desirable to perform the keratin degradation process stage at high solids loadings to maximise product titer and reduce process water, energy usage, and reactor size (Gong et al., 2015). As this is an industrial process in its infancy, the enzymatic hydrolysis mechanism is not well documented, rendering current industrial application limited. Therein lies a strong incentive towards developing a model of the keratin hydrolysis process, to facilitate computational simulations and process optimisation for the emerging technology.

3.2 Industrial Beer Fermentation

The production of beer is well documented, with suggestions that it is one of the world's oldest prepared beverages, dating as early as the early Neolithic period (Arnold, 2005). Today beer is the most widely consumed alcoholic beverage in the world (Rehm et al., 2003) with the global beer market estimated to be over 500 billion USD in 2015 (Research and Markets, 2013). The continual growth of the alcohol industry as a whole has resulted in an ever-increasing demand for beer products, with a rapid increase in the demand for super premium and craft beer products observed in the last 5 years. Market competitiveness makes it imperative that brewers operate their production processes effectively: the ability to improve any stage of production will have a significant effect on profitability and the ultimate success or failure of a brewery. While many variations of the beer manufacturing process exist, industrial production almost invariably follows the scheme outlined in Figure 3.5. Beer production is a complex chemical process: nevertheless, its only prerequisite is the use of the same four essential ingredients: a starch source, yeast, hops and water (Southby, 1885). Beer production requires few raw materials and many rudimentary processing techniques, however what is produced is a highly complex mixture of chemical species which govern product quality and flavour. It is the varying combinations of these compounds which are

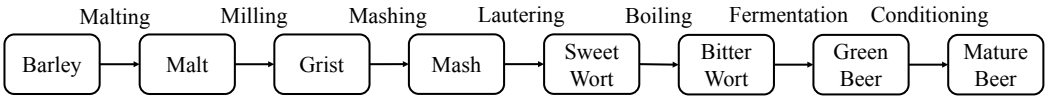

Figure 3.5: Block flow diagram of the beer production process.

responsible for the unique taste of each beer brand, however many are unpleasant at certain concentrations. Diacetyl (2,3-butanedione) has a pungent butter-like aroma (Izquierdo-Ferrero et al., 1997), similar to banana flavouring agents (Hanke et al., 2010), and is often produced well above the flavour threshold in brewing. Due to their volatility, esters also contribute significantly to beer aroma; ethyl acetate is often used as an indicator of all esters present, and is described as having the odour of nail varnish remover. It is essential that efforts to improve fermentation efficacy are mindful of the degrading effect which these compounds have on product quality, if present in substantial quantity.

3.2.1 Beer Fermentation Background

Fermentation is an essential brewing process unit operation, and the focus of this study. Yeast is introduced once the cooled wort (a sugar-rich brewing intermediate, Hough et al., 2012) from the boiling process (Hudson and Birtwistle, 1966) enters fermentation vessels (pitching). The primary chemical reaction pathway is the conversion of two sugar molecules into one ethanol and one carbon dioxide molecule, which is coupled with biomass growth and exothermic reaction heat generation. Concurrently, a wide range of species are formed at low concentrations by a multitude of side reactions, many of which contribute to beer flavour. Fermentation progression is sensitive to yeast pitching rate (Guido et al., 2004), dissolved oxygen content, batch pressure and system temperature, which strongly affects yeast growth and metabolic rate: as long as yeast cells are not damaged and are kept below 30 ^{o}C, high temperature accelerates fermentation. Nevertheless, ethanol and volatile flavour component loss rates are too severe at higher temperatures, coupled with increased production of undesirable aromatic compounds and bacterial growth promotion. Therefore, brewers control temperature inside the fermentor as the batch progresses, to accelerate fermentation while

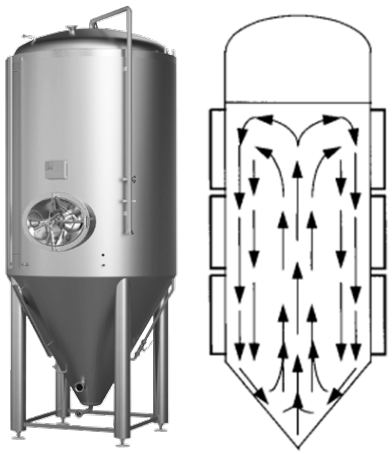

Figure 3.6: Industrial fermentation vessel and mixing pattern.

ensuring that yeast is not denatured and that no undesired by-product species are produced. Online measurements can be cumbersome: each beer brand or line may have a proprietary temperature manipulation profile used for every batch, to ensure product consistency (Trelea et al., 2001). Offline measurements to assess fermentation progression are often limited to wort density or specific gravity. The Plato (specific gravity) scale represents equivalent sucrose concentration: sugar depletion is a useful indicator of the extent of fermentation.

A primary concern of the brewing industry is the selection and implementation of an appropriate dynamic temperate profile throughout the fermentation process, to ensure high product quality, eliminate batch variations and ensure brand consistency and customer satisfaction. Fermentation duration varies by product sought. Lagers are fermented at temperatures around 10 ^{o}C, requiring a fermentation time of about a week. Ales are fermented at higher temperatures (22 ^{o}C) and thus require $3-4$ days (Boulton and Quain, 2008). The worldwide diversity of brewing plants and operations has induced an enormous variety of fermentor vessel types. Many fermentors are cylindro-conical stainless steel vessels (Fig. 3.6a), thus promoting circulation and mixing due to CO_2 bubbling, since contents are not agitated mechanically: a uniform vessel temperature is easier and quicker to achieve. Yeast recovery is thus facilitated via settling into the cone (lager-producing bottom yeasts) or flotation and skimming of the free surface in the cylinder (ale-producing top yeasts). Fermentors typically comprise a cooling

jacket, controlling the wort temperature in order to follow the prescribed profile. Larger tanks may include separate cooling mechanisms on the conical and cylindrical portions (Fig. 3.6b), allowing for control of the circulation pattern (Boulton and Quain, 2008).

Following primary fermentation, beer maturation and finishing (also known as secondary fermentation) achieves numerous objectives: insoluble material is removed, stability is increased, flavour is finalised and the beverage is carbonated by 3 distinct strategies employed for conditioning:

1. Lagering: the beer is cooled causing a considerable portion of the yeast to flocculate: beer is then transferred to a new vessel where any remaining sugar is fermented slowly, while the CO_2 produced remains entrapped toward natural carbonation.

2. Aging: the temperature of the green beer is reduced below freezing (0 ^{o}C) and maintained for up to 2 weeks, after which external beer carbonation with pressurised CO_2 is conducted.

3. Krausening: a portion of wort which has only recently begun fermenting is added to the green beer, which is maintained at a moderately low temperature ($T = 8$ ^{o}C) for several weeks. During this period, additional sugars are slowly consumed and the CO_2 which is produced achieves natural carbonation.

During maturation, concentrations of certain undesirable flavour-modifying compounds are reduced by conversion to substances which do not discernibly influence beer flavour. Beer is then filtered to achieve a clear final product (haze is perceived as a negative product trait), and stabilising agents are added to ensure prolonged beer clarity until consumption. Chill-haze is a well-known undesirable phenomenon during which beer develops opacity when chilled prior to drinking, as a result of the protein/polyphenol content in the beverage. Speciality chemicals remove such compounds, ensuring that beer remains attractive to the consumer; it is then ready to be sealed into cans, kegs or bottles for distribution and sale.

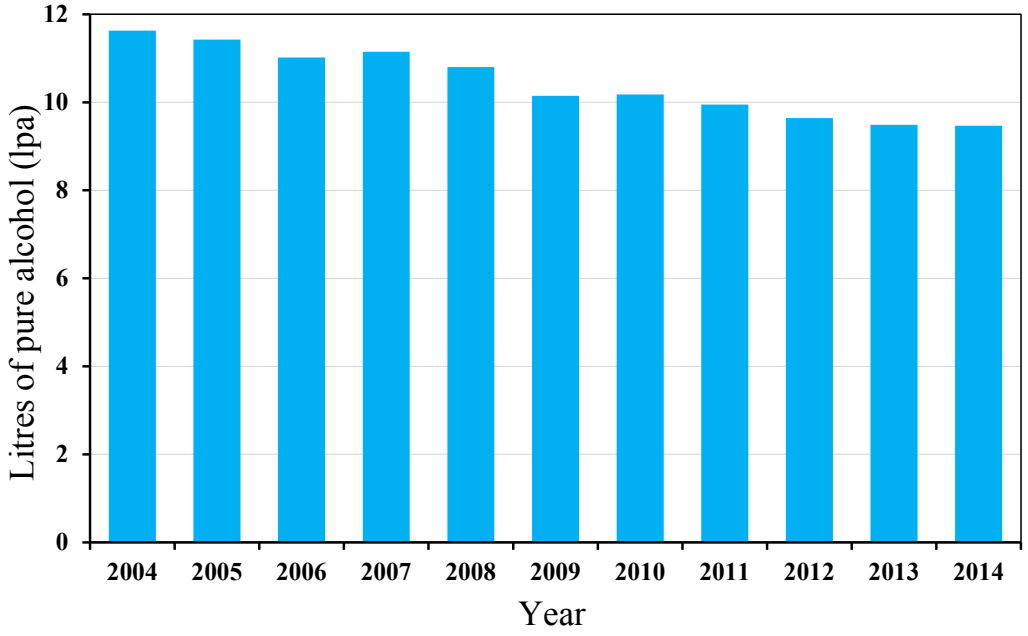

Figure 3.7: UK alcohol consumption per capita. (van de Walle, 2015).

3.2.2 Motivation

An investigation into the beer manufacturing industry in the UK has been performed to determine if a strong incentive for process intensification and optimisation exists. The alcohol industry as a whole has been in decline in recent years within the UK as shown in Fig. 3.7, where annual litres of pure alcohol per capita is the metric used to normalise for beverages of differing alcoholic strength. This a result of several factors: people are drinking from a later age and regular drinkers are turning away from high strength products, towards more costly and lower strength drinks, such as craft beer. Beer is however one of the few exceptions from the trend of a declining sector. The growing market share fuelled by recent increased demand for high value craft beer products produced on a small scale has led to the beer industry growing both in terms of production volume and market value. 1% year on year growth is predicted over the next 3 years, with the annual production volume in the UK expected to exceed 4.6 billion litres by 2019, compared to 4.2 billion in 2015. Fig. 3.8 shows the number of breweries in operation over the last 6 years in the UK: it is evident that there is very steady increase which is predicted to continue moving forward.

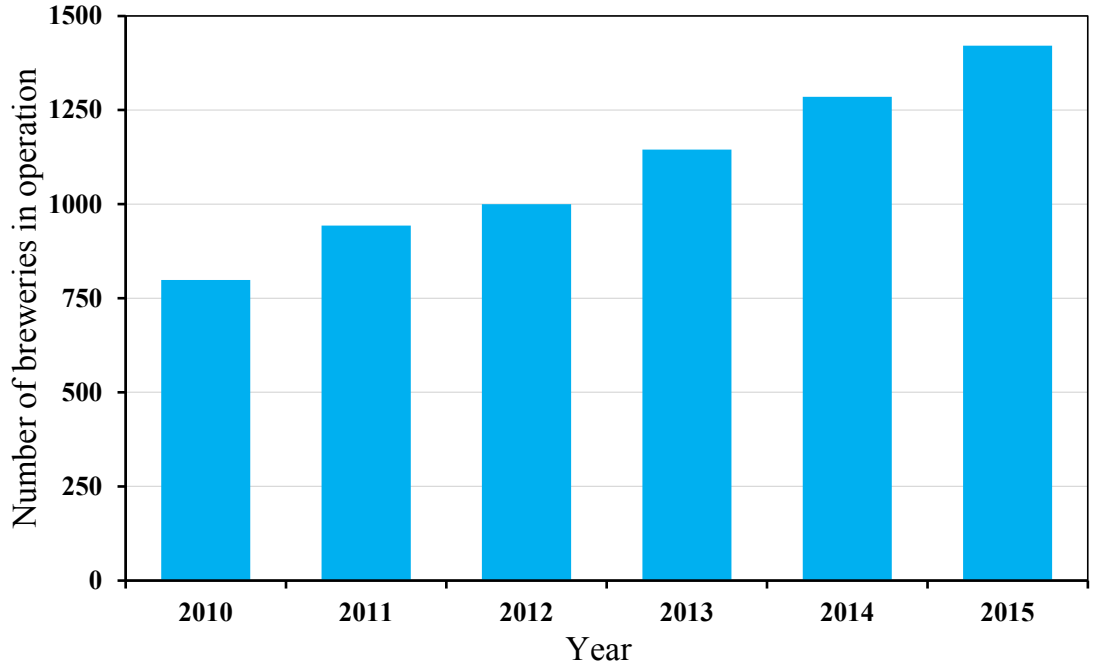

Figure 3.8: Number of UK breweries in operation (van de Walle, 2015).

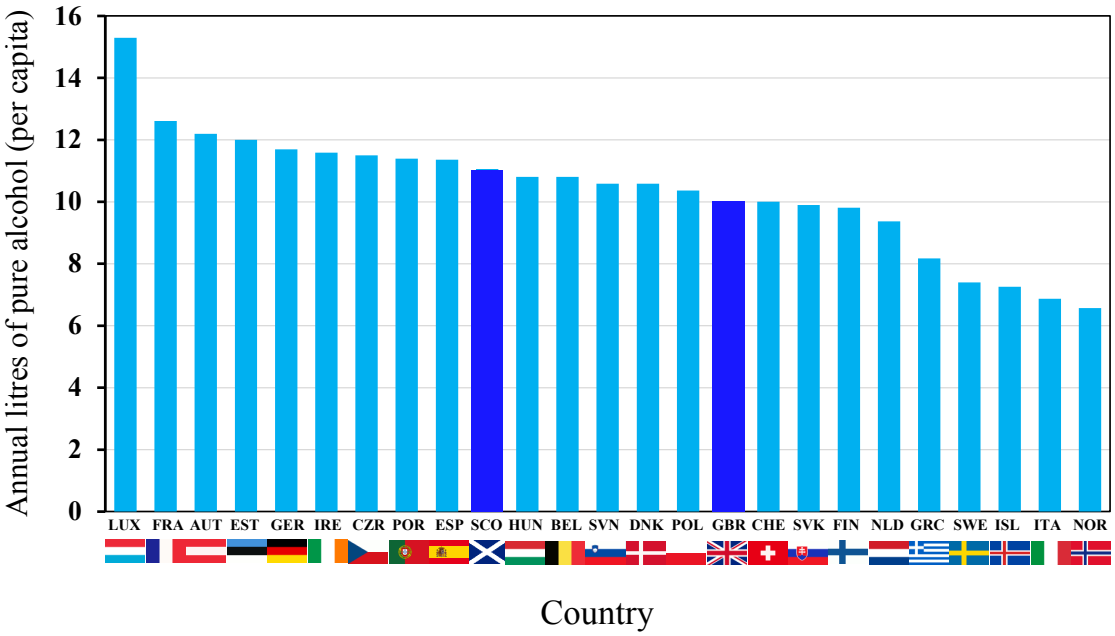

Figure 3.9: Alcohol consumption by country (van de Walle, 2015).

Fig. 3.9 depicts the UK's alcohol consumption in context of the rest of Europe. While Scots may have a reputation of being heavy drinkers it is evident that while their per capita consumption is above the average for the rest of the UK, it is still a very typical value within Europe. The result of the declining alcohol industry and the surge in supply of beer products has created an extremely competitive environment for producers, many of whom must look towards process intensification if they are to remain profitable, forming the motivation for this study. Within the beer production process the fermentation stage is generally the system bottle neck (Lodolo et al., 2008), with batch times in excess of one week not uncommon. Fermentation progression depends on many variables (Engasser et al., 1981; Gee and Ramirez, 1988), however progression is dominated by the influence of the temperature of the involved substrates. As such, it is necessary to determine the temperature manipulation profile capable of steering the process to competition in an optimal manner.

3.2.3 Review of Published Models and Optimisation

Computational prediction and performance assessment of a biochemical process toward process optimisation requires a mathematical model representing species consumption/production, as well as cell growth and death. Given the complexity of the fermentation process, and the numerous (over 600) species present (Vanderhaegen et al., 2006), many chemical interactions are not quantitatively understood and the construction of a comprehensive dynamic process model is thus infeasible. Lumped-parameter dynamic fermentation models considering only the key chemical reaction pathways, using parameters computed from experimental campaign data. The extreme industrial importance of dynamic modelling for high-fidelity simulation and optimisation of fermentation processes is not confined to brewing only. Achieving high efficiency is vital in producing a wide array of therapeutic molecules (i.e. antibiotics), so process intensification is of enormous interest, particularly in the context of continuous pharmaceutical manufacturing (Engell and Toumi, 2005; Schaber et al., 2011).

3.2.3.1 Beer Fermentation Modelling

The earliest kinetic model of beer fermentation has been published by Engasser et al. (1981), based on fundamental biochemical pathways and the manner in which the evolution of alcohol and sugars depends on total biomass (yeast) concentration. Gee and Ramirez (1988) adapted this work to include temperature effects on rate expressions. The model includes three ordinary differential equations (ODEs) predicting consumption of glucose, maltose and maltotriose (assumed to be the limiting nutrients) via Monod kinetics. Gee and Ramirez (1994) also published a subsequent paper to extend the model and consider further compounds, while also incorporating a simple feedback inhibition mechanism on cell growth rate. The model considers a total of twelve species affecting product flavour, in addition to the five described in the original growth model (Gee and Ramirez, 1988), however new parameters are only stated for isothermal conditions. de Andrés-Toro et al. (1998) proposed an alternative kinetic model for beer production under industrial operating conditions. Unlike the model of Gee and Ramirez which is based on sugar uptake rate, this later model relies on predicting yeast evolution in order to subsequently compute chemical species production/consumption. Five responses are considered; ethanol, sugar, biomass and two flavour-contributing compounds (diacetyl and ethyl acetate). Here, the single sugar compound represents the sum of all sugars present in the wort. The suspended biomass within this model is distinguished into three distinct types; active, latent and dead cells. Latent (lag) cells cannot promote fermentation: over time, they are transformed into active cells, responsible for consumption of fermentable sugars. Active cells duplicate and grow over time, but a portion of them will die, settle and no longer contribute to fermentation. The fermentation process is distinguished into two observable phases; in the first (lag phase), the majority of biomass introduced comprises of latent yeast cells, so minimal fermentation takes place as latent cells undergo activation. Once approximately half of the suspended cells are activated, the second (fermentation phase) begins: therein, active cell concentration is sufficient to induce the enzymatic effect, converting the sugar substrate to ethanol product. An overview of the reaction scheme is given in Fig. 3.10a. Evolution of

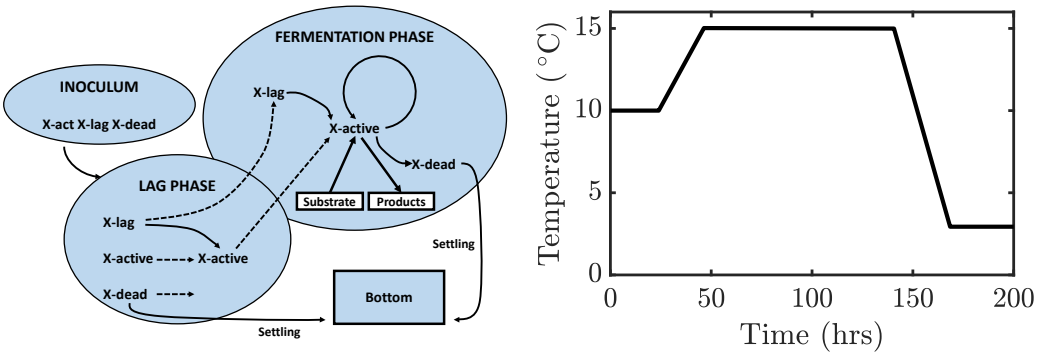

Figure 3.10: (a, left) Process scheme considered in the kinetic model; (b, right) Generic industrial temperature profile.

each cell type is predicted by the respective ODE, where growth rates are Arrhenius temperature functions of the corresponding species maximum growth rate. This allows the total suspended cell (lag, active and dead) population growth to be defined as the rate of active cell growth minus the rate of dead cells settling. Sugar consumption is related to active biomass concentration with its own growth rate: ethanol production is predicted similarly, but with an inhibition factor used to account for its decreasing production rate with time. Ethyl acetate production is related to sugar consumption with a stoichiometric factor as in the Gee and Ramirez (1994), which however includes explicit temperature dependence. Diacetyl growth modelling is more elaborate: the respective ODE includes two terms, one accounting for its production early in the fermentation process and another representing its consumption toward partial conversion to 2,3-butanediol during fermentation progression.

The seven ODEs of the model depend on 10 parameters which vary with temperature and have been modelled using Arrhenius relationships and parameter values estimated from experimental data. Isothermal fermentations have been carried out in a lab-scale 3 L vessel at 5 different temperatures in order to obtain online measurements of species concentrations. Following model parameter estimation, the authors performed a non-isothermal fermentation in a pilot plant-scale 100 L tank using a generic industrial temperature profile (Fig. 3.10b). Published profile predictions are in good agreement with the pilot-plant experimental data; the validated model has been successful in predicting process

behaviour in a variety of operating conditions and in completing relevant optimisation studies. Moreover, it has undergone further experimental validation, on the basis of over 200 fermentation campaigns carried out over a period of three years (de Andrés-Toro et al., 2004). Trelea et al. (2001) developed fermentation models based on CO_2 production, using real-time CO_2 concentration data obtained with commercially available sensors (Corrieu et al., 2000). This is deemed an appropriate basis for a fermentation model, as it has been validated to represent a reliable indicator of ethanol and yeast production and sugar consumption (Stassi et al., 1987). Three dynamic models to predict CO_2 production are considered based on varying knowledge of the underlying biochemical phenomena (Trelea et al., 2001). The first model is a neutral network (black box) and is purely statistical, based on experimental data and computed parameters which are not representative of any physical property. The second (empirical) model is based on a posteriori analysis of the form of the experimental profiles recorded: parameter selection and definition occurs after observing the shapes of these curves, however they have little biological significance. Finally, the third (knowledge-based) model is developed in order to represent the true kinetic pathways, producing a complex model formulation which is challenging to validate structurally as well as computationally.

3.2.3.2 Prior Work

Numerous authors have used the de Andrés-Toro (1998) beer fermentation model for optimal control studies seeking a suitable temperature profile for operation. Authors have proposed different optimisation strategies with unique objective functions, publishing the fermentation temperature profile they have determined as most favourable. Carrillo-Ureta et al. (2001) used an evolutionary algorithm in order to determine such an optimal profile; the procedure is based on the natural selection principal, employing historical simulations to predict new conditions toward achieving greater performance. Their objective function considers the final concentration of ethanol as well as both flavour-degrading species diacetyl and ethyl acetate), and penalises high temperature gradients in the temperature

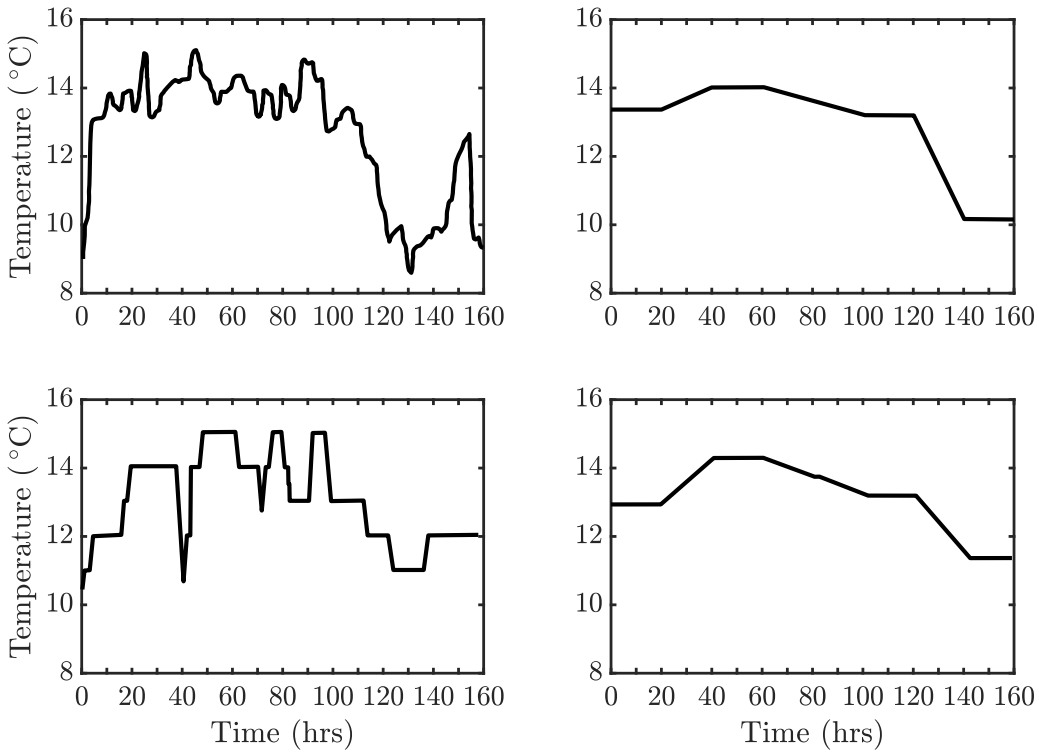

Figure 3.11: Optimal temperature profiles: Carrillo-Ureta et al., (2001): (a) as determined, (b) smoothed; Xiao et al., (2004): (c) as determined, (d) smoothed.

profile, which are undesirable due to operational adjustment limitations related to cooling jacket maximum capacity and operability. The evolutionary algorithm has successfully generated the same profile maximising the objective function irrespective of the initial profile considered, showing that a global optimum has been reached. However, the solution profile produced (Fig. 3.11a) is highly variable (temperature to be manipulated up and down sporadically), despite the gradient penalty within the objective function, hence impractical for industrial use. By averaging the original profile over 40-hour intervals, the authors produced a manipulation protocol which is more suitable for industrial implementation (Fig. 3.11b). Genetic algorithms constitute a powerful stochastic methodology which is successfully used for multi-objective optimisation of numerous biological processes (Lee et al., 2007; Singh et al., 2009; Taras and Woinaroschy, 2011). Xiao et al. (2004) also used the de Andrés-Toro model to compute their own optimal temperature profile. The authors developed a stochastic (ant colony system) algorithm to arrive at the optimal solution: this powerful heuristic tool can be used

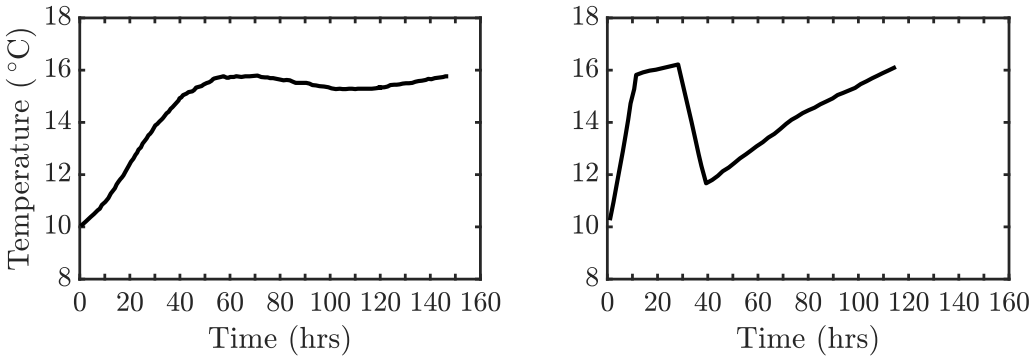

Figure 3.12: De Andrés-Toro et al. (2004) optimal temperature profiles: (a) improved control, (b) minimum time.

to determine the most suitable path through a graph, based on the behaviour of actual ant colonies. The algorithm relies on moving randomly across the domain, determining the value of the objective function continuously. This data (representing the pheromone which ants leave) gives an indication of how desirable a path decision has been, thus rendering subsequent passes less random and more closely following the most desirable historical routes. The procedure is carried out iteratively until paths through the domain converge on the optimal solution, the equivalent of an ant colony having found the quickest route to a food source. The objective function in this work resembles one used previously (Carrillo-Ureta et al., 2001) but without considering batch time minimisation, as the optimisation procedure requires the target domain, and thus time to simulate fermentation, to be a priori defined. The profile produced (Fig. 3.11c) is prohibitively varying for industrial application, so a similar averaging procedure has been used to generate a smoothed form of the optimal manipulation (Fig. 3.11d).

de Andrés-Toro et al. (2004) also performed multi-objective optimisation using the original kinetic model. An evolutionary algorithm (similar to that of Carrillo-Ureta et al., 2001) is used, where each gene can represent a variable time interval between discrete temperature points. The objective function used considers eight goals: three high-priority targets are treated as system constraints, ensuring ethanol concentration is above (while diacetyl and ethyl acetate concentrations are below) specified levels. The five lower-priority targets consider contamination risk (bacterial formation at high temperature), temperature pro-

file smoothness, batch time as well as instantaneous heat flow and heat flow smoothness. The last two aspects are used to improve process control (prior work has not considered implications of temperature and heat flow profiles on coolant demand). Assigning different weights to the respective targets within the objective function yields different temperature profiles which address unique goals: this strategy can thus achieve (a) improved process control as a result of improved heat smoothness (Fig. 3.12a), and (b) reduce total batch fermentation time (Fig. 3.12b).

More recently, Bosse and Griewank (2014) have used the kinetic model to generate optimal control profiles using a sweeping dynamic optimisation methodology (Radwan and Griewank, 2011). The process involves guessing a control path and using this to integrate the states forward in time. This allows the costates to be integrated backwards through the process time span: a new control profile is thus deduced by maximising the Hamiltonian for all $t \in [t_0, t_f]$, and the process is repeated until path convergence is attained. The authors were able to compute a more preferable temperature profile using the same objective, compared to a prior stochastic approach (de Andrés-Toro et al., 1997).

3.3 Chapter Conclusions

Two drastically different biochemical processes have been identified for an extensive simulation and dynamic optimisation study, to explore scope for viable process improvement, within this thesis.

Beer fermentation is an extremely established and widespread industrial bioprocess, having been performed globally for thousands of years. Despite this current operation is often far from optimal, and market conditions mean that operators currently seek any means to reduce operating costs and improve plant throughput. Optimising the fermentor temperature control profile is identified as a potentially favourable route to achieve this, to relax the existing bottleneck without the requirement for plant modification or any significant capitol investment.

Enzymatic keratin hydrolysis on the other hand is an extremely novel emerging technology. At present the process has only been performed on a lab-scale, with little knowledge of the precise underlying reaction mechanisms. As this new strategy for waste treatment appears environmentally favourable over existing approaches, it is highly desirable to develop the technology to determine whether it has potential for economic viability. In order to perform computational simulations and attempt to dynamically optimise the system the construction and validation of a simplified model for the hydrolysis process on the basis of experimental data is first necessary.

Part II

Parameter Estimation & Dynamic Simulation

Chapter 4

Parameter Estimation & Sensitivity Analysis for Beer Fermentation Modelling

The accuracy of all model based computational optimisation relies upon a high fidelity parametrisation of the model. Where model parameters cannot be directly measured a regression is commonly performed. The discrepancy between model predictions and process data is minimised by estimation of the unknown parameters, an optimisation problem in its self. Herein it is often assumed that the best fit (least squares error) corresponds to the most accurate values of all the parameters under estimation in the regression. To ensure model robustness and to explore the importance of estimating a uniquely identifiable parameter set, in contrast to only ensuring least squares minimisation, the parameter estimation problem for beer fermentation modelling is considered.

4.1 Fermentation Model

Several mathematical models for the beer fermentation process have been proposed (Engasser et al., 1981; Gee and Ramirez, 1988; de Andrés-Toro et al., 1998; Trelea et al., 2001). Models are lumped parameter, considering only the key species of the several hundred present (Vanderhaegen et al., 2006), due to sys-

tem complexity rendering exhaustive modelling extremely cumbersome: in fact to date many of the specific chemical interactions in the fermentation process are not understood. The kinetic model of beer fermentation by Gee and Ramirez (1988) is used here: the model considers the uptake of three sugars, namely glucose (G), maltose, (M) and maltotriose (M_r), as functions of the total biomass concentration (X):

$$\frac{dG}{dt} = -\mu_G \cdot X(t) \tag{4.1}$$

$$\frac{dM}{dt} = -\mu_M \cdot X(t) \tag{4.2}$$

$$\frac{dM_r}{dt} = -\mu_N \cdot X(t) \tag{4.3}$$

The foregoing ordinary differential equations (ODEs) have consumption rates (μ_i) defined with Monod-type kinetics with inhibition effects on higher sugars:

$$\mu_G = \frac{V_G(T) \cdot G(t)}{K_G(T) + G(t)} \tag{4.4}$$

$$\mu_M = \frac{V_M(T) \cdot M(t)}{K_M(T) + M(t)} \cdot \frac{K'_G(T)}{K'_G(T) + G(t)} \tag{4.5}$$

$$\mu_N = \frac{V_N(T) \cdot M_r(t)}{K_N(T) + M_r(t)} \cdot \frac{K'_G(T)}{K'_G(T) + G(t)} \cdot \frac{K'_M(T)}{K'_M(T) + M(t)} \tag{4.6}$$

Where V_i is the maximum reaction velocity for sugar i, K_i is the Michaelis constant for sugar i, and K'_i is an inhibition constant for sugar i. The rates of biomass (X) and ethanol (E) production are proportionally related to the uptakes of the individual sugars by constant yield coefficients determined from stoichiometry:

$$\frac{dE}{dt} = R_{E_G} \cdot \frac{dG}{dt} + R_{E_M} \cdot \frac{dM}{dt} + R_{E_N} \cdot \frac{dM_r}{dt} \tag{4.7}$$

$$\frac{dX}{dt} = R_{X_G} \cdot \frac{dG}{dt} + R_{X_M} \cdot \frac{dM}{dt} + R_{X_N} \cdot \frac{dM_r}{dt} \tag{4.8}$$

Where R_{i_j} is the ratio of j consumption to i production. The fermentation model comprises of eight unknown model parameters, summarised in Table 4.1.

Table 4.1: Beer fermentation model parameters for determination.

Symbol	Description	Units
V_G	Maximum reaction velocity for glucose	h^{-1}
V_M	Maximum reaction velocity for maltose	h^{-1}
V_N	Maximum reaction velocity for maltotriose	h^{-1}
K_G	Maximum reaction velocity for maltotriose	mol m^{-3}
K_M	Michaelis constant for maltose	mol m^{-3}
K_N	Michaelis constant for maltotriose	mol m^{-3}
$K_G^{'}$	Inhibition constant for glucose	mol m^{-3}
$K_M^{'}$	Inhibition constant for maltose	mol m^{-3}

4.2 Global Parameter Estimation (all-at-once)

An experimental campaign has been performed by Gee and Ramirez (1988), where the authors monitored the concentrations of the three sugar species over time during an isothermal batch fermentation by HPLC. This was carried out repeatedly over a range of feasible temperatures for effective fermentation, resulting in four distinct data sets at $T = [4, 8, 12, 16]$ °C. The batches were fermented in 100 L non-agitated conical fermentors using *S. carlsbergensis*. Despite the lack of external mixing, the CO_2 generation acts to keep the vessel contents well mixed. The lumped parameter model relies upon a CSTR approximation of the system, found to be not too far from reality, even on pilot plant and small-industrial scale. The parameter estimation problem is defined to determine the values of the eight unknown parameters by minimising the discrepancy between the experimental data set and the model state trajectories. Physical boundaries act as lower parameter non-negativity constraints, and upper limits can be proposed from literature and related fermentation processes, giving a finite span in which the parameter value must lie. Several different objective functions may be used as the minimisation criteria. A sum squared error objective is often used, however this will prove bias in favour of matching states of greater absolute magnitude. It can make more sense to divide the discrepancy at each data point by the mean state value, to normalise the significance of matching the individual states. Alternatively, a chi-squared objective may be used given that sufficient data quality exists to determine standard deviations. For any objective function used the resulting

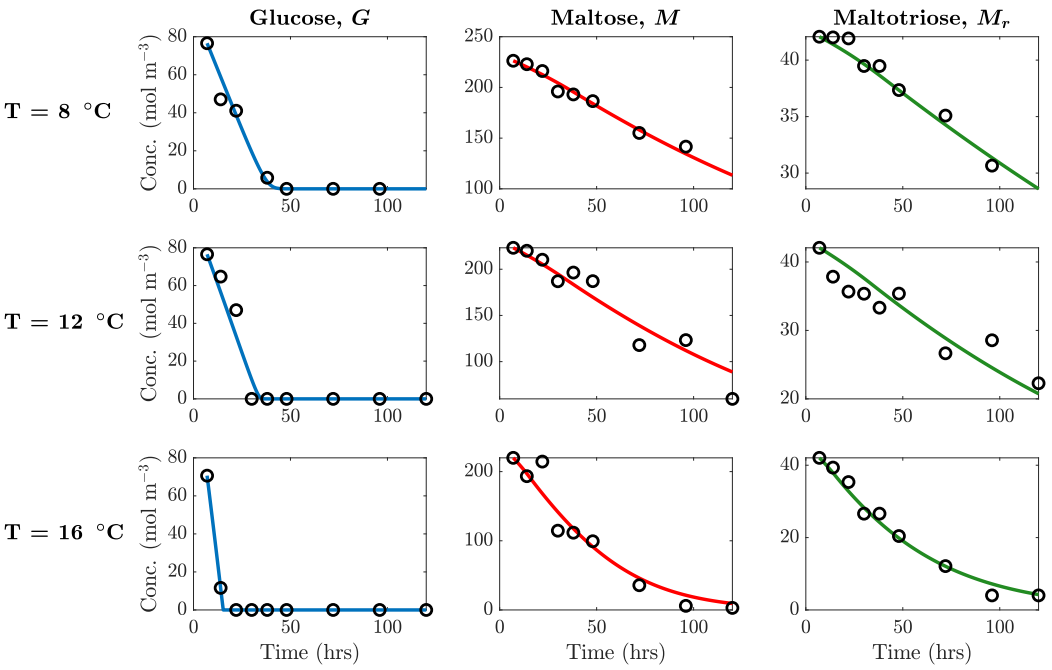

Figure 4.1: Model fit to experimental data: all at once parameter estimation.

problem optimisation problem is non-convex, being well established that kinetic parameter estimation problems can be extremely challenging to solve to global optimality. A method has been developed which utilizes a branch and bound algorithm to guarantee global optimality (Singer et al., 2006). This is particularly useful because if the global solution to the parameter estimation problem still does not fit the data suitably, the model structure can be confidently dismissed. In this work a standard local method is implemented so we can visualize the effect of multi-start initialisation which can highlight some properties about the problem (Martí et al., 2016). Given the resolution of the available data set, the sum squared error minimisation approach is considered in this work, normalizing the fit at each data point by the mean state value over the time span, where the objective is defined by Eq. 4.9.

$$min \sum_i \sum_j \left[\frac{(data - model)}{(\bar{data}_i)} \right]^2 \tag{4.9}$$

Starting from 1000 points (initial parameter guesses) via Latin-Hypercube sampling (McKay et al., 1979; Stein, 1987) of the input space, the parameter estimation problem has been solved for each instance using IPOPT (Wächter and

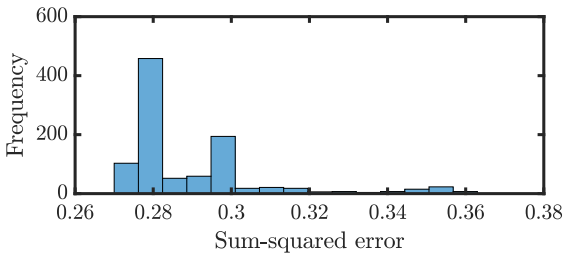

Figure 4.2: Multi-start objective distribution.

Biegler, 2006) via OPTI's MATLAB® implementation (Currie et al., 2012). Taking the parameter set from the 1000 result sets computed which obtains the lowest value of Eq. 4.9, we can plot the approximation of the globally optimal fit, shown in Fig. 4.1 for three of the temperatures considered in the experimental campaign. Visually the model fit appears excellent, however consideration must be given to how appropriate this method is for determining the actual parameter values. Considering the different objective values obtained from the 1000 unique start points, it can be shown how consistently the best solutions are obtained (Fig. 4.2). Under 10% of cases are realizing the minimum value of the sum squared error objective, with a high number of local solutions being produced.

The distributions of the parameter values can be inspected (Fig. 4.3), showing large ranges for most parameters. This is a result of local solution attainment, as well as cases where approximately the same objective value is produced with significantly different parameter sets. This is a result of an ill conditioned problem where model parameters are highly correlated and thus cannot be uniquely estimated simultaneously: the are not uniquely identifiable. This results from the fact that Monod-like models are found to have growth yield parameters which are significantly correlated with the maximum growth rate terms (Sin et al., 2009). It is thus necessary to consider which parameters have the most significant bearing in the model state trajectories, and which less influential ones may be assigned directly from literature to avoid co-dependence issues in the parameter estimation problem. The parameter co-dependence can be confirmed by looking at the covariance matrix (Table 4.2). When the absolute value of the correlation for a parameter pair is greater than ~0.95 it may not be possible to estimate the 2 parameters uniquely using the available regression data, as changing the parameter

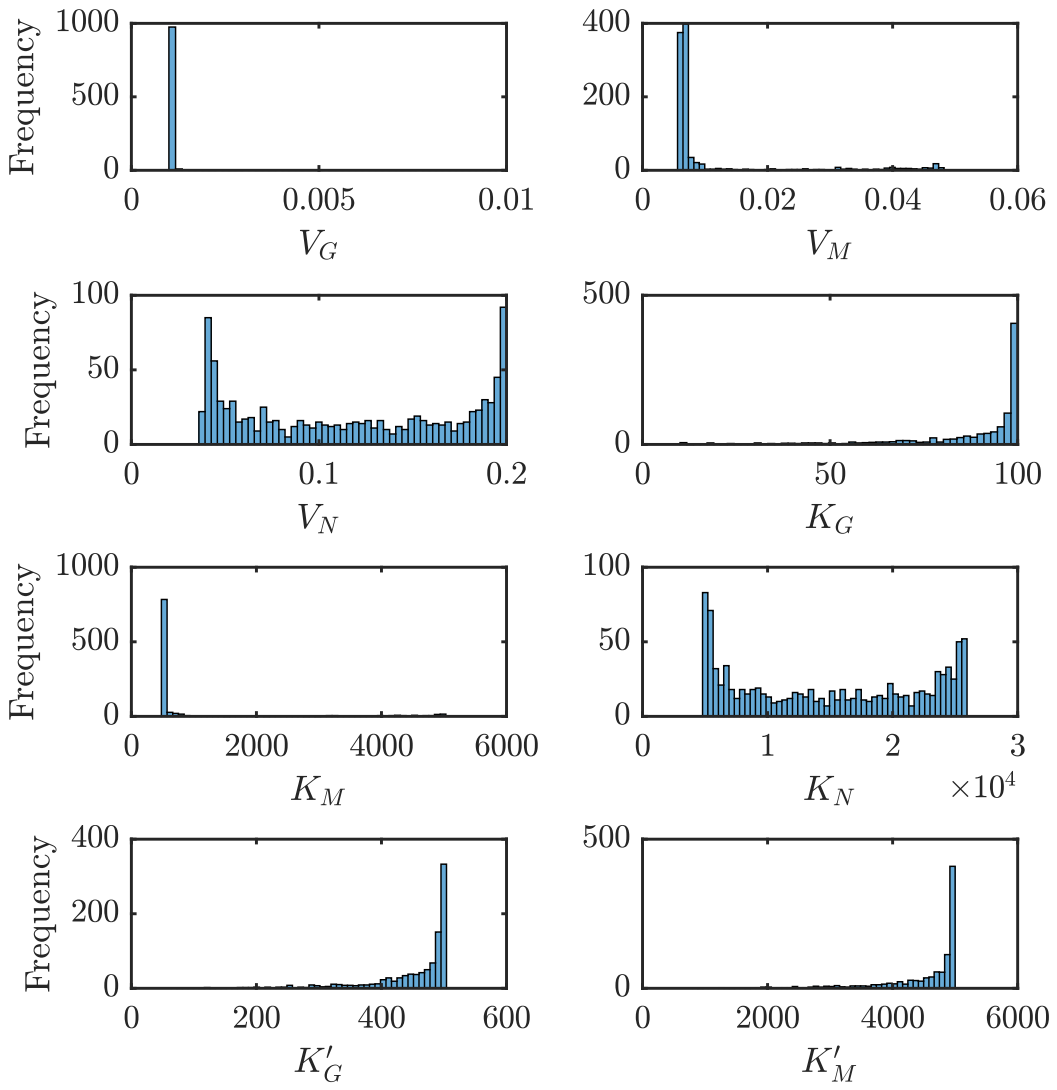

Figure 4.3: Multi-start parameter distribution.

values in a coordinated manner may produce very similar model results.

4.3 Sensitivity Analysis

As it is not effective to directly estimate the entire parameter vector, it is desirable to inspect how the parameters influence the model states: to perform a rigorous sensitivity analysis. A range of methods for sensitivity analysis have been developed and published in the engineering literature, reviewed by Sin et al. (2009). Local methods can perturb parameters around nominal or base values to observe the effect on model outputs. These are generally easy to implement and take little time to solve, however are non explorative due to their local nature,

Table 4.2: Parameter covariance matrix.

	K_G	K_M	K_N	$K_G^{'}$	$K_M^{'}$	V_G	V_M	V_N
K_G	1.000	-0.004	0.185	0.971	-0.004	0.185	-0.001	-0.185
K_M		1.000	-0.124	0.004	1.000	-0.124	-0.942	0.127
K_N			1.000	0.144	-0.123	1.000	0.167	-1.000
$K_G^{'}$				1.000	0.004	0.144	-0.006	-0.144
$K_M^{'}$					1.000	-0.123	-0.940	0.125
V_G						1.000	0.167	-1.000
V_M							1.000	-0.170
V_N								1.000

meaning key effects can be missed. Global methods in contrast can give a fuller picture but are much costlier for implementing.

4.3.1 One-at-a-time (OAAT) Perturbation

To visualise the relative impact and importance of the 8 model parameters one-at-a-time (OAAT) perturbations have been performed given three perturbation sizes, 10, 20 and 50%, with both positive and negative perturbations considered. Nominal values from which perturbations are performed are taken from Gee and Ramirez (1988), with the 4 °C reaction conditions presented in this instance. Figure 4.4 depicts the resultant effect of these parameter perturbations on the total species consumption over the entire reaction duration, with the terminal ($t = t_f$) concentrations under 10% perturbations stated in Table 4.3. Red bars correspond to the effect of negative perturbations, with blue bars the same for the positive permutations. A positive blue bar thus highlights a positive perturbation having a positive effect, with a negative blue bar representing the positive perturbation resulting in a decrease in the species' consumption. The three columns in the figure represent the three perturbation sizes, with the 5 rows showing the effect on the five model states one by one. It is observed that the effect sizes scale with the perturbation sizes in all cases, seen by comparing the figure rows. The relative parameter effects remain unchanged, with all effects scaling with the increase in perturbation size. It can be noted that the maximum effect size is approximately equal to the perturbation size in all cases, suggesting a near linear dependence of each model state on a specific model parameter in each case.

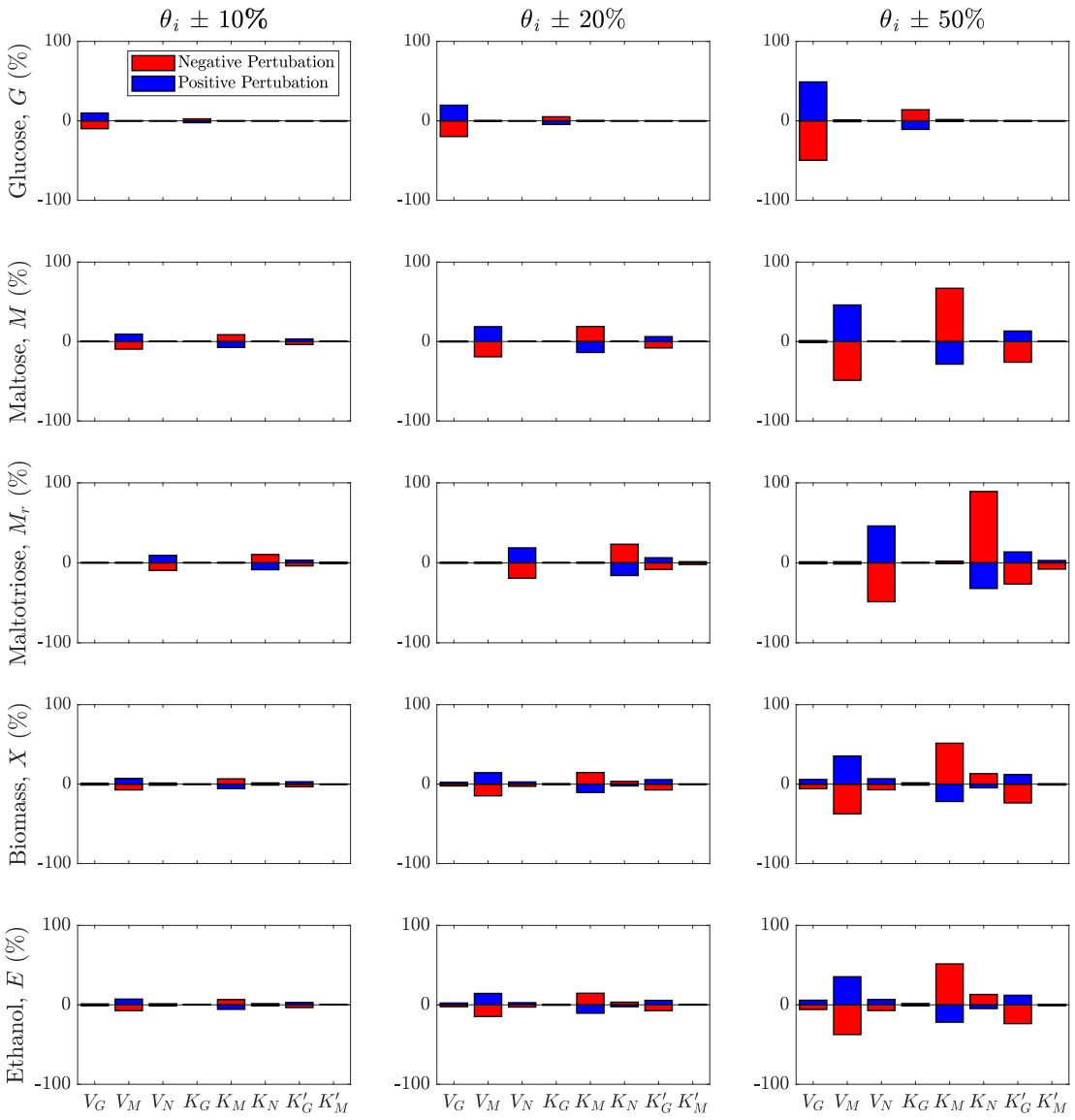

Figure 4.4: OAAT parameter perturbation effects.

Table 4.3: Terminal state concentrations (mol m^3): OAAT perturbations.

Species	t_f (θ_0)	$\theta_i \pm 10\%$	V_G	V_M	V_N	K_G	K_M	K_N	$K_G^{'}$	$K_M^{'}$
Glucose, G	67.36	(+10%):	68.27	67.38	67.37	67.13	67.34	67.36	67.37	67.36
		(−10%):	63.45	67.34	67.36	67.58	67.38	67.37	67.35	67.36
Maltose, M	189.60	(+10%):	189.69	193.10	189.62	198.58	186.42	189.59	190.98	189.60
		(−10%):	37.46	186.14	189.62	189.62	192.31	189.62	188.39	189.60
Maltotriose, M_r	37.45	(+10%):	37.44	37.47	37.89	37.45	37.44	36.97	37.63	37.50
		(−10%):	218.41	34.44	37.02	37.46	37.46	37.85	37.30	37.42
Biomass, X	218.56	(+10%):	218.72	217.62	218.38	218.60	219.43	218.76	218.12	218.55
		(−10%):	182.92	219.5	218.74	218.53	217.83	218.40	218.95	218.58
Ethanol, E	185.10	(+10%):	182.92	171.54	182.51	185.65	197.43	187.93	178.76	184.84
		(−10%):	187.27	198.5	187.66	184.58	174.60	182.75	190.66	185.31

It is shown for the three sugars that the maximum reaction velocity parameter has a very large and positively correlated effect on the sugar consumption, with a smaller and negative trend shown for the Michaelis-Menten constants. Given the structure of the model, it is demonstrated that the effects on ethanol and biomass are identical, as there are both defined as ratios of the different sugars consumption rates. Here the relative effect of the parameters is influenced by the relative initial concentrations of these sugars, with the Maltose parameters having the largest influence on biomass and ethanol trajectories as a result of being the most abundant species in the feed.

4.3.2 Morris Screening

A more useful method for model sensitivity analysis, developed by Morris (1991), takes favourable properties of both local and global methods – local sensitivities are computed, but with sampling to approximate global effects, to give greater insight when compared to strictly OAAT local perturbations only, described previously. The model inputs (parameters) are each equally discretised into p bands between their lower and upper bounds. A random nominal parameter set, θ^0, is then selected from the finite number of values each discretised input can take, and the model is evaluated by numerical integration. Subsequently a single input variable is perturbed by a fixed fraction of the input space, Δ, and the model is revaluated, allowing the elementary effect, EE_i, of that parameter on a function of the model output to be computed as defined by Eqs. 4.10–4.13 for a generic ODE model.

$$\frac{dx}{dt} = f(x, \theta, u, t) \tag{4.10}$$

$$x(t = 0) = x_0 \tag{4.11}$$

$$y = g(x, \theta, u, t) \tag{4.12}$$

$$EE_i^0 = \frac{y(\theta_1^0, \theta_2^0, \ldots, \theta_i^0 + \Delta, \ldots \theta_m^0) - y(\theta^0)}{\Delta} \tag{4.13}$$

The input vector is then updated with a perturbation to an additional parameter, differing from OAAT perturbation in that the prior perturbation is retained

Table 4.4: Uncertainty sets for Morris screening.

Uncertainty Set	V_G	V_M	V_N	K_G	K_M	K_N	$K_G^{'}$	$K_M^{'}$
High	0.5	0.5	0.5	0.5	0.5	0.5	0.5	0.5
Low	0.05	0.05	0.05	0.05	0.05	0.05	0.05	0.05
Assigned	0.05	0.05	0.25	0.05	0.5	0.05	0.25	0.25

in the updated vector, and the elementary effect is computed once more. This is repeated until each parameter has been perturbed in turn, essentially generating a single random trajectory through the input space from which a single EE of each parameter is determined. This is repeated from alternative random start points in the input space r times to produce r trajectories through the input space. In doing so r elementary effects of each parameter are efficiently samples across the input space such that the local measure is sampled globally. The Morris method requires $r \cdot (n+1)$ model evaluations, where n is the number of inputs/parameters. This is in contrast to p^n model evaluations which would be required to exhaustively map the parameter sensitivities given the same discretisation for fractional factorial design. For example when $n = 8$, $p = 8$ and $r = 15$, the Morris method performs $15 \cdot (8+1) = 450$ model simulations compared to $8^8 = 1.7{\times}10^7$ simulations for fractional factorial design.

To define parameter ranges across which the sensitivities are sampled, nominal values for each parameter are assigned as those from Gee and Ramirez (1988). The lower and upper values considered are defined by the range between the nominal value ± a factor describing the parameter 'expert uncertainty' which we consider in three discreet bands: 0.05 = low, 0.25 = moderate and 0.5 = high. In this study three different cases are considered to observe the impact the 'expert uncertainty', and thus the sample range, has on the ranking of elementary effects:

- Uniform high uncertainty across the entire parameter set
- Uniform low uncertainty across the entire parameter set
- Arbitrarily assigned uncertainty across the entire parameter set

This is performed for 50 samples with 8 parameter levels in each case, with the range of resultant 450 state trajectories shown in Fig. 4.5 corresponding to the $T = 4$ °C case with assigned uncertainty (Table 4.4).

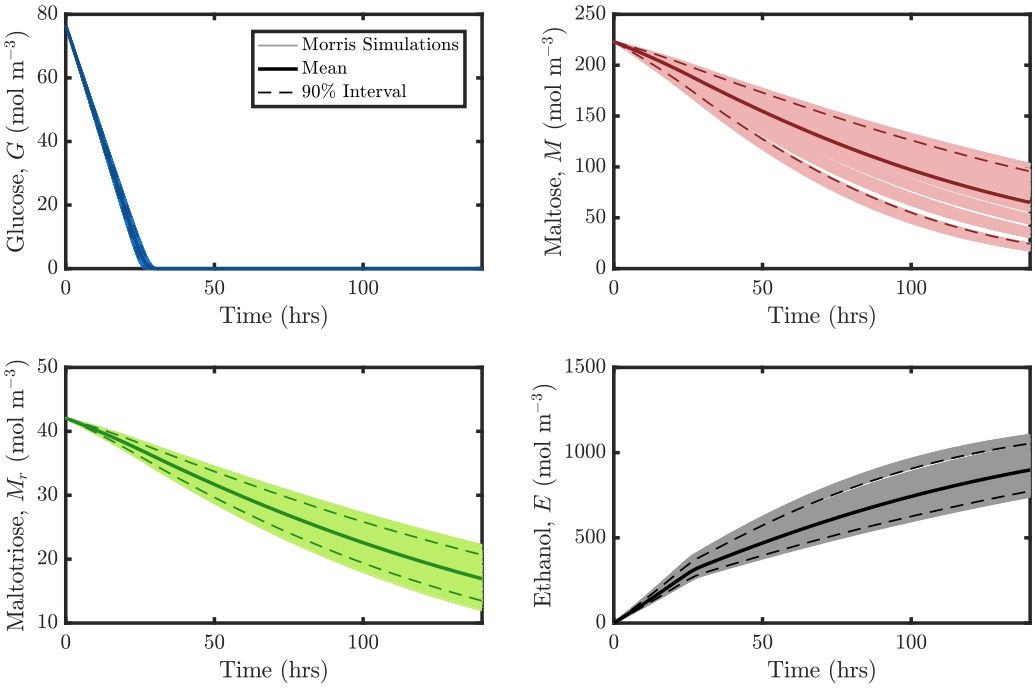

Figure 4.5: Morris model simulations where samples $(r) = 50$, parameter bands $(p) = 8$ and perturbation factor $(\Delta) = 4/7$.

It is demonstrated that glucose shows minimal trajectory variation compared to the other states, as a result of the fewest parameters having influence on this model ODE. Additionally, trajectory banding is clearly observed in the maltose plot due to discrete number of parameter levels considered. It should be noted that ethanol and biomass are affected by all parameters in the same way, as a direct consequence of the ODE model considering both as linear functions of sugar uptake, such that both states are affected in the exact same way by all parameters and the elementary effect is thus always identical. Each histogram in Fig. 4.6 shows the distribution elementary effects of parameter i, EE_i, (Eq. 4.13) on glucose, with Figs. 4.7, 4.8 and 4.9 showing the same for maltose, maltotriose and ethanol respectively. In all figures the 3 columns correspond to the 3 sets of parameter uncertainties defined in Table 4.4. These histograms allows the mean EE as well as the standard deviation to be visualised, acting as useful metrics for determining which parameters are most strongly correlated with the state trajectories of interest. The first two columns of histograms represent the elementary effect distributions with the parameter uncertainty considered to

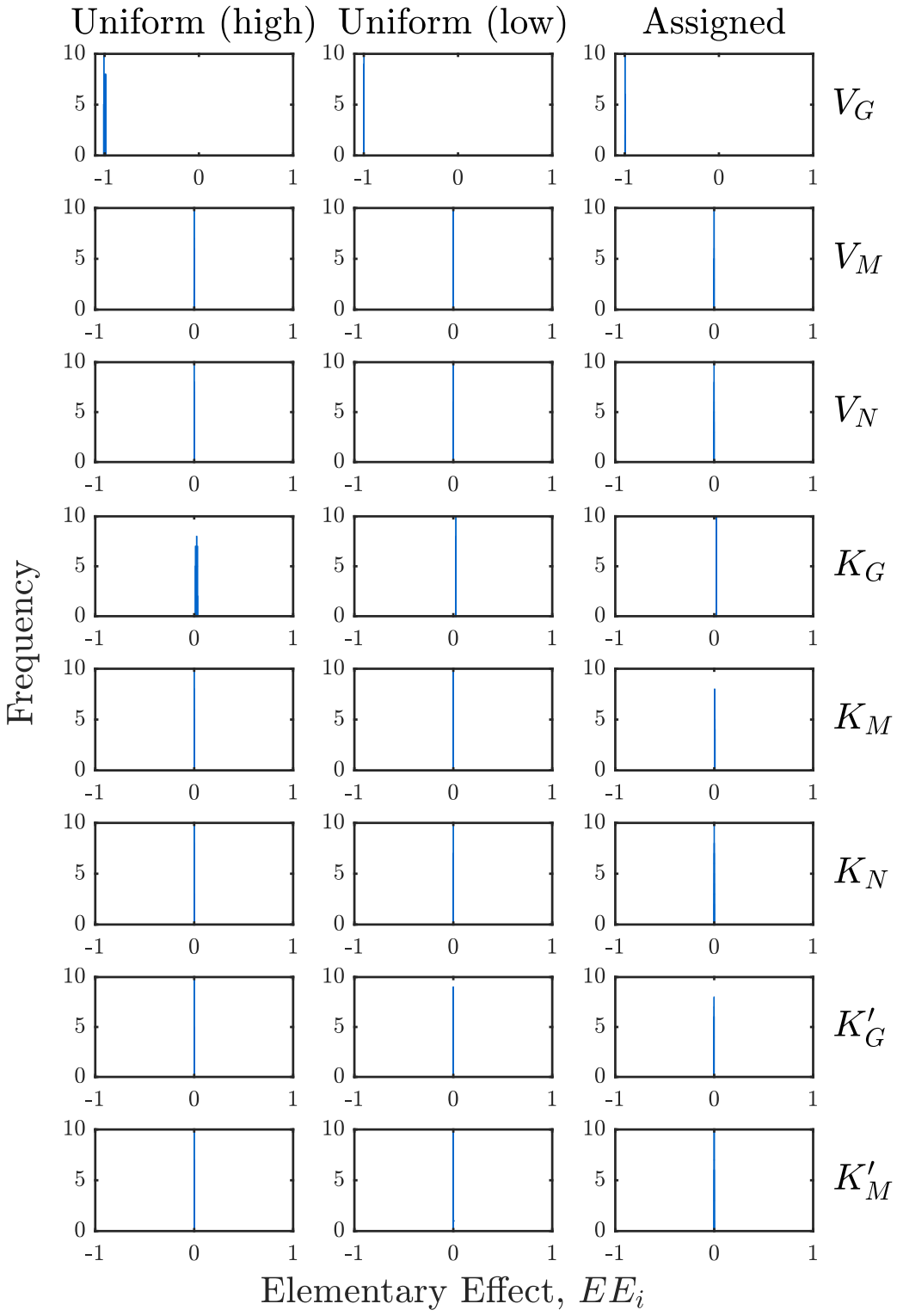

Figure 4.6: Morris screening elementary effects of each parameter on glucose.

be uniformly high and low respectively. In the final column 3 four parameters are assigned low uncertainty, three moderate, with only K_M defined as having a high uncertainty (Table 4.4). The EE's on glucose (Fig. 4.6) are conclusive, with the maximum reaction velocity for glucose uptake, V_G, shown to be the only significant parameter value to predict this specific model state, regardless of the associated parameter uncertainty being assigned. Here V_G shows a linear negative correlation (EE = -1), with all other parameters having essentially no effect (full frequency of EE at 0). This could be inferred directly form the model structure where only this single parameter is directly proportional to the model ODE. Comparing the low and high uncertainty parameter set Morris histograms for EE on maltose, maltotriose and ethanol shows how the uncertainty magnitudes influence the EEs. Between the two cases (column 1 and 2 in these plots) the mean EE is not changed significantly when increasing uncertainty fivefold, however, the standard deviation is much greater when uncertainty is high. Both sets of results show V_G, V_M and K_M to have the greatest EE. This is in contrast to the final case considered, where K_M significantly outshone the others in terms of mean EE and suggested relative importance. This is a result of the greatest concentration of maltose (M) being present, causing the parameters associated with its consumption having the greatest effect on absolute model trajectories. In this scenario it is suggested that V_N, V_M and $K_G^{'}$ have a moderate effect on these states, with a small positive correlation shown in all three cases. These are all of little significance compared to the very large negative correlation shown for K_M. This would suggest that K_M has considerably stronger bearing in the trajectory of ethanol, however consideration must be given to whether it makes sense to have a priori defined this parameter to have at least twice the uncertainty to all other parameters. This highlights the importance of accurately defining the expert uncertainty in model parameters before applying the sensitivity analysis method, or if such expert knowledge is missing a reasonable analysis can be made by defining all uncertainties as equivalent.

A full set of 8 histograms for any single uncertainty set can be summarised with σ versus μ plots (Fig. 4.10). The 8 histograms from Fig. 4.9 map into the plot in the bottom right of Fig. 4.10, with the other 3 panels showing the

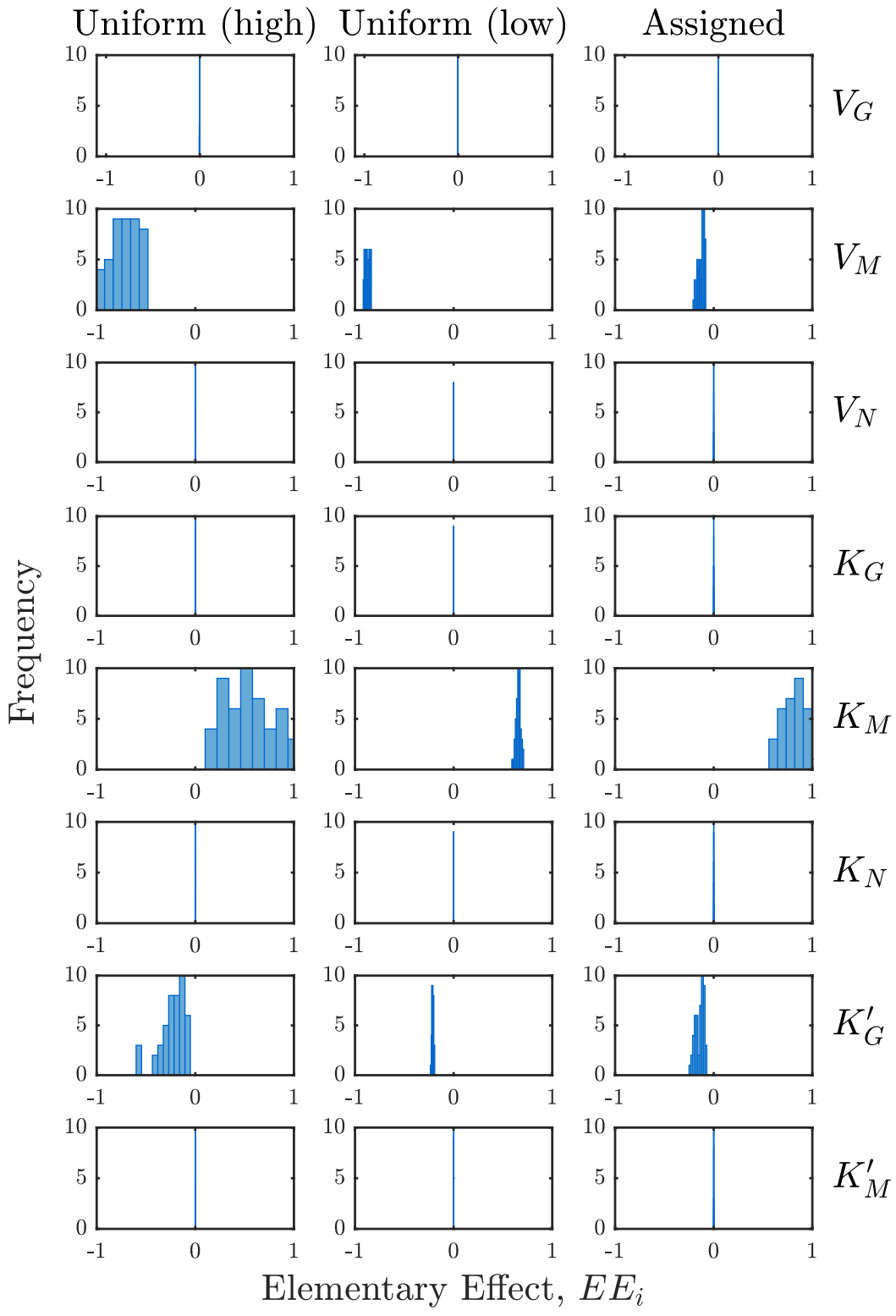

Figure 4.7: Morris screening elementary effects of each parameter on maltose.

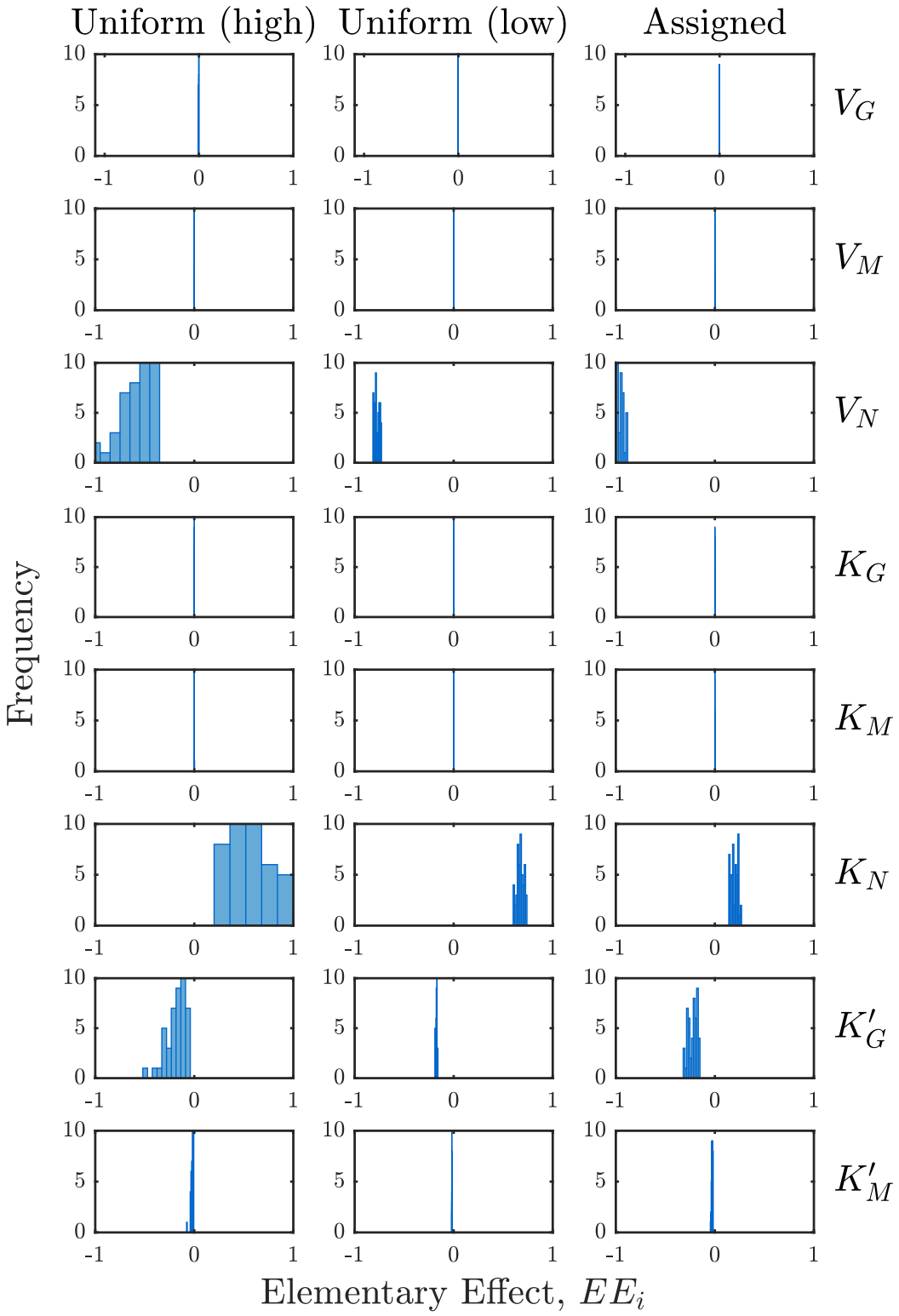

Figure 4.8: Morris screening elementary effects of each parameter on maltotriose.

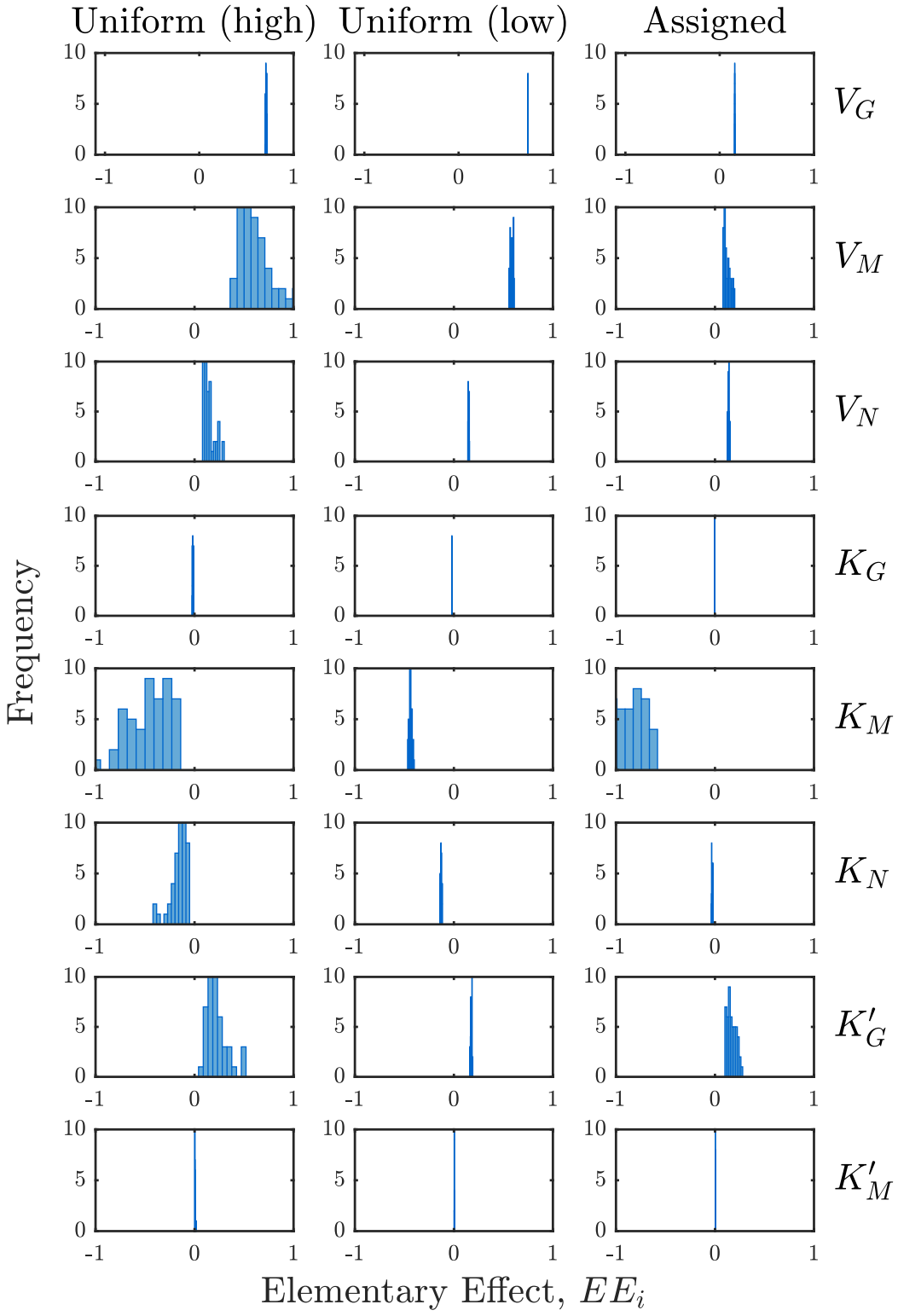

Figure 4.9: Morris screening elementary effects of each parameter on ethanol.

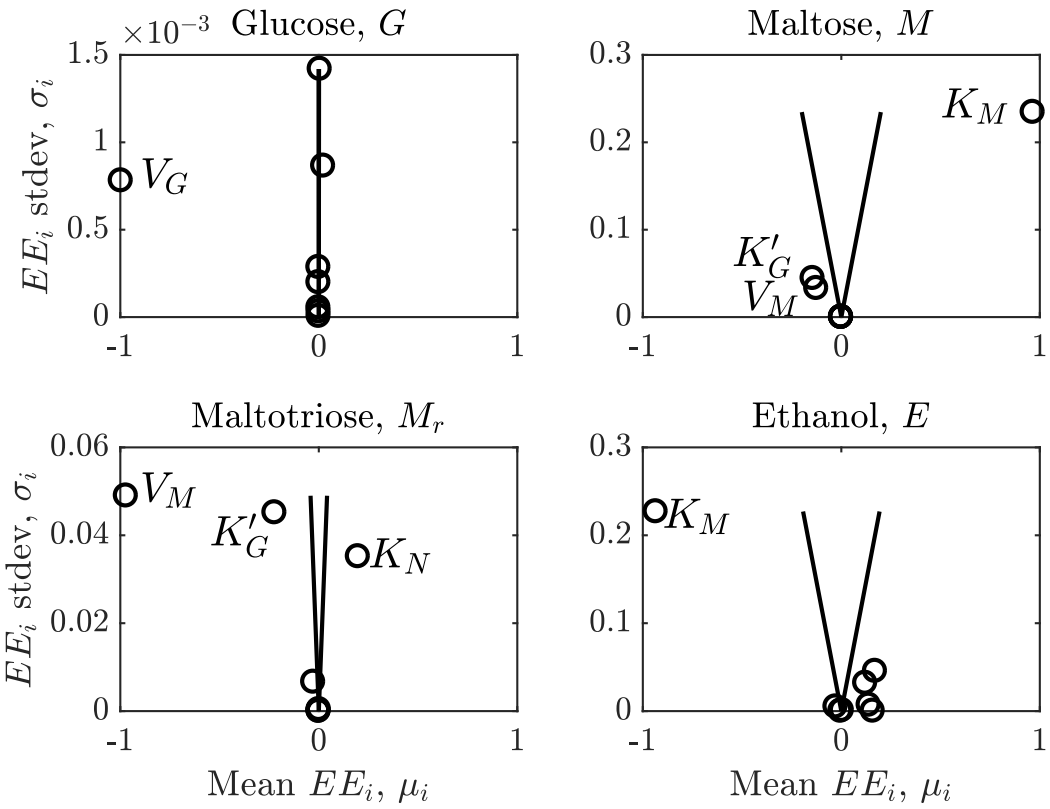

Figure 4.10: Morris mean EEs and standard deviation distribution.

equivalent for the sugar states. The solid lines represent the estimated standard error of the mean, such that if the parameter (circle) lies within the bands it is deemed to have a negligible effect on the state.

The significance of each parameter on each state according to the absolute mean elementary effect can be ranked, highlighting which are the most influential and this most important for accurate estimation (Table 4.5). The table shows that only a single parameter, V_G, is significantly influential on glucose, which could be inferred from the model directly (Eqs 4.1 - 4.8. More insightful is the ranking of the parameter significance on the other states, highlighting that the inhibition constants ($K_i^{'}$) and maximum reaction velocities (V_i) have much more significance than the Michaelis constants (K_i). As ethanol and biomass are linearly related in the model structure, the dimensionless parameter elementary effects for these two states are identical. Given the small size of the fermentation model, many of the outcomes of this investigation could be inferred by simply inspecting the ODE of each model state. It is often apparent when a parameter

Table 4.5: Elementary effect ranking on each model state.

Rank	Glucose, G		Maltose, M		Maltotriose, M_r		Biomass, X	
	θ	μ_{EE}	θ	μ_{EE}	θ	μ_{EE}	θ	μ_{EE}
1	V_G	-1.000	K_M	0.954	V_N	-0.935	K_M	-0.923
2	K_G	0.021	$K_G^{'}$	-0.144	$K_G^{'}$	-0.217	$K_G^{'}$	0.171
3	K_M	0.006	V_M	-0.117	K_N	0.193	V_G	0.150
4	$K_G^{'}$	-0.001	V_G	-0.001	$K_M^{'}$	-0.027	V_N	0.133
5	V_N	-0.001	V_N	0.000	V_G	0.001	V_M	0.114
6	V_M	-0.001	K_N	0.000	V_G	-0.001	K_N	-0.028
7	K_N	0.000	K_G	0.000	V_M	0.000	$K_M^{'}$	0.004
8	$K_M^{'}$	0.000	$K_M^{'}$	0.000	K_G	0.000	K_G	-0.003

value is essentially proportional to the effect it will have on the model state, or when it is highly correlated with an additional model parameter, meaning such analysis can potentially be omitted, or at least accelerated in such cases.

4.3.3 Differential Sensitivity Analysis

First-order derivative model outputs (states) can be taken with respect to model inputs (parameters) to assess their relative effect (Brun et al., 2002):

$$s_{i,j}(t) = \frac{\partial y_j(t)}{\partial \theta_i} \tag{4.14}$$

Where $s_{i,j}$ is the dynamic sensitivity function of parameter θ_i on model state y_j. This allows visualisation of the time dependent sensitivities of model states to each parameter, shown in Figure 4.11. It is shown that the maximum glucose uptake rate, V_G, is initially instrumental on both Glucose and Ethanol, falling to 0 once the glucose is consumed. For maltose and maltotriose it is evident that the maximum reaction velocity has a negative correlation, while the Michaelis constant has a positive correlation of similar magnitude. This is indicative of the highly correlated nature of these two parameters with regard to the state trajectory. The mean squared summary of these profiles, $\delta_{i,j}^{msqr}$, can be used as a means to quantitatively compare and rank the effect of each parameter on each model state (Fig. 4.11), determined by Eq. 4.15 where the model has been evaluated at n discrete time points. The parameters which dictate the sugars evolution are unsurprising, but interestingly the effect of the inhibition constants

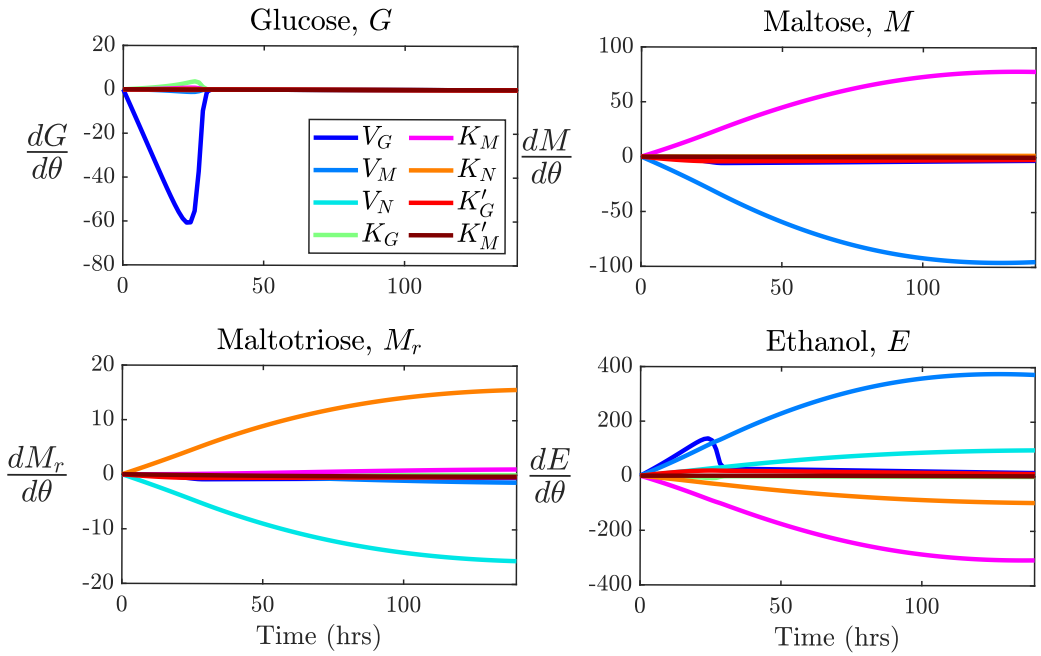

Figure 4.11: Dimensionless sensitivity functions with respect to each parameter.

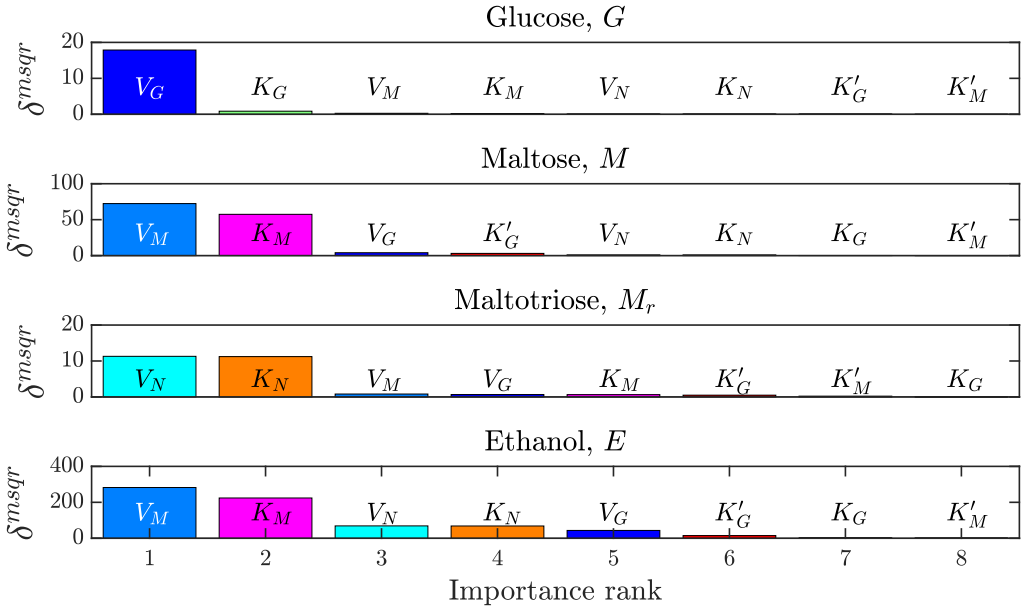

Figure 4.12: Mean squared summary of time series sensitivity function ranks.

are never among the most influential. It is shown how five parameters have significant bearing on Ethanol model predictions. There is a high level of similarity between the results from Morris screening and from differential sensitivity analysis, however a noteworthy difference is that the inhibition constant from glucose is not flagged up here as important, while it was from Morris screening, highlighting the importance of considering multiple strategies for sensitivity analysis to elucidate the key influential model parameters.

$$\delta_{i,j}^{msqr} = \sqrt{\frac{1}{n}\sum s_{i,j}^2(t)} \tag{4.15}$$

4.4 Estimation of a More-Readily Identifiable Parameter Subset

As the most influential model parameters have been identified it is desirable to solve the parameter estimation problem again, focusing specifically on the key parameters while taking those less important from suitable literature sources. To do this we must ensure that the parameter set taken forward for estimation is not ill-conditioned, and that linearly correlated parameters are not considered in the problem. A useful way to do this is to consider the collinearity index (γ_K): a measure of how aligned the sensitivity functions are between pairs of model parameters. With 8 parameters there are 247 subsets which could be estimated, ranging from all pairwise combinations, to the final set where all 8 are estimated. This latter case is as performed initially (Fig 4.2), showing poor solution attainment due to the very large collinearity index. Of the 247 sets, a range of low γ_K cases are presented in Table 4.6.

Typically the set with the most parameters and lowest index should be taken for estimation. However, it has been identified that neither sensitivity analysis method found the maltose inhibition parameter, $K_M^{'}$, to be impactful, so there is little benefit in including this in the estimation. Of those remaining several appear suitable, with subset number 197 selected to estimate the 5 corresponding parameters. This subset incorporates the most influential parameters, while

Table 4.6: Collinearity index for parameter subset examples.

Subset	Components							γ_K
9	V_M	K_G						1.3
79	K_G	K_N	$K_G^{'}$					2.4
151	V_G	V_M	V_N	$K_G^{'}$				10.6
154	V_G	V_M	V_N	K_G				7.6
195	V_G	V_M	K_G	$K_G^{'}$	$K_M^{'}$			8.7
196	V_G	V_M	K_G	K_N	$K_M^{'}$			13.5
197	V_G	V_M	K_G	K_N	$K_G^{'}$			10.7
201	V_G	V_M	V_N	$K_M^{'}$	$K_N^{'}$			18.3
205	V_G	V_M	V_N	K_M	$K_G^{'}$			90.3
207	V_G	V_M	V_N	K_M	$K_M^{'}$			13.5
208	V_G	V_M	V_N	K_G	$K_G^{'}$			10.7
225	V_G	V_M	K_G	K_M	$K_G^{'}$	$K_M^{'}$		18.2
233	V_G	V_M	V_N	K_G	K_M	$K_M^{'}$		18.4
237	V_G	V_M	V_N	K_G	K_M	$K_G^{'}$		90.4
241	V_G	V_M	V_N	K_G	K_M	$K_G^{'}$	$K_M^{'}$	241.0

ensuring the most heavily correlated pairs are omitted. The values of the three parameters omitted from the estimation have been taken from Gee and Ramirez (1988), and the same equivalent multi-start parameter estimation problem has been repeated for the remaining five unknowns, again from 1000 randomly sampled initial guesses. The resultant parameter value distributions are shown in Figure 4.13, for the $T = 4$ °C data set. These results show extremely consistent parameter values are being obtained, regardless of the initialisation, due to *a priori* ensuring a well-conditioned problem is being solved. It can be seen that there is slight variation in the values of V_M and $K_G^{'}$, as a result of a local method being used, however this is a vast improvement versus estimating the entire set. The model fit is visually identicle to Fig. 4.1, thus is omitted to avoid repetition. Repeating the well-conditioned parameter estimation problem for each of the datasets allows for the temperature dependence of each key parameter to be determined: ensuring temperature dependent model parameters have been determined consistently is vital for ensuring the model may be used towards dynamic optimization of the fermentor temperature profile accurately. Sensitivity analysis and parameter estimation results using the Gee and Ramirez (1988) model have been presented within this chapter, demonstrating how SA methods can be

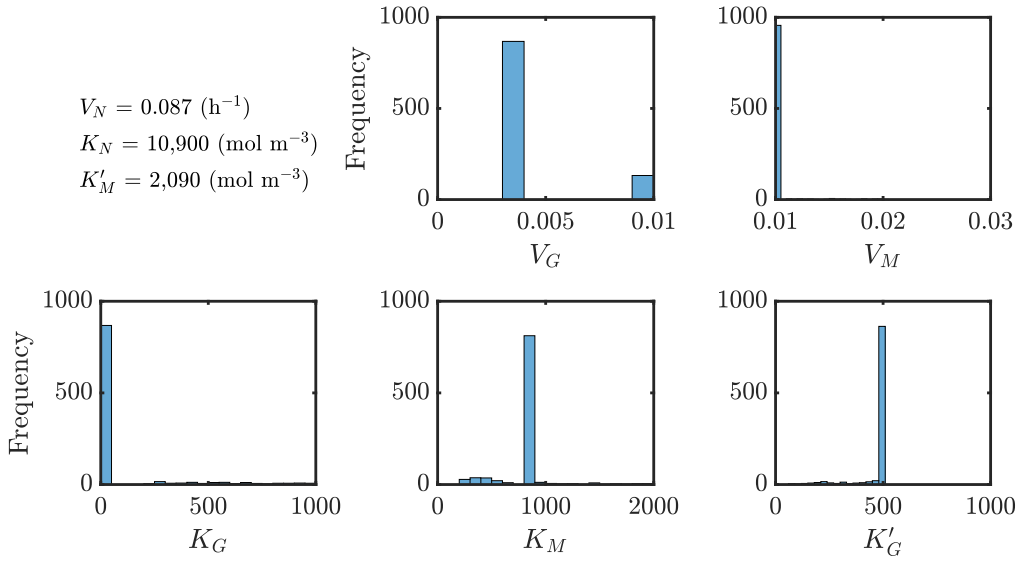

Figure 4.13: Multi-start parameter estimates for a non-correlated subset.

used to determine uncorrelated parameter subsets for effective estimation. This represents the most appropriate beer fermentation model for such an extensive investigation, on the basis that the only available fermentation data concerns the uptake of the three sugars, with no other state data monitored. The Gee and Ramirez model is the only published beer fermentation model which considers each sugar species independently, with other authors electing to use one bulk term as the summation of all sugars present. Much of the work in the later chapters of this thesis employ an alternative fermentation model from de Andrés-Toro et al. (1998), introduced in Chapter 7, which is favourable for process optimisation due to the inclusion of flavour degrading by-products. Unfortunately insufficient data availability prohibits performing a parameter estimation study for this later model, as the different cell types, by-products etc. are very cumbersome and costly to monitor and out with the scope of this work.

4.5 Chapter Conclusions

This thesis involves utilising lumped parameter fermentation models towards dynamically simulating and optimising the process. Doing so requires a high fidelity parametrisation of the model from experiential data, so it can accurately represent the real world process. It is demonstrated that attempting to estimate the

complete unknown parameter set results in an ill-conditioned problem and poor solution attainment. Systematic sensitivity analyses using two established methods is performed to assess and elucidate the relative significance of parametric discrepancy on the validity of dynamic simulation of the evolution of certain concentration observables. In doing so the parameters of least importance have been identified and removed from the regression by assigning appropriate values from literature. Doing so permits high fidelity estimation of the remaining more significant and influential parameters using an experimental data set. Accurate values for these model parameters are instrumental towards valuable dynamic optimisation efforts within the beer fermentation process.

Chapter 5

Experimental Methods, Sensitivity Analysis and Parameter Estimation for a Novel Hydrolysis Process

The enzymatic hydrolysis of keratin waste is an industrial process in its infancy. The specific hydrolysis mechanism is not well documented leading to limited industrial implementation. Therein lies a strong incentive towards developing a simplified lumped parameter model, to facilitate computational simulations and preliminary process optimisation. A simple multiplicative reaction model is used to describe consumption of the substrate, given that the underlying mechanism is still not precisely known to date.

5.1 Proposed Model for Keratin Hydrolysis

The following model is proposed for the enzymatic hydrolysis of keratin, based on the high level of similarity the process shared with the extensively studied depolymerisation process of cellulose into glucose, and the observed dynamics. The substrate is considered to consist of both hydrolysable, $[K]_H$, and non-readily

hydrolysable, $[K]_{NH}$, components (Eq. 5.1):

$$[K] = [K]_{NH} + [K]_H \tag{5.1}$$

The hydrolysable fraction, H, is defined by Eq. 5.2, representing keratins which the enzyme is able to digest.

$$[K]_H = H \cdot [K] \tag{5.2}$$

The consumption rate of the readily hydrolysable substrate, r, is considered as the product of three factors (Eq. 5.4).

$$\frac{d[K]_H}{dt} = -r \tag{5.3}$$

$$r = \varphi_1 \cdot \varphi_2 \cdot \varphi_3 \tag{5.4}$$

Firstly, the Michaelis–Menten expression, φ_1, describes the reaction kinetics (Eq. 5.5) as a function of two parameters. V_{max} is the maximum reaction velocity (as initial substrate mass tends to 0), while K_m is the Michaelis–Menten constant.

$$\varphi_1 = \frac{V_{max} \cdot [K]_H}{K_m + [K]_H} \tag{5.5}$$

Secondly, φ_2 defines the to the keratinase enzymatic activity, where e_i is the initial activity and k_D is a decay constant. This term differs from a conventional two parameter first order activity decay expression by the addition of residual activity (R_A).

$$\varphi_2 = [E] = e_i \cdot \exp(-k_D \cdot t) + R_A \tag{5.6}$$

This is a result of an enzyme cocktail being present in place of a single cell type, where components of the cocktail have drastically differing decay timescales at this reaction temperature. The residual activity represents the activity of the cells that do not notably decay within the hydrolysis timescale, which is visible from the activity in Figure 5.4 plateauing well above 0. Lastly, an inhibition term, φ_3, is considered as a function of the product concentration (Eq. 5.7), representing

Table 5.1: Keratin hydrolysis model parameters.

Parameter	Symbol	Units
Hydrolysable substrate fraction	H	-
Maximum reaction velocity	V_{max}	g L^{-1} hr^{-1}
Michaelis–Menten constant	K_m	g L^{-1}
Initial enzymatic activity	e_i	kU L^{-1}
Enzyme decay constant	k_D	hr^{-1}
Residual enzyme cocktail activity	R_A	kU L^{-1}
Product inhibition constant	K_I	g L^{-1}
Product ratio	f_r	-

the proteins being produced impeding the keratin-enzyme interaction.

$$\varphi_3 = \frac{K_I}{K_I + [P]} \tag{5.7}$$

A product ratio, f_r, relates protein production to substrate consumption, with the remainder of the consumed substrate mass consisting of released fats, lipids, peptides etc. All unknown model parameters are summarised in Table 5.1.

$$\frac{d[P]}{dt} = f_r \cdot r \tag{5.8}$$

5.2 Model Sensitivity Analysis

It can be highly useful to consider the model sensitivity to specific parameters, to better inform parametrisation and data acquisition experiments, as well as highlighting identifiability characteristics of correlated parameters. A range of methods and tools exist for doing so, as considered within Chapter 4.

The Morris method (1991) is applied to the proposed hydrolysis model, with the state trajectories shown in Figure 5.1. The method is defined by Eqs. 4.10–4.13 for a generic system model, and described in full in Section 4.3.2. The Morris method has been performed for the proposed hydrolysis model. For the keratin consumption the corresponding trajectories are shown in blue for each Morris simulation, where the discreet banding is a result of the finite values any given

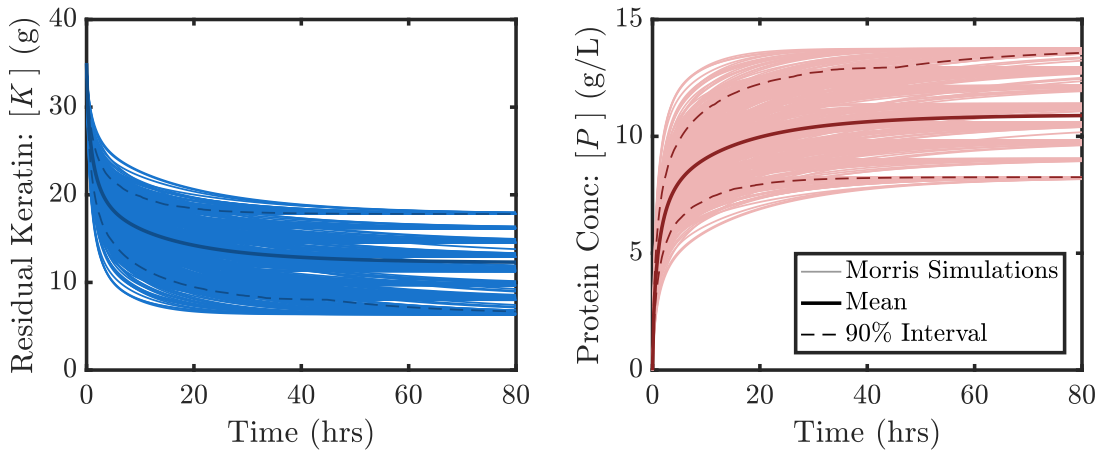

Figure 5.1: Morris simulation trajectories from the proposed model.

parameter can be assigned. Additionally, the wide range in terminal residual keratin clearly shows how at least some of the parameters do have instrumental effect on the model outputs. Similarly, the corresponding plots for protein production are shown in pink, however with this simple model structure the states are proportional to one another, and as such the elementary effects on these two states are also proportional. The parameters are ranked in Table 5.2 according to their absolute mean elementary effect, identifying four parameters as significantly contributing to the model state predictions. It is useful to plot the distributions of elementary effects of each parameter (Figure 5.2). The 8 plots allow visualisation of the mean and the distribution of the elementary effects from each parameter. Where the bars are tightly grouped and close to 0 EE, the parameter is said to have a minimal or negligible effect: the values of these parameters in the model are not very impactful. EE's far from 0 however are much more important: the parameter is said to have a significant elementary effect in these cases and therefore are essential for accurate estimation. For the proposed model it is demonstrated that four parameters appear to be highly influential: V_{max}, the maximum reaction velocity; e_i, the initial or maximum enzymatic activity; H, the fraction of the substrate readily hydrolysable and K_I, the inhibition constant. On the basis of this information the experiments to take place can be refined: it is desirable to directly measure the average value for H from hydrolysis experiments run to completion. It is also determined that the targeted experiments should be

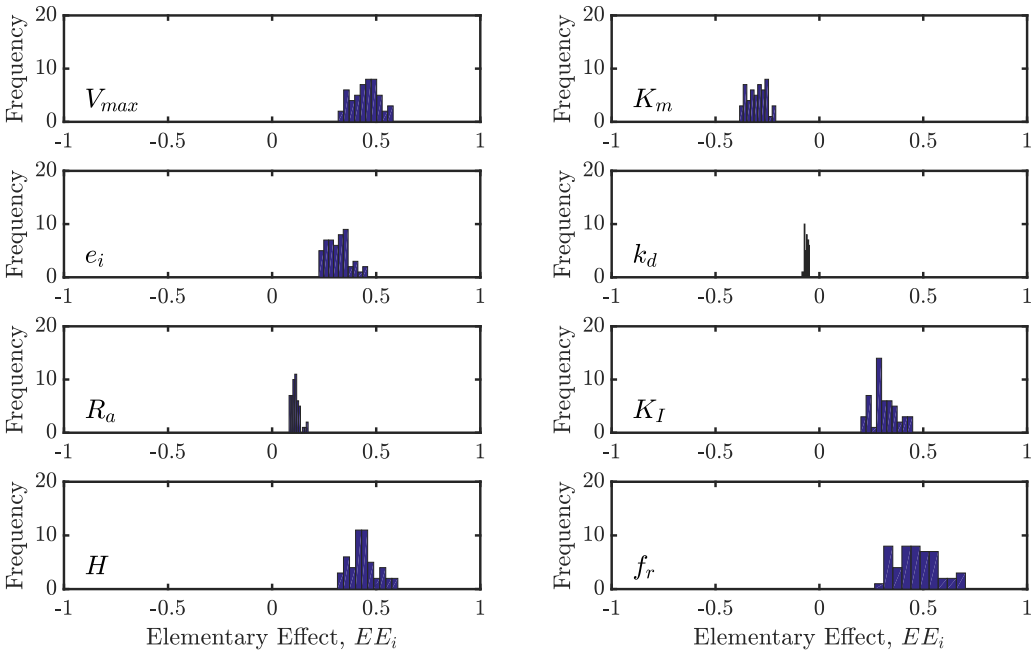

Figure 5.2: Keratin model elementary effect distribution.

Table 5.2: Model parameters ranked by absolute elementary effect.

Rank	θ	Description	μ_{EE_i}
1	V_{max}	Maximum reaction velocity	-0.57
2	H	Hydrolysable substrate fraction	0.53
3	e_i	Initial enzymatic activity	-0.44
4	K_I	Product inhibition constant	-0.44
5	R_A	Residual enzyme cocktail activity	0.10
6	f_r	Product ratio	-0.07
7	k_D	Enzyme decay constant	-0.04
8	K_m	Michaelis–Menten constant	0.03

performed to elucidate the enzymatic activity decay parameters for Eq. 5.6, including e_i. Performing the classical Lineweaver–Burk double inverse plot method (Lineweaver and Burk, 1934) for the Michaelis–Menten equation parameters (Eq. 5.5) then ensures that only one influential model parameter, K_I, remains in the sub-set to be fit from experimental state data.

5.3 Experimental Methods & Results

Collaboration with the Process and Systems Engineering Centre (PROSYS) at the Technical University of Denmark (DTU) was undertaken thanks to the gen-

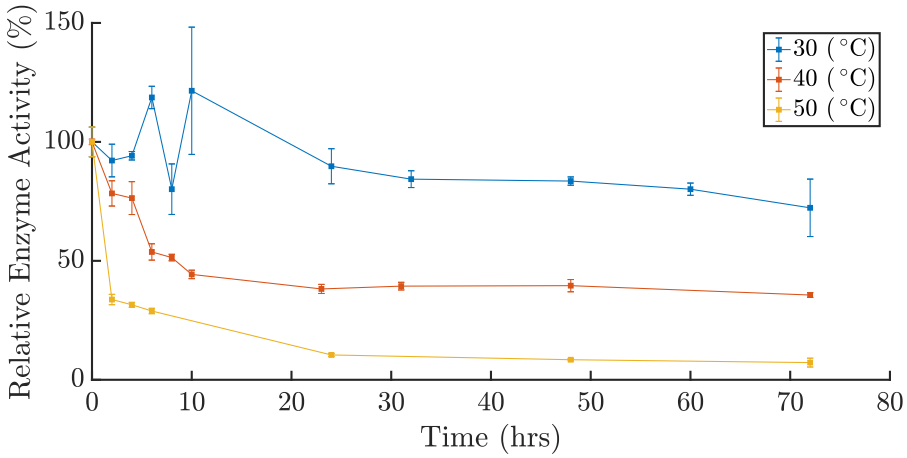

Figure 5.3: Enzymatic activity screening.

erous award of a Royal Society of Edinburgh (RSE) John Moyes Lessells Travel Scholarship. A lab scale experimental campaign has been performed towards parametrising the first kinetic model for this novel process. Significant work towards the characterisation of the particular bacterium involved has been performed the Gernaey group within PROSYS at DTU (i.e. Falco et al., 2019), whose assistance was instrumental in the experimental portion of this work. This was performed in collaboration with Hakan Ayyaldaz, who also presents a portion of the data obtained (Ayyaldaz, 2018).

5.3.1 Enzyme Preparation

Lab scale hydrolysis experiments have been performed using a keratinolytic enzymatic cocktail with the filamentous bacterium *Amycolatopsis keratiniphila D2* (DSM 44409), first reported by Al-Musallam et al. (2003). The bacterium was cultivated on mineral keratin medium with the following composition: 0.75 g L^{-1} NaCl, 1.75 g L^{-1} K_2HPO_4, 0.25 g L^{-1} $MgSO_4 \cdot 7H_2O$, 0.055 g L^{-1} Ca Cl_2, 0.010 g L^{-1} $FeSO_4 \cdot 7H_2O$, 0.005 g L^{-1} $ZnSO_4 \cdot 7H_2O$ and 1% w/w poultry by-product meal (PBM) keratin powder (Falco, 2018). The medium was sterilized at 121 °C for 20 minutes, with the free keratinase extract taken for the laboratory scale hydrolysis experiments presented in this thesis.

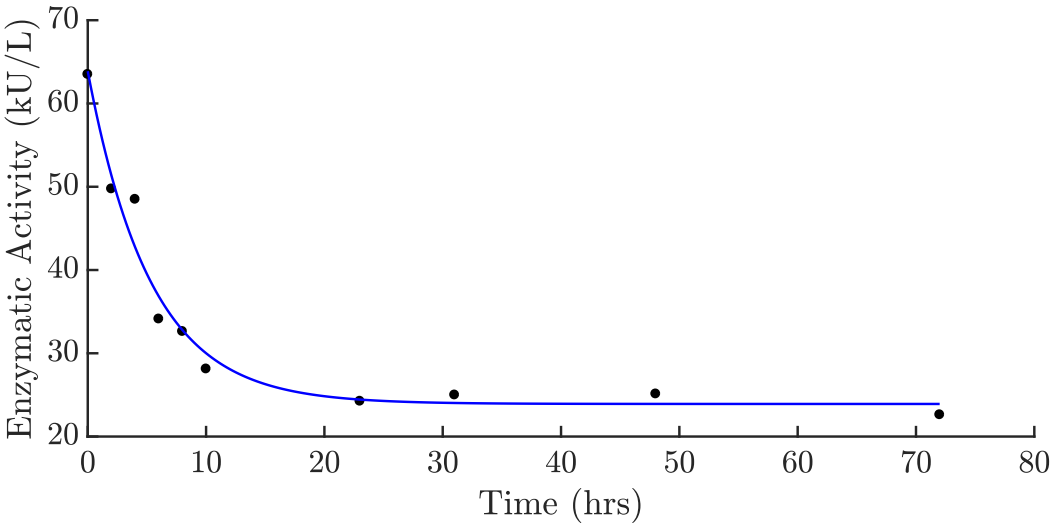

Figure 5.4: 40 °C enzyme activity decay and model fit.

5.3.2 Enzymatic Activity Screening

Prior work by the experimental group at DTU PROSYS characterised the effect of both temperature and pH on observed initial enzymatic activity (Falco, 2018). Optimal conditions were identified to maximise initial activity (T = 65 °C, Ph = 8), however it was demonstrated that at this temperature the enzyme is very rapidly denatured and unable to promote sustained hydrolysis. To screen for suitable reaction temperatures, enzymatic activity was monitored over the entire timespan required for hydrolysis, following isothermal incubation, by assaying with azokeratin as a substrate. A range of temperatures were screened: 30, 40 and 50 °C, where an inherent trade-off exists between increased initial activity and increasing activity decay rate (Fig. 5.3). It was found that at 40 °C the activity was suitably high and did not decay prohibitively quickly, and has thus been implemented as the experimental and model reaction temperature. The same keratinase activity profile at 40 °C can be seen in Figure 5.4, to which the parameters for Eq. 5.6 have been fit. It is shown that the activity falls to a level well above 0, with the enzyme still able to act after 72 hours. This observation can be explained by the fact the experiments are not performed with an isolated a single enzyme strain, rather are using the cocktail produced by the amycolatopsis bacterium. It is found that components of the cocktail have drastically differing decay timescales, and as such there is a fraction which does not

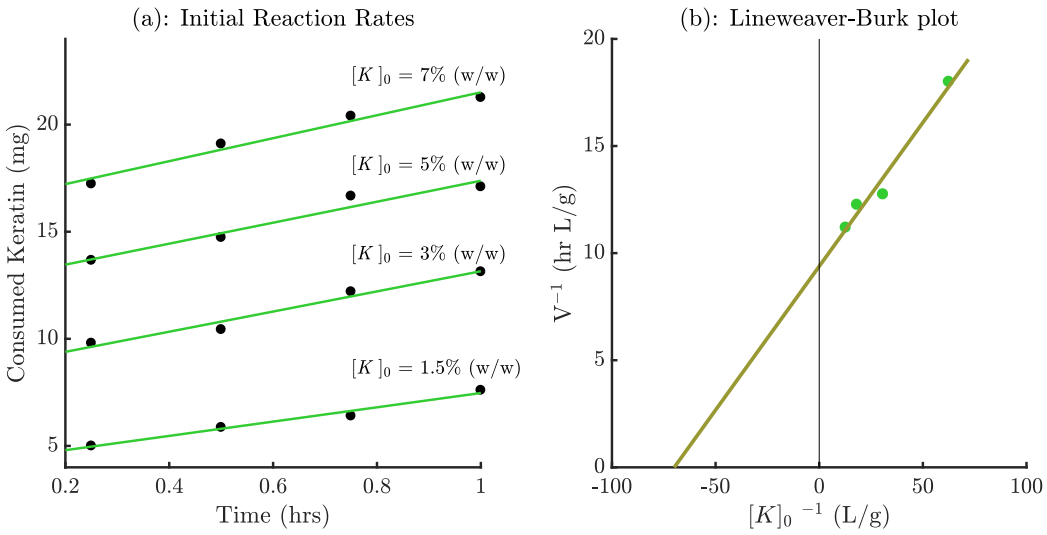

Figure 5.5: (a): Initial hydrolysis reaction rates, (b): Lineweaver-Burk plot.

notably decay in the reactive time-frame at this temperature. To incorporate this phenomenon into the model and the additional term is considered in the activity decay function: the residual activity, R_A, is defined as the activity level below which the activity does not drop (Eq. 5.6).

5.3.3 Initial Reaction Kinetics

Vials containing 2 mL keratinase preparation and varying solids loading (PBM meal) were placed in a thermoshaker at 40 °C and 600 rpm. At fixed time intervals, triplicate vials were removed for each solid loading considered. A sample from each vial was taken and the protein content determined by bicinchoninic acid (BCA) assay, and the remaining vial contents vacuum filtered, dried and weighed to determine residual substrate mass. Initial reaction kinetics for four substrate concentrations (1.5, 3, 5 and 7% w/w) were considered: samples were taken over time in the first hour, a period in which the consumption rate is approximately constant at the maximum (initial) value. Figure 5.5a presents the consumed keratin for the four loading cases in the first hour of the reaction. In all cases linear consumption is observed across the whole hour validating that the reaction rate is approximately constant and that these rates may be used to accurately determine V_{max}. The gradients from Figure 5.5a are used in the Lineweaver-Burk plot (circular markers in Figure 5.5b), to elucidate initial reaction kinetics via

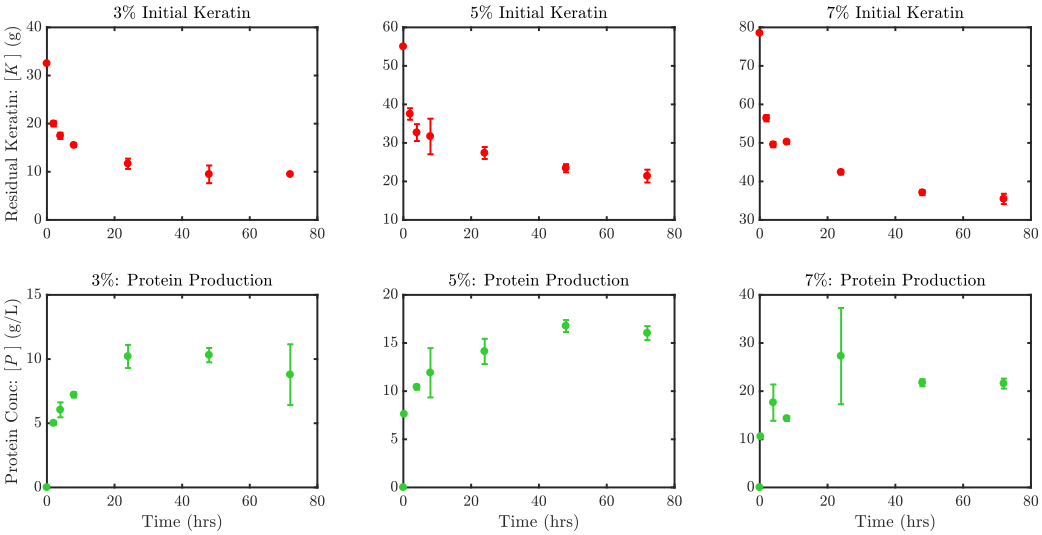

Figure 5.6: Experimental state data.

the classical approach: reading V_{max} and K_m off the figure from the x-intercept ($-K_m^{-1}$) and y-intercept ($-V_{max}^{-1}$) (Lineweaver and Burk, 1934).

5.3.4 Dynamic State Data

A second hydrolysis campaign is performed where three substrate concentrations were considered (3, 5 and 7% w/w) with the hydrolysis now performed for 72 h to construct state profiles for both substrate (keratin) and product (protein) throughout the entire reaction duration. Figure 5.6 presents the experimental state data across the 72 hour experimental campaign. Experiments are performed in triplicate with the corresponding error-bars presented on the figure.

5.3.5 Parameter Estimation

Of the eight model parameters, three (e_i, k_D and R_A) can be fit from the activity assay profile (Figure 5.4), whose solid line shows the fit using parameter values from Table 5.3. Two parameters (V_{max} and K_m) are determined directly using the initial kinetics via the Lineweaver-Burk plot method, (Lineweaver and Burk, 1934), shown in Figure 5.5b). Additionally, the product ration, f_r, can be directly inferred as the ratio between the protein and keratin state derivatives in Figure 5.6 Similarly the fraction of the substrate which is digestible by the enzyme, H,

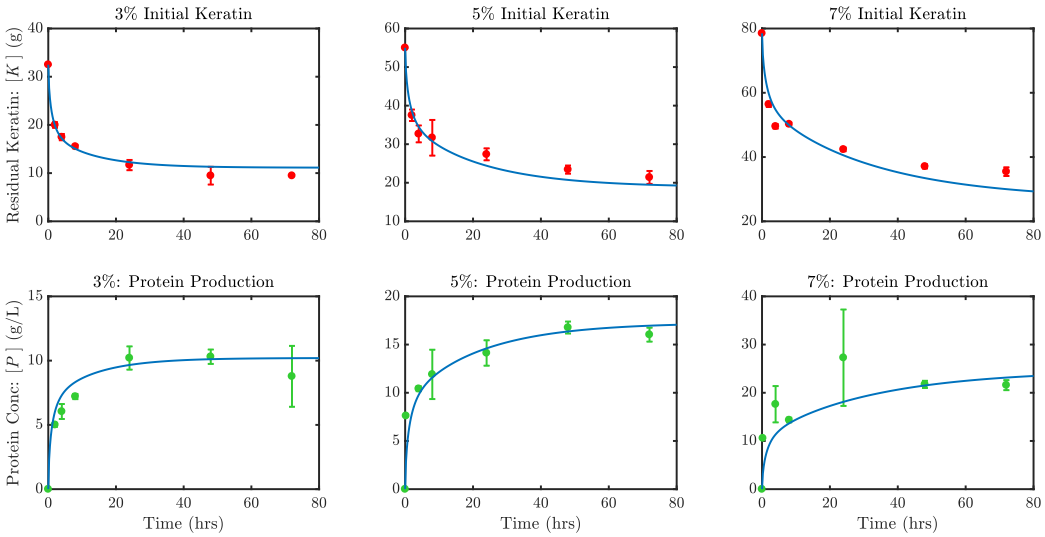

Figure 5.7: Experimental state data and model fit.

can be considered as the average of the total substrate fraction digested after the reaction is completed. Subsequently, the single remaining model parameter, K_I, to be estimated. This is formulated as a standard parameter estimation problem, minimising the sum squared error between model and experimental data points, defined by Eq. 5.9, where the NLP is solved with MATLAB's fmincon function, calling the inbuilt ode45 function for model integration to evaluate the objective in each iteration of the NLP solver.

$$min \sum (f(x_j, \theta) - y_j)^2 \tag{5.9}$$

Here, $f(x_j, \theta)$ is the model predicted keratin and protein state trajectory for experiment j, θ is the parameter vector and y_j is the experimental state trajectory. The data sets for 3% and 7% w/w initial substrate concentration were used in the fitting, leaving the 5% w/w profile as a supplementary dataset to compare the model to for validation. The model fit is presented with the blue trajectories in Fig. 5.7, alongside the prior state data.

5.3.6 Discussion

It can be seen from Figure 5.7 that the proposed model is able to effectively describe the key behaviour observed in the experimental data, both for keratin

Table 5.3: Keratin hydrolysis model parameter values.

Parameter	Symbol	Value	Units
Hydrolysable substrate fraction	H	0.63	-
Maximum reaction velocity	V_{max}	3.20	g L^{-1} hr^{-1}
Michaelis–Menten constant	K_m	14.29	g L^{-1}
Initial enzymatic activity	e_i	39.96	kU L^{-1}
Enzyme decay constant	k_D	0.188	hr^{-1}
Residual enzyme cocktail activity	R_A	23.91	kU L^{-1}
Product inhibition constant	K_I	0.328	g L^{-1}
Product ratio	f_r	0.548	-

consumption and protein production. The dataset not used in the model parameter determination (5% w/w loading) shows good agreement between experimental data and the model prediction, suggesting the model can accurately describe keratin hydrolysis at 40 °C with *A. keratiniphila D2*. The model assumption of a fixed fraction of the substrate being hydrolysable, H, is not able to fully capture the observed phenomena where yield decreases with solids loading. As a result, the model under-predicts keratin consumption at 3% w/w solids, and over predicts for 5% and 7% w/w (Figure 5.7). If the value of H is defined individually for each solid loading campaign according to the observed experimental yield in that campaign and the model parameters re-determined, the fit is exceptional. This indicates that if the mechanism behind diminishing yield with increasing substrate concentration can be incorporated into an updated model it would be even more accurate in representing the dynamic system. It is known that as solids loading increases, factors that were insignificant in low-solid systems become more prominent (Modenbach and Nokes, 2013), which can restrict substrate conversion yield at higher loading and is found to be the case here. It is possible that mass transfer between the keratin and enzyme is becoming impeded at high substrate concentrations due to reduced free water content as the liquid absorbs into the biomass, as has been observed in high-solids enzymatic cellulose hydrolysis (Hodge et al., 2009), a reactive system known to have many parallels to keratin hydrolysis; however further experimental work is necessary to confirm whether this is the precise mechanism responsible for the observed phenomena.

5.3.7 Chapter Conclusions

The first dynamic model for enzymatic hydrolysis of keratin is proposed. Michaelis–Menten kinetics with product inhibition allows the observed behaviour of the reactive system to be captured, with the model fit showing good agreement with experimental data. The assumption of a fixed fraction of the substrate being hydrolysable is not able to fully capture the observed phenomena where by yield in fact decreases with solids loading. Further experimental work is necessary to explore this with the aim of better describing the apparent inhibitory effect at higher substrate content to increase model fidelity towards more robust optimisation results, with the aim of increasing the cost competitiveness of this novel means to treat the abundant quantities of keratin-rich waste produced annually.

Chapter 6

Dynamic Simulation & Visualisation

6.1 Visualisation of Attainable Performance for Beer Fermentation

To assess the potential for process improvements in current plant operation at an industrial partners brewery, an algorithm has been developed to rapidly generate plausible temperature manipulations which adhere to realistic operability constraints at a suitable level of temporal domain discretisation. The systematic investigation of potential improvements relies on generating a vast number of potentially suitable temperature profiles and simulating fermentation for each dynamic manipulation. Plotting the entire set of different performance indicators obtained from each dynamic simulation along with those known from the current industrial manipulation can thereafter reveal the entire performance envelope towards pinpointing which precise process improvements are feasible.

6.1.1 Industrial Beer Fermentation Model

The lumped-parameter kinetic model of beer fermentation by de Andrés-Toro et al. (1998) has been selected for industrial fermentation process simulation for

several reasons: Published parameters are derived from a very large array of experiments, resulting in a wide temperature range (8 – 24 °C) which ensures high fidelity and applicability. The model includes all prominent by-products which degrade beer product quality in terms of taste and aroma, rendering the model valuable for assessing performance. Predicted profiles indicate the highest fidelity with experimental and pilot-plant data in comparison to other models, due to successful validation against over 200 fermentations. A description of this kinetic model corresponds to the schematic diagram presented (Fig. 3.10a). The model has been validated under non-isothermal operation within the prescribed temperature bounds, so is particularly suitable for exhaustive simulation and subsequent dynamic optimisation.

The initial cell culture pitched into the fermentor, $[X_{inc}]$, has a specific composition of active ($[X_{act}]$), latent ($[X_{lag}]$) and dead yeast cells ($[X_{dead}]$), which is defined as (de Andrés-Toro et al., 1998):

$$0.02 \cdot [X_{act}]_0 + 0.48 \cdot [X_{lag}]_0 = [X_{dead}]_0 = 0.5 \cdot [X_{inc}] \tag{6.1}$$

Following their introduction to the system, yeast cells are immediately suspended in the wort, rendering the total suspended cell concentration at any time, $[X_{sus}]$, equal to the sum of all respective cell types:

$$[X_{sus}]_t = [X_{act}]_t + [X_{lag}]_t + [X_{dead}]_t \tag{6.2}$$

During the fermentation lag phase, yeast cells undergo conversion into active cells, which have an enzymatic effect on the sugar substrate:

$$\frac{d[X_{lag}]}{dt} = -\mu_L(T) \cdot [X_{lag}]_t \tag{6.3}$$

The specific rate of activation (μ_L) is highly sensitive to temperature. During the lag phase, active cells are not considered to grow; their concentration changes due to cell activation:

$$\frac{d[X_{act}]}{dt} = -\frac{d[X_{lag}]}{dt}, \; t < t_{lag} \tag{6.4}$$

During the lag phase, cell death is not considered: the suspended dead cell concentration is governed only by the settling rate of cells escaping the suspension toward the tank bottom:

$$\frac{d[X_{dead}]}{dt} = -\mu_{SD}(T,t) \cdot [X_{dead}]_t,\ t < t_{lag} \tag{6.5}$$

The dead cell settling rate (μ_{SD}) depends on wort density, which is in turn related to the initial sugar concentration ($[S]_0$):

$$\mu_{SD} = \frac{\mu_{SD_0}(T) \cdot 0.5 \cdot [S]_0}{0.5 \cdot [S]_0 + [EtOH]_t} \tag{6.6}$$

The maximum settling rate (μ_{SD_0}) occurs at the beginning of the process, and is also highly sensitive to temperature. An Arrhenius equation is used to describe the temperature dependence of all rate parameter expressions within the model, where the constants A and B are estimated on the basis of experimental data at different temperatures (Table 6.1):

$$\mu_{i_0} = exp(A_i + \frac{B_i}{T(t)}) \tag{6.7}$$

Combining Eq. 6.2 with the aforementioned rate expressions for each cell type produces the overall suspended cell balance for the lag phase:

$$\frac{d[X_{sus}]}{dt} = -\frac{d[X_{dead}]}{dt},\ t < t_{lag} \tag{6.8}$$

Once active cells constitute a significant portion of suspended biomass, the lag phase is completed and the fermentation phase begins. Active cell growth occurs thereafter; suspended cell concentration evolves as a function of both active cell growth and dead cells settling:

$$\frac{d[X_{sus}]}{dt} = \mu_x(T,t) \cdot [X_{act}]_t - \mu_{SD}(T,t) \cdot [X_{dead}]_t,\ t \geq t_{lag} \tag{6.9}$$

The specific growth rate (μ_x) is a function of sugar and ethanol concentrations:

$$\mu_x = \frac{\mu_{x_0}(T) \cdot [S]_t}{k_x + [EtOH]_t} \tag{6.10}$$

The rate at which active cell concentration evolved during the fermentation phase is a combination of active cell growth, active cell death and latent cell activation:

$$\frac{d[X_{act}]}{dt} = \mu_x(T,t) \cdot [X_{act}]_t - \mu_{DT}(T) \cdot [X_{act}]_t + \mu_L(T) \cdot [X_{lag}]_t,\ t \geq t_{lag} \tag{6.11}$$

Throughout the fermentation phase, the evolution of latent cells is governed by Eq. 6.3, however the suspended dead cell ODE must incorporate an additional term to account for the death of active cells:

$$\frac{d[X_{dead}]}{dt} = -\mu_{SD}(T) \cdot [X_{dead}]_t + \mu_{DT}(T) \cdot [X_{act}]_t,\ t \geq t_{lag} \tag{6.12}$$

The rate of cell death (μ_{DT}) depends on wort temperature, described with an Arrhenius equation (Table 6.1). The uptake of sugar from wort is proportional to active biomass concentration:

$$\frac{d[S]}{dt} = -\mu_S(T,t) \cdot [X_{act}]_t \tag{6.13}$$

The consumption rate (μ_S) has been assumed to follow Michaelis-Menten kinetics: the maximum rate (μ_{s0}) at $t = 0$) corresponds to the maximum sugar concentration which obeys an explicit temperature dependence:

$$\mu_s = \frac{\mu_{s0}(T) \cdot [S]_t}{k_s(T) + [S]_t} \tag{6.14}$$

Ethanol concentration data shows that its production rate is not constant, so it is necessary to include an inhibition factor (f) in the formulation:

$$\frac{d[EtOH]}{dt} = f(t) \cdot \mu_e(T,t) \cdot [X_{act}]_t \tag{6.15}$$

This factor accounts for the ethanol inhibiting effect in the wort, and is defined

Table 6.1: Experimentally determined Arrhenius constants

Symbol	Description	A_i	B_i
μ_{SD_0}	Maximum dead cell settling rate	33.82	-10033.28
μ_{x_0}	Maximum cell growth rate	108.31	-31934.09
μ_{s_0}	Maximum sugar consumption rate	-41.92	11654.64
μ_{e_0}	Maximum ethanol production rate	3.27	-12667.26
μ_{DT}	Specific cell death rate	130.16	-38313
μ_L	Specific cell activation rate	30.72	-9501.54
$k_e = k_s$	Affinity constant	-119.63	34203.95
Y_{EA}	Ethyl acetate production stoichiometric factor	89.92	-26589

along with the specific growth rate (μ_e):

$$f = \frac{1 - [EtOH]_t}{0.5 \cdot [S]_0} \tag{6.16}$$

$$\mu_e = \frac{\mu_{e0}(T) \cdot [S]_t}{k_e(T) + [S]_t} \tag{6.17}$$

Ethyl acetate production rate is considered proportional to active cell growth; the stoichiometric factor (Y_{EA}) is an Arrhenius function of system temperature.

$$\frac{d[EA]}{dt} = Y_{EA}(T) \cdot \mu_x(T,t) \cdot [X_{act}]_t \tag{6.18}$$

The model considers two chemical pathways for diacetyl evolution; the first term accounts for its production rate (proportional to sugar concentration) while the second term represents its conversion rate to other components (proportional to ethanol concentration):

$$\frac{d[DY]}{dt} = \mu_{DY} \cdot [S]_t \cdot [X_{act}]_t - \mu_{AB} \cdot [DY]_t \cdot [EtOH]_t \tag{6.19}$$

Parameter values required in all modified Arrhenius temperature equations defined in Eq. 6.7 use the ideal gas law constant (R = 8.314 J K^{-1} mol^{-1}) and are reported for T in degrees Kelvin (Table 6.1). The original model (de Andrés-Toro et al., 1998) describes the specific appearance and disappearance rates of diacetyl (μ_{DY} and μ_{AB} respectively) using second-order temperature polynomials: this description predicts erroneous species profiles, entirely different from those shown in the paper and reported in all experiential studies published. Subsequent

Table 6.2: Additional model parameters

Symbol	Parameter Description	Value	Units
μ_{DY}	Diacetyl production rate	$1.27672 \cdot 10^{-7}$	$g^{-1}h^{-1}L$
μ_{AB}	Diacetyl consumption rate	$1.13864 \cdot 10^{-3}$	$g^{-1}h^{-1}L$

papers (Carrillo-Ureta et al., 2001; Xiao et al., 2004) use experimentally determined constants for these growth rates and present profiles in closer agreement with experimental data (Table 6.2).

While investigating the predictive power of the various kinetic models, the present study has discovered that the original de Andrés-Toro kinetic model publication (1998) did not produce the ethyl acetate profile presented in the paper. This error has been reproduced by numerous authors referencing the model, despite not presenting profiles which follow this mathematical description (Carrillo-Ureta et al., 2001; Xiao et al., 2004). Carrillo-Ureta (1999) defines an ethyl acetate ODE identical to that of de Andrés-Toro (1998):

$$\frac{d[EA]}{dt} = Y_{EA}(T) \cdot \frac{d[S]}{dt} = Y_{EA}(T) \cdot \mu_S(T,t) \cdot [X_{act}]_t \tag{6.20}$$

6.1.2 Methodology

To generate a finite set of dynamic profiles, the temperature domain must be discretised. The domain limits have been defined by Eqs. 6.21 - 6.22: the time span is such that any profile producing reasonable performance will be run to completion, while avoiding unreasonable computational load for all profiles which imply a prohibitively long batch time. The lower temperature limit excludes scenarios in which the system lacks enough energy to promote cell growth; the upper limit ensures bacteria which are present above this temperature cannot thrive, while also preventing the temperature from reaching a level at which undesirably high by-product concentrations are known to be produced.

$$0 < t < 160 \text{ (hours)} \tag{6.21}$$

$$9 < T < 16 \text{ (°C)} \tag{6.22}$$

An extremely large number of paths within this finite domain exists, so discretisation is necessary in order to obtain a manageable finite set. Temperature control of industrial fermentation vessels is extremely challenging, given the complex flow patterns in fermentors: consequently, attempting to manipulate the temperature to a finer level than 1 °C is not practical. The temperature range considered has thus been discretised per degree, for profile nodes/corners, between which the temperature is is piecewise linear. For a manipulation profile to be useful, the temperature must not change abruptly with time, to avoid imposing unrealistic demands on the cooling system. To accommodate this, the fermentation time span is broken down into 20-hour intervals, so 9 values are considered along the time axis, thus producing temperature profiles which all consist of 8 linear segments. This discretised grid will produce 9^8 total unique paths, a value too vast for exhaustive numerical dynamic simulation. Many of these paths are evidently not industrially useful, so it is necessary to select and simulate only technically promising cases. Constraints must be applied in order to reduce the number of paths, removing those which evidently produce poor performance and induce an unnecessary computational burden. An investigation has been performed in order to identify appropriate profile constraints, which must reduce the total number of profiles (paths) to a manageable level, selecting those likely to produce good performance while also allowing a reasonable range of different paths to be considered so that the effect of various operating conditions can be assessed. A set of different rules for profile constraints has been developed conceptually. Rule A states that temperature may only increase to any level within the domain limits or remain constant when progressing to the next discretised point in time.

$$\text{Rule A: } T(t_{n+1}) \geq T(t_n) \tag{6.23}$$

In rules B and C, the temperature can remain constant, increase or decrease when progressing to the next time point. Rules B uses $\Delta T_{max} = 1$ °C and rule C considers $\Delta T_{max} = 2$ °C to limit the temperature change between each interval; e.g. in the latter a step of 0, 1 and 2 °C in both directions is permitted at every 20 hour time step.

Table 6.3: Number of profiles for constraint rules and time domain resolutions.

Rule:		A	B	C	D	E	F
ΔT_{max} (°C)			1	2	1	2	3
Equation(s)		6.23	6.24	6.24	6.25, 6.26	6.25, 6.26	6.25, 6.26
N	t_{step} (hrs)	Number of unique manipulation profiles:					
4	53.33	120	62	512	29	59	94
5	40	330	176	4.1×10^3	55	157	309
6	32	792	502	3.3×10^3	106	434	1.1×10^3
7	26.67	1.7×10^3	1.4×10^3	2.6×10^3	201	1.1×10^3	3.2×10^3
9	20	6.4×10^3	1.2×10^4	1.7×10^8	730	7.8×10^3	2.7×10^4

$$\text{Rules B \& C: } T(t_n) - X \leq T(t_{n+1}) \leq T(t_n) + \Delta T_{max} \tag{6.24}$$

One more set of rules have been considered, in which the constraint is split in time such that the temperature may only increase up to ΔT_{max} degrees for the first half of the process, and then only decrease up to ΔT_{max} degrees between successive time steps for the second half of the fermentation. Rule D selects $\Delta T_{max} = 1$ °C, rule E imposes $\Delta T_{max} = 1$ °C and F considers $\Delta T_{max} = 3$ °C. This early increase and later decrease represents the form generally employed in fermentation.

Rules D, E, F:

$$T(t_n) \leq T(t_{n+1}) \leq T(t_n) + \Delta T_{max}, \text{ for } t < \frac{t_{max}}{2} \tag{6.25}$$

$$T(t_n) - \Delta T_{max} \leq T(t_{n+1}) \leq T(t_n), \text{ for } t \geq \frac{t_{max}}{2} \tag{6.26}$$

The number of profiles generated when following each of these constraints is listed in Table 6.3, for increasing levels of time domain discretisation (N). Rule A produces a low number of paths, but limiting temperature evolution such that it can only increase is highly restrictive because cases which include a later decrease in temperature (as often shown in literature) are excluded. Rules B and C are much less restrictive, as temperature increase or decrease at any point is permitted. However, the number of paths produced increases explosively as the allowable ΔT between time points increases. This is clear in Table 6.3, where increasing the allowable temperature variability from 1 °C (Rule B) to 2 °C (Rule C) drastically influences the number of profiles, with the difference increasing very

dramatically as the permitted temperature change is further increased. Rules D, E and F show a much less severe impact on the number of paths when increasing ΔT, while still including typical fermentation cases, and has been found to be the most suitable of all novel constraints we have developed. To allow a greater range of potentially suitable paths to be simulated, Eqs. 6.25–6.26 are modified to remove the permitted temperature step limit, allowing any level of temperature variation between time points while still following the same multi-region constraint rule, as seen in Eqs. 6.27–6.28. This double constraint states that all levels of temperature increase within the domain limits are considered for every time step before the midpoint, and all levels of decrease are considered for every step after the midpoint. Accordingly, a large set of potentially applicable profiles has been obtained for the fermentation process. The applied constraint:

$$T(t_{n+1}) \geq T(t_n), \text{ for } t < \frac{t_{max}}{2} \tag{6.27}$$

$$T(t_n) \geq T(t_{n+1}), \text{ for } t \geq \frac{t_{max}}{2} \tag{6.28}$$

6.1.3 Simulation Results

The temperature and time limits, discretisation level and constraints considered in the present study produce 175,252 unique temperature profiles. Simulating dynamic species evolution for the entire set of manipulations requires 3 hour of total CPU time. Key performance indicator data from all dynamic simulations are plotted and compared to the performance of an industrial partners fermentation manipulation, represented by the circular blue marker on the scatter plots (Figs. 6.1–6.2). Fig. 6.1a illustrates all final concentrations of ethanol, diacetyl and ethyl acetate after fermentation for 160 hours, for every single scenario simulated, providing a three-dimensional indicator of product quality. Fig. 6.1b presents a measure of process performance by correlating fermentation efficiency (measured by maximum ethanol production) and fermentation time (measured by the time to produce 99.5% of that value). Here the desirable region is the upper left corner of the figure, representing maximum ethanol concentration in minimum

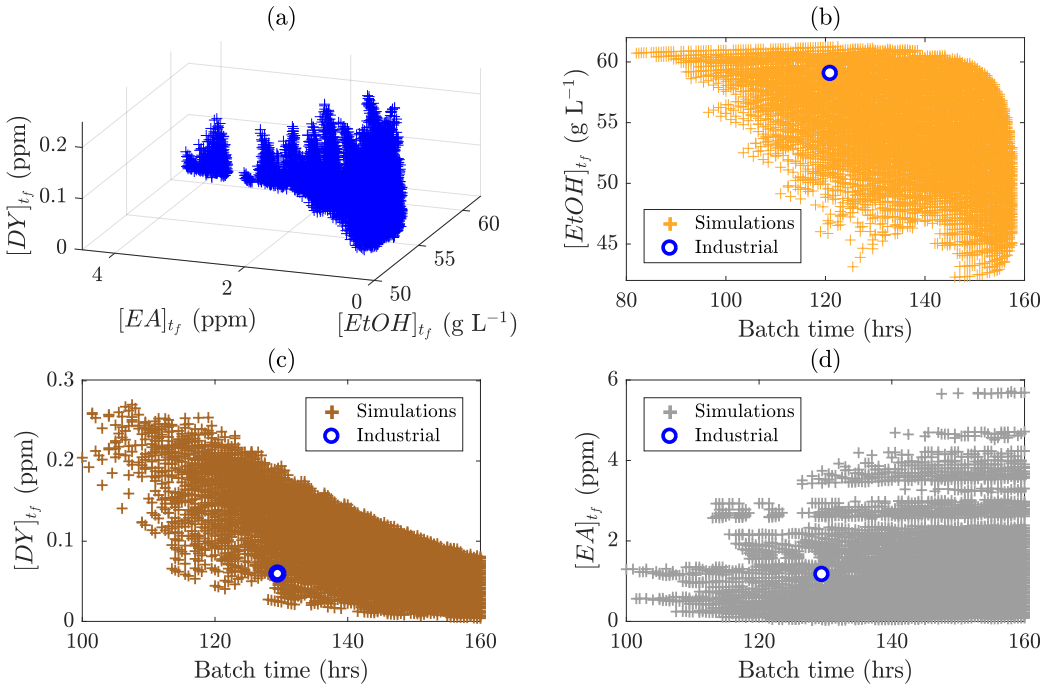

Figure 6.1: (a) Attainable product envelope; Concentration of (b) ethanol, (c) diacetyl, (d) ethyl acetate vs time.

time. Fig. 6.1(c-d) similarly show produced aromatic compound concentrations against fermentation time, which is now measured by the time to almost entirely consume the initial wort sugar concentration. While measuring fermentation time by sugar consumption and ethanol production do yield marginally different times, their strong correlation renders either of the two as a reliable indicator of process performance, providing ethanol production and sugar consumption are both adequately high. Using sugar consumption as an indicator removes cases where undesirably high residual sugar concentration remains in the product, which consequently do not feature in Fig. 6.1(c-d) or Fig. 6.2.

The process lag phase length is also considered for each simulation in order to determine if it has a strong effect on the total batch time. Thus, Fig. 6.2a presents the length of the lag phase vs. batch time, while Fig. 6.2b shows the effect of the lag phase length on the maximum active cell concentration observed within the yeast culture. Figs. 6.2(c-d) present the active cell population against batch time: Fig. 6.2c compares fermentation time to maximum active cell population, while Fig. 6.2d considers the final active yeast cell concentration after fermentation is complete: the latter is of high industrial interest, as it is desirable

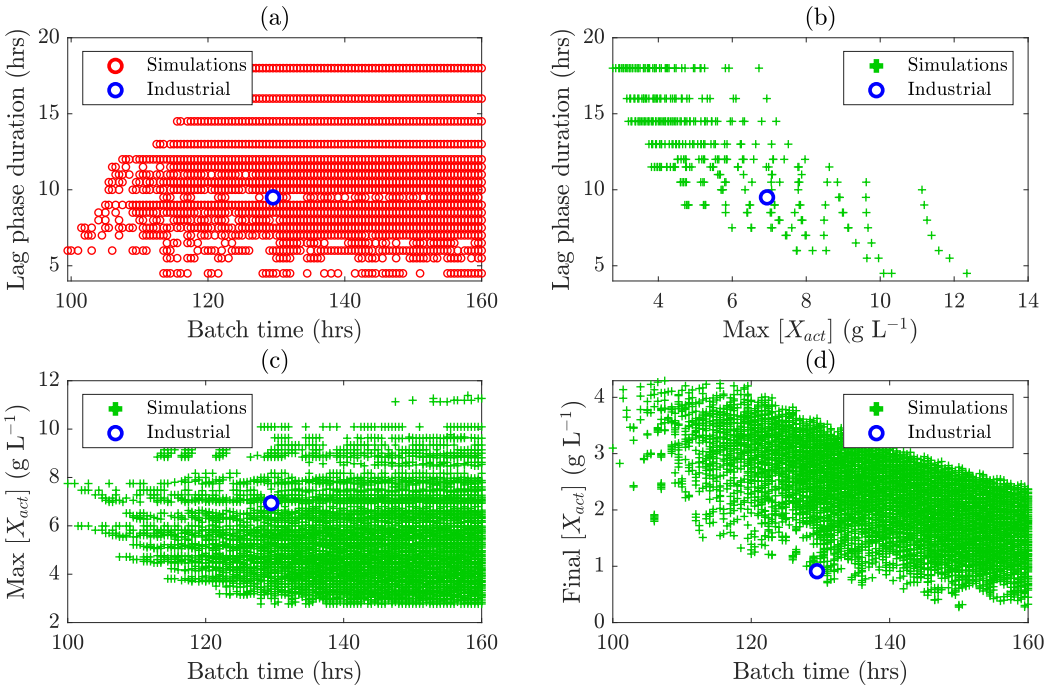

Figure 6.2: Fermentation performance for all simulations; Lag phase length vs. (a) Batch time, (b) Active cell concentration; Fermentation time vs. (c) Maximum active cell concentration, (d) Final cell concentration.

to recover the yeast toward using it in subsequent fermentation batches. All fermentation performance indicators suggest that the industrial operational profile has reasonably high performance, better than a large portion of the simulated alternatives. It is also evident there is significant potential to improve any single variable, however often not without compromising on another target parameter. Thus, Fig. 6.1a shows the relationship between final product concentrations: it can be seen that the greatest ethanol production also corresponds to the highest production of aromatic by-products, well exceeding acceptable levels. It also indicates that a small sacrifice in final ethanol concentration can lead to large reductions in the concentrations of aromatic compounds present. Moreover, Fig. 6.1b shows that it is possible to both increase ethanol production and reduce processing time relative to the industrial manipulation (upper left quadrant data points). However, the implications on all other design variables must be considered; the most desirable simulation according to Fig. 6.1b is the upper leftmost point on the graph, which corresponds to isothermal operation at $T = T_{max}$, but also to very high by-product production and sugars remaining unconsumed. It

is more beneficial to retain or marginally reduce the current ethanol production in order to reduce batch time while not impairing product quality. Furthermore, Fig. 6.1c illustrates that a reduction in batch time is correlated with an increase in diacetyl in the beer product.

The current industrial plant manipulation is producing a low ethyl acetate concentration given the batch time (t_f = 130 hours), close to the Pareto front of this plot, which follows the minimum concentration boundary for any fermentation time. Diacetyl concentration is the most challenging variable to reduce without suffering a detrimental effect on other process parameters. Because it is well below the levels produced by most fermentations, it is possible to allow diacetyl concentration to increase within acceptable limits in order to achieve a process improvement in terms of batch cycle time. Conversely, Fig. 6.1d shows that such a high level of a correlation between ethyl acetate concentration production and batch time does not exist. Simulation data points are spread out widely, however it is clear that longer batch times can coincide with higher aromatic compound levels, while shortest batch times correspond to the lowest concentrations. The current industrial manipulation produces approximately the average ethyl acetate concentration for all fermentations of this duration. No apparent trend between the length of the lag phase and the total fermentation time is observed (Fig. 6.2a). The industrial manipulation corresponds to the average lag phase duration for this batch time, t_f, = 130 hours. The lag phase duration does influence the maximum concentration of active yeast cells which are produced (Fig. 6.2b): a shorter duration for this lag phase leads to an increased maximum cell concentration. Also, Fig. 6.2c reveals that the maximum cell concentration is not closely related to the batch fermentation time, highlighting that this is not an essential parameter for evaluating process performance. The average concentration of active cells is of higher importance, given that a short-lived high maximum does not influence fermentation rate for a long period of time. It is desirable to ensure there is an active cell population when fermentation is complete: Fig. 6.2d illustrates that while the points are highly spread, the overall trend indicates that rapid fermentations facilitate a higher concentration of active cells at the end of the process. This is extremely significant in case of successfully reducing batch

Table 6.4: Proposed fermentation process improvements.

Parameter	Units	Existing Manipulation	A	B	C
Batch Time	hrs	129.5	119.5	115	119.5
$[EtOH]$	g L^{-1}	59.0	58.9	58.0	58.9
$[EA]$	ppm	1.16	1.19	0.99	1.28
$[DY]$	ppm	0.06	0.10	0.16	0.09

time, because material costs for fresh yeast can be reduced in addition to improving plant throughput. Simulation results have been analysed to evaluate which cases reduce fermentation time with acceptable effect on product quality. The time for sugar consumption of the industrial manipulation is 130 hours (Table 6.4). A 10-hour reduction of fermentation time would have a significant impact on brewery production capacity, so all simulated profiles which produce a batch time under 120 hours must be considered as potentially viable process improvements. Hence, of the profiles simulated, 2759 take 120 hours or less to consume 99.5% of the initial sugars. Many of these differ only after fermentation completion (120 hours), so only 826 potentially suitable profiles can improve the first 120-hours.

Three promising process improvement cases are highlighted in Table 6.4, with the corresponding profiles illustrated in Fig. 6.3. A considerable batch time reduction is demonstrated in each case, with minimal impact on product quality. Options A and C show similar performance, a 10-hour reduction in fermentation time, with a small (0.1 g L^{-1}) reduction in ethanol produced and a marginal increase in both aromatic compound concentrations. Option B is more preferable if a more significant decrease in ethanol concentration is permitted: a decrease of 1 g L^{-1} can reduce batch time by 15 hours (Table 6.4), while also reducing the product ethyl acetate concentration by over 15%. Diacetyl concentration is also increased, however it remains comparatively low compared to other manipulations considered (Table 6.4). Depending on a brewer's particular product targets, numerous dynamic simulations performed in this study represent clear and measurable process improvements, which can be attained by tolerating small sacrifices in areas considered as process targets of lower priority.

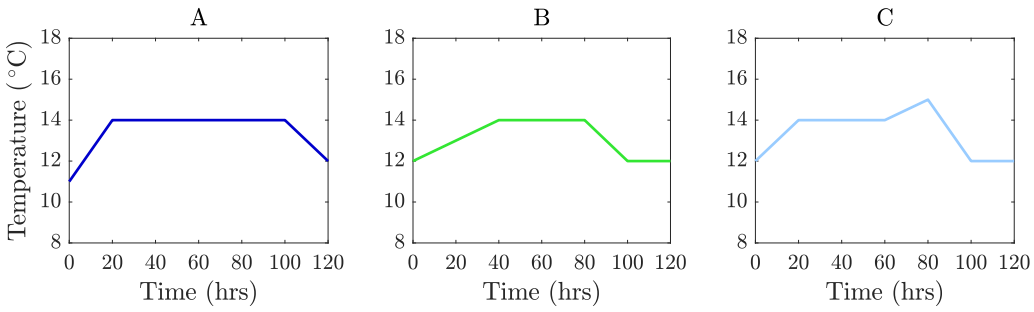

Figure 6.3: Dynamic temperature manipulation profiles producing clear and measurable process improvements.

6.1.4 Optimal Temperature Profile Determination

The attainable envelope of product final concentrations (Fig. 6.1) compiled from the entire data set of simulation results clearly illustrates that numerous plausible manipulations promise superior performance (hence process improvements) over current industrial practice. The precise determination of the most suitable and advantageous temperature manipulations is hence the next essential step for achieving the best feasible performance (optimal operation). First, Simulated Annealing (SA) has been implemented to determine the optimal temperature manipulation profile from the simulation set. Secondly, the performance of each of the 175,000 profiles has been quantified for a range of objective function weights by exhaustive evaluation, in order to validate stochastic results from SA, as well as investigate the sensitivity the solution shows to potentially arbitrary objective function component weights.

6.1.4.1 Simulated Annealing (SA)

Simulated Annealing (SA) is a valuable approach for approximating a global optimum (Kirkpatrick et al., 1983), requiring significantly less CPU time compared to exhaustive techniques, while effectively exploring the design space. The metaheuristic for approximate global optimisation is applicable to the large search space here, and has been applied to biochemical network processes for parameter estimation previously (Gonzalez et al., 2006). The computational procedure is analogous to the thermal annealing of solids, in which the material is heated and then cooled slowly, allowing atoms to reach a minimal energy state. In simulated

(much like in material thermal) annealing, the current candidate solution (system state) may move to another of worse objective function value (akin to a higher energy state), particularly in the early stages of the process. This occurs so that early local minima or maxima can be escaped in the search for the globally optimal solution: as the SA temperature is gradually reduced, the corresponding probability of accepting a worse solution is reduced. An objective (cost) function is essential to define in order to quantify and compare the performance of fermentation temperature profiles: in principle, it can account for final product concentrations (ethanol, diacetyl and ethyl acetate) and batch time as terminal pay-offs, while energy consumption is not considered as a running pay-off, in accordance to most previous studies and the model (de Andrés-Toro et al., 1998) employed. The objective function formulated only considers final ethanol concentration maximisation and batch time minimisation, and is given by Eq. 6.29: therein, W_E and W_t are the respective weights of the two components, $\frac{1}{t}$ is the inverse batch time (normalised by division with the maximum value recorded) and $[\tilde{EtOH}]$ is the ethanol concentration (normalised in the same way). In doing so the normalised ethanol concentration $[\tilde{EtOH}]$ ranges from 0.68 when $[EtOH]$ = 42 g L^{-1} to 1 when $[EtOH]$ = 61.3 g L^{-1}, similarly the normalised inverse batch time ($\frac{1}{\tilde{t_f}}$) ranges from 0.62 to 1 when t is 99 hrs and 160 hrs respectively. By-product species (diacetyl and ethyl acetate) final concentrations are considered as constraints, since they must be kept below threshold values in the final product, and are given in Eqs. 6.30 - 6.31; further reductions below these limits are welcome but not essential, as they do not induce any discernible effect on flavour (resulting product quality improvements cannot be quantified).

$$J_{min} = -W_E \cdot [\tilde{EtOH}] - W_t \cdot \frac{1}{\tilde{t_f}} \tag{6.29}$$

$$\text{s.t. } [EA]_{t_f} \leq 2 \text{ ppm} \tag{6.30}$$

$$[DY]_{t_f} \leq 0.1 \text{ ppm} \tag{6.31}$$

The SA algorithm employed is based on published MATLAB® code (Hedengren, 2015). Firstly, the data set produced via exhaustive simulation is compared to the

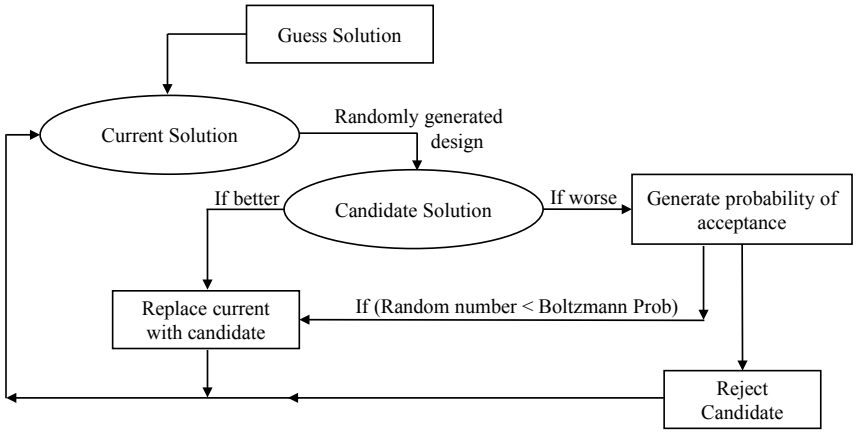

Figure 6.4: Simulated annealing flow diagram (Hedengren, 2015).

tolerable by-product limits, Eqs. 6.30 - 6.31, and all cases in which the latter are exceeded are removed (feasible region identification). Secondly, an ethanol concentration is initially assumed, and the corresponding production (batch) time is retrieved: the objective function value corresponding to the respective temperature profile can then be computed using Eq. 6.29. The SA algorithm then follows the flow diagram given in Fig. 6.4.

A new potential ethanol concentration is generated by stepping randomly from the current value. The corresponding batch time is recorded and the objective function value is computed again: if the latter shows improvement, it replaces the current solution. If the solution is worse, it may still replace the existing solution if a randomly generated number is less than the Boltzmann probability, Eq. 6.32 where ΔE is the energy displacement (difference in objective function values for successive iterations), k_b is the is the Boltzmann constant and T_{SA} is the SA temperature (not to be confused with fermentation temperature):

$$p = exp(\frac{-\Delta E}{k_b T_{SA}}) \tag{6.32}$$

This procedure has been performed for a wide range of objective function component weights (Eq. 6.29), for several starting points (initial guesses): the optimal point determined is independent of the starting point selected, provided that a suitable cooling rate is used. While a multi-start algorithm has been used,

the same initialisation could be used repeatedly since the method is stochastic. The number of iterations required and the appropriate starting SA temperature depend on the accuracy of the initial guess. A wide variation of component weights have been used, but only three cases are illustrated (Fig. 6.5): for each of them, three different starting points (A, B, C) are considered and all three SA trajectories are clearly shown to converge to the same optimal point (which depends on weight allocation), albeit at quite variable performance (iterations). The figure depicts the entire set of simulations results as to allow the SA trajectories to be readily visualised, however the data is not an inherent part of the procedure. The top row of plots within Fig. 6.5 present product $[EtOH]$ versus batch time on an ethanol basis - defined as the time to produce 99.5% of the ethanol produced after 160 hours by any profile, denoted by (*). The remaining plots in the Figs. 6.5, 6.7 and 6.9 still depict batch time in the x-axis, however these refer to a sugar basis - defined as the time to consume 99.5% of the feed sugars. Furthermore, a remarkable observation is that (while dependent on weight allocation for $W_t < 10\%$), the optimal temperature profile remains identical (and independent of weight allocation) for all cases where $W_t > 10\%$; this trend is significant, because it indicates that the optimal manipulation displays almost no sensitivity to the arbitrary balance of objective function terms. A minimal reduction of ethanol concentration (Fig. 6.5, first column) can therefore facilitate a considerable batch time reduction, while also ensuring that Eqs. 6.30 - 6.31 constraints are satisfied. The temperature profile presented (Fig. 6.5, second and third columns) can thus be conclusively determined as the optimal result for the fermentation process considered, excluding the unrealistic case of extreme (and virtually exclusive) importance of ethanol concentration only ($W_E > 90\%$), in which batch duration is disregarded ($W_t < 10\%$). A larger number of SA iterations are required when the initial point lies far from the optimal result; also, a higher initial SA temperature is required in these cases so that local maxima can be overcome. In the first case ($W_t = 1\%$, $W_E = 99\%$), the solution lies closer to the starting points, so a lower initial SA temperature and fewer iterations were required. Conversely, the other two weight allocation cases required a higher initial temperature, in order to prevent convergence entrapment in a local minimum

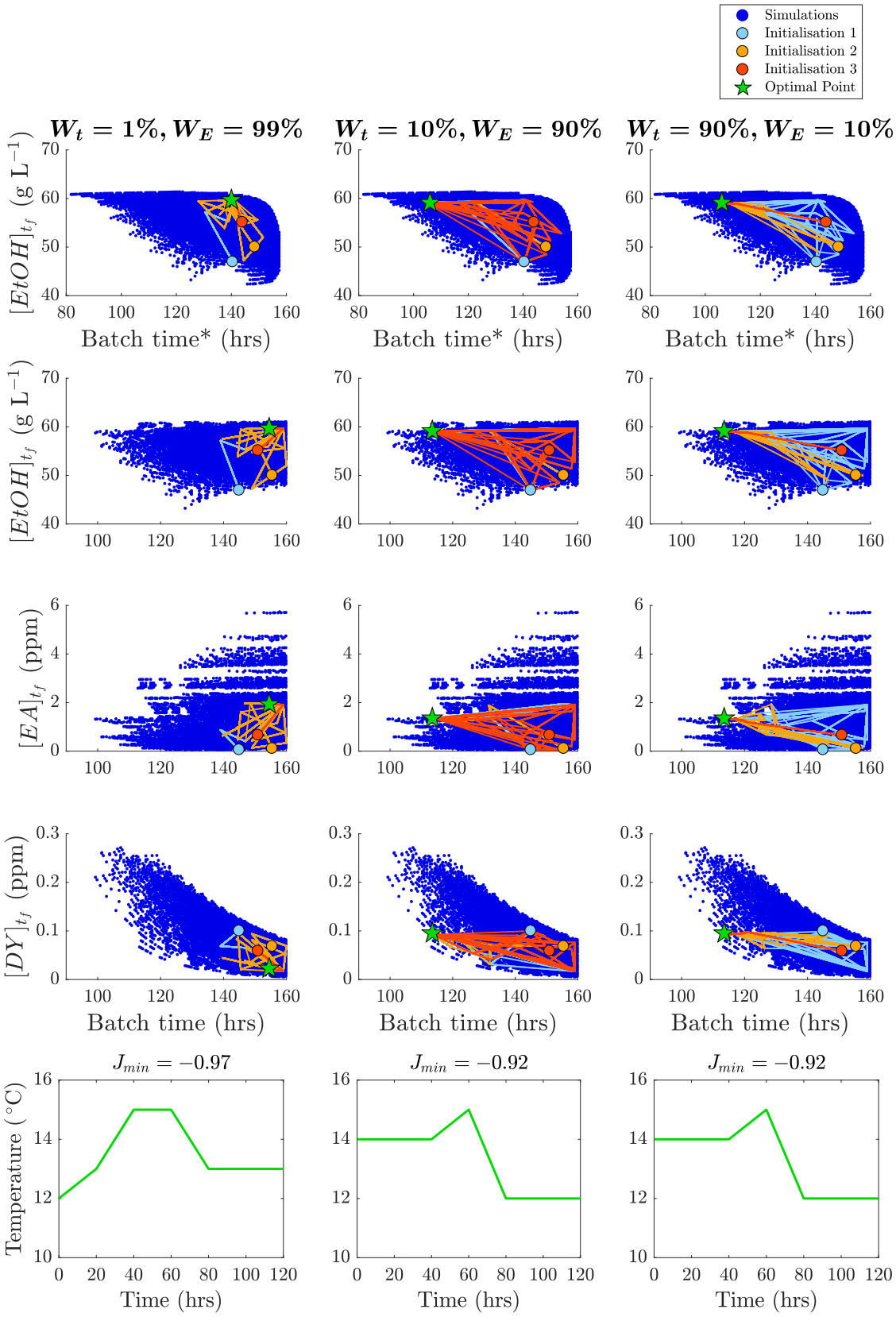

Figure 6.5: SA optimisation results for varying J-function component weights.

Table 6.5: SA solution methods.

Weights	$T_{initial}$	$p_{initial}$	T_{final}	p_{final}	Iters	Simulations	J_{min}
W_t= 1% W_E = 99%	0.621	0.2	0.1087	0.0001	10	103	-0.97
W_t= 10% W_E = 90%	9.491	0.9	0.1087	0.0001	30	364	-0.92
W_t= 90% W_E = 10%	9.491	0.9	0.1087	0.0001	30	324	-0.92

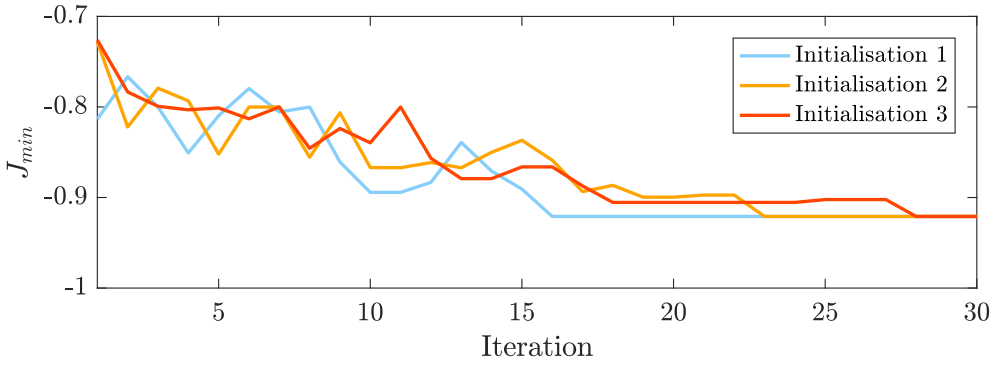

Figure 6.6: SA objective function per iteration from 3 initial points (W_t = 90%, W_E = 10%).

and attain the global solution. Fig. 6.5 (second and third columns) indicates that the SA algorithm passed through the point corresponding to optimal operation in the first case (W_t = 1%, W_E = 99%), as the latter constitutes a local (but not global) maximum for the other two cases. Table 6.5 shows the required parameters to consistently reach the optimal solution for any starting point in each case. Objective function convergence from various initialisations is illustrated in Fig. 6.6 for the second case (W_t = 90%, W_E = 10%).

6.1.4.2 Exhaustive Enumeration

The exhaustive evaluation of all (175,000) candidate temperature manipulation profiles has been pursued in order to validate the Simulated Annealing (SA) algorithm constructed and results obtained: the same objective function given in Eq. 6.29 has been used in order to calculate J values for every single temperature profile, using the same component weights.

Figure 6.7 illustrates the top 10% (red points) and the optimal (green point) product quality combinations achieved, respectively, superimposed on the entire

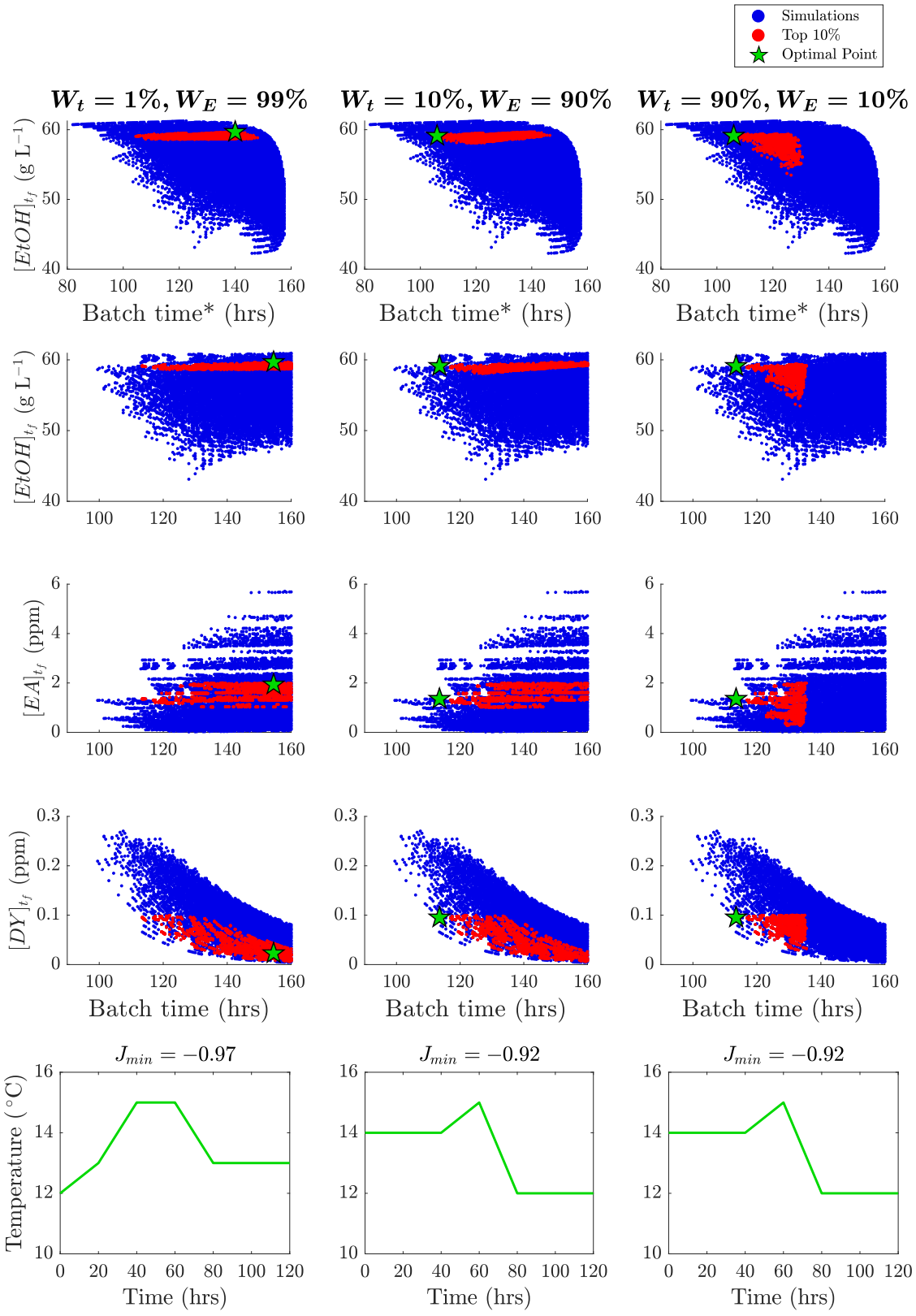

Figure 6.7: Exhaustive optimisation results for varying J-function component weights.

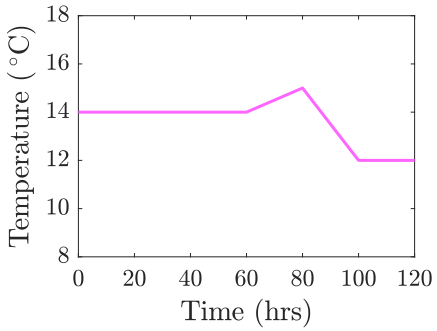

Figure 6.8: Optimal temperature profile from exhaustive search.

Table 6.6: Optimal fermentation profile performance.

Parameter	Units	Existing Manipulation	New Profile (Figure 6.8)
Batch Time	hrs	129.5	113.5
$[EtOH]$	g L^{-1}	59.0	59.1
$[EA]$	ppm	1.16	1.35
$[DY]$	ppm	0.06	0.09

attainable envelope (blue points). The optimal points identified are precisely those determined via simulated annealing, which is however a lot more efficient as it performs only a fraction of objective function evaluations. Both simulated annealing (SA) and exhaustive evaluation approaches arrive at the same temperature profiles to minimise the objective function of Eq. 6.29 and satisfy the constraints of Eqs. 6.30 - 6.31. For the vast majority of objective function weight allocation values, the optimal temperature profile determined remains the same (Fig. 6.8); its performance is compared to the current industrial manipulation in Table 6.6. The batch time reduction achieved is spectacular (12.3%), and it is accompanied by a small desirable increase in final ethanol concentration; while both by-product concentrations do increase marginally as well, they are well below tolerable thresholds and do not affect flavour.

6.2 Visualisation of the Impact of Wort Composition

The dynamic simulation and visualisation analysis of beer brewing is conducted considering two (low/high) values for each of the three system parameters of in-

terest. Initial wort sugar concentration ($[S]_0$), pitching rate ($[X_{INC}]_0$) and active yeast fraction concentration ($[X_{act}]_0$) have been varied between realistic bounds for industrial operation, thus producing 8 distinct initial condition combinations. The base case considered is the one for which all foregoing initial condition parameters are set at the lower bound values. Dynamic process simulation for all initial condition triplets and all 175,252 plausible temperature manipulation profiles has been performed in order to visualise and comparatively evaluate the impact and relative importance of each condition parameter on each beer quality attribute, i.e. $[EtOH]$, $[DY]$, and $[EA]$ (ethanol, diacetyl and ethyl acetate final concentrations, respectively). Dynamic simulation results are summarised in Fig. 6.9 via three-dimensional attainable envelopes of attributes (row 1) and two-dimensional sensitivity analysis plots (rows 2-5), illustrating the output ensembles of all measurable attributes versus all three ($[S]_0$, $[X_{INC}]_0$, $[X_{act}]_0$) initial condition steps. Two-dimensional plots are attainable envelope projections constructed in order to facilitate pairwise comparisons of possible operational changes against the industrial base case. Final ethanol concentration is the main beer quality attribute, whose maximisation is the foremost process efficiency index. The time axis has been normalised (rows 3-5) to portray the required interval to consume 99.5% of initial sugar feed, $[S]_0$; it has also been represented (row 2) as the required interval to achieve 99.5% of final ethanol concentration, $[EtOH]_{max}$, to elucidate the full envelope of attainable alcohol production. Filled black circles represent this base case in all Fig. 6.9 plots, while open grey circles depict each other alternative scenario.

6.2.1 Initial Wort Sugar Concentration

The impact of raising the initial wort sugar concentration (from 130 to 150 g L^{-1}) on fermentation process performance and beer quality attributes is illustrated in Fig. 6.9 (column 1). Evidently, increasing fermentable material correspondingly increases final attainable ethanol concentrations (rows 2-3). The maximum attainable limit (row 2) is horizontal (virtually independent of batch time), but shorter times lead to higher flavour compound contents and thus compromise

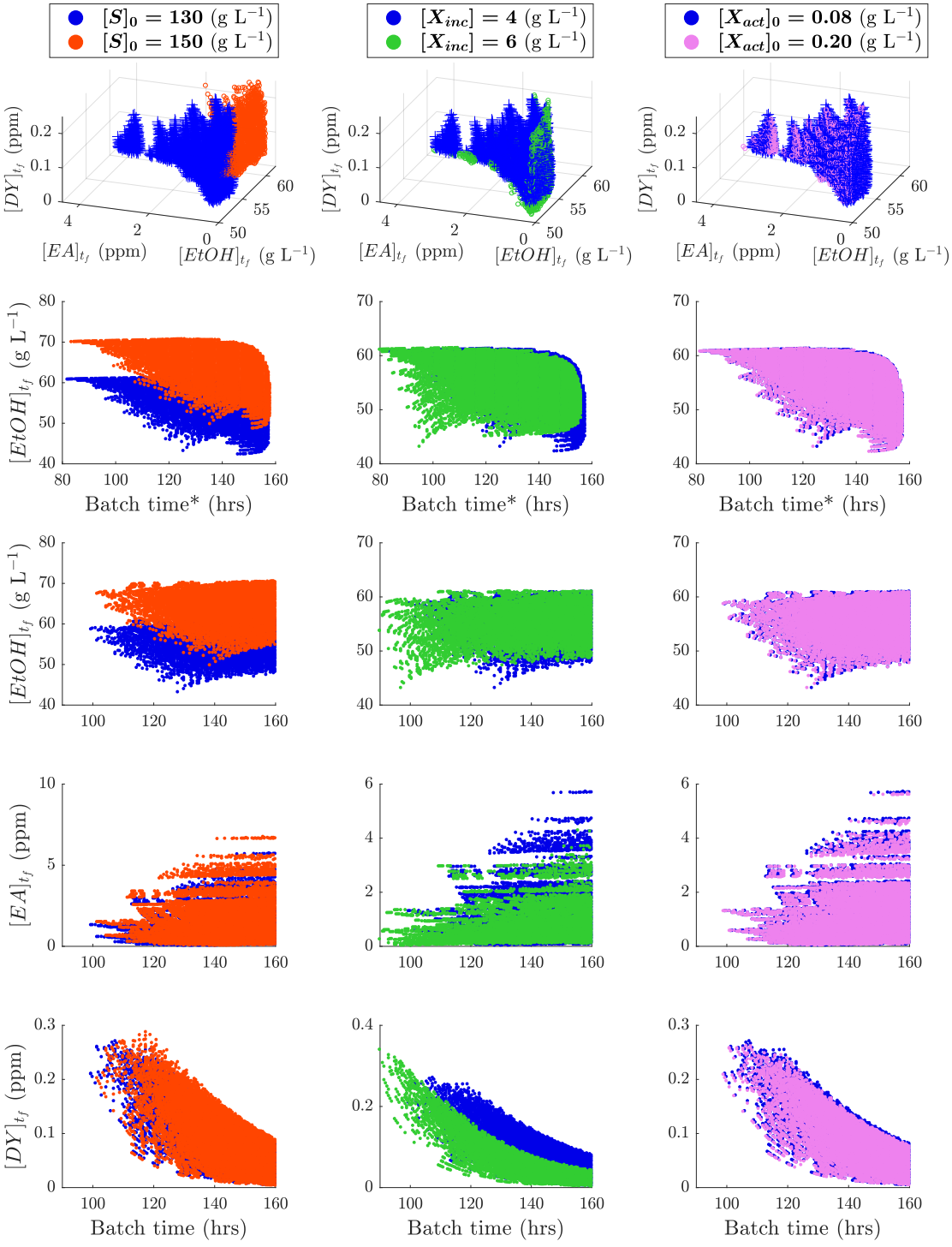

Figure 6.9: Effect of fermentation initial conditions on beer flavour and quality for the set of temperature manipulation profiles.

beer taste. Moreover, identical temperature manipulations require longer fermentation time at higher initial sugar concentrations, due to the inhibition on ethanol production in the relevant ODE (this minimal time penalty is quite acceptable in high-gravity brewing strategies, as it offers the benefit of even higher final product capacity due to the post-processing dilution stage). Both flavour compounds attain higher final concentrations for increased initial sugar concentration, a trend which implies that high-intensity fermentation practice should be monitored judiciously in order to remain safely below taste thresholds. This effect is apparent but limited for $[DY]$ (row 4), and more pronounced for $[EA]$ (row 5) in the entire duration spectrum.

6.2.2 Initial Yeast Concentration (Pitching Rate)

The effect of raising the initial yeast concentration (pitching rate) from 4 to 6 g L^{-1} is highlighted in Fig. 6.9 (column 2). The maximum attainable ethanol concentration barely varies: it is slightly higher for shorter and lower for longer batches, as initial fermentable sugar content is constant for all profiles. Lower pitching rates induce longer fermentation durations, as shown by the consistent black band on the right (row 2); thus, a few more hours are required for most $[EtOH]$ targets. High pitching rates may though induce cases in which short batches yield low $[EtOH]$ concentrations (Guido et al., 2004), even lower than that for low $[X_{INC}]_0$ (grey triangular swarm). Another remarkable observation is that higher pitching rates also yield a few cases in which fermentation is spectacularly accelerated without any discernible loss in attainable ethanol. Flavour compound production levels strongly depend on the initial pitching rate and demonstrate extreme variability. Lower pitching rates induce higher by-product concentrations of diacetyls and ethyl acetate; higher initial yeast loads drastically reduce maximum $[DY]$ and $[EA]$ levels produced. For both pitching rates, the shortest batch times correspond to the highest final concentrations of undesirable compounds. The diacetyl concentration Pareto front (row 4) embodies the trade-off observed for both pitching rates: maximum diacetyl concentration decreases monotonically with batch duration. Higher pitching rates narrow the

$[DY]$ concentration range for all batch times (high $[X_{INC}]_0$ reduces variability by 50%). By-product formation is higher in many faster fermentations, but there is a subset of $T(t)$ profiles which can simultaneously reduce batch durations as well as by-product concentrations.

6.2.3 Active Yeast Cell Fraction

The active yeast fraction value used in previous studies (2%) has been compared to a higher (5%) level (Fig. 6.9 , column 3). Dynamic simulation results indicate remarkable similarity and identical trends for all observables in both $[X_{act}]_0$ cases, with very limited variation seen in all attainable sets ($< 2\%$). Higher initial active cell population marginally reduces the final concentration of undesirable compounds (rows 4-5); nevertheless, this minimal effect is barely discernible and therefore not useful in improving current industrial practice.

6.3 Instantaneous Heat Dynamics

Simulations presented in this chapter have relied upon universal assumption of direct and instantaneous control of fermentor temperature. With the addition of only two more ODEs to the system model the heat transfer dynamics can be approximated. A comprehensive visualisation of the attainable performance maps for key process variables is presented, obtained via a large-scale dynamic simulation campaign of viable heat transfer (cooling) policies. These attainable performance maps are compared to equivalent results produced previously, to elucidate how fermentor performance varies once production scale increases beyond where the assumption of instantaneous temperature control can apply.

The model is extended to consider heat transfer between the exothermic fermentor contents and the surrounding cooling jacket. Eq. 6.33 defines the bulk temperature inside the vessel, where energy generated by sugar fermentation at a rate of (ΔH) heats the wort according to its mean physio-thermal properties (ρ_R, C_{p_r}). The cooling rate is a function of the jacket temperature (T_C), the jacket:fermentor heat transfer area (A_h), overall heat transfer coefficient

Table 6.7: Heat transfer model parameters.

Symbol	Definition	Units	Value
T	Reaction Temperature	°C	-
T_C	Jacket Temperature	°C	-
T_{C_0}	Coolant Feed Temperature	°C	4
F_C	Coolant Feed Rate	$m^3\ hr^{-1}$	-
ΔH	Enthalpy of Reaction	$kJ\ kg^{-1}$	587
ρ_R	Mean Density of Wort	$kg\ m^{-3}$	1030
ρ_C	Density of Coolant	$kg\ m^{-3}$	1042
C_{p_R}	Wort Heat Capacity	$J\ kg^{-1}K^{-1}$	4065
C_{p_C}	Coolant Heat Capacity	$J\ kg^{-1}K^{-1}$	3914.65
A_h	Heat Transfer Area	m^2	221.4
U	Overall Heat Transfer Coefficient	$kJ\ kg^{-1}$	200
V_R	Wort Volume	m^3	400
V_C	Jacket Volume	m^3	3.8

$(OHTC, U)$ and wort volume (V_h). The temperature of the jacket (volume = V_C) is described by Eq. 6.34, cooled with fresh coolant at $(T = T_{C0})$ at a volumetric rate (F_C). Heat losses to the surroundings are negated as the vessel jacket is operating close to ambient conditions.

$$\frac{dT}{dt} = \frac{\frac{dC_S}{dt} \cdot \Delta H}{\rho_R \cdot Cp_R} + \frac{(A_h \cdot U)}{V_R \cdot \rho_R \cdot Cp_R} \cdot (T - T_C) \tag{6.33}$$

$$\frac{dT_C}{dt} = \frac{F_C}{V_C} \cdot (T_{C_0} - T_C) + \frac{(A_h \cdot U)}{(V_C \cdot \rho_C \cdot Cp_C))} \cdot (T_C - T) \tag{6.34}$$

A typical large capacity industrial specification fermenting vessel is modelled. The 400,000 L vessel has a 3,800 L jacket, cooled by a propylene glycol:water mixture. A 4 °C coolant temperature is first assumed, along with an OHTC of 200 W m^{-2} K^{-1}. Table 6.7 details the additional parameter values used in Eq. 6.33 - 6.34 (Scheer, 2014).

6.3.1 Impact on Attainable Performance

Prior work investigating potential for process improvement versus current plant fermentation operation involved an algorithm which rapidly generated and simulated plausible temperature manipulations adhering to realistic operability heuristics, all the while relying on the simplifying assumption that vessel temperature

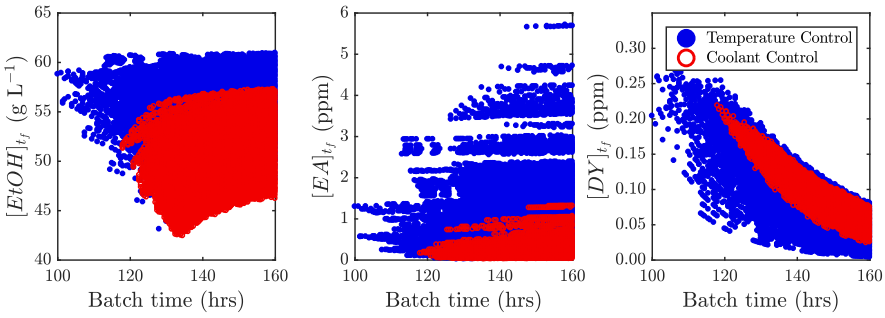

Figure 6.10: Comparison between attainable envelopes: direct $T(t)$ control vs $F(t)$ control.

may be directly manipulated. Attainable performance maps were generated, allowing rapid visualisation of the viable output space permitted by operational modifications. To elucidate how fermentor performance varies once production scale increases beyond the point of the previous simplifying assumption, we perform a similar simulation campaign using the extended model. To exhaustively enumerate comparable performance maps for the most simple cooling policies five discreet coolant rates (F=[0:5:20]) are permitted, which may be only be switched at the end of a 20 hr interval across the 160 hr span considered.

Thus 5^9 = 1,953,125 cooling policies are considered. Figure 6.10 depicts the performance maps from the new cooling policy campaign (red markers) alongside those from Section 6.1, which assumed direct temperature control (blue markers). An immediate observation across all metrics is that the addition of the temperature model considerably reduces the broad range of viable terminal product concentrations, particularly for both the by-product species. This is despite the solution set for coolant control being significantly larger (∼1.9M policies) than that for direct temperature control (∼175k). The observation can be attributed to the fact that in the absence of any external heat source the vessel temperature can only rise from its initial temperature at a rate governed by the exothermic fermentation reaction: there is considerably less scope to vary the vessel temperature during primary fermentation, where the temperature is capped by how quickly it can rise from the reaction enthalpy. This contrasts prior work where the vessel temperature could instantaneously rise as high as 16 °C, something not feasible in practice, leading to a subset of simulations corresponding to very short batch

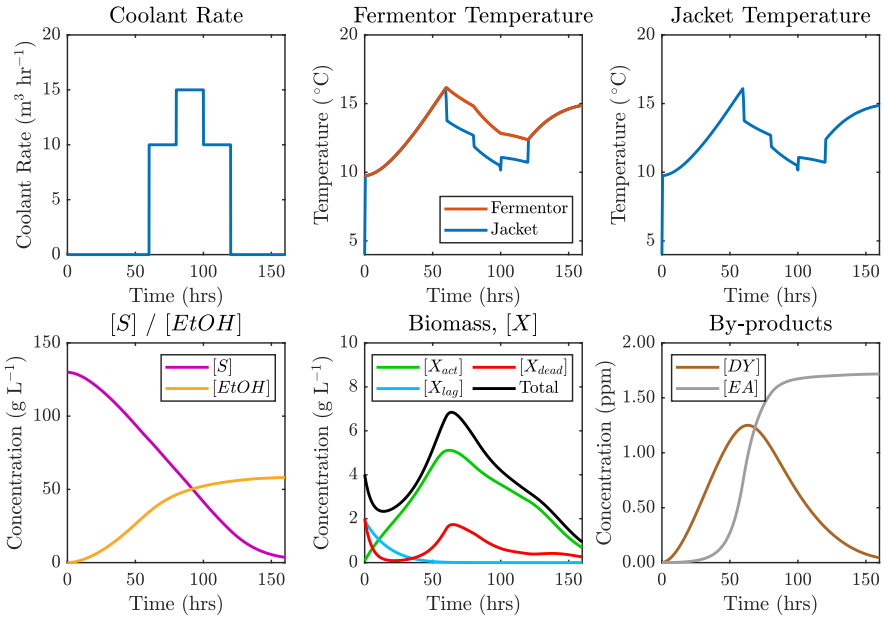

Figure 6.11: Favourable cooling policy from exhaustive simulation set.

times and high by-product concentrations, highlighted by the black markers lying to the upper left of their grey counterparts in Fig. 6.10a. Of all cooling policies considered the most favourable for alcohol maximisation ($J_{min} = -[EtOH]$) is presented in Fig. 6.11 alongside the corresponding state trajectories under this manipulation. Here the preferable approach is to begin cooling the jacket once the temperature exceeds 15 °C after 60 hours, increasing the cooling duty at 80 hours and reducing it at 100 hours before turning the coolant flow off at 120 hours to allow the temperature to rise again. In doing so the active yeast population is effectively managed, preventing the substantial cell death if the temperature were allowed to further rise.

6.4 Chapter Conclusions

Dynamic simulation and visualisation of attainable envelopes of beer fermentation are extremely useful techniques in order to pictorially capture industrial brewing operation protocols, capitalize on embedded organizational knowledge but most notably identify, suggest and evaluate feasible improvements. This thesis chapter employs a widely validated beer fermentation model (de Andrés-Toro et al.,

1998) which has been implemented in order to predict species concentration evolution for any set of initial and operating (temperature profile) conditions; the code has been successfully validated computationally against profiles previously published by other research groups. A range of operating temperature profiles published in the literature have been simulated, and their performance has been assessed using several quantitative indicators of fermentation performance (final concentrations of ethanol and aromatic by-products, batch production time). The trade-off between product quality and batch time is evident: results clearly show that aromatic by-product concentrations can be reduced during longer fermentation. This balance of operational objectives makes the determination of a single optimal temperature a very challenging problem: the latter depends on each brewer's target product composition, and arbitrary target variable weighting appears a popular but also questionable methodology. A simulation-based optimisation procedure has been developed, facilitating the comparison of over 175,000 unique scenarios against the current industrial temperature manipulation. Each scenario represents a unique temperature profile, generated using suitable constraints which are representative of manipulations that are indeed applicable to the real process. This procedure also ensures that the degree of domain discretisation only produces temperature profiles which are implementable, without the need for a secondary smoothing process. A small sacrifice in ethyl acetate concentration (to a level not exceeding the acceptable beer flavour threshold) allows for a considerable reduction of batch time, while maintaining the ethanol and diacetyl concentration levels close to those achieved in the industrial process. Three unique novel manipulations have been identified, each with the potential to drastically reduce batch time (by up to 15 hours), with no discernible impact on beer flavour and quality. A simulated annealing (SA) algorithm has also been developed in order to rapidly investigate the entire solution space and determine the optimal temperature manipulation profile which maximises a weighted objective function considering both ethanol maximisation and batch time minimisation, subject to explicit by-product constraints; several weight assignment cases have been solved and presented, indicating limited result sensitivity to weight value allocation. A novel temperature profile (with a conspicuous heating peak) has

been discovered, indicating that this non-trivial manipulation can reduce fermentation time by 16 hours, but also increase ethanol concentration and maintain by-product concentrations below threshold values.

A multi-dimensional sensitivity analysis of key beer quality attributes versus plausible initial condition modifications for an enormous ensemble (hundreds of thousands of possible temperature manipulation profiles possible for prescription) demonstrates that initial sugar concentration clearly affects final ethanol concentration and thus beer product quality; the most remarkable finding is that fermentation efficiency and batch duration can be improved by manipulating the initial biomass concentration (yeast pitching rate) fed to fermentors. Moreover, what is also noteworthy is that the active fraction of fed yeast has a quite minor (virtually insignificant) effect on process efficiency (as long as a potent yeast strain is used) because the active cell population quickly rises if enough heat is provided by the selected temperature manipulation profile. Exploring and identifying improved temperature profiles enhancing fermentor productivity in tandem with beer quality has been a focal point (Rodman and Gerogiorgis, 2016) which has been further accentuated by the present results. The vast operational space of plausible $T(t)$ profiles has been reduced on the basis of previously published heuristics and explored via large-scale dynamic simulations which have been visualised to identify promising profile improvements. These plots are useful in capturing and mapping differences in current practice (and possible changes) for various products. Consideration of explicit fermentor jacket heat transfer marks a significant improvement over the fidelity of prior work which assumed temperature may freely manipulated. Visualisation of attainable performance reveals that a vast portion of operation cases considered previously are unobtainable on an industrial scale.

Part III

Dynamic Optimisation

Chapter 7

Initialisation Strategies for Effective Dynamic Optimisation

A wide range of optimisation methodologies exist for solving optimal control trajectory problems, as considered in Chapter 1. With most approaches it is necessary to solve iteratively, starting from an initialising solution (often referred to as an initial guess). This chapter presents an investigation into the performance of two different dynamic optimisation strategies for batch beer fermentation temperature control, using different initialisation strategies and solvers. A simultaneous strategy (CVP) with an interior point algorithm is presented first, followed by a complete discretisation (CD) approach: orthogonal collocations on finite elements. The objective function remains from Chapter 6, here with $W_E = 0.75$, $W_t = 0.25$, with the same constraint thresholds dictating the product quality is suitable:

$$J_{min} = -W_E \cdot [E\tilde{t}OH] - W_t \cdot \frac{1}{\tilde{t_f}} \tag{7.1}$$

$$\text{s.t. } [EA]_{t_f} \leq 2 \text{ ppm} \tag{7.2}$$

$$[DY]_{t_f} \leq 0.1 \text{ ppm} \tag{7.3}$$

7.1 Control Vector Parametrisation

The sequential approach to direct dynamic optimisation (often referred to as control vector parametrisation, CVP) involves discretising the control trajectory to a function of a few parameters, while the state equations remain in ODE/DAE form (Biegler et al., 2012). By defining a finite number of equal size piecewise segments within the temperature profile a NLP problem can be formulated for Eqs. 1.2–1.9, which any one of many large scale non-linear programming (NLP) solvers may be applied. Herein function evaluations still invoke integration across the time horizon, as the state trajectories remain continuous.

7.1.1 Control Profile Encoding Strategies

The first encoding applied to describe the $T(t)$ profile is a simple piecewise constant representation, where the decision vector passed to the NLP solver is:

$$d_{PWC} = [T_1, T_2..., T_N, SF] \tag{7.4}$$

Where the corresponding profile consists of Nequal length periods of temperature T_i, of length equal to $t_{max} \cdot SF/N$. The additional variable SF acts to scale the profile length and allow variable process duration, without the requirement to double the problem size by considering each time point as a variable. This is expanded to the piecewise linear case, with the addition of only one further variable:

$$d_{PWL} = [T_1, T_2..., T_N, T_{N+1}, SF] \tag{7.5}$$

Now the profile consists of Nlinear segments between N+1 nodes, again of equal length scaled by SF.

7.1.2 Solution Strategy

Model integration in the CVP method in this work is performed using the ode45 function based on an explicit Runge-Kutta (4, 5) formula, the Dormand-Prince pair (Dormand and Prince, 1980; Shampine and Reichelt, 1997), allowing the

objective to be evaluated and the value reported to the NLP solver applied, computing objective and constraint derivatives numerically. Two NLP solvers are compared: fmincon from the MATLAB optimisation toolbox (Waltz et al., 2006), and the open source Interior Point OPTimizer (IPOPT). IPOPT is a leading open source software package for large-scale non-linear optimisation. It solves general non-linear programming problems of the form:

$$\min_{x \in R^n} f(x) \tag{7.6}$$

$$g_L \leq g(x) \leq g_U \tag{7.7}$$

$$x_L \leq x \leq x_U \tag{7.8}$$

Where $x \in \mathbb{R}^n$ are the optimisation variables (possibly with lower and upper bounds, $x_L \in (\mathbb{R} \bigcup -\infty)^n$ and $x_U \in (\mathbb{R} \bigcup +\infty)^n$, $f : \mathbb{R}^n \to \mathbb{R}$ is the objective function, and $g : \mathbb{R}^n \to \mathbb{R}^m$ are the general non-linear constraints. The functions $f(x)$ and $g(x)$ can be linear or non-linear and convex or non-convex. The constraints, $g(x)$, have lower and upper bounds, $g_L \in (R \bigcup -\infty)^m$ and$g_U \in (R \bigcup +\infty)^m$. Equality constraints of the form $g_i(x) = \bar{g}_i$ are treated as inequality constraints with equal lower and upper bounds: $g_i^U = g_i^L = \bar{g}_i$. IPOPT implements an interior point line search filter method that determines a local solution of Eqs. 7.6–7.8. Details of the full mathematical algorithm can be found in several publications (Wachter, 2003; Wächter and Biegler, 2005, 2006; Nocedal et al., 2009). Both IPOPT and fmincon has been called via OPTI's MATLAB® toolbox (Currie et al., 2012) for the CVP portion of this Chapter.

7.1.3 Results

7.1.3.1 Piecewise Constant Control Profiles

Profiles which are piecewise constant between discreet time points are first computed to investigate the performance of the algorithm and its sensitivity to the input initial guess (initialising solution, T^0), and as to how performance is affected by varying the degree of discretisation (N). To achieve this a range of cases are

systematically considered: four discretisation levels have been considered: $N = [3, 6, 12, 18]$ along with four isothermal initialising solutions: T^0 (°C) = [11, 12, 13, 14], producing 16 permutations to be solved in turn. The optimal profile computed in each case is shown in Fig. 7.1, with the performance criteria from each case shown in Fig. 7.2 using MATLAB's fmincon solver. The equivalent results are also shown in Fig. 7.3–7.4, where the only difference is that IPOPT is now used for solving the NLP. The performance of each solution presented from the CVP method is tabulated in Table 7.1.

Effect of Initialising Temperature Profile Computed optimal control profiles on an identically discretised $T(t)$ domain for numerous initialising temperature profiles can be seen in each column in Figs. 7.1 and 7.3. From top to bottom isothermal profiles at 11, 12, 13 and 14 °C were used for the initial iteration respectively. It is observed that the same general solution form is produced in all cases presented from this method. This tends initially to the highest permitted temperature for the first stages of the process (16 °C) to accelerate the yeast growth and promote fermentation immediately. For the solutions from fmincon (Fig. 7.1) this is followed by a sudden drop in temperature, below 10 °C, before climbing back over 15 °C and subsequently re-dropping. Differences between the four solutions in each column (same N) demonstrate how the solver is exhibiting relatively significant sensitivity to the initialisation profile. As such it is evident that the method employed is unable to converge to global optimality, using the fmincon solver. In contrast, the profiles produced via PWC CVP with IPOPT show a slightly different solution: again starting the process at the maximum permitted temperature, but rather than a sudden drop, a parabolic-like temperature 'dip' is observed. The temperature is reduced only to 13 °C over approximately 20 hours, before gradually heating back to 16 °C in a symmetric fashion. The solution profiles obtained via IPOPT (Fig. 7.3) no longer show sensitivity to the initialisation, converging to the same solution profile for all initialisations, suggesting the algorithm is more robust and less dependent on selecting a favourable seed solution. The industrial practicalities of fine manipulations to the temperature of the bulk vessel contents should be noted. While the large batch fermentors

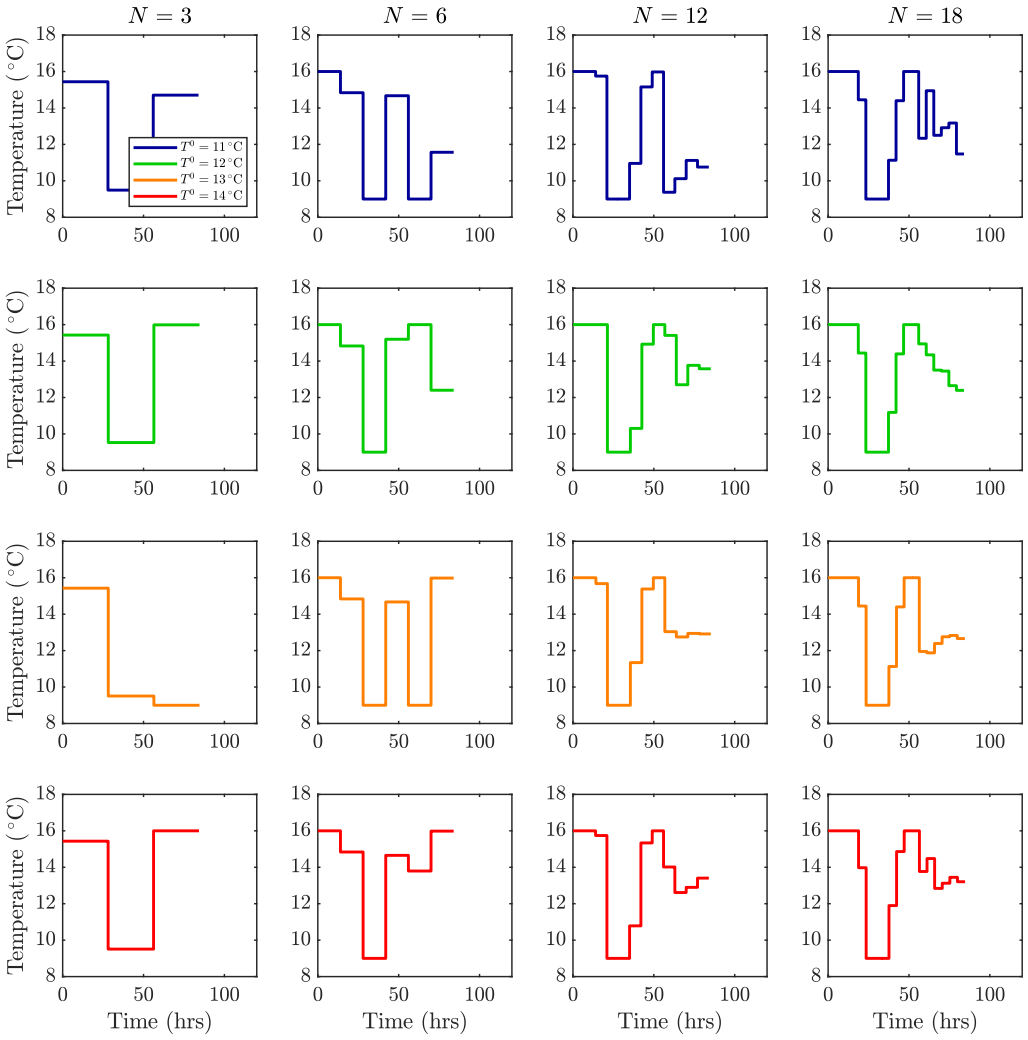

Figure 7.1: CVP $T(t)$ solutions: PWC with fmincon.

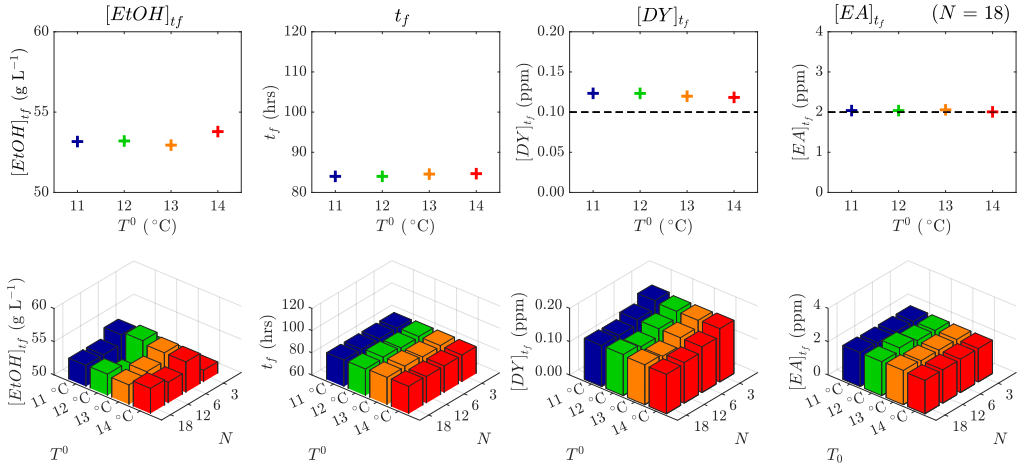

Figure 7.2: Performance metrics of CVP $T(t)$ solutions: PWC with fmincon.

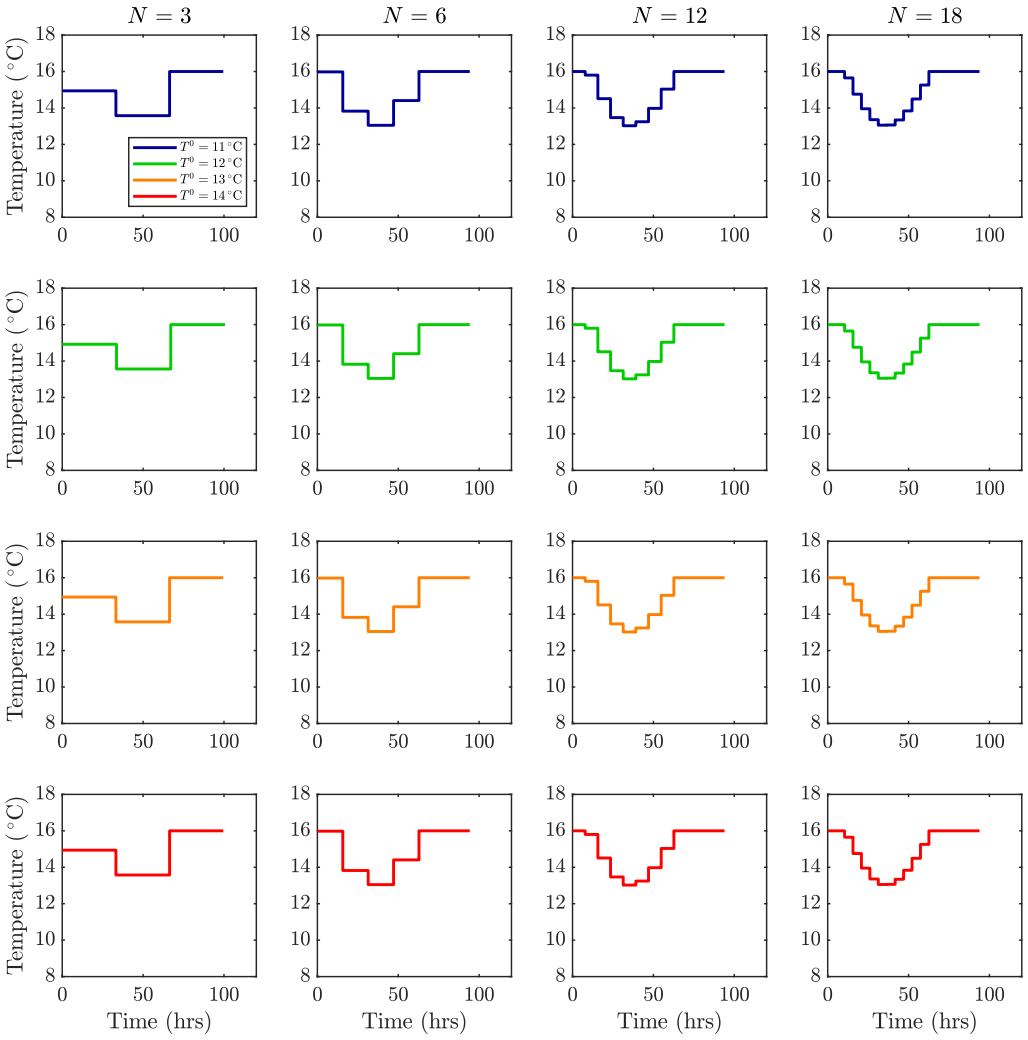

Figure 7.3: CVP $T(t)$ solutions: PWC with IPOPT.

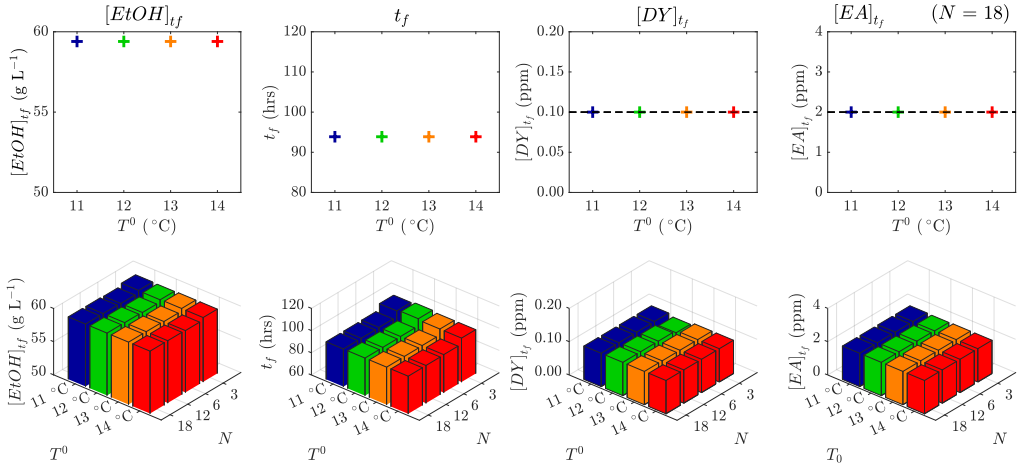

Figure 7.4: Performance metrics of CVP $T(t)$ solutions: PWC with IPOPT.

used for industrial scale brewing are capable of accurately regulating temperature, temperature gradients inevitably exist and manipulations < 0.5 °C likely lie within the unavoidable variation present throughout the tank, having implications on the accuracy of model predictions.

Effect of Increasing Time Domain Discretisation To access the effect of increasing the discretisation level of the control profile, the computed results for $N = 3$, 6, 12 and 18 (representing the number of equispaced time segments in which the fermentor temperature is piecewise constant) are shown in each row Figs. 7.1 and 7.3 for a specific initialising isothermal temperature and NLP solver. In both cases it is observed that increasing N does not drastically alter the solution form, rather a gradual refinement is observed. This is particularly true for the IPOPT profiles (Fig. 7.3) which appear to tend towards a smooth parabola as the discretisation increases. Improvements in objective function value become marginal once N exceeds 6 suggesting that optimality is being approached for the specific objective and that perhaps little value exists in increasing discretisation drastically. A trade-off exists as the required CPU time for computing the profiles increases rapidly with increasing discretisation level, so unnecessary discretisation is undesirable. It is noteworthy that the majority of profiles produced from CVP with an IPOPT are not highly changeable in form. That is to say there is minimal abrupt changes in temperature so no secondary smoothing procedure is required, which often the case with stochastic techniques (Carrillo-Ureta et al., 2001; Xiao et al., 2004) which often computed abrupt changes in the control profile which would not be attainable in a real world application.

Control Profile Performance The upper rows in Fig. 7.2 and Fig. 7.4 compares the performance of the profiles computed for $N = 18$ with each initialising isothermal profile considered. The second row of plots in these figures considers a third axis to simultaneously visualise the effect of both discretisation level and initialising profile on the resulting fermentation performance. These results produced with IPOPT (Fig. 7.4) demonstrate effective independence to the initialisation profile and the discretisation level, once N is increased past 6. In contrast

Fig. 7.2 shows how the results produced with fmincon are highly variable. It is observed that the ethanol concentration varies non-monotonously when N is increased for all values of T^0. Surprisingly, all solutions where $N = 6$ with fmincon produce a greater ethanol yield than any of those under greater discretisation, indicating a local solution has been reached which was not found in the other N cases. The product concentrations of undesirable fermentation by-products are shown in the right half of Figs. 7.2 and 7.4. It is apparent that the ethyl acetate concentration constraint is universally fulfilled, however the constraint imposed on the diacetyl concentration consistently violated in the solutions from fmincon solver (Eq. 7.3) in Fig. 7.2 panel 7. The algorithm has converged at unfeasible solutions due to not being able to fulfil the imposed constraint the objective, rendering their little reason to progress to higher. The product concentration of $[DY]$ is shown to systematically drop with N, however even when $N = 18$ the constrained is still violated (Fig. 7.2 panel 3). In contrast the solutions obtained by the IPOPT solver are able to meet all constraints imposed (Fig. 7.4), outperforming all solutions from fmincon.

7.1.3.2 Piecewise Linear Control Profiles

The equivalent result plots to Figs. 7.1–7.4 for the PWL profile encoding (Eq. 7.5) are presented in Figs. 7.5–7.8. It is apparent that such instantaneous temperature gradients as shown in Fig. 7.1 are not attainable in large scale process equipment. Piecewise linear profiles are computed using the same methodology, as to see how these more readily implementable solutions compare to the more simple piecewise constant profiles, and if the additional degrees of profile freedom will enable constraint satisfaction across the range of N and T^0 considered. The same 16 cases have been solved in turn: $N = [3, 6, 12, 18]$, T^0 (°C) $= [11, 12, 13, 14]$, the optimal profile computed in each case is shown in Fig. 7.5, with the performance criteria from each case shown in Fig. 7.6 from the fmincon solver, with the IPOPT equivalent in Fig. 7.7–7.8. Comparing Fig. 7.5 to Fig 7.1 and Fig. 7.7 to Fig 7.3 shows how the profiles differ for equivalent N and T^0 between piecewise linear and piecewise constant for each solver. It can be seen that the profile

Table 7.1: Performance of presented CVP solutions.

Figure	Optimisation Method	Initialisation Profile	N	J_{min}	$[EtOH]$ (g L^{-1})	t_f (hrs)	$[DY]$ (ppm)	$[EA]$ (ppm)
7.1	CVP PW Constant fmincon Isothermal T^0	11 °C	3	-0.93	51.68	84.00	0.16	2.00
			6	-0.96	54.60	84.00	0.14	2.01
			12	-0.95	53.17	84.00	0.12	2.00
			18	-0.95	53.17	84.00	0.12	2.04
		12 °C	3	-0.93	51.80	84.60	0.16	2.00
			6	-0.97	55.06	84.00	0.14	2.03
			12	-0.92	51.47	85.20	0.11	2.24
			18	-0.95	53.20	84.00	0.12	2.04
		13 °C	3	-0.93	51.76	84.60	0.16	2.00
			6	-0.96	54.60	84.00	0.14	2.01
			12	-0.94	53.35	85.20	0.11	2.00
			18	-0.94	52.95	84.57	0.12	2.06
		14 °C	3	-0.93	51.74	84.30	0.16	2.00
			6	-0.96	54.59	84.00	0.14	2.01
			12	-0.94	53.11	84.00	0.12	2.00
			18	-0.95	53.79	84.67	0.12	2.01
7.3	CVP PW Constant IPOPT Isothermal T^0	11 °C	3	-0.98	59.70	99.56	0.10	2.00
			6	-0.99	59.32	94.22	0.10	2.00
			12	-0.99	59.38	93.97	0.10	2.00
			18	-0.99	59.40	93.87	0.10	2.00
		12 °C	3	-0.98	59.64	100.66	0.09	1.98
			6	-0.99	59.32	94.22	0.10	2.00
			12	-0.99	59.38	93.97	0.10	2.00
			18	-0.99	59.40	93.87	0.10	2.00
		13 °C	3	-0.98	59.70	99.56	0.10	2.00
			6	-0.99	59.32	94.22	0.10	2.00
			12	-0.99	59.38	93.97	0.10	2.00
			18	-0.99	59.40	93.87	0.10	2.00
		14 °C	3	-0.98	59.70	99.56	0.10	2.00
			6	-0.99	59.32	94.21	0.10	2.00
			12	-0.99	59.38	93.97	0.10	2.00
			18	-0.99	59.40	93.87	0.10	2.00
7.5	CVP PW Linear fmincon Isothermal T^0	11 °C	3	-0.98	56.00	84.00	0.19	2.00
			6	-0.95	53.26	84.00	0.14	1.40
			12	-0.96	54.61	84.00	0.13	2.00
			18	-0.95	53.64	84.00	0.12	2.03
		12 °C	3	-0.98	56.01	84.00	0.19	2.00
			6	-0.95	53.27	84.00	0.14	1.40
			12	-0.96	54.61	84.00	0.13	2.00
			18	-0.95	53.61	84.00	0.12	2.03
		13 °C	3	-0.98	56.01	84.00	0.19	2.00
			6	-0.95	53.28	84.00	0.14	1.40
			12	-0.96	54.65	84.00	0.13	2.00
			18	-0.95	53.42	84.60	0.12	2.04
		14 °C	3	-0.98	56.01	84.00	0.19	2.00
			6	-0.94	53.33	85.20	0.13	1.44
			12	-0.96	54.51	84.00	0.13	2.00
			18	-0.95	53.57	84.64	0.12	1.98
7.7	CVP PW Linear IPOPT Isothermal T^0	11 °C	3	-0.98	59.96	98.99	0.10	2.00
			6	-0.99	59.32	93.78	0.10	2.00
			12	-0.99	59.40	93.80	0.10	2.00
			18	-0.99	59.39	93.73	0.10	2.00
		12 °C	3	-0.98	59.96	98.99	0.10	2.00
			6	-0.99	59.32	93.78	0.10	2.00
			12	-0.99	59.40	93.80	0.10	2.00
			18	-0.99	59.39	93.73	0.10	2.00
		13 °C	3	-0.98	59.96	98.99	0.10	2.00
			6	-0.99	59.32	93.78	0.10	2.00
			12	-0.99	59.40	93.80	0.10	2.00
			18	-0.99	59.39	93.73	0.10	2.00
		14 °C	3	-0.98	59.96	98.99	0.10	2.00
			6	-0.99	59.32	93.78	0.10	2.00
			12	-0.99	59.40	93.80	0.10	2.00
			18	-0.99	59.39	93.73	0.10	2.00

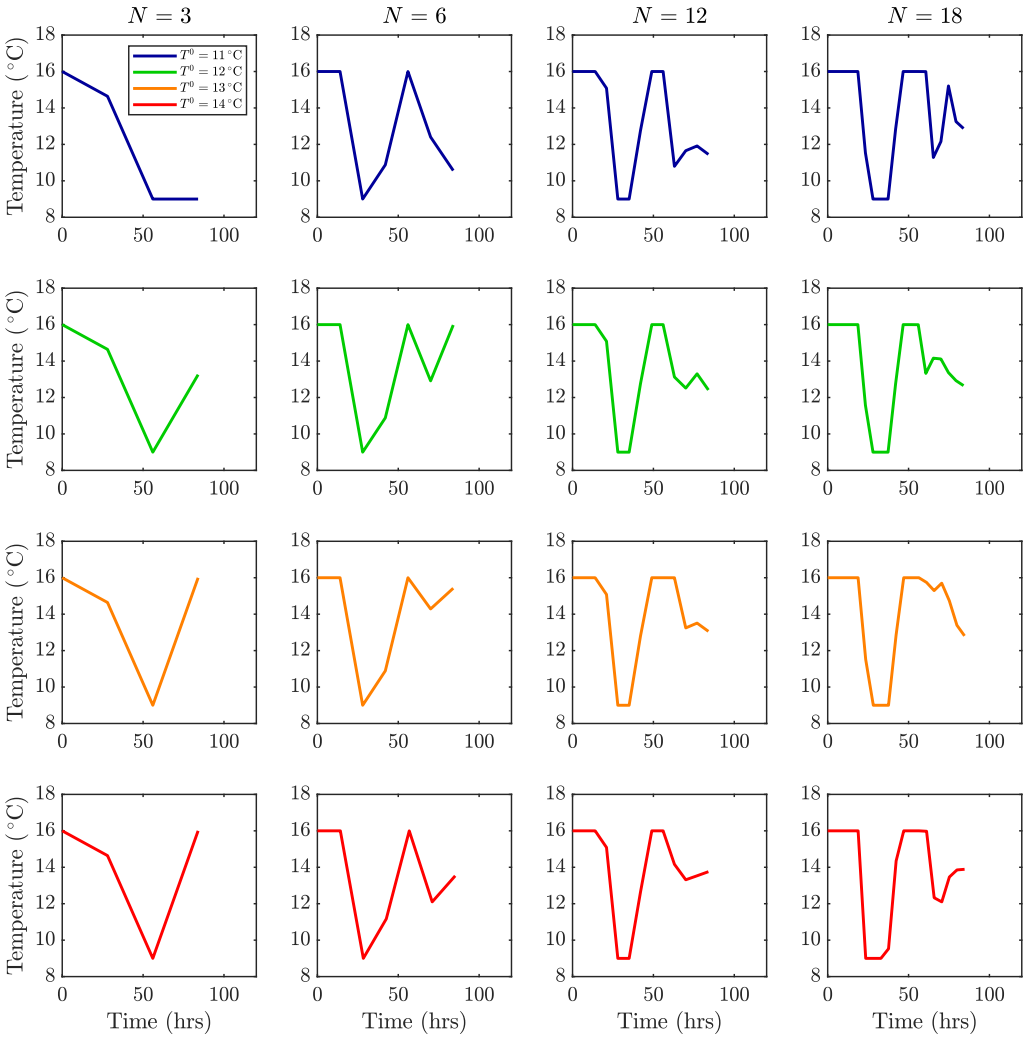

Figure 7.5: CVP $T(t)$ solutions: PWL with fmincon.

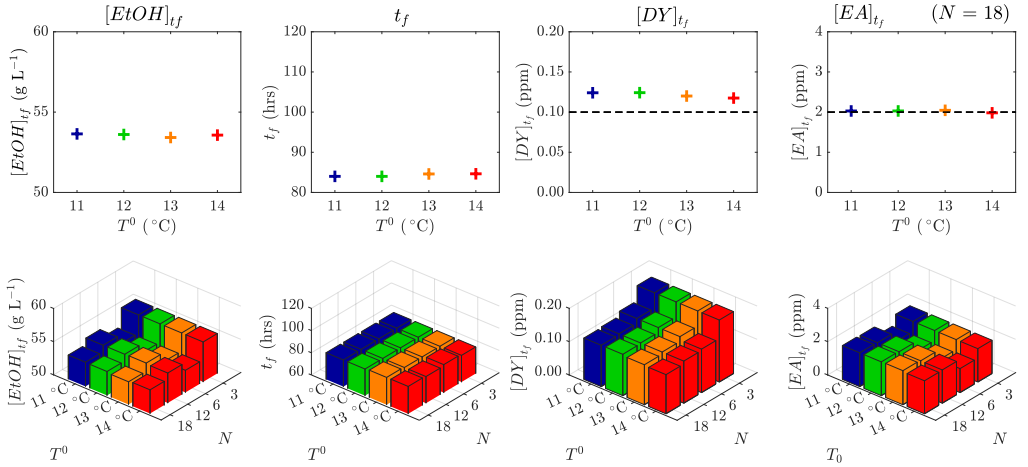

Figure 7.6: Performance metrics of CVP $T(t)$ solutions: PWL with fmincon.

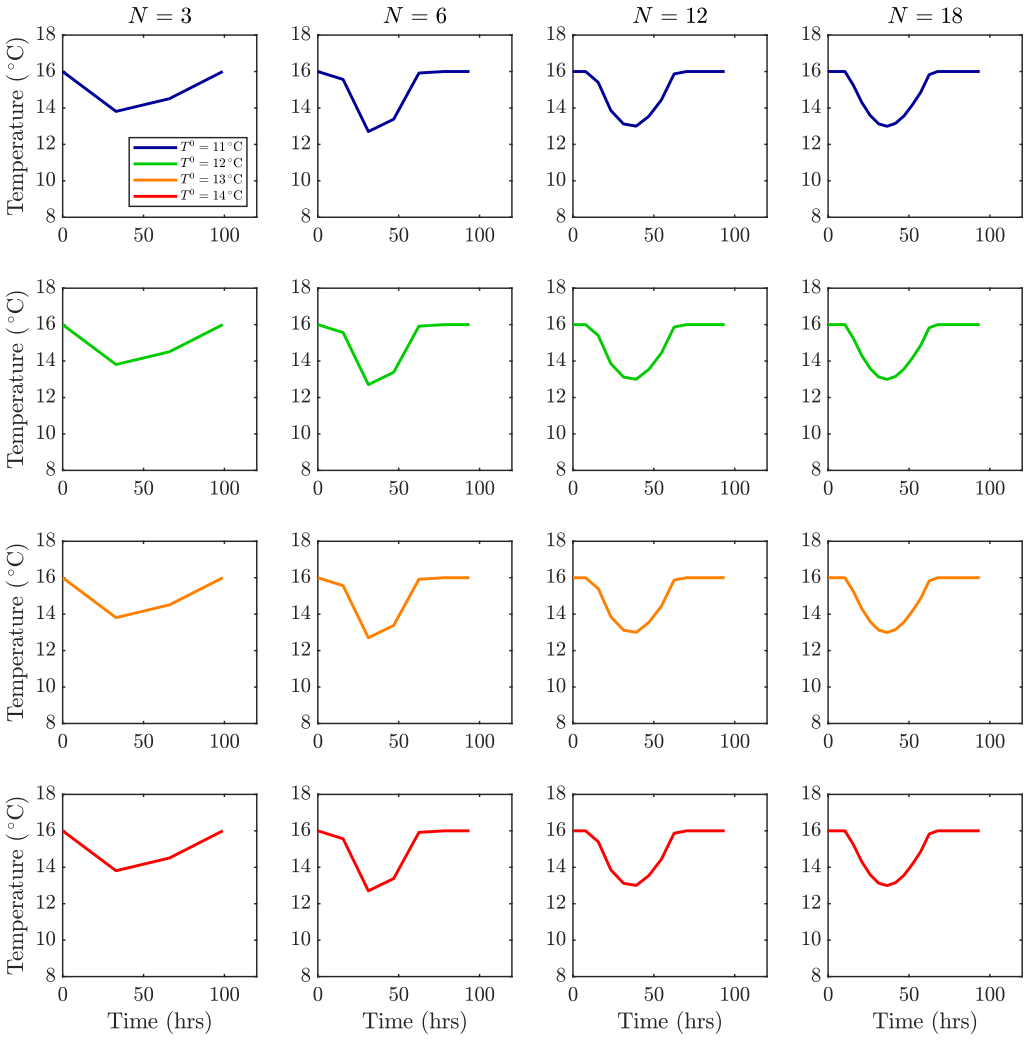

Figure 7.7: CVP $T(t)$ solutions: PWL with IPOPT.

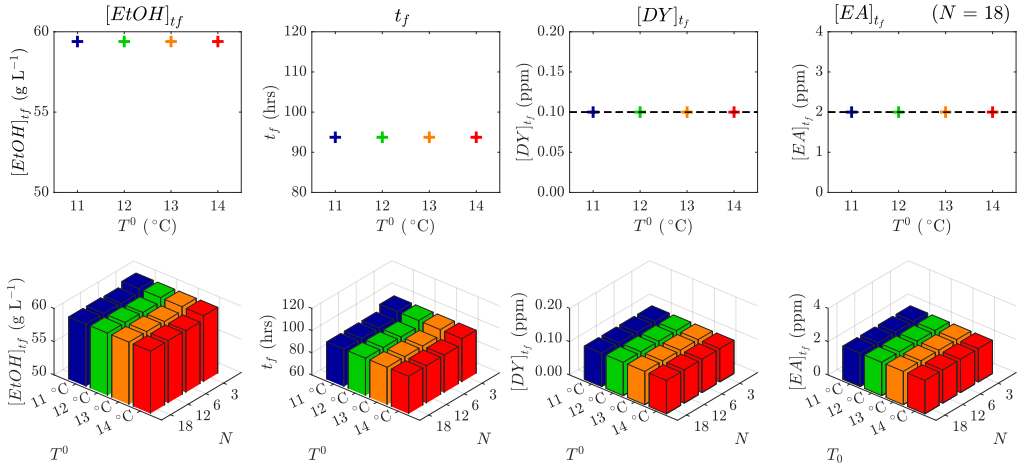

Figure 7.8: Performance metrics of CVP $T(t)$ solutions: PWL with IPOPT.

forms are extremely similar, with intermediate cooling prevailing as a strategy for optimal fermentation performance. The PWL solutions appear to mirror the PWC solutions, now with gradual and sustained temperature manipulations in place of instantaneous ones. Once more the solutions produced via fmincon are unable to satisfy the $[DY]$ threshold (Fig. 7.6), despite reducing this value as N increases. The ethanol yield also shows surprising behaviour, now producing the highest concentration when $N = 3$, followed by $N = 12$. In contrast again, results from IPOPT do not show such sensitivity to initialisation, or discretisation (once $N > 3$) with the profiles presented in Fig. 7.7 very closely resembling those in Fig. 7.3, with the benefit of being more readily realisable due to the lack of instantaneous temperature manipulations. While prescribing a profile with large instantaneous jumps in temperature may be challenging to realise in industrial practice, it is in fact considerably easier for an operator to input a PWC strategy as a vector of set points for plant equipment, in place of a continuous function which shall require many more set points to follow.

7.2 Complete Discretisation

7.2.1 Collocation on Finite Elements

An alternative direct method for dynamic optimisation (a simultaneous strategy) has also been performed in this study. Orthogonal polynomials on finite elements are used to approximate the control and state trajectories, allowing the continuous problem to be converted to NLP form. Implementation has been performed using the DynOpt package for MATLAB (Cizniar et al., 2005). The DAE system is converted to a system of algebraic equations, where decision variables of the derived NLP problem are the coefficients of the linear combinations of these AEs. Precision is known to vary with collocation point locations and element lengths used (Tanartkit and Biegler, 1995; Logsdon and Biegler, 1989). The methodology is to approximate the state variables with Lagrange polynomials

over each element, i:

$$\boldsymbol{x}_{K_x}(t) = \sum_{j=0}^{K_x} \boldsymbol{x}_{ij}\phi_j(t) \tag{7.9}$$

Where ϕ_j is defined by:

$$\phi_j(t) = \prod_{k=0,j}^{K_x} \frac{(t - t_{ik})}{(t_{ij} - t_{ik})} \tag{7.10}$$

Similarly the control trajectory is approximated by:

$$\boldsymbol{u}_{K_u}(t) = \sum_{j=1}^{K_u} \boldsymbol{u}_{ij}\theta_j(t) \tag{7.11}$$

Where θ_j is defined as follows:

$$\theta_j(t) = \prod_{k=1,j}^{K_u} \frac{(t - t_{ik})}{(t_{ij} - t_{ik})} \tag{7.12}$$

With $k = 0, j$ representing k starting form 0 and that $k \neq j$. Wherex_{K_x} is a piecewise polynomial of order Kx+1, u_{K_x} is a piecewise polynomial of order Ku+1. Figure 7.9 shows orthogonal collocation with $K = Kx = Ku$: defining basis functions so that they are normalised over each profile element, $\Delta\xi_i$, such that the residual equation becomes:

$$\Delta\xi_i r(t_{ik}) = M\sum_{j=0}^{K_u} x_{ij}\phi_j(\tau_k) - \Delta\xi f(t_{ik}, x_{ik}, u_{ik}, p) \tag{7.13}$$

Which may be evaluated at shifted roots of Legendre polynomials.

The NLP formulation now consists of the beer fermentation ODE model discretised as a finite element approximation, continuity equations for state variables and the inequality constraints on the system, and is compatible with the same NLP solvers applied in the partial discretisation (CVP) approach, fmincon and IPOPT. Both solvers are applied once more, with shall also help understand whether IPOPTs superior performance in the CVP problem was a consequence of the formulation, or the solver being superior in general. Similarly to the CVP solution set, a range of discretisation levels (N) and initialising profiles (T^0)

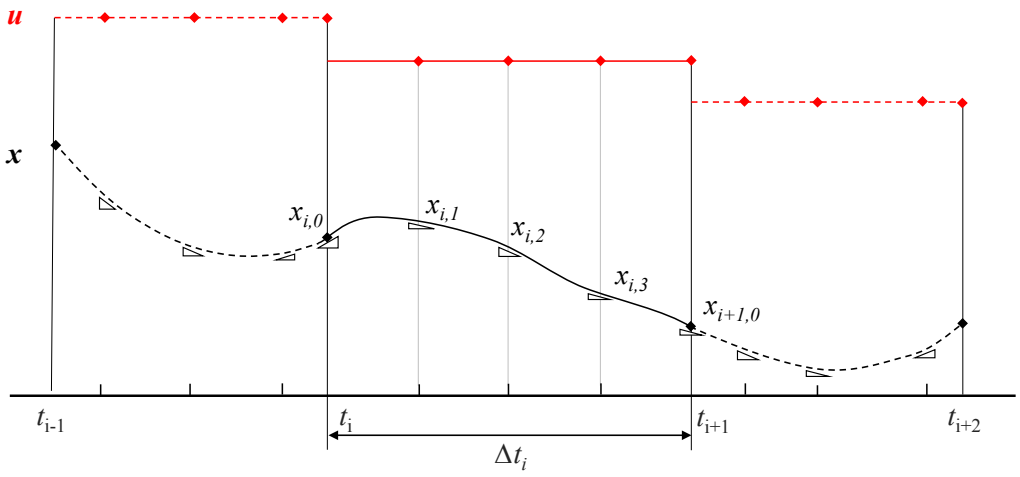

Figure 7.9: Collocation method for state and control profiles.

are considered: N = [6: 6: 36], T^0 (°C) = [11, 12, 13, 14]. Three collocation points have been used for state trajectories, with one collocation point being used for control profiles, resulting in the computation of profiles which are piecewise-constant. For both solvers considered, objective and constraint gradients are defined analytically, requiring no finite difference approximations as the solver iterates.

7.2.2 Results

The methodology described above has been used to compute control profiles for 6 levels of temporal domain discretisation (N = [6, 12, 18, 24, 30, 36]) along with four isothermal initialising solutions, T^0 (°C) = [11, 12, 13, 14], producing 24 permutations solved in turn. The solution profiles produced with the fmincon solver are presented in Figure 7.10, while the equivalent solution profiles from IPOPT are given in Figure 7.11. The performance of all presented CD solutions is tabulated in Table 7.3.

Comparing Fig. 7.10 (simultaneous) with Fig. 7.1 (sequential) shows the differing profile forms favoured by the two methods employing the fmincon NLP solver. The differences are relatively significant: the sequential (CVP) profiles show a very drastic temperature drop, meanwhile the results obtained from CD favour a less significant and more gradual temperature reduction and re-heating, akin to the parabolic CVP solutions from IPOPT (Fig. 7.3). The primary differ-

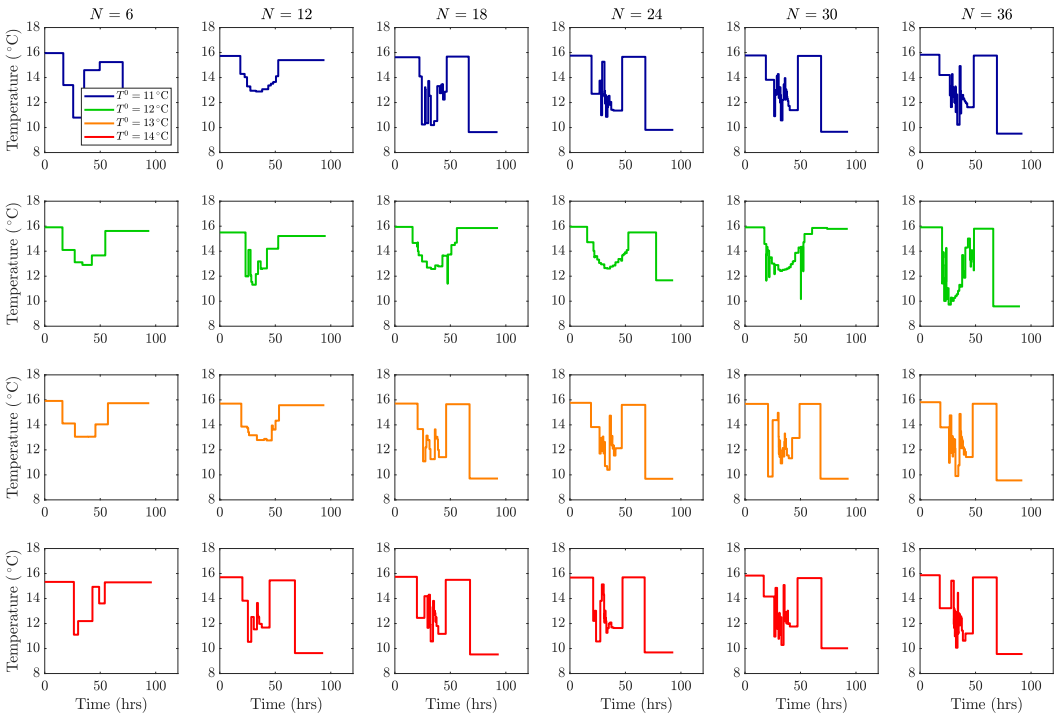

Figure 7.10: CD $T(t)$ solutions: Isothermal T^0, PWC with fmincon.

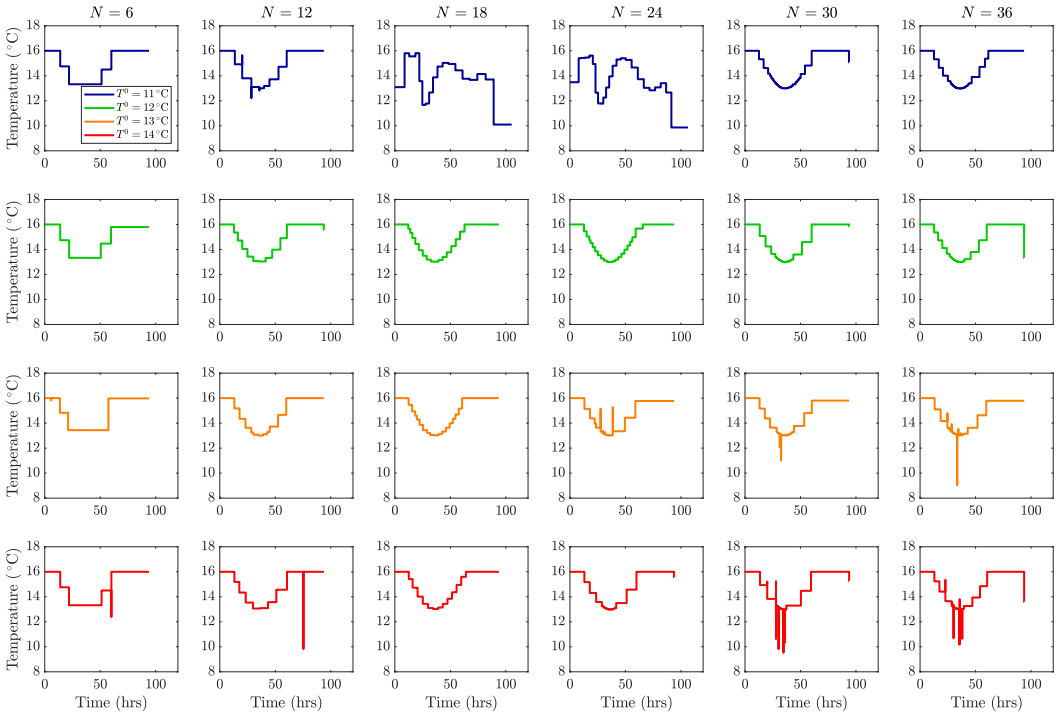

Figure 7.11: CD $T(t)$ solutions: Isothermal T^0, PWC with IPOPT.

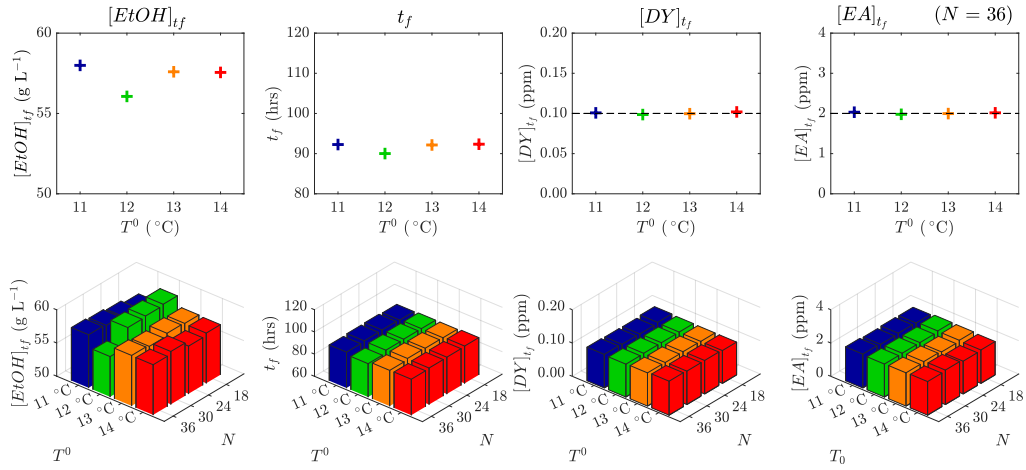

Figure 7.12: Influence of discretisation level (N) and initialising isothermal profile (T^0) on profile performance - CD with fmincon.

ence is that most of the solutions in Fig. 7.10 exhibit extremely rapidly fluctuating temperature during the 'dip' portion, as the solver struggles to converge. Excluding this discrepancy, the profile form is similar in the IPOPT solution set (Fig. 7.11), which are essentially identicle to those produced in the CVP IPOPT case (Fig. 7.3), and believed to be the globally optimal solution to this specific problem. The primary exception are the two outlier cases in Fig. 7.11 ($T^0 = 11$ °C; $N = 18$–24). In only these two cases an alternative solution is produced, somewhat similar to those observed in Fig. 7.1. This local solution is less favourable than the other cases presented, highlighting that the IPOPT solver can also exhibit sensitivity to the initialisation profile in certain circumstances and get trapped in less favourable local solutions. Additionally, select IPOPT CD solutions show artefacts of the solution method, whereby instantaneously the temperature profile goes up and down (vertical lines off the profile path). Such behaviour is observed in solutions for $T^0 = 13$ and 14 °C, particularly at higher N, however this has no bearing on the performance of the profile or the solution method, and can be readily removed from the profile prior to implementation.

Control Profile Performance The upper row in Figs. 7.12–7.13 compares the performance of the profiles computed for $N = 36$ with each initialising isothermal profile for the fmincon and IPOPT solvers respectively. The second row of plots in these figures considers a third axis to simultaneously visualise the effect

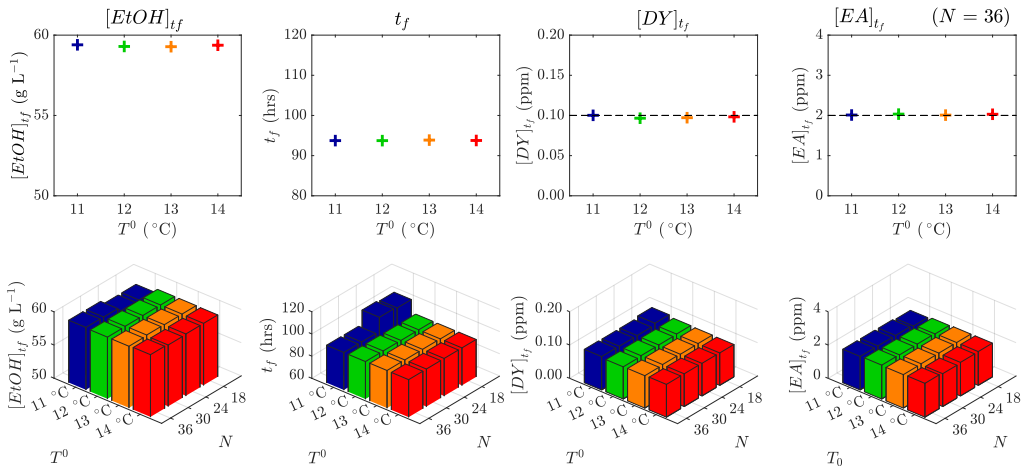

Figure 7.13: Influence of discretisation level (N) and initialising isothermal profile (T^0) on profile performance - CD with IPOPT.

of both discretisation level and initialising profile on the resulting fermentation performance. Firstly looking at the fmincon solutions (Fig. 7.12), it is now shown that all by-product constraints are universally satisfied, such that all solutions obtained are feasible. It is also shown that aside from ethanol concentration, the performance of all solution profiles do not have significant differences in any other metric. The unusual trend in ethanol concentration obtained with different N and T^0 can be understood by looking at the profiles in Fig. 7.10. The greatest ethanol concentration is produced when $T^0 = 12$ °C, and only when $N = 18$–30. The corresponding profiles are those which show the least erratic variations around the 'dip', and closely resemble the profiles which have been obtained IPOPT in Fig. 7.11. Interestingly this was not reproduced when N was increased to 36, as this solution now resembles the inferior strategy favoured in Figs. 7.1 (fmincon CVP). In contrast to the fmincon performance plots, the corresponding plots from IPOPT (Fig. 7.13) show no variation in any metric with T^0 or N, with the exception being the two profiles highlighted above for having a different form ($T^0 = 11$ °C; $N = 18$–24). Panel 6 in Fig. 7.13 highlights these outliers, showing that these profiles require significantly greater batch times, and are this significantly inferior solutions, outperformed by both lower and higher N solutions for the same T^0. While CD with IPOPT appears to be the most favourable strategy considered, the method shows some sensitivity to the initial-

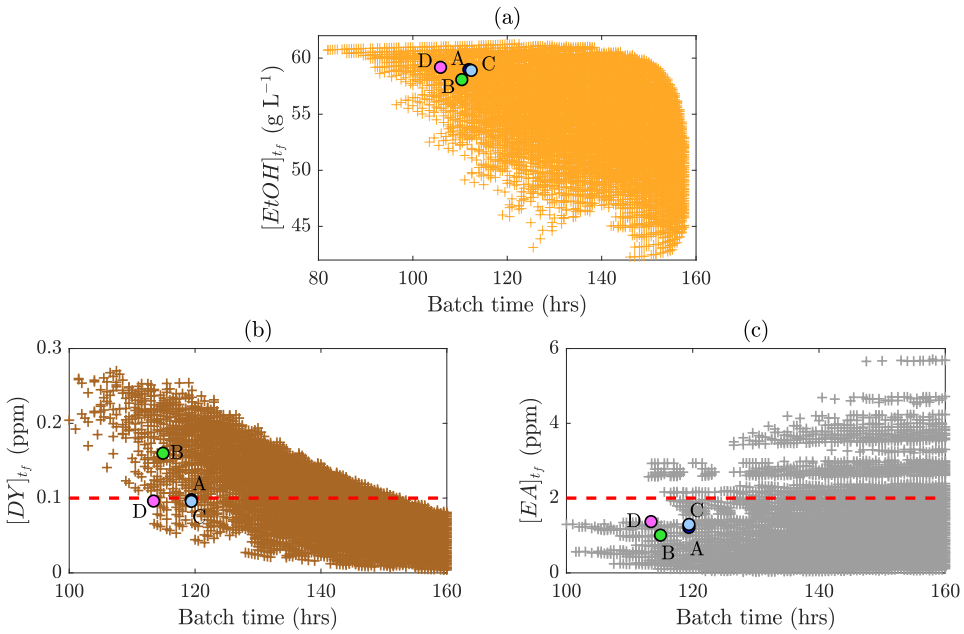

Figure 7.14: Performance of promising profiles from exhaustive simulation.

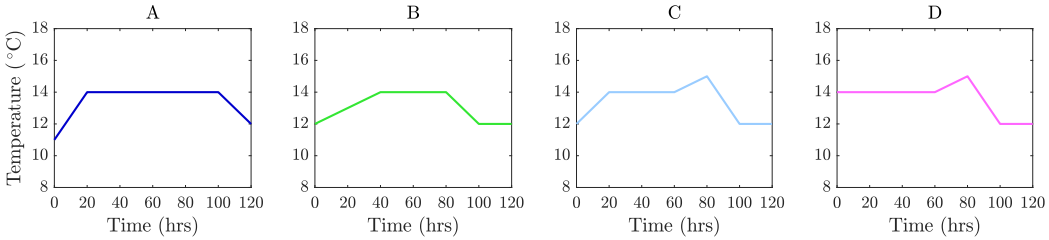

Figure 7.15: Promising profiles from exhaustive simulation for initialisation.

isation profile supplied to the optimiser, which can be problematic when it is not know whether solutions generated are inferior to undiscovered global optima.

7.2.3 Initialisation with Promising Candidate Profiles

Initialising with isothermal profiles may be considered as a means to assess the blind performance of the optimisation strategies. This can be highly beneficial not only in assessing the algorithm performance, but also in preventing the narrowing of the attainable solution space by starting in the vicinity of local solutions. It is however shown that for the beer fermentation problem the solutions produced from isothermal initialisations, specifically when using fmincon, are of limited applicability, due to their highly changeable nature. It is now desirable to take solutions already showing promise, and see how the optimisation algorithm per-

Table 7.3: Performance of presented CD solutions.

Figure	Optimisation Method	Initialisation Profile	N	J_{min}	$[EtOH]$ (g L^{-1})	t_f (hrs)	$[DY]$ (ppm)	$[EA]$ (ppm)
7.10	CD PW Constant fmincon Isothermal T^0	11 °C	6	-0.97	58.06	95.78	0.10	2.01
			12	-0.99	59.22	94.32	0.10	1.92
			18	-0.97	57.02	92.52	0.10	1.99
			24	-0.97	57.52	93.15	0.10	2.01
			30	-0.97	57.81	92.89	0.10	1.98
			36	-0.98	57.99	92.26	0.10	2.03
		12 °C	6	-0.99	59.33	94.20	0.10	2.04
			12	-0.98	58.70	95.43	0.10	1.92
			18	-0.99	59.18	92.97	0.10	2.06
			24	-0.99	58.99	93.01	0.10	1.99
			30	-0.99	58.84	92.63	0.10	1.99
			36	-0.96	56.06	90.01	0.10	1.98
		13 °C	6	-0.99	59.26	94.19	0.10	2.02
			12	-0.99	59.17	94.22	0.10	2.00
			18	-0.97	57.65	92.93	0.10	2.04
			24	-0.97	57.75	93.04	0.10	1.98
			30	-0.97	57.37	93.36	0.10	2.03
			36	-0.97	57.59	92.15	0.10	2.00
		14 °C	6	-0.98	58.76	96.50	0.10	1.99
			12	-0.97	57.69	93.14	0.10	2.05
			18	-0.97	57.56	93.61	0.10	2.00
			24	-0.97	57.18	93.13	0.10	1.97
			30	-0.98	57.96	92.90	0.10	2.07
			36	-0.97	57.55	92.34	0.10	2.02
7.11	CD PW Constant IPOPT Isothermal T^0	11 °C	6	-0.99	59.33	93.94	0.10	1.96
			12	-0.99	59.35	93.81	0.10	1.98
			18	-0.95	58.76	105.24	0.10	1.93
			24	-0.95	58.74	106.36	0.10	2.00
			30	-0.99	59.37	93.68	0.10	2.01
			36	-0.99	59.40	93.74	0.10	2.01
		12 °C	6	-0.99	59.33	94.20	0.10	2.04
			12	-0.98	58.70	95.43	0.10	1.92
			18	-0.99	59.18	92.97	0.10	2.06
			24	-0.99	58.99	93.01	0.10	1.99
			30	-0.99	58.84	92.63	0.10	1.99
			36	-0.96	56.06	90.01	0.10	1.98
		13 °C	6	-0.99	59.34	94.11	0.10	2.01
			12	-0.99	59.30	93.73	0.10	2.00
			18	-0.99	59.36	93.68	0.10	2.03
			24	-0.99	59.35	93.85	0.10	2.03
			30	-0.99	59.38	93.84	0.10	2.02
			36	-0.99	59.28	93.87	0.10	2.01
		14 °C	6	-0.99	59.34	93.94	0.10	1.96
			12	-0.99	59.41	93.77	0.10	2.04
			18	-0.99	59.32	93.76	0.10	2.03
			24	-0.99	59.31	93.80	0.10	2.02
			30	-0.99	59.24	93.81	0.10	1.97
			36	-0.99	59.37	93.77	0.10	2.03
7.17	CD PW Constant IPOPT Novel T^0	*A*	6	-0.99	59.35	93.94	0.10	1.97
			12	-0.99	59.32	93.72	0.10	2.00
			18	-0.99	59.38	93.89	0.10	2.01
			24	-0.99	59.29	93.86	0.10	1.99
			30	-0.99	59.33	93.69	0.10	1.98
			36	-0.99	59.38	93.71	0.10	2.00
		B	6	-0.99	59.40	93.74	0.10	2.03
			12	-0.99	59.40	93.73	0.10	1.99
			18	-0.99	59.42	93.80	0.10	2.04
			24	-0.99	59.36	93.65	0.10	2.03
			30	-0.99	59.38	93.70	0.10	2.00
			36	-0.99	59.41	93.74	0.10	2.00
		C	6	-0.99	59.34	94.06	0.10	2.05
			12	-0.99	59.36	93.79	0.10	2.00
			18	-0.99	59.44	93.72	0.10	2.05
			24	-0.99	59.38	93.75	0.10	2.05
			30	-0.99	59.41	93.69	0.10	2.03
			36	-0.99	59.37	93.67	0.10	1.99
		D	6	-0.99	59.13	93.27	0.10	1.94
			12	-0.99	59.34	93.73	0.10	1.99
			18	-0.99	59.32	93.77	0.10	2.02
			24	-0.99	59.34	93.36	0.10	2.13
			30	-0.99	59.35	93.52	0.10	2.04
			36	-0.99	59.37	93.71	0.10	1.99

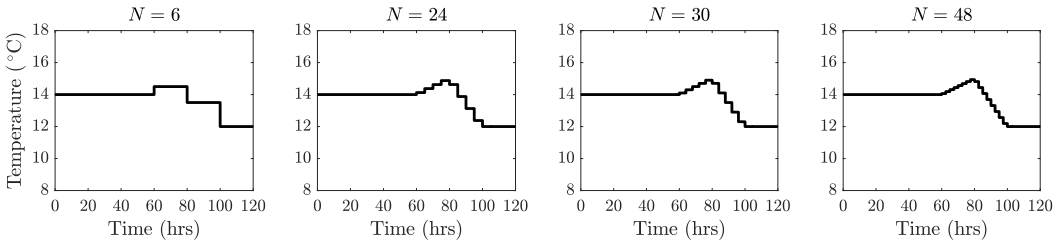

Figure 7.16: PWC approximations of profile D (Fig. 7.15) for varying N.

forms, if the output profile solutions are more suitable for industrial manipulation than those from an isothermal initialisation. A range of promising profiles from the prior exhaustive simulation campaign, performed with a low discretisation level, $N = 6$ (Chapter 6) are selected to use as T^0 profiles (Fig. 7.15). To visualise how these profiles perform, the corresponding marker is highlighter over the entire exhaustive solution set in Fig. 7.14. The top plot (ethanol vs. batch time) shows that the four profiles taken forward from exhaustive simulation for initialising the simultaneous optimisation procedure all fall towards the more desirable portion of the plot. The vast number of points which correspond to lesser batch time and greater ethanol concentration (top left corner of Fig. 7.14) suggest that there is potential scope to improve upon these profiles. The lower two plots (by-products vs. batch time) show that profiles A, C & D all universally fulfil both base limits of the by-product species, while profile B in fact does violate the diacetyl limit for the base case. This is of interest to observe how a constraint violation in the initialising solution affects the performance of the algorithm in producing optimal $T(t)$ profile outputs.

As these profiles are PWL and the CD method employed is computing PWC temperature profiles, it is necessary to approximate the profiles in Fig. 7.15 to a piecewise constant form, which will differ for each discretisation level solved. This approximation is performed by averaging the temperature over N steps of equal duration: this transformation is shown in Fig. 7.16 for profile D. It is demonstrated that N increases the profile tends to the original piecewise linear form. Solution profiles obtained for the same set of cases solved in Section 7.2.2 are presented in Fig. 7.17, only now $T^0 = [A, B, C, D]$.

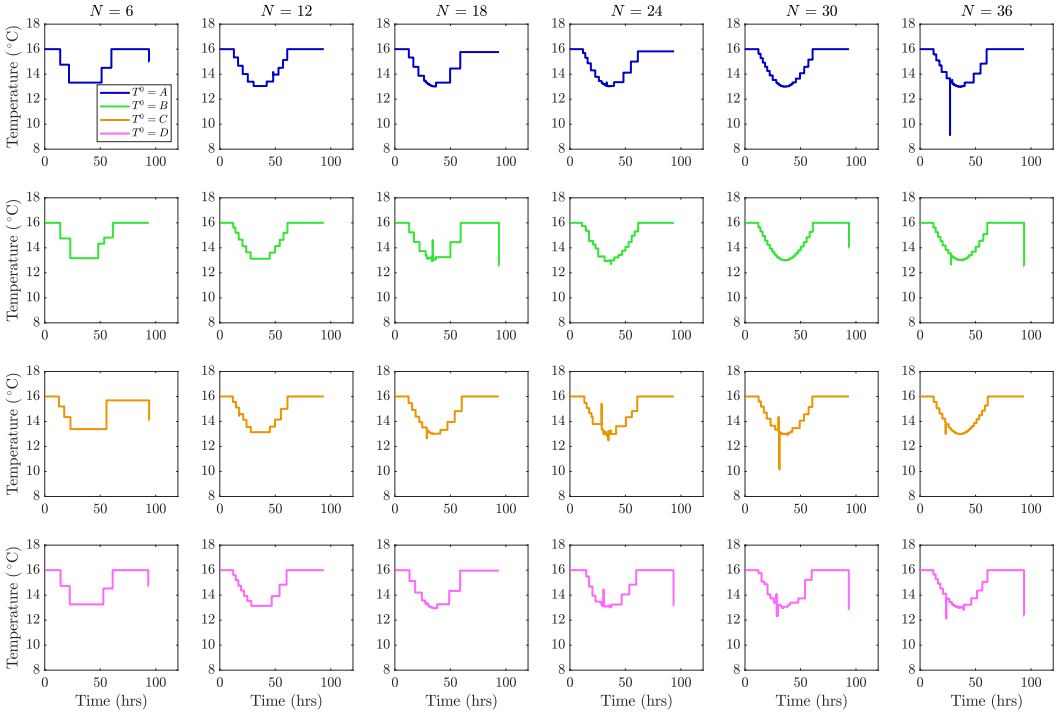

Figure 7.17: CD $T(t)$ solutions: Novel T^0, PWC with IPOPT.

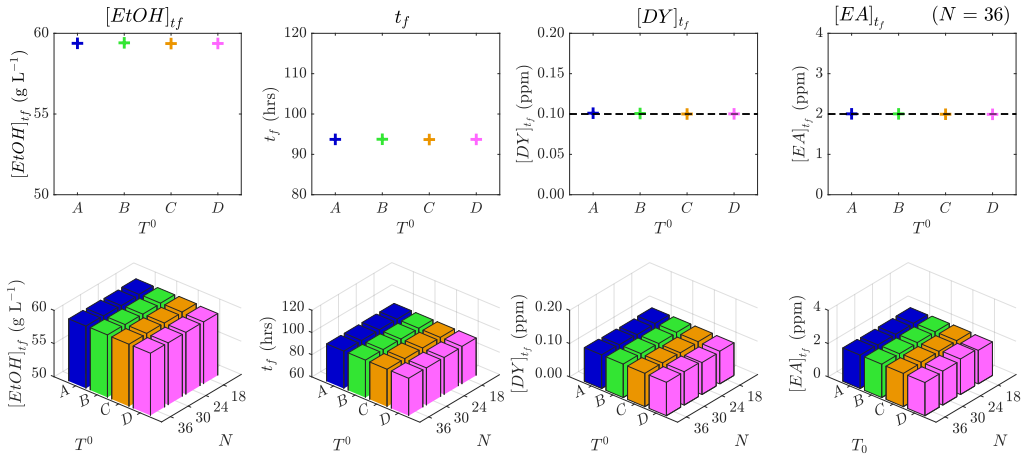

Figure 7.18: Influence of discretisation level (N) and initialising novel profile (T^0) on profile performance - CD with IPOPT.

Results

A very high level of similarity is observed between the solution temperature profiles in Fig. 7.17 and Fig. 7.11. Similarly to the isothermal initialisations, the profiles obtained following novel initialisations converge to the same solution trajectory, irrespective of the discretisation level or initialisation. The only difference is that the two inferior sub-optimal solutions produced when $T^0 = 11$ °C (Fig. 7.11) are no longer re-produced, suggesting that supplying favourable profiles as a starting point for the NLP solver can potentially prevent or limit convergence to less preferable solutions. Within Fig. 7.17 every single profile produced appears to follow the same optimal path. Once more select solutions show artefacts where instantaneously the temperature profile goes up and down, however as this is instantaneous it has no bearing on the performance and may be readily removed from the profile. The upper row in Fig. 7.18 compares the performance of the profiles computed for $N = 36$ with each initialising isothermal profile considered, while second row of plots introduces a third axis to visualise the effect of discretisation level on the resulting fermentation performance. It is evident that the method employed is extremely effective in converging to the same optima, given that the performance metrics and solution appearance are both identicle across the solution set. Furthermore the fact that the 3D bar plots are all flat shows that when $N > 18$, increasing the discretisation level has absolutely no benefit on the performance of computed profile solutions. An interesting exception to this trend is the case where $T^0 = D$ and $N = 24$. In this one instance the limit on $[EA]$ is exceeded by 0.13 ppm, despite the solver reporting a feasible solution. This can be attributed to the slight deviations that exist between the approximated state trajectories from the collocation equations, and later integration of the DAE model given the solution profile, which depend on the accuracy of the piecewise polynomial representation of the continuous state trajectories. Deviations are shown to be non-significant as the algorithm used captures the state trajectories effectively. Figure 7.19 shows an alternative performance plot of the output profiles computed from the 3 CD solution sets (Figs. 7.10, 7.11 and 7.17). Plotting batch time against ethanol concentration represents the bi-criteria ob-

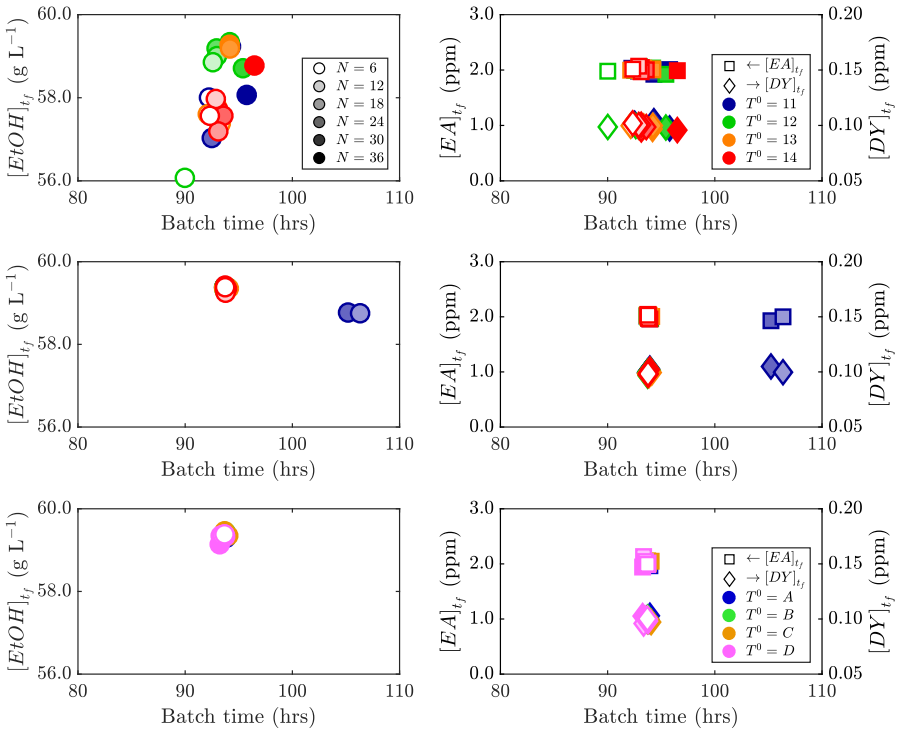

Figure 7.19: Effect of T^0 and N on fermentation performance.

jective function, where the most favourable solutions would exist in the upper left corner. The first row (isothermal T^0, fmincon) shows significant variation in batch time and ethanol concentration. Despite the solution profiles all exhibiting similar objective values, the weighted sum approach means that they can still differ significantly in the objective components. A general trend observed is that higher N solutions tend to have a longer batch time with a greater ethanol yield. Furthermore, the markers in the plot are grouped together depending on their initialisation profile, reiterating that the method was converging to local solutions in the vicinity of the initialisation. The second row in plot Fig. 7.19 presents the solution performance from Fig. 7.11 (isothermal T^0, IPOPT) shows significant less variation. In fact all the points lie on top of each other, excluding the two solutions previously identified as outliers converging to a different solution ($T^0 = 11$ °C; $N = 18$ - 24). The final row (now T^0, IPOPT) now shows every single marker centred around the same point (believed to be globally optimal), as no convergence issues have been found to occur when supplying favourable initialisation profiles to the CD method with the IPOPT NLP solver.

7.3 Chapter Conclusions

A control vector parametrisation strategy has been used to compute temperature profiles to minimise a bi-criteria problem considering ethanol maximisation and batch time minimisation. Two NLP algorithms are compared, fmincon and IPOPT, for the computation of both piecewise constant (stepwise) and piecewise linear temperature profiles to for a range of levels of discretisation and initialising temperature profiles. It is demonstrated that even at low discretisation levels the CVP strategy is extremely effective at computing the control profile for optimal beer fermentation, with little benefit found in increasing the problem size to from PWC to PWL. While PWL control trajectories can be more realistic to adhere to in practice, since instantaneous temperature gradients are omitted, it is considerably easier for an operator to input a PWC profile as a vector of set points for plant equipment, and is the favourable approach of those considered here.

A second dynamic optimisation method is applied, discretisation of the state trajectories in addition to the control vector using orthogonal collocations to generate a large scale NLP problem. It is demonstrated that both NLP solvers considered can converge to local solutions when blindly initialised with isothermal profiles, which restricts the performance of computed solution profiles. Electing to initialise with promising candidate profiles is shown to be highly beneficial, with the simultaneous optimisation approach being able to improve upon the input profiles in all cases. The robustness and computational performance of the interior point NLP solver (IPOPT) is clearly superior to that of the alternative solver (fmincon) considered: while global optimisation is not the purpose of the present study, it is clear that poor initialisations can result in suboptimal temperature manipulation profiles, particularly when less powerful solvers are being used.

A highly novel optimal fermentation temperature profile is identified: a symmetrical parabola dip in temperature across the majority of the duration effectively manages the active yeast population, slowing down cell death and maintaining a sustained high concentration of active yeast cells. Doing so permits very rapid fermentation, while also preventing excessive accumulation of the two

flavour degrading by-products under consideration. The form of these solutions (e.g. high initial temperature, progressive cooling and reheating) carry technical merit with respect to plant implementations (e.g. feeding warm wort to the fermentor straight from the mashing stage under insulation, rather than allowing cooling), and appear to be a viable route towards significant process improvement for industrial beer fermentation.

Chapter 8

Dynamic Optimisation of Fed-Batch and Batch Fermentation Reactors

The favourable dynamic optimisation methodology and initialisation strategies from the previous chapter are herein applied to two reactor optimisation studies.

8.1 Keratin Hydrolysis Optimisation

The hydrolysis model developed for batch operation in Chapter 5 (where the substrate is all introduced at $t = 0$ hrs) is applied to a fed batch system. In practice it is not viable to increase the reactor solids content far above 7% (w/w), with the viscous broth becoming restrictive of the reaction kinetics. To circumvent this, it can be favourable to perform the hydrolysis reaction in fed-batch operation: allowing a portion of the substrate to be digested before supplementing additional solids. In doing so a greater amount of the waste material can be hydrolysed while ensuring the solids content does not become restrictively high. It is of great interest to determine the feed schedule (dosage quantities and timings) for optimal performance, to consume the largest portion of a given substrate mass in a fixed time-frame.

8.1.1 Problem Formulation

The proposed model structure is unable to capture the observed behaviour at elevated substrate concentrations, due to the lack of mass transfer consideration or inhibitory effects under high solid content. This would result in any attempt to use the model for unconstrained dynamic feed profile optimisation to return batch operation as the preferred strategy, with no benefit existing (as far as the model is concerned), in keeping the solids content low to promote consumption (shown experimentally), compared to feeding the entire substrate mass initially. As such the concentration of solids in the reactor across the entire timespan is constrained (Eq. 8.6) to not exceed 7% (w/w), with the assumption that it is above this level where the viscosity becomes prohibitive for reaction progression (Modenbach and Nokes, 2013). Additionally, this ensures the model is not applied out with the substrate range in which the data used for model fitting was obtained. As feed additions are instantaneous (manual solid addition) the process is modelled as a series of batch reactors, with the output from one reactor fed to the next with the supplemented substrate mass. A favourable strategy identified in Chapter 7 is applied: given the small problem size CVP is used with the IPOPT solver (Wächter and Biegler, 2006) interfaced in MATLAB through OPTI (Currie et al., 2012). A NLP problem is formulated, where decision variables define the feeding profile: after the initial substrate, K_{F_0}, is introduced at $t = 0$ hrs subsequent additions K_{F_i} are made at times t_{F_i}, such that the decision vector is defined as d:

$$d = [K_{F_0}, K_{F_1}, ..., K_{F_i}, ..., K_{F_N}, t_{F_1}, ..., t_{F_i}, ..., t_{F_N}] \tag{8.1}$$

An equality constraint (Eq. 8.2) ensures the various additions of substrate sum to desired amount of waste to be treated, K_T. Inequality constraints (Eqs. 8.3–8.5) are imposed to ensure the solver only considers feasible feed profiles. The objective (Eq. 8.7) is to minimise the residual substrate after the reaction time-frame has elapsed, which coupled with Eq. 8.2 equates to maximising the mass of substrate hydrolysed.

$$\sum K_{F_i} = K_T \tag{8.2}$$

$$0 < t_{F_1} \tag{8.3}$$

$$t_{F_i} < t_{F_{i+1}} \tag{8.4}$$

$$0 \leq K_{F_i} \leq K_T \tag{8.5}$$

$$K \leq K_C \text{ for all } t \in [t_0, t_f] \tag{8.6}$$

$$\min_d J = K_{(t=t_f)} \tag{8.7}$$

8.1.2 Results

The solution when the number of permitted feeds (excluding t_0) is equal to three, with a total substrate mass to be treated, K_T, equal to 135 g L^{-1} (12% w/w) is shown in Figure 8.1, compared to a generic feed profile where equal feeds are added every 24 hours. It can be observed that the optimal protocol involves supplementing the substrate quantity such that it reaches the constrained threshold (slack variable equal to 0), which is intuitive given that in the unconstrained case the solution with such a model is to feed the entirety of K_T as early as possible. What is less intuitive is the feeding times: an inherent trade-off exists between adding the substrate early while the enzyme cocktail retains a higher fraction of its potency, and delaying the addition so that a greater amount may be added to approach the constraint threshold, K_C. The solution presented shows additions favouring each of these: the first supplementation of keratin is made after only ∼5 hours, quickly replenishing the permitted concentration while enzyme activity remains favourable. The two subsequent additions are made after more prolonged time periods, allowing a sufficient portion to be consumed before topping back up to the threshold, a result of the finite number of additions and the requirement to feed the total mass defined by Eq. 8.2. It is demonstrated that the terminal concentration, $K_{t=t_f}$, is around 5 g L^{-1} lower following the optimised schedule compared to a generic strategy (addition after each 24 hours). This highlights the potential benefit in applying such a method towards determining the optimal strategy for maximising substrate consumption. It should be noted that this is only a modest improvement in yield and does little to improve the viability of this

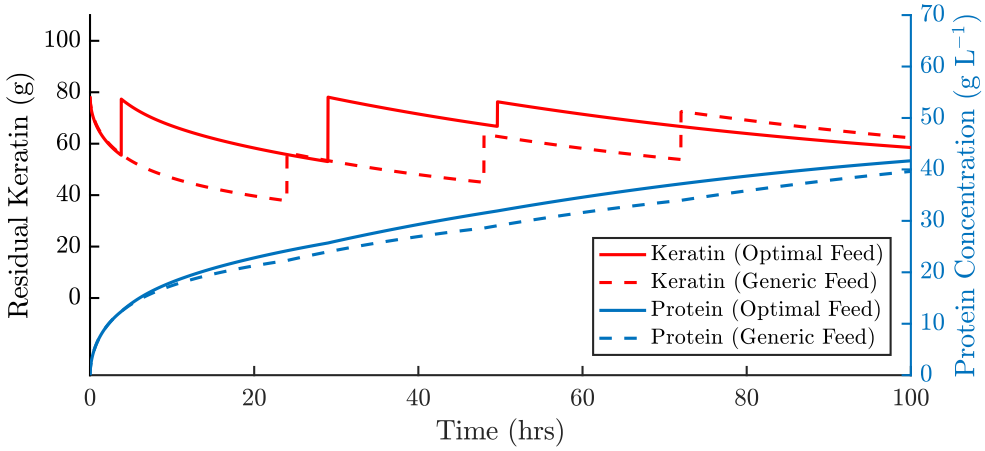

Figure 8.1: Optimised fed-batch substrate feed profile.

technology versus conventional thermal processing. Given the model uncertainty and lack of validation for fed-batch operation, it is highly desirable to perform the optimised feed profile experimentally as to ascertain whether the model can indeed be applied to fed-batch mode, and whether the 5 g L^{-1} hydrolysis improvement may be achievable.

8.2 Fermentor Jacket Cooling Optimisation

Beer fermentor optimisation results presented in the previous chapter rely upon universal assumption of direct and instantaneous control of fermentor temperature. As with the dynamic simulation and performance mapping in Chapter 6.3, heat transfer dynamics are now incorporated into the dynamic optimisation problem so that the implications of such an assumption may be addressed. The most favourable strategy identified for this specific problem is applied: CD with collocation on finite elements, solving the NLP produced with IPOPT. Once more orthogonal polynomials on finite elements are used to approximate the model control (coolant rate) and state (model species) trajectories using the DynOpt package for MATLAB (Cizniar et al., 2005). Batch time is fixed at 160 hours, to investigate cooling strategies for very high yield fermentations where time pressure is not a concern. The objective is defined to maximise ethanol yield:

$$J_{min} = -[EtOH]_{t_f} \tag{8.8}$$

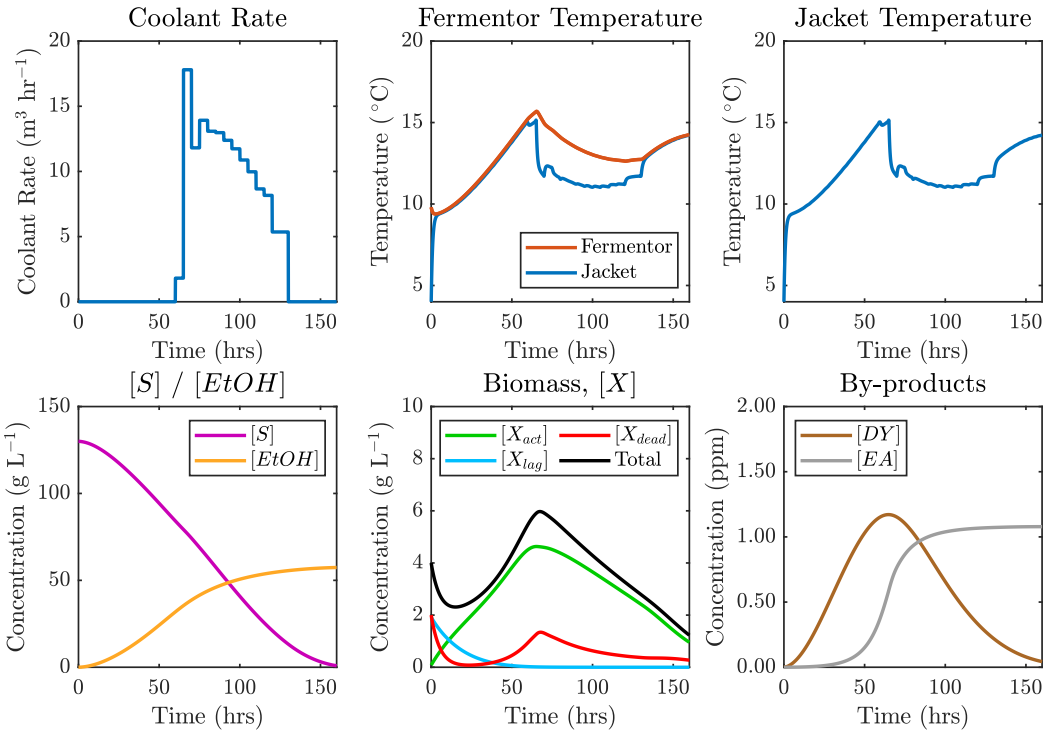

Figure 8.2: Optimal $F(t)$ solution for maximum $[EtOH]$ in 160 hrs.

Fixing 16 elements across the time horizon, with 3 collocation points per element for the nine state ODEs and one collocation point (piecewise constant) per element for the control (F) leads to a $16 \times (3+1) \times 9 + 16 \times 1 \times 1 = 592$ variable NLP, able to accurately approximate the continuous dynamics of the system. For a single objective ethanol maximisation problem the NLP is solved using IPOPT (Wächter and Biegler, 2006). The local solver uses an interior point line search filter method, with multi-start initialisation used to best approximate global optimality. The optimal control profile produced is presented in Figure 8.3, alongside the corresponding jacket and vessel temperature trajectories. Similarities are observed between profiles in Chapter 7 (i.e. Fig 7.17) and Fig. 8.2, where using intermediate cooling to manage the active cell population is evident as a lucrative and viable policy to maximise ethanol yield. With considerably greater degrees of freedom than the policies in the exhaustive search (Fig. 6.10), the optimal policy computed here is to rapidly begin cooling after a favourable temperature is reached (~15 °C), and to graduate lower the coolant rate over the following 70 hours such that gradual and sustained cooling of the wort is facilitated.

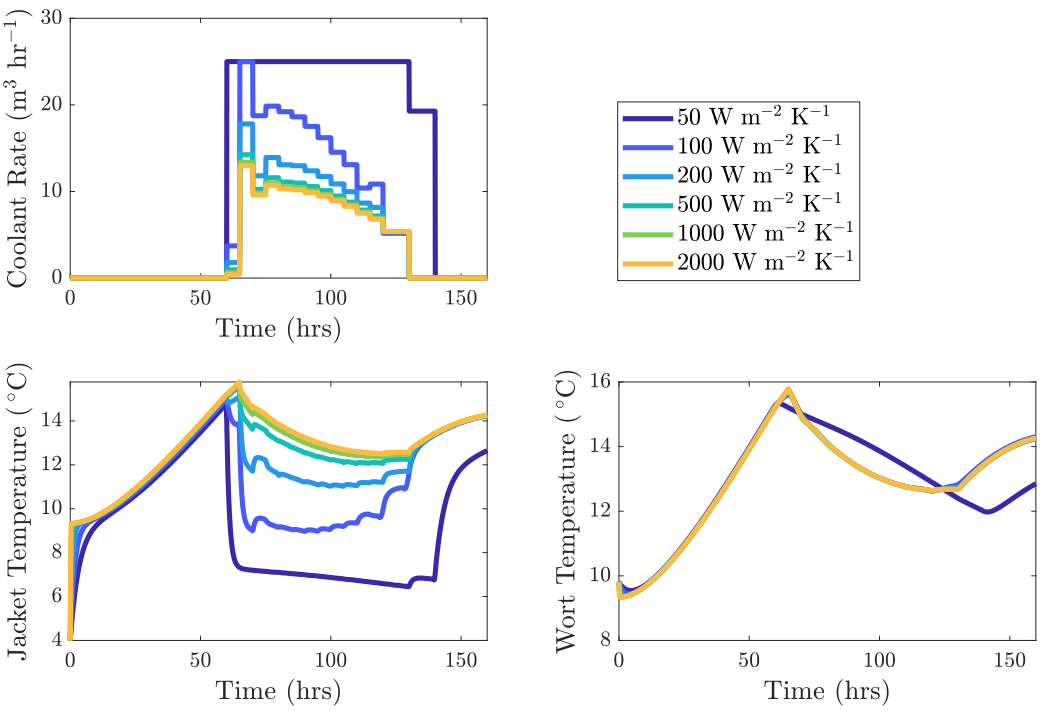

Figure 8.3: Overall heat transfer coefficient effect on optimal coolant supply rate.

Solution Sensitivity to Process Parameters

To investigate the impact of the coolant temperature and overall heat transfer coefficient OHTC on the optimal cooling policy, the same dynamic optimisation problem is repeatedly solved for a range of realistic values for this parameter. Figure 8.3 shows the solution profile for a range of values of U, while Fig. 8.4 shows the same for coolant temperatures. It is demonstrated in Fig 8.3. that with decreasing OHTC the same cooling policy profile form is utilised, with increasing required coolant rate. After a critical point ($U < 100$ W m^{-2} K^{-1}) the maximum coolant rate is insufficient and the solution is to run the coolant at the maximum rate. The bottom left panel highlights how the jacket temperature differs in these cases with the increasing coolant rate, which leads to near identical temperature trajectories in the fermentor (bottom left panel), with the exception of the dark blue case ($U = 50$ W m^{-2} K^{-1}) which takes a less favourable path due to being limited by the maximum coolant rate.

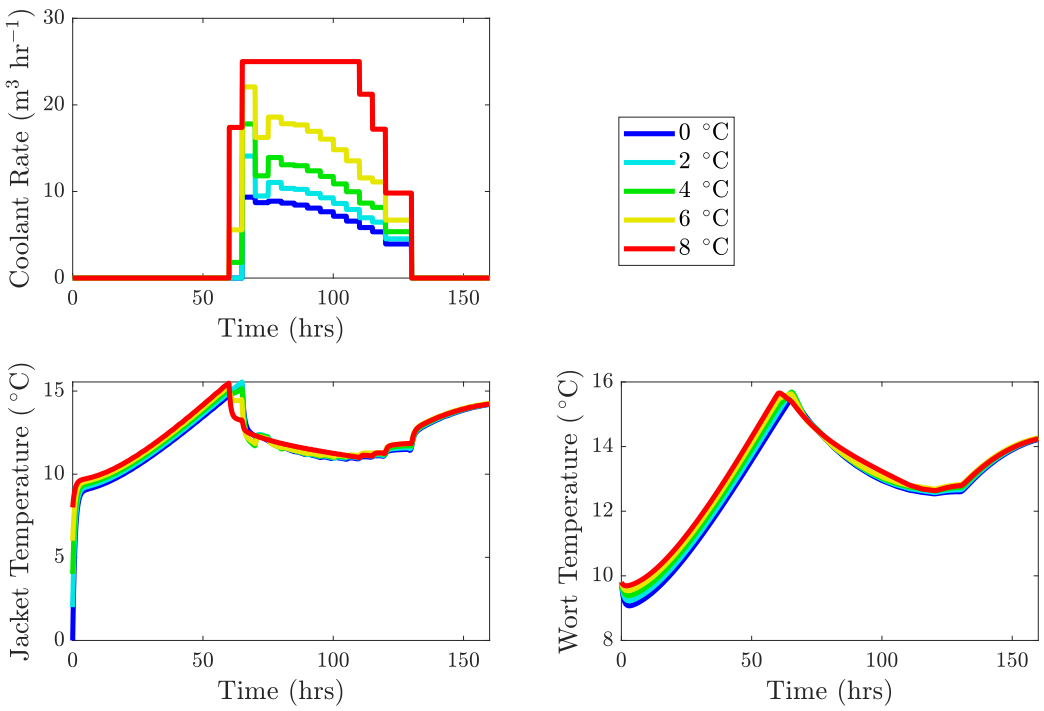

Figure 8.4: Coolant temperature effect on optimal coolant supply rate.

Figure 8.4 similarly demonstrates how the same cooling policy form is computed regardless of the coolant temperature. Across all cases considered it is possible to maintain essentially the same jacket-side temperature by adjusting the coolant rate accordingly, such that the wort temperature and corresponding fermentation progression are unchanged. This highlights that in the common scenario where coolant feed temperature varies over time (ambient condition variability), adjustments can be readily made by increasing or decreasing the volumetric supply rate to adhere to the same temperature progression within the batch itself.

8.3 Chapter Conclusions

The hydrolysis of keratin-rich material with keratinolytic bacteria is an attractive way of transforming undesirable waste from agro-industrial activities into products of practical industrial value. It is demonstrated how the proposed model may be applied towards fed-batch feed-schedule optimisation. An improvement (reduction) in terminal keratin concentration of around 5 g L^{-1} can be made following the optimised schedule compared to a generic strategy (addition after

each 24 hours). This highlights the potential benefit in applying such a method towards determining the optimal strategy for maximising substrate consumption. It is essential to consider that such a modest improvement in yield does little to improve the viability of this technology versus conventional thermal processing. Given the model uncertainty and lack of validation for fed-batch operation, it is highly desirable to perform the optimised feed profile experimentally, or at least a fed-batch experimental campaign, as to ascertain whether the model can indeed be applied to fed-batch mode, and to verify whether a 5 g L^{-1} hydrolysis improvement is achievable.

The beer fermentation dynamic optimisation problem considered in Chapter 7 is extended with the inclusion of realistic, indirect temperature manipulation via coolant federate, while all prior work assumed direct temperature control. Consideration of explicit fermentor jacket heat transfer marks a significant improvement over the fidelity of prior work which assumed temperature may freely manipulated. Optimal operation involves a novel cooling policy to effectively manage the active yeast population in the reactor, capable of improved performance versus established approaches. Sensitivity analysis of the solution dependence on thermal process parameters shows how adjustments in the coolant rate can be made to maintain the preferred optimal temperature trajectory of the fermenting wort in the vessel.

Chapter 9

Dynamic Optimisation as a Tool to Gain Process Insight

Applying dynamic optimisation methodologies to compute single and unique control vector solutions, minimising a given objective function, is an invaluable tool in process engineering. However doing so relies upon a concise problem formulation, whereby the objective function and system constraints can be readily and meaningfully defined. In the food and drinks manufacturing industry there is often varying specifications for different product lines, so such a unique formulation becomes less useful when exploring potential for new or alternative products. Herein this chapter considers repeatedly solving a finite set of modified versions of the original dynamic optimisation problem, as a means to gain significant insight into process characteristics and as to how attainable process performance is potentially dictated specific constraints. The effect of by-product species thresholds on optimal beer fermentation performance is explored, as to identify how the variable by-product limits in different products impacts the potential efficiency of production.

9.1 Methodology

9.1.1 Solution Strategy

The formulated dynamic optimisation problem in Chapter 7 for beer fermentation is extended. Here the same objective (Eq. 9.1) is used, systematically varying the specific constraint thresholds on diacetyl and ethyl acetate, as to elucidate the impact these flavour compounds have on attainable process performance.

$$J_{min} = -W_E \cdot [\tilde{EtOH}] - W_t \cdot \frac{1}{\tilde{t_f}} \tag{9.1}$$

$$\text{s.t. } [EA]_{t_f} \leq [EA]_{max} \tag{9.2}$$

$$[DY]_{t_f} \leq [DY]_{max} \tag{9.3}$$

The most favourable strategy identified for this specific problem is applied: CD with collocation on finite elements, solving the NLP produced with IPOPT. Three collocation points have been used for each of the eight model state trajectories per element, with one collocation point being used for control profiles per element, resulting in the computation of temperature profiles which are piecewise-constant.

9.1.2 Initialisation

Due to the high number of local extrema which exist when discretising a control vector problem to NLP form, the initialising profile has considerable bearing on the solution obtained, which cannot be guaranteed as globally optimal from most algorithms. To overcome this limitation, it is desirable to input a profile known to have favourable performance, such that the algorithm can act to improve on this. As highlighted in Chapter 7, initialising the solver with favourable candidate profiles can improve the robustness of the algorithms ability to converge to a feasible and favourable solution. As in Chapter 7, a range of favourable profiles from the exhaustive simulation campaign (Chapter 6) are used. The specific profiles which have been used for initialising the solver are shown in the Fig. 7.15, where their position (corresponding performance) is highlighted in Fig. 7.14.

Table 9.1: Summary of solution conditions, producing 200 cases.

	Number of values	Range
$[EA]_{max}$(ppm)	5	[0.5, 1.0, 1.5, 2.0, 3.0]
$[DY]_{max}$(ppm)	5	[0.05, 0.10, 0.15, 0.20, 0.25]
$W_E : W_t$	2	[0.75:0.25, 0.5:0.5]
Initialising profile	4	[A, B, C, D]

9.1.3 Case Definition

To thoroughly investigate effect which by-product constraint thresholds (Eqs. 9.2–9.3) have the attainable fermentation performance, and to access the methodology performance, a campaign of cases have been solved. Five realistic thresholds for ethyl acetate and diacetyl have been selected producing 25 constraint permutations for which the system will be solved. This is performed for different discretisation levels, with the $N = 30$ case presented in this thesis for conciseness, each of which is initialised with each of the four input profiles (Fig. 7.15) in turn. Additionally two different sets of objective weights are considered, as to observe how the solution profiles vary to shorten batch time at the expense of ethanol yield, when the former is given higher priority. The conditions for the set of 200 dynamic optimisation problems are summarised in Table 9.1. All solutions presented represent the best performing case of each solution from the four initialisations, however in the vast majority of scenarios the attained solution is equivalent for all four.

9.2 Results and Discussion

The solution profiles for all 25 by-product threshold cases are presented in Fig. 9.1, for the problem weighted towards Ethanol maximisation ($W_E = 0.75$, $W_t = 0.25$). Each panel depicts the specific $T(t)$ solution (temperature profile) for optimal performance, subject to the corresponding thresholds: $[EA]_{max}$ decreases from left to right, $[DY]_{max}$ decreases moving down each row in the figure. A high level of similarity is evident across all solutions presented. Much like the base case ($[EA]_{max}$ = 2 ppm & $[DY]_{max}$= 0.10 ppm) presented in Chapter 7,

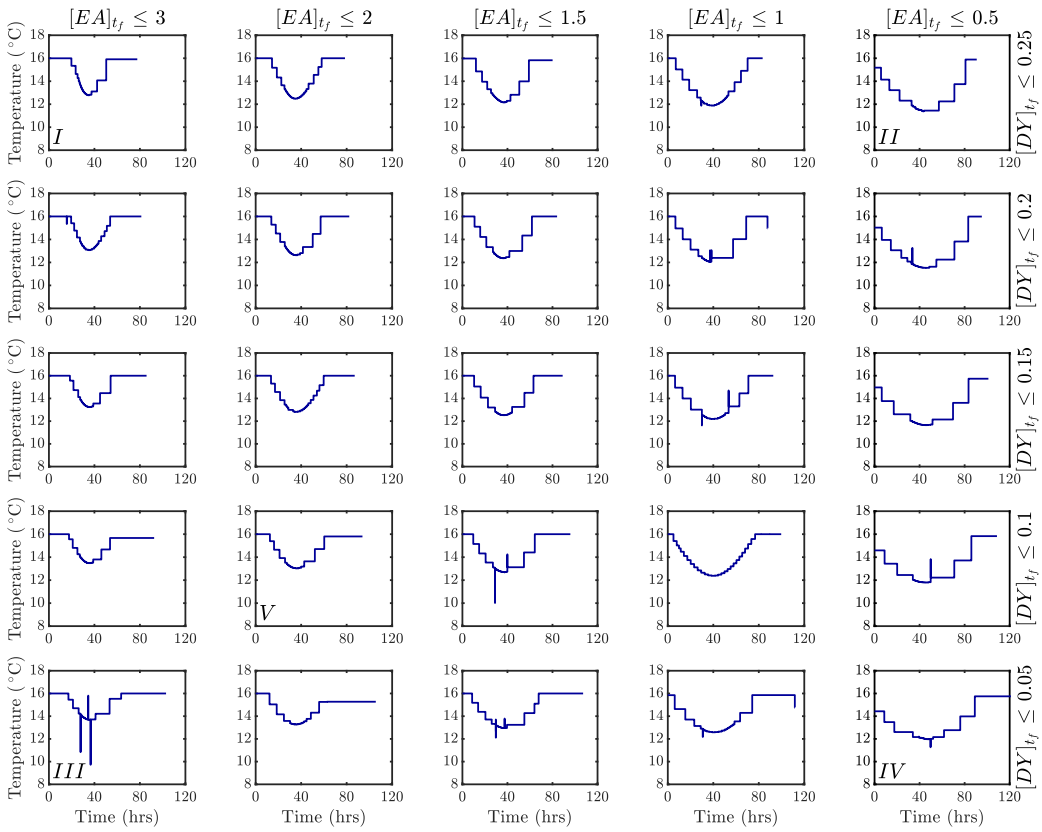

Figure 9.1: Solution profiles ($N = 30$, $W_E = 0.75$, $W_t = 0.25$).

the solution takes the general form of beginning at 16 °C before exhibiting a symmetrical parabola dip in temperature over the majority of the duration, returning to 16 °C shortly before completion. As discussed in Chapter 7 this novel strategy for fermentation very effectively manages the active yeast population, slowing down cell death and maintaining a sustained high concentration of active yeast cells. The permits very rapid fermentation, while also preventing excessive accumulation of the two flavour degrading by-products under consideration. An astonishing result is the fact that that the same approach can similarly optimise fermentation for alternative target product quality specifications, only requiring minor adjustments to the general profile form.

9.2.1 Effect of ethyl acetate limit on optimal solution

Figure 9.1 reveals that in order to satisfy tighter limits on $[EA]$ it is necessary to initiate the temperature drop earlier in the process, which is sustained for

a longer portion of the batch duration. This continues to the tightest bound on $[EA]$ (right most column) where it is no longer possible to start the process at 16 °C, and essentially the parabolic temperature dip is already underway at the start of the batch. This observation can be explained by the simple fact that $[EA]$ is not consumed at any point during the process, so any production leads to accumulation. Since production is accelerated at higher temperatures, sustained initial heating is no longer feasible when $[EA]_{max}$ decreases below 1 ppm. Furthermore, it can be observed that the minimum temperature across each profile (the base of the parabola) decreases with tightening $[EA]_{max}$, which also assists in preventing excess production of this undesirable species.

9.2.2 Effect of diacetyl limit on optimal solution

The specific effect which $[DY]_{max}$ has on the solution profile can similarly be observed by comparing columns within figure 9.1. Unlike for varying $[EA]$,the constraint on $[DY]$ has a negligible effect of the parabolic portion of the profile. In fact the only notable trend is that in order to satisfy an increasingly tight upper bound on the product $[DY]$ (moving down each column in Fig. 9.1) the fermentor is operated for greater time at $T = 16$ °C after the parabolic portion of profile has passed. Once more this observation can be explained by interpretation of the model and the reaction scheme present. Unlike ethyl acetate, diacetyl formed during fermentation can break down, being reabsorbed by the yeast which converts them to acetoin and subsequently to 2,3-butanediol. This is particularly dominant towards the latter stages of the process when primary fermentation has essentially completed. As such, any imposed limit on the product $[DY]$ may be fulfilled by extending the batch duration until the concentration of the species falls below the imposed upper limit.

9.2.3 Effect of by-products on attainable performance

The objective function applied in this chapter is of weighed sum form, so observing the attainable J_{min} for each case can only quantify performance in a general overall sense. To observe more specifically how each constrained species

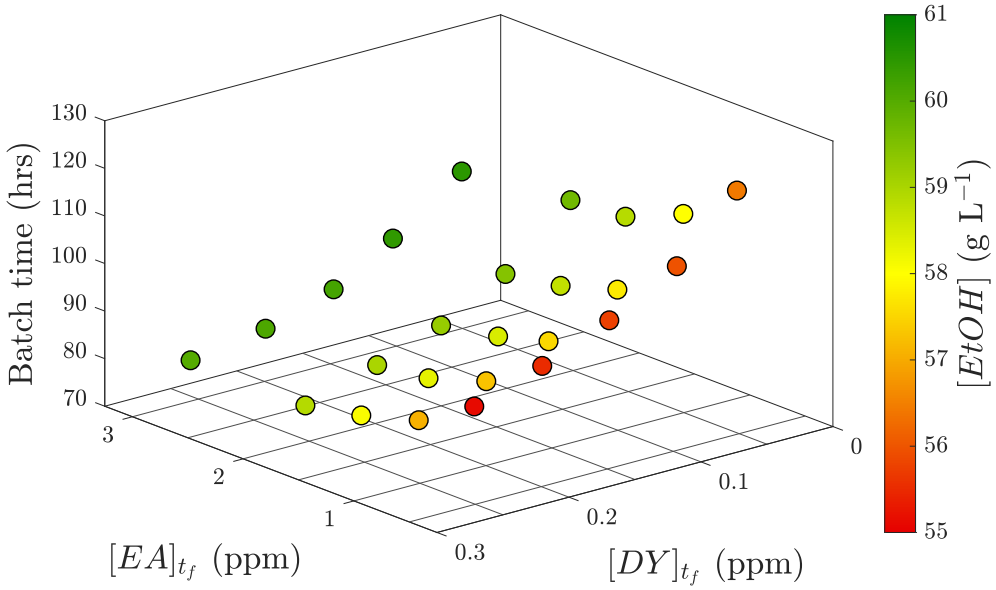

Figure 9.2: Solution performance for all cases ($N = 30$, $W_E = 0.75$, $W_t = 0.25$).

in this study affects the two process targets (batch time and alcohol yield), Figure 9.2 simultaneously depicts all performance metrics. Each circular marker corresponds the performance an output profile from Fig. 9.1; the corresponding by-product concentration limits are represented on the x-y plane with the z axis showing the batch time, t_f, and the marker colour corresponding to the ethanol product concentration, $[EtOH]_{tf}$. The results show a very coherent and consistent pattern, indicating the manner in which fermentation performance is influenced independently by each constrained species. It is shown that batch time universally increases as the acceptable threshold on diacetyl, $[DY]_{max}$, is reduced. Batch time does indeed also increase as $[EA]_{max}$ is reduced, however the relationship is far less significant, with the dependency on the diacetyl threshold much stronger. The marker colours show how it is exclusively the ethyl acetate threshold, $[EA]_{max}$, which influences the final ethanol yield. In all cases when $[EA]_{max} = 0.5$ ppm the product ethanol, $[EtOH]_{tf}$, is very low (under 56 g L^{-1}), which increases steadily towards 61 g L^{-1} as this permitted $[EA]_{max}$, threshold is relaxed towards 3 ppm. These results reveal as to how the two components of the bi-criteria objective are dictated by the two inequality constraints on the by-product concentrations:

- $[DY]_{max}$ has very strong influence on batch time.
- $[EA]_{max}$ is shown to dictate the attainable ethanol concentration.

This finding can be explained by the phenomena discussed in Section 9.2.1 – 9.2.2. In summary, as $[EA]$ is promoted at higher temperatures along with $[EtOH]$, and can not be reduced by any side-reactions. Thus a milder fermentation must be performed if $[EA]_{max}$ is reduced, which unavoidably reduced the potential ethanol yield. On the other hand, $[DY]$ can be reabsorbed by the yeast in the later stages of fermentation, converting to compounds without an adverse effect on the product flavour. As such, it simply becomes a case of extending the batch duration until the $[DY]$ falls below the desired thresholds, leading to prolonged batch times.

9.2.4 Effect of objective weights

The exact same procedure performed with the objective weights $W_E = 0.75$, $W_t = 0.25$ is now repeated, increasing the weight allocated to batch time reduction ($W_E = 0.5$, $W_t = 0.5$). Similarly to Fig. 9.1, Fig. 9.3 depicts each $T(t)$ solution for the same 25 constraint cases, where $[EA]_{max}$ decreases from left to right and $[DY]_{max}$ decreases moving down each row. Solution forms remain highly similar in nature to the prior results with differing objective weightings (Fig. 9.1). Once more the profile 'dip' is elongated when the permitted $[EA]$ is reduced, again to prohibit the unnecessary production which would occur if the fermentor returned to its maximum temperature sooner. Similarly the profile duration after the 'dip' portion has passed increases with the tightening $[DY]$ threshold, so that sufficient time remains for the concentration to be reduced to an acceptable level. These solutions differ to those presented prior in that the 'dip' region is no longer parabolic in form, and may better be described as a V-profile. The V region is asymmetric in most cases, unlike the earlier consistently symmetrical parabolas produced. Since less favour is given to ethanol yield all solutions represent extremely rapid fermentation, accelerated by controlling the active yeast population in this manor, at the expense of a sacrifice in the product $[EtOH]$. Figure 9.4 presents the three dimensional performance plot for all scenarios, analogous to

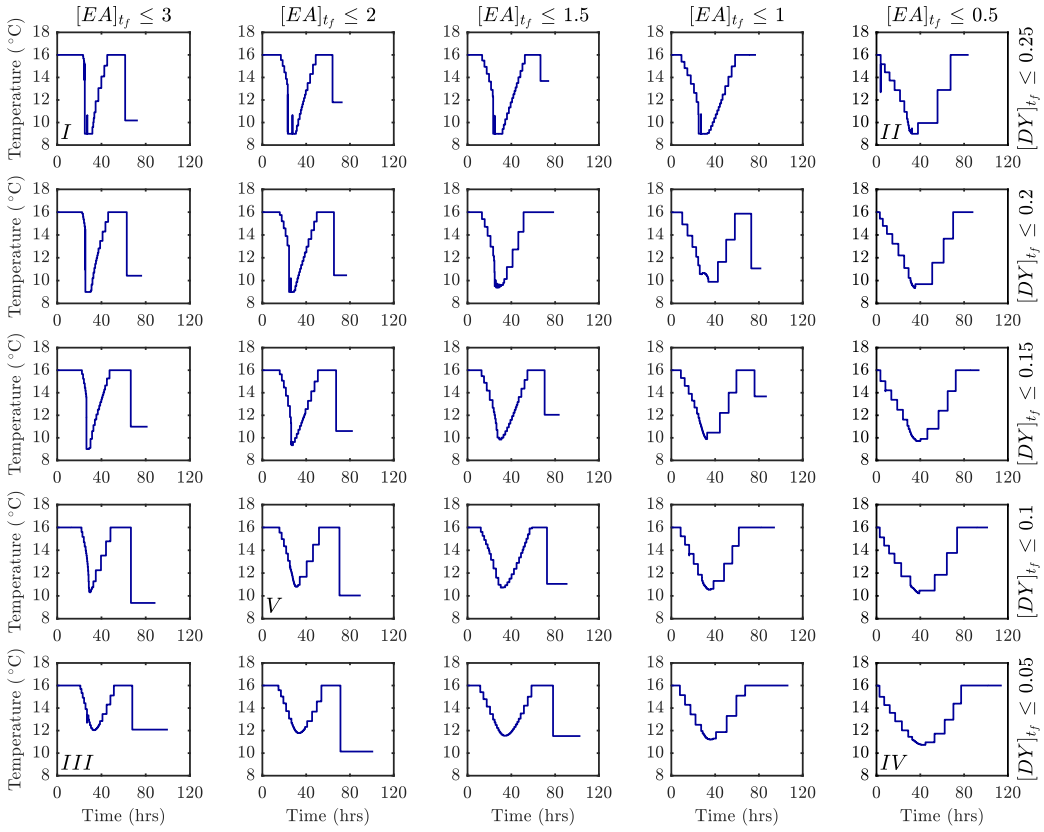

Figure 9.3: Solution profiles ($N = 30$, $W_E = 0.5$, $W_t = 0.5$).

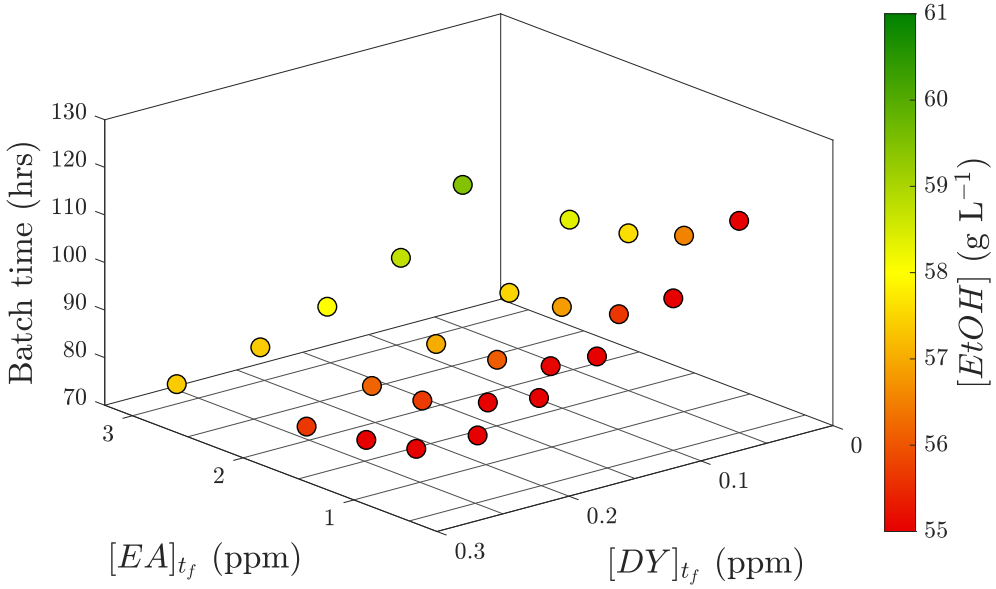

Figure 9.4: Solution performance for all cases ($N = 30$, W_E= 0.5, W_t= 0.5).

Fig. 9.2 from the prior result set. Comparing the two 3D performance plots show a high level of similarity, where the points in Fig. 9.4 are essentially the same as these in Fig. 9.2, only shifted down in the z-axis (reduced batch time), and considerably more red in colour (reduced ethanol yield). It is apparent that the way each objective component is uniquely effected by each by-product limit is unchanged from the previous case, which is fact shown to be independent of the specific objective function.

Figure 9.5 depicts the projection of both Fig. 9.2 and Fig. 9.4 on the by-product concentration plane. Here the marker size is scaled relative to inverse batch times: smaller makers show the worst performing solutions (longest batch times) while larger markers show the best performance (shortest batch times). It is shown that a small selection of solutions do not fall directly on the intersect of the two by-product limits imposed for the particular case being solved. There are two factors responsible for this; firstly there are several cases where the constraints are comfortably fulfilled, i.e. the solution produced for the case $[EA] < 3.0$ ppm & $[DY] < 0.10$ ppm in fact has a lower $[EA]$ of only 2.85 ppm. This could suggest sub optimality in the solution, perhaps with a shorter batch time possible if the concentration of diacetyl were to increase more towards the bound. Secondly, all performance results presented in this work have been computed after reintegration of the system using the computed control profile. Slight deviations exist between the performance of the profile during the collocation approximation in the optimiser and later integration of the solution, depending on the accuracy of the piecewise polynomial representation of the continuous state trajectories. Deviations have are shown to be non-significant as the algorithm used captures the state trajectories effectively.

9.2.5 Performance of key output profiles

Of the entire solution set computed it is of interest to visualise the model state trajectories which correspond to the extrema by-product thresholds, and how these compare to the base case solutions shown in Chapter 7. The following five cases are considered, both for the first solution set (W_E= 0.75, W_t = 0.25), and

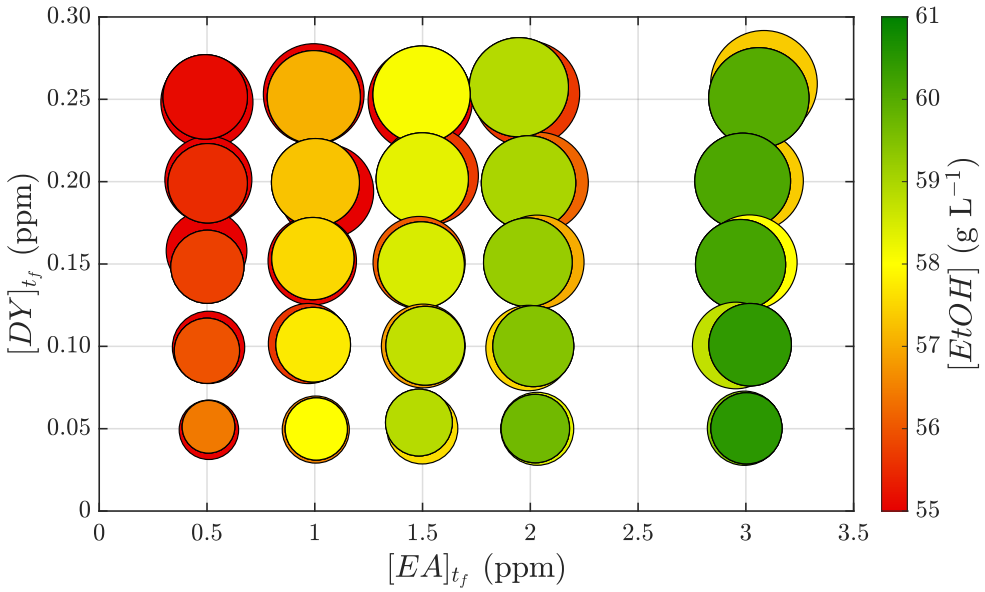

Figure 9.5: Performance projection ($N = 30$): marker size scaled with t_f^{-1}.

that with modified weights ($W_E = 0.5$, $W_t = 0.5$). The corresponding solution within Fig. 9.1 and Fig. 9.3 are denoted with the appropriate Roman numeral in the bottom left of the panel (four corner panels plus the base case).

I: Most relaxed constraints ($[EA]_{max} = 3.0$ ppm, $[DY]_{max} = 0.25$ ppm)

II: Minimum $[EA]_{max}$ (0.5 ppm) and maximum $[DY]_{max}$ (0.25 ppm)

III: Maximum $[EA]_{max}$ (3.0 ppm) and minimum $[DY]_{max}$ (0.05 ppm)

IV: The tightest constraint set ($[EA]_{max} = 0.5$ ppm, $[DY]_{max} = 0.05$ ppm)

V: The base case constraints ($[EA]_{max} = 2.0$ ppm, $[DY]_{max} = 0.10$ ppm)

The corresponding trajectories are shown in Figs. 9.6–9.7 for all model states, with the numerical performance metrics summarised in Table 9.2. Figures 9.6–9.7 allow the manor in which these novel temperature profiles steer fermentation to optimal completion to be visualised. It can be observed how the 'dip' region of the profile can prevent cell death in all cases, and promote very rapid sugar uptake by the yeast. The right most column in both cases provides some insight as to the optimal 'dip' timing varies with each case. It can be seen that the 'dip' is only initiated once $[EA]$ is approaching the permitted upper limit,

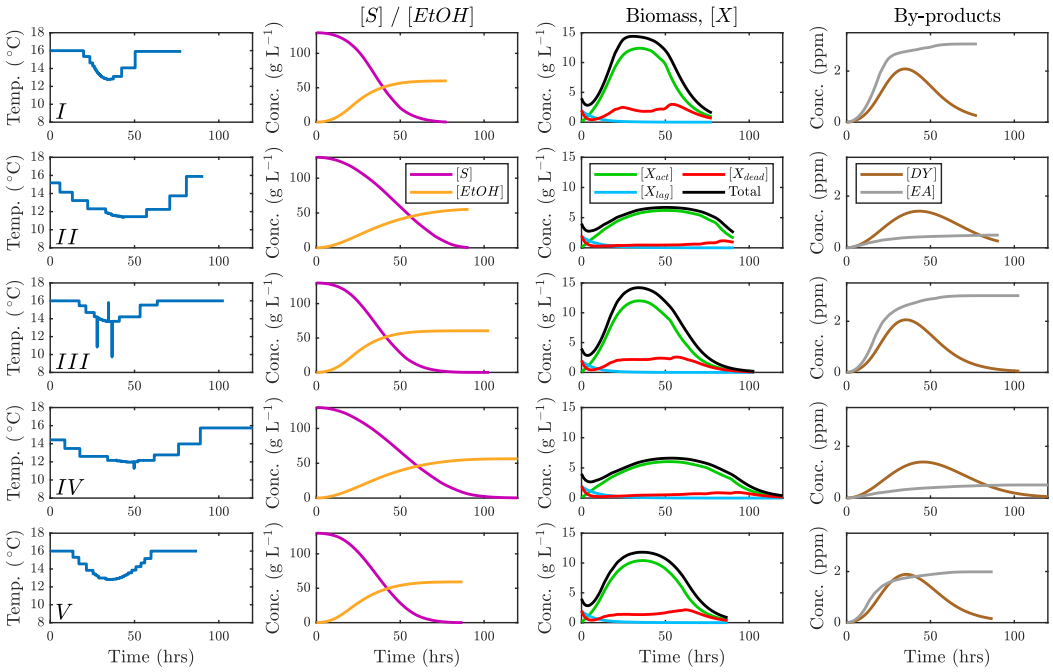

Figure 9.6: Trajectories of key solution profiles ($N = 30$, $W_E = 0.75$, $W_t = 0.25$).

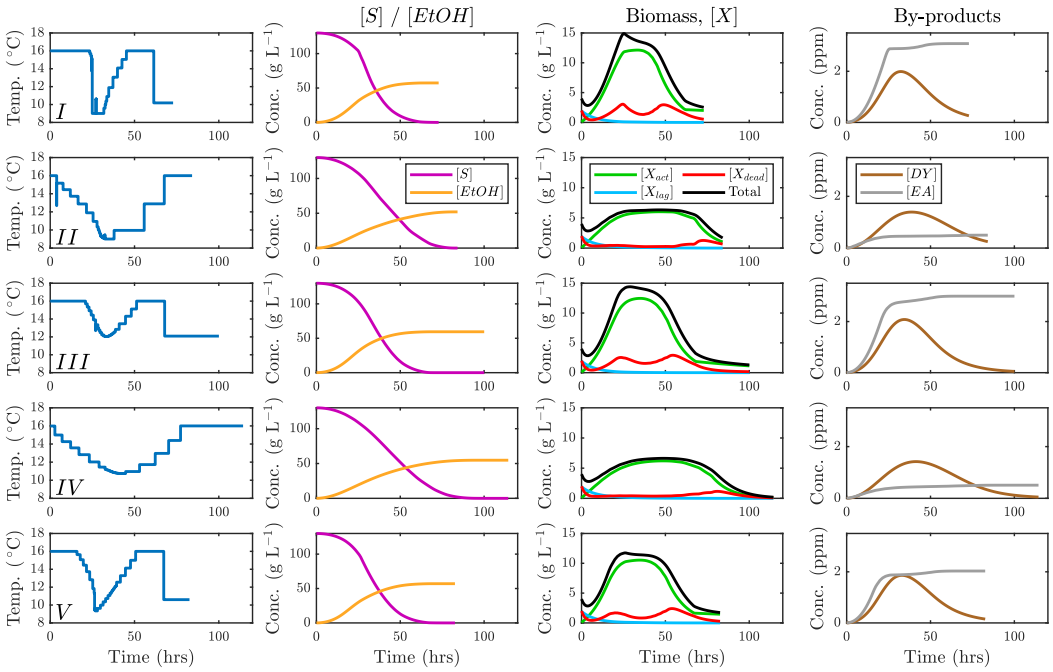

Figure 9.7: Trajectories of key solution profiles ($N = 30$, $W_E = 0.5$, $W_t = 0.5$).

Table 9.2: Performance of extrema profiles plus base case.

$W_E : W_t$	Profile	$[EtOH]_{tf}$(g L^{-1})	t_f (hrs)	$[DY]_{max}$ (ppm)	$[DY]_{max}$ (ppm)
W_E= 0.75 W_t= 0.25	I	60.00	77.7	3.0	0.25
	II	55.14	90.7	0.5	0.25
	III	60.48	103.0	3.0	0.05
	IV	56.42	121.1	0.5	0.05
	V	59.42	93.9	2	0.1
W_E= 0.5 W_t= 0.5	I	57.38	72.9	3.0	0.25
	II	52.00	84.1	0.5	0.25
	III	59.45	100.0	3.0	0.05
	IV	54.75	114.39	0.5	0.05
	V	57.52	89.84	2	0.1

preventing this level from being exceeded for the remainder of the batch duration. Similarly, the way in which $[DY]$ dictates batch time can be visualised, as the moment $[DY]$ (brown profile) drops to the threshold the batch is deemed complete and the profile terminates.

9.3 Chapter Conclusions

The investigation into the influence of by-product threshold limits on obtainable fermentation performance has revealed new insight into how each by-product uniquely affects different aspects of the performance of the fermentor under optimal operation. It is found that the permitted diacetyl concentration in the product has very strong influence on batch time, with lower limits requiring considerably longer batches. Ethyl acetate is shown to dictate the attainable ethanol concentration, such that low limits prohibit a reasonable alcohol content in the product. Repeatedly solving a finite set of modified versions of a dynamic optimisation problem is demonstrated as a useful means to gain process insight, and my be used to visualise the effect constraint thresholds have on the performance ceiling for bioprocess operation.

Chapter 10

Problem Reduction Towards Rapid Pareto Approximation

A weighted sum approach for optimal fermentor operation has been applied in Section 9.2.4; varying the respective objective weights allowed alternative optimal solutions to be produced. Doing so provided insight into the inherent process trade off between batch time and ethanol yield, and how optimal solution profiles for temperature control are affected by the weightings, however only two sets of weights were considered. The weights assigned to the various process targets to produce a single objective function may be considered arbitrary in many cases, with decision-makers (brewers) not necessarily able to quantify a priori the relative importance of competing objectives. Systematically exploring the trade-off and visualising Pareto optimal temperature manipulations for efficient fermentation is desirable to gain greater insight and assist brewers with the selection of the most preferable operation strategy. A number of multi-objective optimisation algorithms have been successfully applied to a wide range of engineering problems, where visualisation of the trade-offs can provide decision makers with valuable insight (Gujarathi et al., 2015; Zhang et al., 2015; Fraga and Amusat, 2016; Che et al., 2017; Maria and Crişan, 2017; Keßler et al., 2017).

It could be suggested to further vary the objective weights and repeatedly re-solve the same problem to construct the entire Pareto set. However, difficulty

exists in determining which weighting-sets to solve, as equally spaced weights are unlikely to map to equispaced points unless the trade off is linear. Furthermore unsupported points can be omitted from the solution set when using a weighted sum approach if the true front is non-convex, even if they are Pareto optimal. Additionally, the large scale NLPs produced following the complete discretisation of the continuous dynamic optimisation problem can show large solution times and convergence issues when the problem size rapidly grows with the level of discretisation applied. Herein an alternative approach is developed, whereby the problem size is drastically reduced while still encapsulating the vast scope for variability of potential operational schemes, in order to rapidly map the full Pareto solution set and trade-off front between the two objectives.

10.1 The Strawberry Algorithm

It is desirable to develop a novel profile representation (control profile to decision vector encoding) which permits efficient search of feasible candidate temperature manipulations for effective fermentation. Such a representation would allow the bi-criteria trade-off to be mapped using multi-objective optimisation methods such as NSGA-II (Deb et al., 2002), or for exploration with single objective methods with weighted sum or ε-constraint approaches. The Strawberry algorithm (Salhi and Fraga, 2011)is a nature-inspired stochastic evolutionary optimisation method which has been successfully applied to a single objective dynamic optimisation problem in the built environment (Fraga et al., 2015). Recently, using a new fitness function for multi-objective problems, the algorithm has been applied to integrated energy systems design for off-grid mining operations (Fraga and Amusat, 2016). Given the demonstrated success of the algorithm for gaining insight into a bi-criteria objective trade-off we propose using the Strawberry Algorithm evaluate our solution representations and compute Pareto optimal solution sets for the industrial beer fermentation process. The fermentation objective in this chapter is thus no longer the weighted sum formulation from Chapter 6 – 9; rather the multi-objective problem is now defined by Eqs. 10.1–10.3, subject to

the base-case constraint thresholds on by-product species (Eqs. 6.30–6.31):

$$\min_{d} f_1, f_2 \tag{10.1}$$

$$f_1 = -[EtOH]_{tf} \tag{10.2}$$

$$f_2 = t_f \tag{10.3}$$

Where d is the encoded decision vector which translates to a specific $T(t)$ profile. The Strawberry algorithm (Salhi and Fraga, 2011) is a nature inspired stochastic evolutionary optimisation method. It emulates the behaviour of strawberry plants, encapsulating the two key aspects of effective global optimisation algorithms: solution exploration and intensification. In nature, strawberry plants exploit their surroundings through the propagation of runners. In a favourable environment, they will generate a greater number of runners, most within their local vicinity. Less frequently, the plants which are not as well situated will reproduce through the propagation of fewer yet longer runners. This inspires the Strawberry algorithm: each member of the population (an individual solution) is evaluated (objective functions computed) and a fitness function is assigned. The fitness value influences both the number of runners (exploitation, proportional to fitness) and the distance which each runner travels (exploration, inversely proportional to fitness). The population evolves over a pre-defined number of generations. The evolutionary process is characterised by only two parameters: the maximum number of runners to generate for any given solution and the number of solutions to consider for propagation in each generation. The Strawberry algorithm has previously been successfully applied to a single objective dynamic optimisation problem in the built environment (Fraga et al., 2015). Recently, using a new fitness function for multi-objective problems, the algorithm has been applied to integrated energy systems design for off-grid mining operations (Fraga and Amusat, 2016), also a dynamic optimisation problem. The algorithm can be summarised as follows:

Algorithm 1: The Strawberry Algorithm Pseudo Code

Given: $f(x)$, a vector function; ng, number of generations to perform, n_p, the propagation size; n_r, maximum number of runners to propagate.
Output: z, vector approximation of Pareto front.

```
p ← initial random population of size n_p
for n_g generations do
    prune p, removing similar solutions
    N← fitness(p) ;                          // Use rank based fitness
    p ← φ ;                                  // Empty set
    for i ← 1 . . . n_p do
        x ← select(p, N) ;                   // Tournament fitness
                                                based selection
        for each runner to generate do ;     // Number proportional to
                                                fitness rounded up
            x̃ ← new solution(x, 1 − N);      // Distance inversely
                                                proportional to fitness
            p̃ ←x̃ ⋃ p̃;                        // Add to new population
        end for
        p ← p̃ ⋃ Non-dominated(p) ;           // New population with
                                                elitism
    end for
end for
z ← Non-dominated(p) ;                       // Pareto Set
```

10.2 Control Profile Encoding

In order for any control trajectory optimisation problem to be compatible with such an algorithm like The Strawberry Algorithm, at least the control profile must be discretised. Doing so leads to a partial discretisation approach (CVP), meaning it is necessary to define a function which transforms a vector of decision variables to a unique profile or trajectory (herein referred to specific profile encoding strategy or solution representation). The representation of solutions has a direct impact on the effectiveness of any optimisation method (Fraga et al., 2018). Specifically, the bounds imposed on each variable should restrict the solution form such that only realistically practical cases are considered (omitting unnecessary computational load) while ensuring that a large enough search space exists so that a wide range of solutions may be considered. In this study we consider two strategies for profile encoding, a piecewise linear approach and a piecewise polynomial approach.

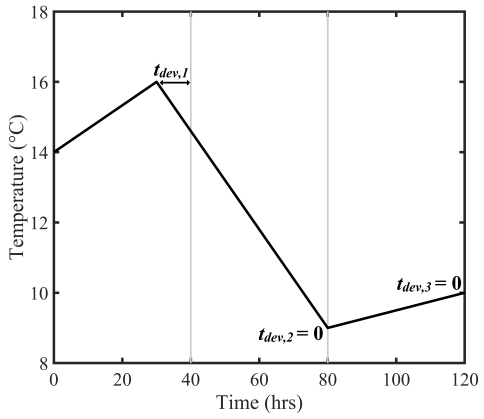

Figure 10.1: (a): Example PWL profile; (b): PWP Profile Structure

10.2.1 Piecewise Linear (PWL) Profile Encoding

For this encoding strategy, each temperature profile consists of N piecewise linear segments, between N+1 nodes of coordinates $[t_i, T_i]$ where $0 \leq i \leq N$. The time domain is discretised into N equal intervals:

$$\Delta t = \frac{t_{max}}{N} \tag{10.4}$$

Where t_{max} is the longest fermentations desirable to be considered, defined using existing industrial practice as a basis:

$$t_{max} = 120 \text{ hrs} \tag{10.5}$$

If uniform spacing were used, t_i would be $i \cdot \Delta t$. However, more effective use of the N+1 points may be possible if non-uniform spacing were allowed, since drastically more variation in the profile is permitted. The variable $t_{dev,i}$ is introduced to represent deviation from the uniform spacing for each time point, excluding t_0, such that each time point (apex of PWL profile) is defined as:

$$t_i = i \cdot \Delta t + t_{dev,i} \tag{10.6}$$

This deviation approach is preferable to permitting completely free movement of the nodes within the time domain. With suitable bounds on the deviations,

this approach acts to regulate the segment lengths: preventing a large portion of the segments bunching together which would require unachievable and undesired rapid manipulations to be performed to the vessel. Additionally it ensures that unfavourably long fermentations are not considered: only fermentation times up to $t_{max} + \max(t_{dev})$ can be computed. Bounds imposed on time point deviation prevent subsequent nodes, t_i, from overlapping with the prior, t_{i-1}.

$$\frac{-\Delta t}{2} \leq t_{dev,i} \leq \frac{\Delta t}{2} \tag{10.7}$$

The bounds on the initial temperature and the temperature component of each profile node are given by:

$$T_{min} \leq T_i \leq T_{max} \tag{10.8}$$

Here the values for the bounds taken from Eq. 6.22. In summary, the decision variables consist of the initial system temperature, $T_{t=o} = T_0$, and N couplets of $[t_i, T_i]$:

$$d = [T_0, t_{dev,1}, T_1 ..., t_{dev,N}, T_N] \tag{10.9}$$

As such that the number of decision variables scales linearly with the discretisation level:

$$\text{length}(d) = 2 \cdot N + 1 \tag{10.10}$$

The search domain which may be explored by the stochastic algorithm is fully defined by Eqs. 10.7–10.10, with the manner in which the decision vector translates to a piecewise linear $T(t)$ control profile between $N+1$ nodes $[t_i, T_i]$ $(0 \leq i \leq N)$ defined by Eqs. 10.4–10.6. As an illustrative example of this profile encoding, consider the vector d = [14, -10, 16, 0, 9, 0, 10]. The 7 elements correspond to $N = 3$, from Eq. 10.10 meaning the profile described by 4 $T(t)$ points or 3 linear sections. Three equal time intervals would split the 120 hr horizon into 40 hr sections ($\triangle t = 40$), however the second point in d states a minus 10 hour deviation on the second time coordinate (the first is always $t = 0$ so no deviation applies). This example there-for corresponds to a piecewise linear profile between the four points: [(0,14), (30,16), (80, 9), (120, 10)], as shown in Fig. 10.1.

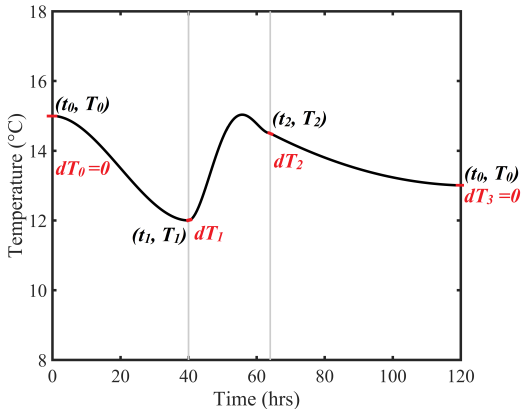

Figure 10.2: PWP Profile Structure

10.2.2 Piecewise Polynomial (PWP) Profile Encoding

To explore the effectiveness of smoother profiles which are not dependent on discretisation level a piecewise polynomial profile representation is considered. It has been demonstrated that problems of slow convergence and non-smooth impractical control strategies can be overcome by representing control profiles with polynomial approximations (Sorek et al., 2017). The authors could achieve significant computational savings, due to seeking the optimal polynomial coefficients rather than optimal control values within many time intervals. The PWP implementation in this thesis considers the time domain to consist of three sub-domains, on the basis of the optimal solutions from exhaustive simulation and dynamic optimisation (Chapters 6, 7 and 9) generally showing three distinct regions in the computed control profiles. In each sub-domain, the solution representation will define a smooth polynomial. Specifically, we construct $T(t)$ profiles from three polynomials: a cubic for first and last sections, with an intermediate quintic. Temperature values and first derivatives of the temperature are defined to be the same for the respective polynomials at each boundary between sub-domains, and the gradients at the very start and the end of the profile are set to 0. With these restrictions, the profile is described uniquely by 5 coordinates and 2 derivatives, shown in Fig. 10.2. The decision vector corresponds to these 5 points and 2 derivatives, requiring 11 variables as the first point will always occur at $t = 0$:

$$d = [T_0, t_1, T_1, dT_1, t_{f2}, T_2, dT_2, t_{fm}, T_m, T_3, t_3] \tag{10.11}$$

The cubic between t_0 and t_1 has 4 degrees of freedom so defined by 2 points (t, T) and 2 gradients (dT). The points $(0, T_0)$ and (t_1, T_1) and gradient dT_1 are known directly from Eq. 10.11, which along with $dT_0 = 0$ fully defines the curve. A linear system of equations can be rapidly solved to give the coefficients of the corresponding polynomial. Similarly, the centre polynomial, here 5th order, is defined by 3 points and 2 derivatives: (t_1, T_1) and dT_1 known from the end of the first section, T_2 and T_m are defined by d (Eq. 10.11) and the corresponding time of these points are defined by:

$$t_2 = t_1 + (t_{2,max} – t_1) \cdot t_{f2} \tag{10.12}$$

$$t_m = t_1 + (t_2 - t_1) \cdot t_{fm} \tag{10.13}$$

This allows the linear system of equations to be solved to in order to obtain the 5 coefficients of the middle quintic. The final cubic is defined with 2 points and 2 derivatives: (t_2, T_2) along with dT_2 are known from the previous segment, dT_0 is set as 0 so only a final point remains to be defined:

$$t_3 = t_3 + (t_{max} - t_2) \cdot t_{f3} \tag{10.14}$$

Herein the profile end point (t_2, T_2) is defined, allowing the coefficients of the final polynomial to be determined. Therefore, the full profile, consisting of three piecewise polynomials, is uniquely represented by Eq. 10.11.

10.3 Results

A variety of discretisation levels were investigated for PWL profiles, in addition to the maximum number of generations (gen) and the number of solutions with each generation to propagate (referred to as the population size herein), to investigate how these variables influence solution performance.

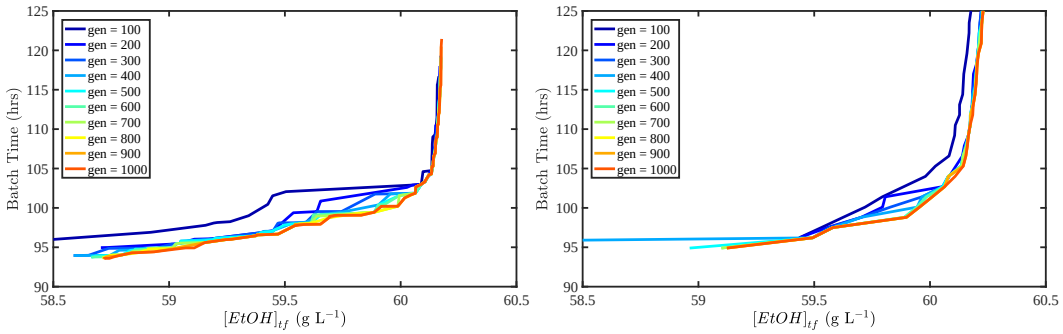

Figure 10.3: Improvement of non-dominated solutions over subsequent generations with population size of 200; left (a): PWL with $N = 6$; right (b): PWP

10.3.1 Solution Convergence

Figure 10.3 depicts how the trade-off curve for the two objectives evolves during the evolutionary process. As batch time minimisation and ethanol maximisation are the two objectives, the desirable solutions will be to the right and the bottom of the plot. Each coloured line joins non-dominated points (where no other solution improves on both objectives simultaneously) from the population which corresponds by colour to a generation number: this can be considered an approximation to the Pareto trade-off front. An elitism rule in place ensures that all non-dominated points pass to subsequent generations: favourable solutions are not lost and performance of the corresponding temperature profiles the beer fermentation from the front can only improve or remain unchanged in subsequent generations. The left panel represents PWL with $N = 6$ with a population of 200 solutions, while the right panel shows the PWP equivalent with the same population size.

In the left plot it can be observed that the front moves to towards the bottom right (improvement) significantly between generation 100 and 200 with PWL profiles. Over the following 500 generations continual improvement occurs, particularly regarding batch time reduction. The last 300 generations show minimal gains in either direction so it can be concluded that convergence has occurred to the final red line which we can consider the Pareto front for $N = 6$. The algorithm was repeated numerous times for the same conditions and settings, with convergence to a similar front achieved in under 1000 generations in all instances. When

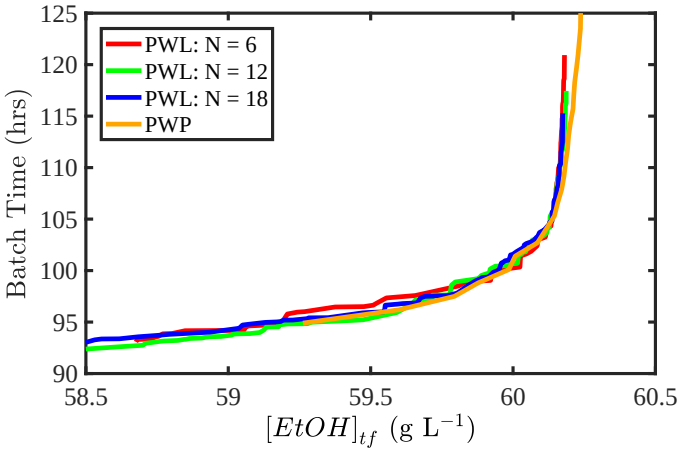

Figure 10.4: Non-dominated front after 2000 generations for various control profile discretisation levels.

N was increased to both 12 and 18 it was found necessary to increase the number of generations to 2000 in order to achieve convergence. This is a direct result of the increased number of decision variables (Eq. 10.9) which leads to an increase in the size of the search space. The right plot again shows a significant improvement over the first 200 generations for PWP profiles, however here it is found that convergence is consistently observed sooner. No discernible improvement is achieved after generation 500, suggesting that the algorithm has converged on the most preferable profiles for this particular $T(t)$ profile encoding. Fig. 10.4 compares the final Pareto front approximation after convergence between the two strategies. The front after 2000 generations, over the same objective axis as Figure 10.3, for increasing discretisation level (N) of PWL profiles, along with the front for PWP profiles after 500 generations. A high level of similarity between the lines is evident. This is surprising between the three PWL cases, given that with three times as many linear profile segments one might expect the considerably increased level of control to permit significant improvements. However, this is not found to be the case. The blue line is significantly smoother than the others as a result of the greater number of non-dominated points in this solution set. It is worth noting that the search for candidate solution profiles for industrial fermentation is not concerned with the number of candidates detected, rather the suitability and effectiveness of the most promising candidates. As the PWP Pareto front very closely follows those from the PWL representation

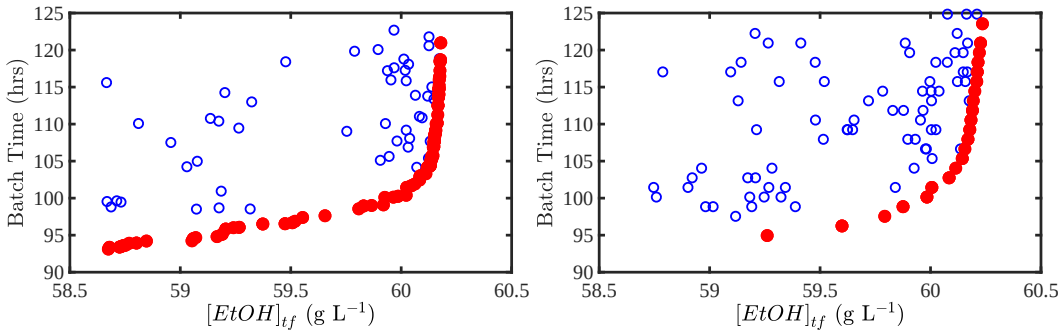

Figure 10.5: Final population (population size of 200) of solutions, left (a): PWL with $N = 6$; right (b): PWP. Solid red markers are non-dominated.

it is demonstrated that neither encoding is particularly favourable for attainable fermentation performance across the majority of the domain, as equivalently performing solutions are generated in both cases. However, it is observed that the lower left portion of front is not reproduced with PWP profiles, highlighting that the piecewise polynomial encoding restricts the solution space such that very low batch time (and low ethanol) solutions are not able to be produced. This is a results of near instantaneous temperature adjustments not being permitted with PWP profiles, the implications of which are considered subsequently.

10.3.2 Final Solution Populations

The plots shown in Fig. 10.5 represent the final populations from unique instances of the Strawberry algorithm being executed for the two different encoding strategies. Each hollow blue circular marker corresponds to the performance of a solution profile in the current population; those which are non-dominated are coloured red. The algorithm was executed numerous times using varying population sizes, and it has been found that a very similar Pareto approximation is produced with population sizes as low as 20 solutions. For both methods the density of the front, thus the number of promising candidate solutions discovered, increases with population size at the cost of required CPU time. Comparing the two plots in Fig. 10.5 shows that unlike PWL the PWP encoding is not able to produce solutions towards the bottom left of the axis; however given the low ethanol concentration this is unlikely to omit realistically desirable scenarios. In addition to the performance of the solutions in terms of objective function values,

it is of critical importance to examine what the solutions represent in terms of control profiles to assess their suitability for industrial application. Fig. 10.6 represents samples of the profiles which make up the non-dominated solutions from the final populations for discretisation levels $N = 6$ and $N = 18$ for PWL profiles, with PWP profiles below. Not all the PWL profiles are of industrial value due to the ability to physically replicate them on real plant equipment. Solutions obtained with low N values are more suitable industrially. The number of manipulations required is smaller and temperature changes more gradual, as can be seen in the figure. Taking this into account, and considering the marginal improvement observed when increasing the discretisation level (Fig. 10.4), it is recommended to only pursue $N = 6$ solutions for the PWL implementation. Not all of the solutions produced for high discretisation levels (i.e. $N = 18$) have undesired temperature variations. The third example presented in the middle row of Fig. 10.6 is a particularly promising case where the improved control permitted with higher discretisation acts to smooth the profile form, rather than to do the opposite as seen in the second plot from the same row. This suggests that merit may exist in refining the definition of the search space, D, by reformulating Eqs. 10.4 - 10.10 so that by design only favourable and implementable solutions may be considered by restricting the ability of the profiles to display a high level of variability in temperature. It must however be noted that simply the omission of rapid temperature changes should be avoided, as both a rapid increase or decrease at some point of the process is not uncommon and can be desirable to assist with the control of by-product production. In contrast, all of the solutions obtained from the PWP method would be considered appropriate for implementation, with no restrictive variability possible due to the polynomial $T(t)$ encoding. Comparing the solution forms between the two methods it can be seen that that there are many similarities. In particular the large temperature drop towards the end of the process appears to be an effective trait for controlling the by-product levels. Given the high similarity in attainable performance and the significantly improved inherent implementability and profile smoothness, using PWP profiles is the most promising strategy for industrial fermentation $T(t)$ profile formulation via the Strawberry algorithm.

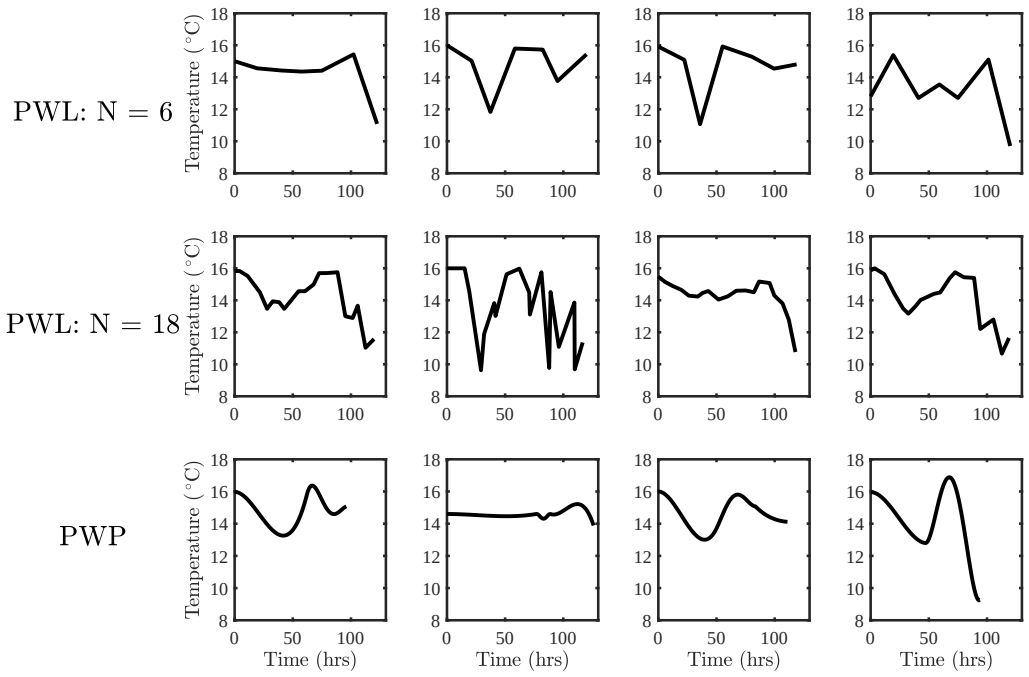

Figure 10.6: Example non-dominated profiles

10.3.3 Solution Profile Performance – design heuristics

Figure 10.7 shows specifically how the solution profiles correspond with their performance on the Pareto front for the preferable PWP method, which provides considerable insight into the fermentation process and as to how the performance is influenced by the temperature manipulation. The profiles which produce extremely short batch times ($t_f < 105$ hrs) at the cost of reduced ethanol concentration all have a comparable form. An initial high temperature is immediately lowered over the first 40 hours (16 °C to 14 °C). The temperature is then raised back to a peak momentarily around 16 °C at the 70 hour point before being reduced once more. Depending on the vessel size this cooling and heating cycle may be attainable on industrial fermentation equipment. In order for the vessel contents to achieve homogeneity, the cylindrical and conical portion of the tank must achieve thermal equilibrium. As such, for the assumptions in the lumped parameter model to apply there is exists a minimum time under which temperature variations cannot be realised, the time for which is a function of the vessel size. In contrast, the longer batch time solutions are more likely to be implementable on any scale of industrial fermentation vessel, as the lesser temperature

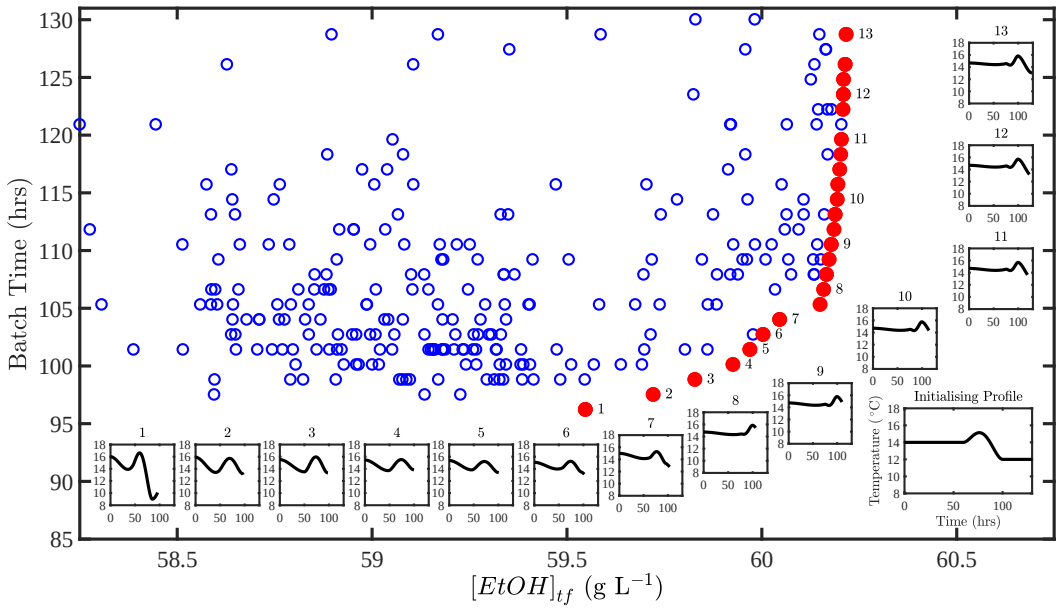

Figure 10.7: Pareto front of non-dominated solutions to the multi-objective problem and corresponding $T(t)$ profiles, for a quasi-A profile initialisation.

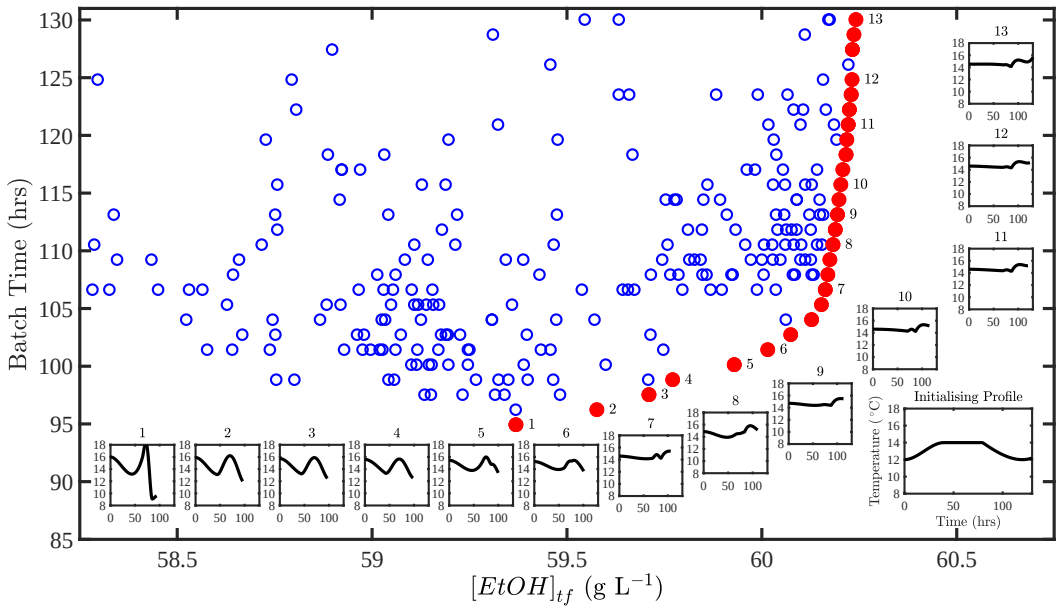

Figure 10.8: Pareto front of non-dominated solutions to the multi-objective problem and corresponding $T(t)$ profiles, for a quasi-B profile initialisation.

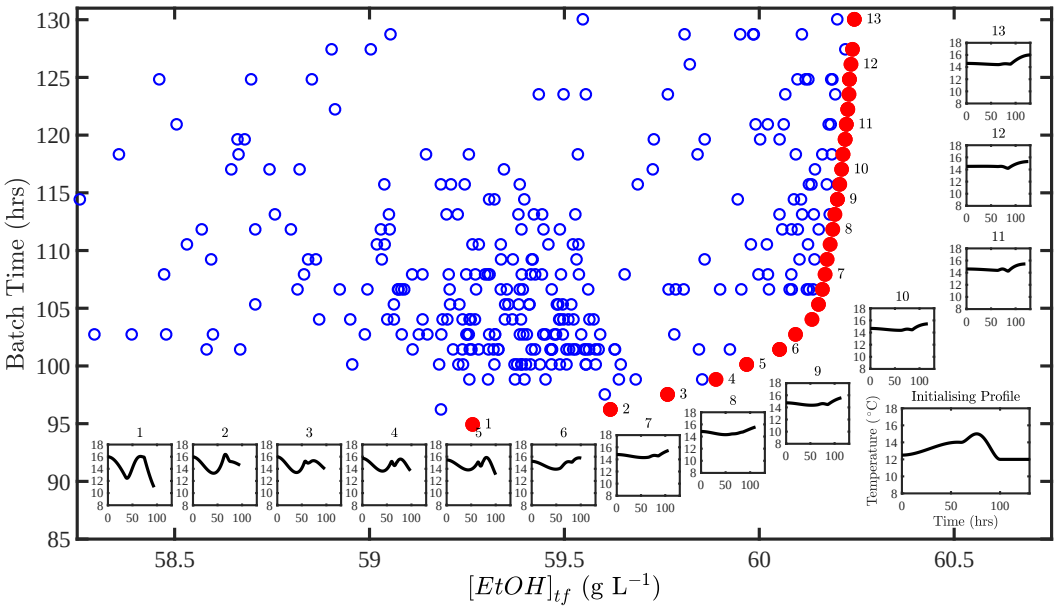

Figure 10.9: Pareto front of non-dominated solutions to the multi-objective problem and corresponding $T(t)$ profiles, for a quasi-C profile initialisation.

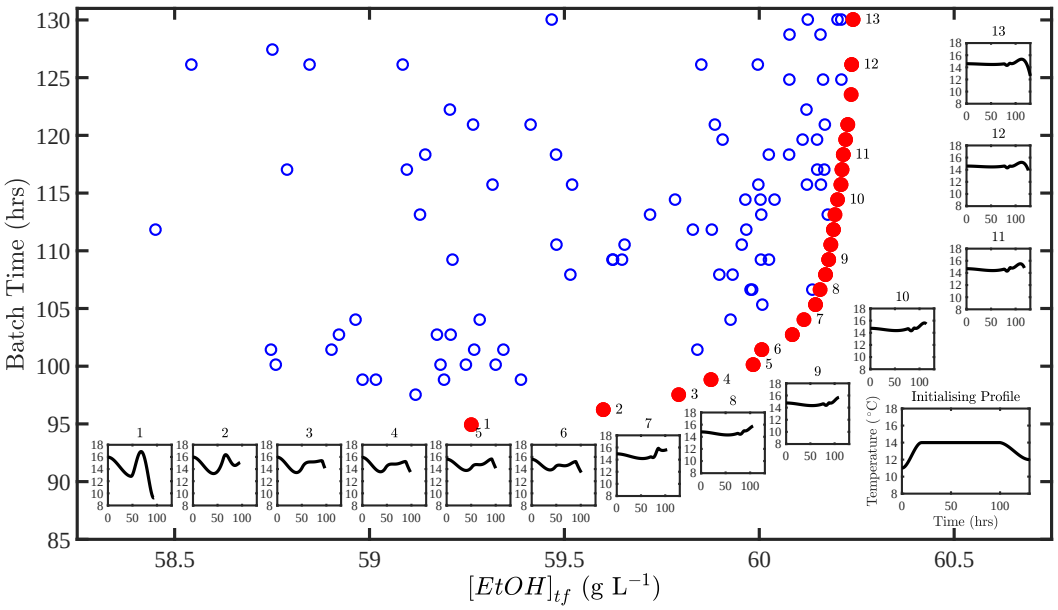

Figure 10.10: Pareto front of non-dominated solutions to the multi-objective problem and corresponding T(t) profiles, for a quasi-D profile initialisation.

variability means that homogeneity will more readily be achieved. In the lower portion of the Pareto set it is demonstrated that magnitude of the batch time range is comparable to the ethanol concentration range, i.e. a sacrifice of 5 hours in batch time can enable a significant 0.5 g L^{-1} increase in ethanol production. In contrast, the longer batch time subset of the front ($t_f > 105$ hrs) shows a very steep form, meaning that very minimal further gains in ethanol concentration are attainable, even upon increasing batch time as high as 130 hrs. A gradual transition is observed in the $T(t)$ profile form along the Pareto front. The initial dip in temperature becomes less pronounced as batch time is increased, an indication that this is an essential component of the temperature profile for extremely rapid beer fermentation. The first half of the profile continues to level off moving up the front, suggesting that this is useful for ensuring a very high ethanol yield. The presence of the later peak and subsequent cooling remains constant throughout the entire front, a feature that is known to assist with efficient fermentation while ensuring that the by-product constraints are not violated. Diacetyl compounds are consumed in the later stages of the process, with this feature of the temperature manipulation accelerating their consumption to fall below the tolerable level rapidly.

It has been demonstrated that the tolerable level of diacetyl in the product is directly restrictive to the attainable batch time, due to the requirement to wait until a sufficient portion has been consumed (Chapter 9), hence why this is an essential profile component for efficient beer fermentation throughout. An important consideration which can be visualised on Fig. 10.7 is how slight variations in the temperature profile can affect the performance of the batch. Of the profiles highlighted in the figure, solutions 12 and 13 is an example of two profiles which are very similar in terms of the $T(t)$ profile. However, the corresponding performance varies drastically, with the later requiring 5 more hours for completion. This stresses the importance of ensuring the temperature is accurately controlled in the fermentor, and that system homogeneity is ensured. Additionally, consideration should be given to solution robustness, ensuring that the manipulation employed will still perform adequately if slight deviations from the profile are encountered.

It has been demonstrated that the initialising profile can influence the solution when using an exact optimisation method (Chapter 7). To investigate whether the stochastic method used in this study exhibits a similar deficiency, a range of initialising profiles have been used, with the corresponding profile maps shown in Figs. 10.7–10.10 for four cases. The initialising profiles presented here are approximations of the 4 candidate solutions highlighted previously from the exhaustive search (Chapter 6), where minor deviations in the profiles are a result of the polynomial representation being unable to fully mirror the PWL form. From Figs. 10.7–10.10 it is shown that the approximate Pareto front of non-dominated points is extremely similar between the four cases, highlighting that attainable performance is not restricted or significantly influenced by the seed profile. While these four cases are initialised with promising candidates, very similar results were found when using either random or isothermal initialisation $T(t)$ profiles, suggesting robustness of the stochastic optimisation strategy employed in this paper. Although the performance of the non-dominated solutions is essentially identical, there are differences observed when comparing the corresponding $T(t)$ profiles. The same overall trends are present, such that postulated heuristics for effective fermentation remain valid. The discrepancies in the profiles across different initialisations are minimal. For example the late peak in the temperature is shown to be less pronounced in the latter three cases, however is still present throughout. The variability in the profiles shown across these four figures is no greater than the differences observed when re-initialising the algorithm numerous times using the exact same seed profile. As such it may be concluded that it is the stochastic nature of the method which is responsible for the solution profiles varying slightly across the four cases presented here, rather than the solution being sensitive to the 'initial guess' or initialising solution.

10.3.4 Evaluation of Profile Encoding Strategies

Table 10.1 presents performance metrics (terminal state concentrations and batch time) comparing the seed solution used for initialising the Strawberry Algorithm to an example of a non-dominated point in the $N = 6$ final population of the

Table 10.1: Example solution profile performance versus initialising profile

Profile	$[EtOH]_{t_f}$(g L^{-1})	t_f(hrs)	$[EA]_{t_f}$(ppm)	$[DY]_{t_f}$(ppm)
Initialisation	59.1	113.5	1.350	0.09
Example solution, PWL	60.0	100.3	1.995	0.10
Example solution, PWP	60.0	100.0	1.996	0.10

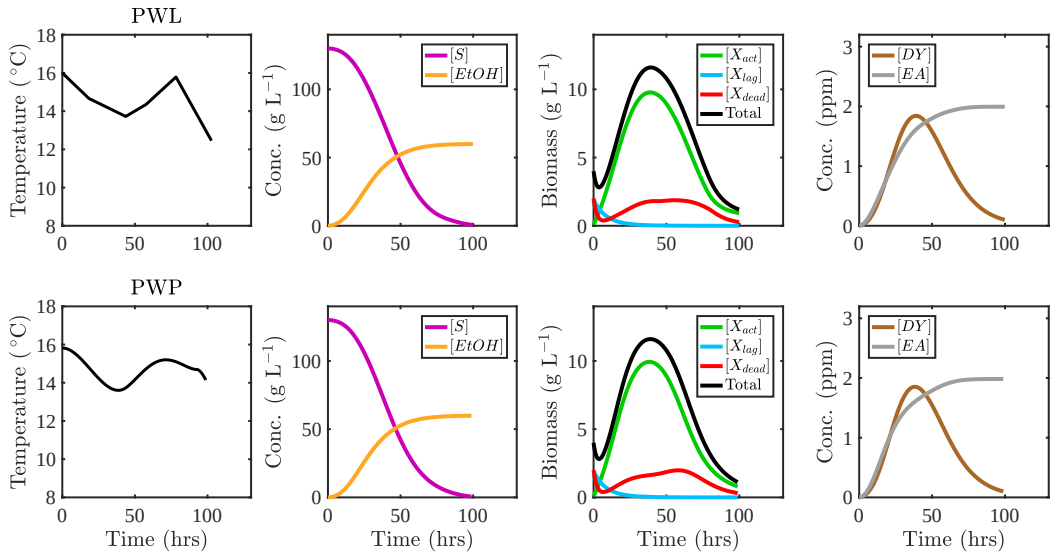

Figure 10.11: Example solution profiles and corresponding state trajectories.

PWL method as well as an example of an attractive PWP solution. The two novel $T(t)$ profiles produced in this study are shown in Fig. 10.11. It can be seen that there is a very high level of similarity the two profiles and the corresponding performance metrics, highlighting that the two unique profile encodings are able to produce comparable favourable solutions. While the upper row of Fig. 10.11 is from $N = 6$ the profile shown consists of 5 sections only: in this case the batch is complete before the final segment, so the profile is terminated. Fig. 10.11 also shows the concentration trajectories over time within the batch while following each example profile. The similarity of the two profiles produces similar concentration progression throughout the respective batch. In both cases the desirable ethanol yield is rapidly achieved by permitting the product concentrations of undesirable species to increase towards the upper limits imposed by the corresponding constraints. The batch time saving of over 12 hours is noteworthy, suggesting the potential for significant process improvement via a potential plant throughput increase.

10.4 Chapter Conclusions

The Strawberry Plant Propagation Algorithm has been used to explore process improvement potential of an industrial beer fermentation process via control vector (temperature profile) optimisation. Two different methods for representing temperature control profiles are investigated, considering batch time minimisation and ethanol yield maximisation as two simultaneous but conflicting objectives. Consistent convergence to the trade-off curve for the two objectives is demonstrated after an adequate number of generations have passed, the required number of which scales with number of decision variables, which in turn scales linearly with the discretisation level for the piecewise linear representation. It is found that a large population size is not necessary for the production of a dense approximation to the Pareto front, due to the inclusion of an elitism rule when generating new solution populations. It has been demonstrated that if a piecewise linear profile is being used it can be beneficial to use a moderately low discretisation level. The minimal performance improvement upon increasing profile complexity is marginal next to the restrictiveness of the highly variable (in temperature) nature of profiles often computed. In contrast low discretisation solutions are inherently more suitable, given the reduced number of manipulations required and the more gradual temperature gradients. A piecewise polynomial encoding has been demonstrated to produce solutions with performance very similar to those from the piecewise linear approach. The added benefit is that these profiles are inherently appropriate for implementation, with no restrictive variability possible due to the improved polynomial $T(t)$ encoding. A dense Pareto front of solution profiles is identified describing the optimal trade-off between these process targets. Such data can be of value as a performance map when operators weigh up the relative importance of these two process targets. A subset of these output profiles can simultaneously reduce batch time and increase product ethanol concentration while satisfying constraints on by-products produced in the fermentors, representing significant improvements versus current industrial practice. A potential batch time reduction of over 12 hours has been

highlighted, which is coupled with a moderate improvement in ethanol content. The ability to identify novel temperature manipulations (control profiles) for improved performance can allow brewers to reduce their batch times and operating costs, highlighting the effectiveness of the multi-objective Strawberry method for efficient dynamic optimisation when the control profile is in such a manor. This approach has the potential to be applied to a range of bioprocess optimisation problems which may benefit from reducing the problem size from the outset, based on fundamental knowledge of the system, in place of constructing very large and complex optimisation problems when not necessary.

Part IV

Research Contributions and Conclusions

Chapter 11

Research Contributions

This thesis has produced several novel research contributions, summarised herein.

11.1 Visualisation of Attainable Fermentation Performance

For the first time a simulation-based optimisation procedure has been applied to a validated industrial scale beer fermentation dynamic model, facilitating the comparison and visualisation of a vast number of unique scenarios against current industrial practice (Chapter 6). Brewers can gain highly valuable insight into the potential for process modifications via such a dynamic simulation campaign of viable and readily implementable modifications to current operation (Rodman and Gerogiorgis, 2016). Each scenario represents a unique fermentation temperature profile, generated using suitable heuristics which are representative of manipulations that are indeed applicable to the real process. Each case can represent a potential new product, with its own characteristic composition and aromatic profile, or a modified version of an established product, produced in a potentially more efficient manor. This procedure favourably ensures that the degree of domain discretisation only produces temperature profiles which are implementable, without the need for a secondary smoothing process. In doing so performance maps are attained: high density plots of performance criteria of all

the manipulations in the simulation set. Analysing these maps in relation to current industrial performance permits brewers the insight necessary to make process decisions and select candidate profiles for implementation and validation. Three unique novel manipulations have been identified, each with the potential to drastically reduce batch time of an industrial collaborator (WEST Brewery, Glasgow, UK) by up to 15 hours, with no discernible impact on beer flavour and quality. These candidate profiles are also later shown as highly effective for initialisation or 'initial guesses' for deterministic and stochastic dynamic optimisation methodologies, compared to blind or random initialisation (Chapter 7). This procedure is extended, comparing performance maps under differing simulation conditions to ascertain, visualize and quantify the global effect wort components have on process performance. Multi-dimensional sensitivity analysis of key beer quality attributes versus plausible initial condition modifications for an enormous ensemble (hundreds of thousands of possible temperature manipulation profiles possible for prescription) demonstrates that initial sugar concentration clearly affects final ethanol concentration and thus beer product quality; the most remarkable finding is that fermentation efficiency and batch duration can be improved by manipulating the initial biomass concentration (yeast pitching rate) fed to fermentors. Moreover, what is also noteworthy is that the active fraction of fed yeast has a quite minor (virtually insignificant) effect on process efficiency (as long as a potent yeast strain is used) because the active cell population quickly rises if enough heat is provided by the selected temperature manipulation profile. These plots are extremely useful in capturing and mapping differences in current practice (and possible changes) for various products.

11.2 Multi-Objective Dynamic Optimisation of Beer Fermentation

A range of studies into model based optimisation of beer fermentation are reported in the literature, however prior work relies on the assumption that the precise process targets are know precisely; allowing a single explicit objective

function to quantify performance and ultimately be minimised. Given the vast range in global brewing operations and the diverse spectrum of products in the market, extreme difficulty exists in formulating a meaningful objective: this depends on each brewer's target product composition, and arbitrary target variable weighting appears a popular but also questionable methodology. Additionally, prior work elects to consider flavour-degrading by-product aromatic species minimisation as a component of their objective function. Liaising with industrial collaborators reveals the reality whereby such a minimisation is often redundant: rather any specific product features strict threshold upper limits which specific compound concentrations must adhere to. To this end the first multi-objective dynamic optimisation beer fermentation study has been performed, considering batch minimisation and product yield maximisation as the two process targets, subject to explicit terminal constraints on by-product species concentrations (Chapter 10). Mapping the Pareto front trade-off via multi-objective dynamic optimisation can be used by decision makers to better inform process decisions with significant economic implications, in place of computing a single solution scenario deemed optimal by an *a priori* determined objective weighting (Rodman, Fraga and Gerogiorgis, 2018).

11.3 Optimisation subject to Variable Constraint Limits to Gain Process Insight

Alcoholic beverages have differing tolerable concentrations of by-product species. As a consequence their exists no universal limits which optimal operation would always be subject to. This thesis presents a strategy for investigating the impact each species threshold has on the attainable process performance (Chapter 9). The dynamic trajectory problem for optimal fermentor operation is repeatedly solved for a spectrum of threshold values on by-product concentrations to investigate the effect which these have on the obtainable process performance. Discretisation of the state trajectories in addition to the control vector using orthogonal collocations permits a large scale NLP problem to be solved, here for piece-wise

constant temperature profiles. This is performed for 25 different pairs of constraint thresholds on ethyl acetate and diacetyl in the beer product to compare the performance of the optimal profiles produced in each case. This investigation into the influence of by-product threshold limits on obtainable fermentation performance has revealed novel insight into how each by-product uniquely affects process performance (Rodman and Gerogiorgis, 2017). It is found that the permitted diacetyl concentration in the product has very strong influence on batch time, with lower limits requiring considerably longer batches as a result of its consumption in secondary fermentation. Ethyl acetate is shown to dictate the attainable ethanol concentration, such that low limits prohibit a reasonable alcohol content in the product.

11.4 Problem Reduction Towards Efficient Optimisation

Much of the work presented in this thesis involves computing precise solutions to large scale NLPs, following the complete discretisation of the continuous dynamic optimisation problem. Limitations with this approach can include very large solution times and convergence issues as the problem size rapidly grows with the level of discretisation applied. Herein an alternative approach is developed, whereby the problem size is drastically reduced while still encapsulating the vast scope for variability of potential operational schemes (Chapter 10). Novel encoding strategies are developed to represent the fermentor temperature profile as a vector of only a few decision variables. Strategies are developed from the insight gained by prior dynamic simulation and optimisation results presented in this thesis. Here in the characteristics of favourable manipulations are ensured alongside inherent industrial implementability and problem size management. Two different representations are presented: piece-wise linear and piece-wise polynomial approaches, where the resultant CVP problem can be solved by a number of approaches, here by the Strawberry Plant Propagation Algorithm. Consistent and rapid convergence to the trade-off curve for the two objectives is demonstrated

after an adequate number of generations have passed, the required number of which scales with number of decision variables, which in turn scales linearly with the discretisation level for the piece-wise linear representation. It is found that a large population size is not necessary for the production of a dense approximation to the Pareto front, due to the inclusion of an elitism rule when generating new solution populations. An added benefit is that these profiles are inherently appropriate for implementation, with no restrictive variability possible under the improved polynomial $T(t)$ encoding. A dense Pareto front of solution profiles is identified describing the optimal trade-off between these process targets. These results highlight the effectiveness of the multi-objective Strawberry method for efficient dynamic optimisation when the control profile is in such a manor. This approach has the potential to be applied to a range of bioprocess optimisation problems which may benefit from reducing the problem size from the outset, based on fundamental knowledge of the system, in place of constructing very large and complex optimisation problems when not necessary (Rodman, Fraga and Gerogiorgis, 2018). .

11.5 Estimation of an Uncorrelated Parameter Set for Beer Fermentation Modelling

All model based optimisations rely on high fidelity parametrisation. Where model parameters cannot be directly measured a regression is commonly performed. An optimisation problem in its self, the discrepancy between the model predictions and data is minimised by parameter estimation. Herein it is often assumed that the best fit (least squares error) corresponds the most accurate values of all the parameters under estimation in the regression. However, it is highly common for bioprocess models to contain parameters which are not uniquely identifiable: Monod-like models generally have growth yield parameters which are significantly correlated with the maximum growth rate term (i.e. V_{max} and K_m in a Michaelis–Menten expression). It is demonstrated that attempting to estimate the complete unknown parameter for a beer fermentation model results in

an ill-conditioned problem and poor solution attainment whereby a large number of parameter sets produce essentially the same model fit. For the first time systematic sensitivity analyses of this beer fermentation model is performed, using two established methods, to assess and elucidate the relative significance of parametric discrepancy on the validity of dynamic simulation of the evolution of certain concentration observables (Chapter 4). In doing so the parameters of least importance have been identified, and by assigning appropriate values from literature it permits high fidelity estimation of the remaining more significant and influential parameters using the experimental data set. Ensuring accurate values for these model parameters is instrumental towards ensuring the robustness and applicability of the dynamic simulation and optimisation results presented in this thesis.

11.6 Heat Transfer Dynamics in Beer Fermentation Modelling

A limitation of much prior work towards beer fermentation optimisation is the universal assumption of direct and instantaneous control of fermentor temperature. With the addition of a heat transfer model fermentor heat dynamics are approximated in this thesis. Herein the manipulatable control becomes the jacket coolant feed-rate in place or the reactor temperature. A novel, comprehensive visualisation of the attainable performance maps for key process variables is presented, obtained via a large-scale dynamic simulation campaign of viable heat transfer (cooling) policies. These attainable performance maps are compared to equivalent results produced previously, to elucidate how fermentor performance varies once production scale increases beyond the point of the previous simplifying assumption (Chapter 6). Consideration of explicit fermentor jacket heat transfer marks a significant improvement over the fidelity of prior work which assumed temperature may freely manipulated. Visualisation of attainable performance reveals that a vast portion of operation cases considering explicit temperature control are unobtainable on an industrial scale, highlighting the importance of

the improved approach. Optimal operation involves a novel cooling policy to effectively manage the active yeast population in the reactor, capable of improved performance versus established approaches. Sensitivity analysis of the solution dependence on thermal process parameters shows how adjustments in the coolant rate can be made to maintain the preferred optimal temperature trajectory of the fermenting wort in the vessel.

11.7 Keratin Hydrolysis Modelling and Optimisation

The hydrolysis of keratin-rich material with keratinolytic bacteria is identified as an attractive way of transforming undesirable waste from agro-industrial activities into products of practical industrial value. A lab scale experimental campaign has been performed allowing the first dynamic model for enzymatic hydrolysis of keratin to be proposed (Chapter 5). Michaelis–Menten kinetics with product inhibition allows the observed behaviour of the reactive system to be captured, with the model fit showing good agreement with experimental data. The model assumption of a fixed fraction of the substrate being hydrolysable is not able to fully capture the observed phenomena where by yield in fact decreases with solids loading. Further experimental work is necessary to explore this with the aim of better describing the apparent inhibitory effect at higher substrate content to increase model fidelity towards more robust optimisation results, with the aim of increasing the cost competitiveness of this novel means to treat the abundant quantities of keratin-rich waste produced annually. It is demonstrated how the proposed model may be applied towards fed-batch feed-schedule optimisation. To circumvent the model not capturing the inhibitory effect of high solids content, the reactor substrate concentration is constrained to a level below which such a phenomenon is observed, allowing an optimal operating protocol to be computed.

Chapter 12

PhD Thesis Conclusions

This PhD thesis presents a framework for bioprocess model parameter estimation, rapid dynamic simulation of viable operational scenarios with visualisation of the attainable performance, followed by multi-objective dynamic optimisation strategies, all applied to select candidate processes identified to benefit drastically from process intensification. The problems of consistent kinetic parameter estimation and systematic determination of optimal operating profiles to improve industrial practice are explored, with best practices presented in this thesis.

Performing an extensive lab scale experimental hydrolysis campaign has allowed the first dynamic model for enzymatic hydrolysis of keratin to be proposed. Michaelis–Menten kinetics with product inhibition allows the observed behaviour of the reactive system to be captured, with the model fit showing good agreement with experimental data. Developing a model for this highly novel process represents an important step towards achieving commercial viability of this emerging technology. Undertaking model sensitivity analysis alongside the experimental campaigns permitted specific experiments to be performed to uniquely identify the most pertinent model parameters, prior to regressing those remaining from the data sets collected. A high-fidelity parametrisation of a previously published fermentation model is also presented, such that it can represent the real world process with maximum accuracy. It is demonstrated that attempting to estimate the complete unknown parameter set results in an ill-conditioned problem and poor solution attainment, a frequent problem in biochemical model parametrisa-

tion. Systematic sensitivity analyses using two established methods is performed to assess and elucidate the relative significance of parametric discrepancy on the validity of dynamic simulation of the evolution of certain concentration observables. In doing so the parameters of least importance have been identified and assigning appropriate values from literature to permit high fidelity estimation of the remaining influential parameters using an experimental data set.

For the first time attainable performance in beer fermentation has been exhaustively mapped under a comprehensive family of realistic time dependent temperature manipulations, providing invaluable insight to industrial brewing collaborators. In addition to providing valuable process insight, it is later shown how favourable solutions from this exhaustive simulation set can be highly valuable for initialisation of both deterministic and stochastic dynamic optimisation methodologies, when local methods are being employed. Optimal dynamic fermentor temperature profiles subject to a range of realistic threshold constraints on flavour degrading compounds have been computed and presented. Herein the influence of each individual by-product level on the achievable process performance can be explicitly quantified and visualised.

Furthermore, the inherent trade-off in brewing process targets has been explored for the first time in this work, mapping the Pareto front via multi-objective dynamic optimisation. These results can be used by decision makers to better inform process decisions with significant economic implications. This is further extended to incorporate realistic, indirect temperature manipulation via coolant feed-rate. Optimal operation involves a novel cooling policy to effectively manage the active yeast population in the reactor, capable of improved performance versus established approaches. Dynamic sensitivity analysis of the solution dependence on thermal process parameters shows how adjustments in the coolant rate can be made to maintain the preferred optimal temperature trajectory of the fermenting wort in the vessel.

Dynamic optimisation using the proposed keratin hydrolysis model towards fed-batch feed-scheduled optimisation has been successfully performed. An improvement (reduction) in terminal keratin concentration of about 5 g L^{-1} can be made, following the optimised schedule compared to a generic strategy (addition

after each 24 hours). This highlights the potential benefit in applying such a method towards determining the optimal strategy for maximising substrate consumption. The case studies presented highlight the immense value in systematic and rigorous model-based simulation and optimisation campaigns for biochemical process systems, and the applicability of the methodologies outlined in this PhD thesis.

Part V

Auxiliary Chapters

Appendix A

Nomenclature

Greek Characters:

ϕ	Running objective pay-off function
Δ	Perturbation step size
$\Delta\xi_i$	Profile element
ΔE	Energy displacement
ΔH	Enthalpy of Reaction
β	Product formation coefficient
γ	Terminal objective pay-off function
γ_K	Collinearity index
$\delta_{i,j\ msqr}$	Mean squared summary of state y_j sensitivity to parameter i
ΔT_{max}	Maximum permitted temperature step
θ	Parameter vector
θ_0	Nominal parameter vector
θ_j	Basis function
μ_{EE}	Mean elementary effect
μ_{AB}	Diacetyl consumption rate
μ_d	Biomass death rate
μ_{DT}	Rate of cell death
μ_{DY}	Diacetyl production rate
μ_e	Ethanol specific growth rate

μ_{e0}	Maximum ethanol specific growth rate
μ_g	Biomass growth rate
μ_G	Glucose production rate
μ_L	Specific rate of activation
μ_M	Maltose production rate
μ_N	Maltotriose production rate
μ_S	Sugar consumption rate
μ_{s0}	Maximum sugar consumption rate
μ_{SD}	Dead cell settling rate
μ_{SD_0}	Maximum cell settling rate
μ_x	Specific cell growth rate
μ_{x0}	Maximum cell growth rate
ρ_C	Density of Coolant
ρ_R	Mean Density of Wort
ϕ_j	Basis function

Roman Characters:

A_h	Heat Transfer Area
A_i	Arrhenius Constant
B_i	Arrhenius Constant
Cp_C	Coolant Heat Capacity
Cp_R	Wort Heat Capacity
d	Decision vector
dT_i	Temperature gradient at interface i
$[DY]$	Concentration of diacetyl compounds
E,$[EtOH]$	Ethanol concentration
$[EA]$	Concentration of ethyl acatate
EE_{i0}	Elementary effect of parameter i around parameter set θ_0
$[E]$	Active enzymatic activity
$[EtOH]$	Concentration of ethanol
e_i	Maximum enzymatic activity
f	Ethanol inhibition factor

F	Reactor feed rate
F_C	Coolant Feed Rate
f_i	Objective i
f_r	Product ratio
g	Inequality constraint function
G	Glucose concentartion
h	Equality constraint function
H	Hydrolysable fraction
J	Objective function value
$[K]$	Keratin concentration
$[K]_H$	Hydrolysable keratin concentration
$[K]_{NH}$	Non-hydrolysable keratin concentration
k_b	Boltzmann constant
k_D	Enzymatic activity decay rate
K_{Fi}	Keratin addition at t_i
K_G	Maximum reaction velocity for maltotriose
K'_G	Inhibition constant for glucose
KI	Inhibition constant
K_M	Michaelis constant
K'_M	Inhibition constant for maltose
K_N	Michaelis constant for maltotriose
k_S	Affinity constant
K_T	Total keratin mass
K_u	Polynomial approximation of control
k_x	Affinity constant
K_x	Polynomial approximation of state
M	Maltose concentration
M_r	Maltotriose concentration
N	Discretisation level
p	Probability
$[P]$	Concentration of protein

p_{final}	Final acceptance probability
$p_{initial}$	Initial acceptance probability
r	Substrate consumption rate
R_A	Residual enzymatic activity
R_{EG}	Yield coefficient (ethanol:glucose)
R_{EM}	Yield coefficient (ethanol:maltose)
R_{EN}	Yield coefficient (ethanol:maltotrisoe)
R_{XG}	Yield coefficient (biomass:glucose)
R_{XM}	Yield coefficient (biomass:maltose)
R_{XN}	Yield coefficient (biomass:maltotrisoe)
$[S]$	Concentration of sugar
$s_{i,j}$	Dynamic sensitivity function of parameter θ_i on model state y_j
t	Time
T	Temperature
T^0	Initialising temperature profile
T_C	Jacket Temperature
T_{C0}	Coolant Feed Temperature
$t_{dev,i}$	Deviation from equispaced time interval i
t_f	Batch Time
T_{final}	Final annealing temperature
t_i	Discreet timepoint i
$T_{initial}$	Initial annealing temperature
t_{lag}	Duration of lag phase
T_{SA}	SA temperature
t_{step}	Time step duration
u	Control variable
U	Overall Heat Transfer Coefficient
V	Reaction volume
V_C	Jacket Volume
V_G	Maximum reaction velocity for glucose
V_N	Maximum reaction velocity for maltotriose

V_M	Maximum reaction velocity for maltose
V_{max}	Maximum reaction velocity
V_R	Wort volume
W_E	Objective weight for ethanol production
W_t	Objective weight for batch time
X	Biomass concentration
$[X_{act}]$	Concentration of active cells
$[X_{dead}]$	Concentration of dead cells
$[X_{inc}]$	Total inoculum concentration
$[X_{lag}]$	Concentration of latent cells
$[X_{sus}]$	Total suspended concentration
Y_{EA}	Ethyl acetate production stoichiometric factor

Appendix B

List of Abbreviations

AE	Algebraic Equation
BCA	BicinChoninic Acid
CD	Complete Discretisation
CPUs	Central Processing Unit seconds
CVP	Control Vector Parametrisation
DAE	Differential Algebraic Equations
DEFRA	Department for Environment, Food & Rural Affairs
EE	Elementary Effect
FAO	Food and Agriculture Organization
HPLC	High Performance Liquid Chromatography
IDP	Itterative Dynamic Programming
ITC	International Trade Centre
IPOPT	Interior Point OPTimizer
MRSA	Methicillin-Resistant Staphylococcus Epidermidis
NSGA	Non-dominated Sorting Genetic Algorithm
NLP	NonLinear Programming
OAAT	One At A Time
ODE	Ordinary Differential Equation
OHTC	Overall Heat Transfer Coefficient
PBM	Poultry By-product Meal

PD	Partial Discretisaton
PWL	PieceWise Linear
PWP	PieceWise Polynomial
SA	Simulated Annealing
VRE	Vancomycin-Resistant Enterococci

Appendix C

Peer-Reviewed Publications

C.1 Journal Articles

1. Rodman, A.D., Gerogiorgis, D.I., An investigation of initialisation strategies for dynamic temperature optimisation in beer fermentation. *Computers and Chemical Engineering,* **124**: 43-61 (2019).

2. Rodman, A.D., Fraga, E. S. and Gerogiorgis, D.I., On the application of a nature-inspired stochastic evolutionary algorithm to constrained multi-objective beer fermentation optimisation. *Computers and Chemical Engineering*, **108**: 448-459 (2018).

3. Rodman, A.D., Gerogiorgis, D.I., Dynamic optimisation of beer fermentation: sensitivity analysis of attainable performance vs. variable product flavour constraint levels. *Computers and Chemical Engineering*, **106**: 582-595 (2017).

4. Rodman, A.D., Gerogiorgis, D.I., Multi-objective process optimisation of beer fermentation via dynamic simulation, *Food and Bioproducts Processing*, **100**: 255-274 (2016).

C.2 Conference Proceedings

1. Rodman, A.D., Falco, F.C., Gernaey, K.V. and Gerogiorgis, D.I., Enzymatic keratin hydrolysis: Dynamic modelling, parameter estimation and validation. *Computer-Aided Chemical Engineering*, **43**: 1553-1558 (2018).

2. Rodman, A.D., Gerogiorgis, D.I., Dynamic simulation and visualisation analysis of fermentation: effect of conditions on beer quality, *IFAC-PapersOnline (DYCOPS 2016)*, **49**(7): 615-620 (2016).

3. Rodman, A.D., Gerogiorgis, D.I., Multi-objective optimisation of flavour and processing time in beer fermentation via dynamic simulation, *Computer-Aided Chemical Engineering*, **38**: 1033-1038 (2016).

C.3 Conference Presentations

Presenting author in **bold**.

1. Rodman, A.D., Weaser, M., Griffiths, L., **Gerogiorgis, D.I.,** Dynamic optimisation and visualisation of industrial beer fermentation with explicit heat transfer dynamics. The 29th European Symposium on Computer Aided Process Engineering (ESCAPE), Eindhoven, Netherlands, (06/2019).

2. **Rodman, A.D.,** Weaser, M., Griffiths, L., Gerogiorgis, D.I., The Industrial Implementation of Validated Dynamic Simulation and Optimisation Tools Towards Superior Beer Fermentation. 2018 AIChE Annual Meeting, Pittsburgh, PA, USA (11/2018).

3. **Rodman, A.D.,** Gerogiorgis, D.I., Multi-Objective Dynamic Optimisation of a Fed-Batch Nosiheptide Reactor. 2018 AIChE Annual Meeting, Pittsburgh, PA, USA (11/2018).

4. **Rodman, A.D.**, Falco, F.C., Gernaey, K.V., Gerogiorgis, D.I., Enzymatic keratin hydrolysis: Dynamic modelling, parameter estimation and validation. The 28th European Symposium on Computer Aided Process Engineering (ESCAPE), Graz, Austria (06/2018).

5. **Rodman, A.D.,** Gerogiorgis, D.I., Parameter estimation and sensitivity analysis for beer fermentation modelling and optimisation. 2017 AIChE Annual Meeting, Minneapolis, MN, USA (11/2017).

6. **Rodman, A.D.,** Fraga, E.F., Gerogiorgis, D.I., Influence of problem formulation on stochastic optimisation efficiency of control trajectories. 2017 AIChE Annual Meeting, Minneapolis, MN, USA (11/2017).

7. Rodman, A.D., **Gerogiorgis, D.I.,** Dynamic optimisation of beer fermentation: sensitivity analysis of attainable performance versus product flavour constraint levels. 2016 AIChE Annual Meeting, San Francisco, CA, USA (11/2016).

8. Riley, S., **Rodman, A.D.,** Gerogiorgis, D.I., Experimentally validated first-principles rheological modelling for drilling nanofluids. PSE@ResearchDayUK, Imperial College London, UK (07/2016).

9. **Rodman, A.D.,** Gerogiorgis, D.I., Dynamic simulation, visualisation and multi-objective optimisation of flavour and batch-time in beer fermentation. PSE@ResearchDayUK, Imperial College London, UK (07/2016).

10. **Rodman, A.D.,** Gerogiorgis, D.I., Multi-objective optimisation of flavour and processing time in beer fermentation via dynamic simulation. The 26th European Symposium on Computer Aided Process Engineering (ESCAPE), Portoroz, Slovenia (06/2016).

11. Rodman, A.D., **Gerogiorgis, D.I.**, Dynamic simulation and visualisation analysis of fermentation: effect of conditions on beer quality. The 11th IFAC Symposium on Dynamics and Control of Process Systems, including Biosystems (DYCOPS-CAB), Trondheim, Norway (06/2016).

12. Rodman, A.D., **Gerogiorgis, D.I.,** Dynamic simulation and multiobjective optimization of flavour and processing time in beer fermentation. AIChE Annual Meeting, Salt Lake City, UT, USA (11/2015).

References

Akinlabi, C. O., Gerogiorgis, D. I., Georgiadis, M. C., and Pistikopoulos, E. N. (2007). Modelling, design and optimisation of a hybrid PSA-membrane gas separation process. *Computer Aided Chemical Engineering*, 24:363–370.

Al-Musallam, A. A., Al-Zarban, S. S., Fasasi, Y. A., Kroppenstedt, R. M., and Stackebrandt, E. (2003). Amycolatopsis keratiniphila sp. nov., a novel keratinolytic soil actinomycete from Kuwait. *International Journal of Systematic and Evolutionary Microbiology*, 53(3):871–874.

Almeida, N. E. and Secchi, A. R. (2011). Dynamic optimization of a fcc converter unit: numerical analysis. *Brazilian Journal of Chemical Engineering*, 28(1):117–136.

Anbu, P., Gopinath, S. C. B., Hilda, A., Lakshmipriya, T., and Annadurai, G. (2007). Optimization of extracellular keratinase production by poultry farm isolate Scopulariopsis brevicaulis. *Bioresource Technology*, 98(6):1298–1303.

Angelopoulos, P. M., Gerogiorgis, D. I., and Paspaliaris, I. (2013). Model-based sensitivity analysis and experimental investigation of perlite grain expansion in a vertical electrical furnace. *Industrial & Engineering Chemistry Research*, 52(50):17953–17975.

Angelopoulos, P. M., Gerogiorgis, D. I., and Paspaliaris, I. (2014). Mathematical modeling and process simulation of perlite grain expansion in a vertical electrical furnace. *Applied Mathematical Modelling*, 38(5-6):1799–1822.

Arashi, A., Konopczynski, M., et al. (2003). A dynamic optimisation technique

for simulation of multi-zone intelligent well systems in a reservoir development. In *Offshore Europe*. Society of Petroleum Engineers.

Arnold, J. P. (2005). *Origin and History of Beer Brewing From Prehistoric Times to the Beginning of Brewing Science and Technology*. BeerBooks, Cleveland, OH.

Ayyaldaz, H. (2018). Optimization of protein recovery from keratin-rich slaughterhouse waste. Master's thesis, Technical University of Denmark.

Aziz, N. and Mujtaba, I. M. (2002). Optimal operation policies in batch reactors. *Chemical Engineering Journal*, 85(2-3):313–325.

Bajpai, R. K. and Reuss, M. (1980). A mechanistic model for penicillin production. *Journal of Chemical Technology and Biotechnology*, 30(1):332–344.

Balsa-Canto, E., Alonso, A. A., and Banga, J. R. (2010). An iterative identification procedure for dynamic modeling of biochemical networks. *BMC Systems Biology*, 4(1):11.

Biegler, L. T. (2007). An overview of simultaneous strategies for dynamic optimization. *Chemical Engineering and Processing: Process Intensification*, 46(11):1043–1053.

Biegler, L. T. (2010). *Nonlinear programming: concepts, algorithms, and applications to chemical processes*, volume 10. SIAM.

Biegler, L. T., Campbell, S. L., and Mehrmann, V. (2012). *Control and optimization with differential-algebraic constraints*. SIAM.

Biegler, L. T., Cervantes, A. M., and Wächter, A. (2002). Advances in simultaneous strategies for dynamic process optimization. *Chemical Engineering Science*, 57(4):575–593.

Bittanti, S., Laub, A. J., and Willems, J. C. (2012). *The Riccati Equation*. Springer Science & Business Media.

Bock, H. G., Eich, E., and Schlöder, J. P. (1987). *Numerical solution of constrained least squares boundary value problems in differential algebraic equations*. Sonderforschungsber., Univ.

Bock, H. G. and Plitt, K.-J. (1984). A multiple shooting algorithm for direct solution of optimal control problems. *IFAC Proceedings Volumes*, 17(2):1603–1608.

Bonvin, D. (1998). Optimal operation of batch reactors: a personal view. *Journal of Process Control*, 8(5-6):355–368.

Bosse, T. and Griewank, A. (2014). Optimal control of beer fermentation processes with Lipschitz-constraint on the control. *Journal of the Institute of Brewing*, 120(4):444–458.

Boulton, C. and Quain, D. (2008). *Brewing yeast and fermentation*. John Wiley & Sons.

Brandelli, A. (2008). Bacterial keratinases: useful enzymes for bioprocessing agroindustrial wastes and beyond. *Food and Bioprocess Technology*, 1(2):105–116.

Brebu, M. and Spiridon, I. (2011). Thermal degradation of keratin waste. *Journal of Analytical and Applied Pyrolysis*, 91(2):288–295.

Brun, R., Kühni, M., Siegrist, H., Gujer, W., and Reichert, P. (2002). Practical identifiability of ASM2d parameters - systematic selection and tuning of parameter subsets. *Water Research*, 36(16):4113–4127.

Bryson, A. E. (2018). *Applied optimal control: optimization, estimation and control*. Routledge.

Carrillo-Ureta, G. (1999). *Optimal control of a fermentation process*. PhD thesis, City University.

Carrillo-Ureta, G. E., Roberts, P. D., and Becerra, V. M. (2001). Genetic algorithms for optimal control of beer fermentation. In *Proceedings of the 2001 IEEE International Symposium on Intelligent Control*, pages 391–396. IEEE.

Cervantes, A. and Biegler, L. T. (1998). Large-scale DAE optimization using a simultaneous NLP formulation. *AIChE Journal*, 44(5):1038–1050.

Cervantes, A. and Biegler, L. T. (2001). Optimization strategies for dynamic systems. *Encyclopedia of optimization*, pages 1886–1897.

Cervantes, A. M., Wächter, A., Tütüncü, R. H., and Biegler, L. T. (2000). A reduced space interior point strategy for optimization of differential algebraic systems. *Computers & Chemical Engineering*, 24(1):39–51.

Chachuat, B., Roche, N., and Latifi, M. (2001). Dynamic optimisation of small size wastewater treatment plants including nitrification and denitrification processes. *Computers & Chemical Engineering*, 25(4-6):585–593.

Che, A., Zhang, Y., and Feng, J. (2017). Bi-objective optimization for multi-floor facility layout problem with fixed inner configuration and room adjacency constraints. *Computers & Industrial Engineering*, 105:265–276.

Cizniar, M., Salhi, D., Fikar, M., and Latifi, M. (2005). Dynopt-dynamic optimisation code for MATLAB. *Technical Computing Prague*, 2005.

Corrieu, G., Trelea, I.-C., and Perret, B. (2000). On-line estimation and prediction of density and ethanol evolution in the brewery. *Technical Quarterly*, 37(2):173–181.

Currie, J., Wilson, D. I., Sahinidis, N., and Pinto, J. (2012). OPTI: lowering the barrier between open source optimizers and the industrial MATLAB user. *Foundations of Computer-Aided Process Operations*, 24:32.

Cuthrell, J. E. and Biegler, L. T. (1987). On the optimization of differential-algebraic process systems. *AIChE Journal*, 33(8):1257–1270.

Dadebo, S. A. and McAuley, K. B. (1995). Dynamic optimization of constrained chemical engineering problems using dynamic programming. *Computers & chemical engineering*, 19(5):513–525.

Daroit, D. J. and Brandelli, A. (2014). A current assessment on the production of bacterial keratinases. *Critical Reviews in Biotechnology*, 34(4):372–384.

de Andrés-Toro, B., Giron-Sierra, J. M., Fernandez-Blanco, P., Lopez-Orozco, J. A., and Besada-Portas, E. (2004). Multiobjective optimization and multivariable control of the beer fermentation process with the use of evolutionary algorithms. *Journal of Zhejiang University-Science A*, 5(4):378–389.

de Andrés-Toro, B., Giron-Sierra, J. M., Lopez-Orozco, J. A., and Fernandez-Conde, C. (1997). Using genetic algorithms for dynamic optimization: an industrial fermentation case. In *Proceedings of the 36th IEEE Conference on Decision and Control*, volume 1, pages 828–829. IEEE.

de Andrés-Toro, B., Girón-Sierra, J. M., López-Orozco, J. A., Fernandez-Conde, C., Peinado, J. M., and Garcia-Ochoa, F. (1998). A kinetic model for beer production under industrial operational conditions. *Mathematics and Computers in Simulation*, 48(1):65–74.

Deb, K., Pratap, A., Agarwal, S., and Meyarivan, T. (2002). A fast and elitist multiobjective genetic algorithm: NSGA-II. *IEEE Transactions on Evolutionary Computation*, 6(2):182–197.

Denbigh, K. G. (1958). Optimum temperature sequences in reactors. *Chemical Engineering Science*, 8(1-2):125–132.

Department of Agriculture, Environment and Rural Affairs (DEFRA) (2018). E&W Poultry Slaughterhouse Survey. Technical report, DEFRA, https://www.defra.gov.uk/.

Department of Agriculture, Environment and Rural Affairs (DEFRA), The Scottish Government, DAERA (NI), and Food Standards Agency (FSA) (2018). Slaughterhouse Surveys. Technical report, DEFRA, https://www.defra.gov.uk/.

DiStefano III, J. (1969). A model of the normal thyroid hormone glandular secretion mechanism. *Journal of Theoretical Biology*, 22(3):412–417.

Dormand, J. R. and Prince, P. J. (1980). A family of embedded Runge-Kutta formulae. *Journal of Computational and Applied Mathematics*, 6(1):19–26.

Engasser, J. M., Marc, I., Moll, M., and Duteurtre, B. (1981). Kinetic modelling of beer fermentation. *Brauindustrie*.

Engell, S. and Toumi, A. (2005). Optimisation and control of chromatography. *Computers & chemical engineering*, 29(6):1243–1252.

Falco, F. (2018). *Microbial degradation of keratin-rich porcine by-products for protein hydrolysate production: a process engineering perspective*. PhD thesis, Technical University of Denmark.

Falco, F. C., Espersen, R., Svensson, B., Gernaey, K. V., and Lantz, A. E. (2019). An integrated strategy for the effective production of bristle protein hydrolysate by the keratinolytic filamentous bacterium amycolatopsis keratiniphila d2. *Waste Management*, 89:94–102.

Fang, Z., Zhang, J., Liu, B., Du, G., and Chen, J. (2013). Biodegradation of wool waste and keratinase production in scale-up fermenter with different strategies by Stenotrophomonas maltophilia BBE11-1. *Bioresource Technology*, 140:286–291.

Farhat, S., Czernicki, M., Pibouleau, L., and Domenech, S. (1990). Optimization of multiple-fraction batch distillation by nonlinear programming. *AIChE Journal*, 36(9):1349–1360.

Food and Agriculture Organization of the United Nations (FAO) (2017). Globefish Highlights: A Quarterly Update on World Seafood Markets. Technical report, FAO, http://www.fao.org/fishery/.

Food and Agriculture Organization of the United Nations (FAO) (2018). Aquaculture Feed and Fertilizer Resources Information System. Technical report, FAO, http://www.fao.org/fishery/.

Fraga, E. S. and Amusat, O. (2016). Understanding the impact of constraints: a rank based fitness function for evolutionary methods. In *Advances in Stochastic and Deterministic Global Optimization*, pages 243–254. Springer.

Fraga, E. S., Salhi, A., and Talbi, E.-G. (2018). On the impact of representation and algorithm selection for optimisation in process design: motivating a meta-heuristic framework. In *Recent Developments in Metaheuristics*, pages 141–149. Springer.

Fraga, E. S., Salhi, A., Zhang, D., and Papageorgiou, L. G. (2015). Optimisation as a tool for gaining insight: An application to the built environment. *Journal of Algorithms & Computational Technology*, 9(1):13–26.

Fraser, R., MacRae, T. P., Sparrow, L. G., and Parry, D. (1988). Disulphide bonding in α-keratin. *International Journal of Biological Macromolecules*, 10(2):106–112.

Garcia, V., Cabassud, M., Le Lann, M. V., Pibouleau, L., and Casamatta, G. (1995). Constrained optimization for fine chemical productions in batch reactors. *The Chemical Engineering Journal and the Biochemical Engineering Journal*, 59(3):229–241.

Gassner, M. and Maréchal, F. (2012). Thermo-economic optimisation of the polygeneration of synthetic natural gas (sng), power and heat from lignocellulosic biomass by gasification and methanation. *Energy & Environmental Science*, 5(2):5768–5789.

Gee, D. A. and Ramirez, W. F. (1988). Optimal temperature control for batch beer fermentation. *Biotechnology and Bioengineering*, 31(3):224–234.

Gee, D. A. and Ramirez, W. F. (1994). A flavour model for beer fermentation. *Journal of the Institute of Brewing*, 100(5):321–329.

Gerogiorgis, D. I., Georgiadis, M., Bowen, G., Pantelides, C. C., and Pistikopoulos, E. N. (2006). Dynamic oil and gas production optimization via explicit reservoir simulation. *Computer Aided Chemical Engineering*, 21(A):179.

Gerogiorgis, D. I. and Ydstie, B. E. (2005). Multiphysics CFD modelling for design and simulation of a multiphase chemical reactor. *Chemical Engineering Research and Design*, 83(6):603–610.

Gong, J.-S., Wang, Y., Zhang, D.-D., Zhang, R.-X., Su, C., Li, H., Zhang, X.-M., Xu, Z.-H., and Shi, J.-S. (2015). Biochemical characterization of an extreme alkaline and surfactant-stable keratinase derived from a newly isolated actinomycete Streptomyces aureofaciens K13. *RSC Advances*, 5(31):24691–24699.

Gonzalez, O. R., Kuper, C., Jung, K., Naval Jr, P. C., and Mendoza, E. (2006). Parameter estimation using simulated annealing for system models of biochemical networks. *Bioinformatics*, 23(4):480–486.

Guebila, M. B. and Thiele, I. (2016). Model-based dietary optimization for late-stage, levodopa-treated, Parkinsons disease patients. *NPJ systems biology and applications*, 2:16013.

Guido, L. F., Rodrigues, P. G., Rodrigues, J. A., Gonçalves, C. R., and Barros, A. A. (2004). The impact of the physiological condition of the pitching yeast on beer flavour stability: an industrial approach. *Food Chemistry*, 87(2):187–193.

Gujarathi, A. M., Sadaphal, A., and Bathe, G. A. (2015). Multi-objective optimization of solid state fermentation process. *Materials and Manufacturing Processes*, 30(4):511–519.

Hanke, S., Ditz, V., Herrmann, M., Back, W., Krottenthaler, M., and Becker, T. (2010). Influence of Ethyl Acetate, Isoamyl Acetate and Linalool on off-flavour perception in beer. *Brewing Science*, 63:94–99.

Hasdorff, L. (1976). *Gradient optimization and nonlinear control*. John Wiley & Sons.

Hedengren, J. (2015). Optimization techniques in engineering. Technical report, APmonitor, http://apmonitor.com/me575/index.php/Main/HomePage.

Henze, M., Gujer, W., Mino, T., and van Loosdrecht, M. (2000). *Activated sludge models ASM1, ASM2, ASM2d and ASM3*. IWA publishing.

Hodge, D. B., Karim, M. N., Schell, D. J., and McMillan, J. D. (2009). Model-based fed-batch for high-solids enzymatic cellulose hydrolysis. *Applied Biochemistry and Biotechnology*, 152(1):88.

Hough, J. S., Briggs, D. E., Stevens, R., and Young, T. W. (2012). *Malting and Brewing Science: volume II hopped wort and beer*. Springer.

Hudson, J. R. and Birtwistle, S. E. (1966). Wort-boiling in relation to beer quality. *Journal of the Institute of Brewing*, 72(1):46–50.

International Trade Centre (2017). Value of products of animal origin exported from the United Kingdom (UK) in 2017, by type (in 1,000 GBP). Technical report, ITC, https://www.trademap.org/.

Izquierdo-Ferrero, J. M., Fernández-Romero, J. M., and de Castro, M. D. L. (1997). On-line flow injection-pervaporation of beer samples for the determination of diacetyl. *Analyst*, 122(2):119–122.

Jeske, J., Doruchowski, W., and Wcislo, H. (1976). The assessment of by-product management in the poultry industry. *Food Industry*, 30:255–257.

Karthikeyan, R., Balaji, S., and Sehgal, P. K. (2007). Industrial applications of keratins - A review. *Journal of Scientific and Industrial Research*, 66(9):710–715.

Keßler, T., Logist, F., and Mangold, M. (2017). Bi-objective optimization of dynamic systems by continuation methods. *Computers & Chemical Engineering*, 98:89–99.

Kirkpatrick, S., Gelatt, C. D., and Vecchi, M. P. (1983). Optimization by simulated annealing. *Science*, 220(4598):671–680.

Korniłłowicz-Kowalska, T. and Bohacz, J. (2011). Biodegradation of keratin waste: theory and practical aspects. *Waste Management*, 31(8):1689–1701.

Lam, M.-C. (2009). *In silico dynamic optimisation studies for batch/fed-batch mammalian cell suspension cultures producing biopharmaceuticals*. PhD thesis, Imperial College London.

Lee, F. C., Rangaiah, G. P., and Ray, A. K. (2007). Multi-objective optimization of an industrial penicillin V bioreactor train using non-dominated sorting genetic algorithm. *Biotechnology and Bioengineering*, 98(3):586–598.

Lentini, M. and Pereyra, V. (1977). An adaptive finite difference solver for nonlinear two-point boundary problems with mild boundary layers. *SIAM Journal on Numerical Analysis*, 14(1):91–111.

Lichtfouse, E., Navarrete, M., Debaeke, P., Souchère, V., Alberola, C., and Ménassieu, J. (2009). Agronomy for sustainable agriculture: a review. In *Sustainable Agriculture*, pages 1–7. Springer.

Lineweaver, H. and Burk, D. (1934). The determination of enzyme dissociation constants. *Journal of the American chemical society*, 56(3):658–666.

Liu, P., Gerogiorgis, D. I., and Pistikopoulos, E. N. (2007). Modelling, investment planning and optimisation for the design of a polygeneration energy system. *Computer Aided Chemical Engineering*, 24:1095.

Lodolo, E. J., Kock, J. L., Axcell, B. C., and Brooks, M. (2008). The yeast saccharomyces cerevisiae–the main character in beer brewing. *FEMS yeast research*, 8(7):1018–1036.

Logist, F. and Van Impe, J. (2012). Multi-objective dynamic optimisation of cyclic chemical reactors with distributed parameters. *Chemical engineering science*, 80:429–434.

Logsdon, J. S. (1991). *Efficient determination of optimal control profiles for differential algebraic systems*. PhD thesis, Carnegie Mellon University.

Logsdon, J. S. and Biegler, L. T. (1989). Accurate solution of differential-algebraic optimization problems. *Industrial & Engineering Chemistry Research*, 28(11):1628–1639.

Logsdon, J. S. and Biegler, L. T. (1993). A relaxed reduced space SQP strategy for dynamic optimization problems. *Computers & Chemical Engineering*, 17(4):367–372.

Luus, R. (1993). Piecewise linear continuous optimal control by iterative dynamic programming. *Industrial & engineering chemistry research*, 32(5):859–865.

Luus, R. (1994). Optimal control of batch reactors by iterative dynamic programming. *Journal of Process Control*, 4(4):218–226.

Maria, G. and Crişan, M. (2017). Operation of a mechanically agitated semi-continuous multi-enzymatic reactor by using the Pareto-optimal multiple front method. *Journal of Process Control*, 53:95–105.

Martí, R., Lozano, J. A., Mendiburu, A., and Hernando, L. (2016). Multi-start methods. *Handbook of Heuristics*, pages 1–21.

McKay, M. D., Beckman, R. J., and Conover, W. J. (1979). Comparison of three methods for selecting values of input variables in the analysis of output from a computer code. *Technometrics*, 21(2):239–245.

Modenbach, A. A. and Nokes, S. E. (2013). Enzymatic hydrolysis of biomass at high-solids loadings–a review. *Biomass and Bioenergy*, 56:526–544.

Morris, M. D. (1991). Factorial sampling plans for preliminary computational experiments. *Technometrics*, 33(2):161–174.

Mujtaba, I. M. and Macchietto, S. (1993). Optimal operation of multicomponent batch distillation: multiperiod formulation and solution. *Computers & Chemical Engineering*, 17(12):1191–1207.

National Research Council (NRC) (1993). *Nutrient requirements of fish*. National Academy Press, Washington, D.C.

Niu, D., Jia, M., Wang, F., and He, D. (2013). Optimization of nosiheptide fed-batch fermentation process based on hybrid model. *Industrial & Engineering Chemistry Research*, 52(9):3373–3380.

Nocedal, J., Wächter, A., and Waltz, R. A. (2009). Adaptive barrier update strategies for nonlinear interior methods. *SIAM Journal on Optimization*, 19(4):1674–1693.

Orzeszko, G. and Sutarzewicz, D. (1979). Bristle utilization. *Meat Management*, pages 48–51.

Osorio, D., Pérez-Correa, J. R., Biegler, L. T., and Agosin, E. (2005). Wine distillates: practical operating recipe formulation for stills. *Journal of Agricultural and Food Chemistry*, 53(16):6326–6331.

Pontryagin, L. S. (2018). *Mathematical theory of optimal processes*. Routledge.

Radwan, A. and Griewank, A. (2011). First order method for optimal control using parmetric optimization. *Proceedings of the World Congress on Engineering 2011, WCE 2011*, I.

Rehm, J., Rehn, N., Room, R., Monteiro, M., Gmel, G., Jernigan, D., and Frick, U. (2003). The global distribution of average volume of alcohol consumption and patterns of drinking. *European Addiction Research*, 9(4):147–156.

Research and Markets (2013). Analyzing the global beer industry. Technical report, Research and Markets.

Reverberi, A. et al. (1993). Optimal solutions of processes described by systems of differential - algebraic equations. *Chemical Engineering Science*, 48(14):2609–2614.

Rodman, A. D. and Gerogiorgis, D. I. (2016). Multi-objective process optimisation of beer fermentation via dynamic simulation. *Food and Bioproducts Processing*, 100:255–274.

Salhi, A. and Fraga, E. S. (2011). Nature-inspired optimisation approaches and the new plant propagation algorithm. In *The International Conference on Numerical Analysis and Optimisation (ICeMATH2011)*, K2, pages 1–8.

Sargent, R. and Sullivan, G. (1979). Development of feed changeover policies for refinery distillation units. *Industrial & Engineering Chemistry Process Design and Development*, 18(1):113–124.

Schaber, S. D., Gerogiorgis, D. I., Ramachandran, R., Evans, J. M. B., Barton, P. I., and Trout, B. L. (2011). Economic analysis of integrated continuous and batch pharmaceutical manufacturing: a case study. *Industrial & Engineering Chemistry Research*, 50(17):10083–10092.

Scheer, F. M. (2014). *Thermal Process Engineering for Brewers - Basics in Theory and Practice*. Krones Inc.

Schlegel, M., Stockmann, K., Binder, T., and Marquardt, W. (2005). Dynamic optimization using adaptive control vector parameterization. *Computers & Chemical Engineering*, 29(8):1731–1751.

Shampine, L. F. and Reichelt, M. W. (1997). The MATLAB ODE suite. *SIAM Journal on Scientific Computing*, 18(1):1–22.

Sin, G., Gernaey, K. V., and Lantz, A. E. (2009). Good modeling practice for PAT applications: Propagation of input uncertainty and sensitivity analysis. *Biotechnology Progress*, 25(4):1043–1053.

Singer, A. B., Taylor, J. W., Barton, P. I., and Green, W. H. (2006). Global dynamic optimization for parameter estimation in chemical kinetics. *The Journal of Physical Chemistry A*, 110(3):971–976.

Singh, V., Khan, M., Khan, S., and Tripathi, C. K. M. (2009). Optimization of actinomycin V production by Streptomyces triostinicus using artificial neural network and genetic algorithm. *Applied Microbiology and Biotechnology*, 82(2):379–385.

Sorek, N., Gildin, E., Boukouvala, F., Beykal, B., and Floudas, C. A. (2017). Dimensionality reduction for production optimization using polynomial approximations. *Computational Geosciences*, 21(2):247–266.

Sørensen, E., Macchietto, S., Stuart, G., and Skogestad, S. (1996). Optimal control and on-line operation of reactive batch distillation. *Computers & Chemical Engineering*, 20(12):1491–1498.

Southby, E. (1885). *A Systematic Handbook of Practical Brewing*. London; Ipswich.

Spann, R., Lantz, A. E., Roca, C., Gernaey, K. V., and Sin, G. (2018). Model-based process development for a continuous lactic acid bacteria fermentation. In *Computer Aided Chemical Engineering*, volume 43, pages 1601–1606. Elsevier.

Stassi, P., Rice, J. F., Munroe, J. H., and Chicoye, E. (1987). Use of CO2 evolution rate for the study and control of fermentation. *MBAA Technical Questions*, 24:44–50.

Stein, M. (1987). Large sample properties of simulations using Latin hypercube sampling. *Technometrics*, 29(2):143–151.

Støren, S. and Hertzberg, T. (1995). The sequential linear quadratic programming algorithm for solving dynamic optimization problems-a review. *Computers & chemical engineering*, 19:495–500.

Suzuki, Y., Tsujimoto, Y., Matsui, H., and Watanabe, K. (2006). Decomposition of extremely hard-to-degrade animal proteins by thermophilic bacteria. *Journal of Bioscience and Bioengineering*, 102(2):73–81.

Tanartkit, P. and Biegler, L. T. (1995). Stable decomposition for dynamic optimization. *Industrial & Engineering Chemistry Research*, 34(4):1253–1266.

Taras, S. and Woinaroschy, A. (2011). Simulation and multi-objective optimization of bioprocesses with MATLAB and SuperPro Designer using a client–server interface. *Chemical Engineering Transactions*, 25:207–212.

Trelea, I. C., Titica, M., Landaud, S., Latrille, E., Corrieu, G., and Cheruy, A. (2001). Predictive modelling of brewing fermentation: from knowledge-based to black-box models. *Mathematics and Computers in Simulation*, 56(4-5):405–424.

Tse, S.-M., Liang, Y., Leung, K.-S., Lee, K.-H., and Mok, T. S.-K. (2007). A memetic algorithm for multiple-drug cancer chemotherapy schedule optimization. *IEEE Transactions on Systems, Man, and Cybernetics, Part B (Cybernetics)*, 37(1):84–91.

Tsikouras, B., Passa, K.-S., Iliopoulos, I., and Katagas, C. (2016). Microstructural control on perlite expansibility and geochemical balance with a novel application of isocon analysis: An example from milos island perlite (greece). *Minerals*, 6(3):80.

van de Walle, M. (2015). Beer Statistics. Technical report, The Brewers of Europe.

Vanderhaegen, B., Neven, H., Verachtert, H., and Derdelinckx, G. (2006). The chemistry of beer aging-a critical review. *Food Chemistry*, 95(3):357–381.

Wachter, A. (2003). *An interior point algorithm for large-scale nonlinear optimization with applications in process engineering.* PhD thesis, Carnegie Mellon University.

Wächter, A. and Biegler, L. T. (2005). Line search filter methods for nonlinear programming: Motivation and global convergence. *SIAM Journal on Optimization*, 16(1):1–31.

Wächter, A. and Biegler, L. T. (2006). On the implementation of an interior-point filter line-search algorithm for large-scale nonlinear programming. *Mathematical Programming*, 106(1):25–57.

Waltz, R. A., Morales, J. L., Nocedal, J., and Orban, D. (2006). An interior algorithm for nonlinear optimization that combines line search and trust region steps. *Mathematical Programming*, 107(3):391–408.

Wright, S. J. (1992). Stable parallel algorithms for two-point boundary value problems. *SIAM Journal on Scientific and Statistical Computing*, 13(3):742–764.

Xiao, J., Zhou, Z.-K., and Zhang, G.-X. (2004). Ant colony system algorithm for the optimization of beer fermentation control. *Journal of Zhejiang University-Science A*, 5(12):1597–1603.

Zhang, P., Chen, H., Liu, X., and Zhang, Z. (2015). An iterative multi-objective particle swarm optimization-based control vector parameterization for state constrained chemical and biochemical engineering problems. *Biochemical Engineering Journal*, 103:138–151.